

AGH

University of Science and Technology in Kraków

Faculty of Electrical Engineering, Automatics, Computer Science and Biomedical
Engineering



PHD DISSERTATION

MGR INŻ. KRZYSZTOF KOGUT

REAL-TIME CONTROL IN AUTOMOTIVE SYSTEMS

SUPERVISOR:

prof. dr hab. inż. Andrzej Turnau

Kraków 2017

Akademia Górniczo-Hutnicza im. Stanisława Staszica w Krakowie

Wydział Elektrotechniki, Automatyki, Informatyki i Inżynierii Biomedycznej



ROZPRAWA DOKTORSKA

MGR INŻ. KRZYSZTOF KOGUT

**STEROWANIE W CZASIE RZECZYWISTYM W SYSTEMACH
AUTOMATYKI SAMOCHODOWEJ**

PROMOTOR:

prof. dr hab. inż. Andrzej Turnau

Kraków 2017

*I would like to express my sincere gratitude to my supervisor, **Professor Andrzej Turnau**, for the continuous support of my PhD studies, for his inspirational guidance, understanding, patience, motivation, and immense knowledge. My special thanks also go to all those whose enormous help contributed to the production of this thesis.*

Abstract

The dissertation concerns real-time control methods applied to the systems from the automotive domain. It gives a comprehensive review of the recent auto-industry related technology and the state of the market in terms of tools and methods. Two laboratory systems, SAS and ABS, are used to conduct experimental research. The development of real-time capable control algorithms is presented as well as the identification of the parameters of dynamic models of the two systems.

In the first part of the paper general aspects of automotive industry are addressed. A brief automobile history overview is given and the most pioneer electric and electronic systems are described. Afterwards, the recent automotive systems are presented. The modern vehicle electric/electronic system consists of a huge network of sub-systems responsible for certain domains such as powertrain, drivetrain, passive and active safety, comfort, convenience and finally communication and entertainment. Next, the design, development and testing of the aforementioned automotive systems is introduced. The entire V-model process is discussed along with the supporting methods and methodologies such as Model Based Design, Model Based Development and Model Based Testing. Widely utilized hardware, modeling, simulation, software tools and environments are presented. Subsequently, the emphasis is placed on real-time control systems. The general-purpose real-time system aspects are presented, followed by an application of real-time control in the automotive domain. Finally, the demonstrative laboratory SAS and ABS setups are introduced and considered as rapid control prototyping platform for further research of real-time control algorithms.

The second part of the dissertation is devoted to semi-active suspension systems. The technology and its application in ground vehicles is briefly described. Next, the modeling of vehicle suspension including dampers, tire and road is presented. Afterwards, the comfort and safety assessment analysis based on quarter vehicle suspension model is performed. This is followed by literature review of both classical control laws and advanced control strategies applied to semi-active suspension systems. Finally, the laboratory SAS system is introduced in detail and its mathematical model is experimentally identified. A number of MR damper control strategies are implemented and evaluated in real-time experiments.

The last part of this paper is concerned with the automotive braking systems. ABS is described and its functionality is presented. Similarly to semi-active suspension, the braking vehicle dynamics modeling

is tackled including the modeling of tire-road dynamics, friction and brake actuator. Next, the state-of-art of the control design for ABS is discussed. Both, the conventional rule-based ABS control strategies and more complex algorithms are outlined. Afterwards, the demonstrative ABS test rig is examined. The laboratory system is modeled and the parameters are determined via identification procedure. Finally, control algorithms are tested. A new wheel slip controller based on the brake DC current measurement is proposed, implemented and evaluated based on the conducted experiments.

The conclusions summarize the dissertation and possible further research is outlined.

Streszczenie

Niniejsza rozprawa dotyczy zagadnień i metod sterowania w czasie rzeczywistym w systemach automatyki samochodowej. W pracy przedstawiono obszerny przegląd obecnych technologii, systemów i metod wykorzystywanych w czasie projektowania automatycznych systemów sterowania w pojazdach. W celu przeprowadzenia eksperymentów w czasie rzeczywistym wykorzystano dwa systemy: SAS i ABS. W szczególności skupiono się na implementacji algorytmów czasu rzeczywistego oraz na identyfikacji parametrów modeli dynamicznych wykorzystywanych systemów.

W pierwszej części pracy zawarto ogólny opis branży automatyki samochodowej. Przedstawiono historie rozwoju przemysłu samochodowego oraz ewolucję najważniejszych systemów elektrycznych i elektronicznych pojazdów. Zaprezentowano również szerokie spektrum systemów spotykanych w dzisiejszych samochodach. W obecnych pojazdach system elektronicznych sterowników tworzy rozbudowaną sieć mikrokontrolerów odpowiadających za: układ napędowy, systemy aktywnego i pasywnego bezpieczeństwa, systemy komfortu jazdy oraz systemy komunikacyjne i rozrywkowe.

W następnej kolejności przedstawiono procesy i fazy projektowania, implementacji i weryfikacji wymienionych komponentów. W szczególności opisano kompletny proces modelu V oraz pozostałe metody i metodologie mające zastosowanie podczas rozwoju systemów automatyki samochodowej takie jak MBD (ang. Model Based Design / Development) oraz MBT (ang. Model Based Testing). Zaprezentowano zestawy narzędzi sprzętowych, programowych i symulacyjnych wykorzystywanych do projektowania, implementacji czy testowania rozwijanych systemów. Następnie przedstawiono zagadnienie systemów czasu rzeczywistego oraz ich realizacji w systemach automatyki samochodowej. Na koniec tej części pracy zaproponowano demonstracyjne systemy SAS i ABS do celów szybkiego prototypowania algorytmów czasu rzeczywistego i jako narzędzie do eksperymentalnej weryfikacji wydajności sterowania.

Część druga rozprawy skupia się w szczególności na systemach półaktywnego zawieszenia pojazdów. Przedstawiono technologie tłumików zarówno aktywnych jak i półaktywnych oraz ich zastosowanie w układach zawieszenia pojazdów. Następnie przeprowadzono przegląd metod modelowania i modeli samochodowego układu zawieszenia, w tym tłumików, opon i drogi. Ponadto, rozważono ocenę jakości komfortu i bezpieczeństwa jazdy na przykładzie modelu

ćwiartki zawieszenia pojazdu oraz przedstawiono przegląd literatury dotyczący algorytmów sterowania tłumików magnetoreologicznych (MR) w celu tłumienia drgań. W następnej kolejności zaprezentowano laboratoryjny system SAS (ang. Semi-Active Suspension) z półaktywnym tłumikiem magnetoreologicznym wraz z modelem matematycznym oraz przeprowadzono eksperymentalną identyfikację parametrów systemu. Następnie przedstawiono wyniki badań skuteczności i wydajności działania zaimplementowanych algorytmów sterowania tłumikiem MR w czasie rzeczywistym.

W trzeciej części pracy podjęto tematykę samochodowych systemów hamulcowych. Zaprezentowano układ ABS (ang. Anti-Lock Braking System) oraz opisano jego zadania i funkcjonalności. Podobnie jak w części drugiej rozprawy, przedstawiono szereg modeli wykorzystywanych do opisu dynamiki hamującego pojazdu, w tym dynamiki oddziaływania opona-droga, tarcia oraz samego hamulca. Następnie przeprowadzono przegląd literatury dotyczącej zarówno konwencjonalnych (regulowych) sterowników ABS, jak i złożonych algorytmów kontroli poślizgu. Na koniec tej części pracy przeprowadzono eksperymenty z wykorzystaniem demonstracyjnego systemu ABS. Analogicznie jak w przypadku systemu SAS, przeprowadzono identyfikację parametrów modelu matematycznego układu. Następnie przeprowadzono testy algorytmów kontroli poślizgu i opracowano nowy sterownik wykorzystujący dodany pomiar prądu silnika sterującego hamulcem w systemie.

Na koniec przedstawiono podsumowanie rozprawy oraz zaproponowano dalsze możliwe kierunki badań.

Contents

Abstract	4
Streszczenie	6
Introduction	14
1. Automotive systems	16
1.1. History of automobiles and early automotive E/E systems	17
1.2. Automotive E/E systems.....	20
1.2.1. Vehicle network systems	21
1.2.2. Powertrain and drivetrain systems	23
1.2.3. Safety systems.....	25
1.2.4. Comfort and convenience systems	28
1.2.5. Communication and entertainment systems	29
2. Automotive systems design, development and testing	31
2.1. V-Model as automotive systems development process.....	31
2.2. MBD of embedded real-time control algorithms and software	34
2.3. Software and hardware tools.....	37
2.3.1. Modeling and simulation software tools	37
2.3.2. RCP and HiL simulation testing software and hardware tools	41
3. Real-time control systems	43
3.1. Real-time digital signals processing and computing	43
3.2. Real-time systems, operating systems and programming languages.....	46
3.3. Real-time control in automotive E/E systems.....	48
3.4. INTECO's SAS and ABS laboratory setups.....	49
3.4.1. Laboratory setup's overview	49
3.4.2. RT-DAC/USB2 I/O card.....	50

3.4.3. PC based real-time control and measurement environment.....	52
4. Semi-active suspension systems	56
4.1. Semi-active suspension application and technology.....	56
4.2. Vehicle suspension modeling.....	62
4.2.1. Quarter vehicle suspension model	62
4.2.2. Half vehicle suspension model.....	65
4.2.3. Full vehicle suspension model	66
4.2.4. Suspension dampers modeling.....	69
4.2.5. Tire modeling	71
4.2.6. Road modeling	72
4.3. Comfort and safety assessment based on quarter vehicle suspension model analysis	73
4.3.1. Comfort and safety assessment	74
4.3.2. Quarter vehicle suspension model analysis.....	75
4.4. Control design for semi-active suspension	79
4.4.1. Classical control laws for semi-active suspension systems	80
4.4.2. Advanced control strategies for semi-active suspension systems	82
5. SAS laboratory demonstrative system	84
5.1. SAS overview	84
5.1.1. Kinetic excitation controller.....	87
5.1.2. MR rotary damper	90
5.2. SAS model and model parameters identification.....	90
5.2.1. Suspension part model identification	91
5.2.2. Identification of the wheel-eccentricity part model	97
5.2.3. MR-damper model improvement.....	106
5.3. MR damper control strategies for SAS system.....	108
6. Automotive braking systems	114
6.1. Description of ABS.....	114
6.2. Braking vehicle dynamics modeling.....	115
6.2.1. Longitudinal slip ratio, tire-road dynamics and friction modeling	115
6.2.2. Brake actuator modeling	118
6.2.3. Vehicle dynamics modeling	120

6.3. ABS functions and wheel slip control goals based on single wheel model analysis.....	122
6.4. Control design for ABS	125
6.4.1. Conventional rule-based ABS control algorithms	126
6.4.2. Other control strategies applications to ABS.....	127
7. ABS laboratory demonstrative system.....	130
7.1. ABS overview	130
7.2. ABS modeling and identification.....	131
7.2.1. Lower wheel with DC motor parameters identification.....	131
7.2.2. Upper wheel parameters identification	133
7.2.3. Complete model introduction.....	135
7.2.4. Slip friction curve estimation.....	136
7.2.5. Brake force profile estimation.....	138
7.3. ABS control	140
7.3.1. Motivation to introduce brake DC current measurement.....	140
7.3.2. The new slip controller based on brake DC current measurement	146
Conclusions.....	152

List of Tables

4.1. The automotive suspensions comparison.....	60
5.1. Identified parameters and quality index values.....	93
5.2. SAS system control algorithms	109
6.1. Burckhardt model parameters.....	117

List of Figures

1.1. An example of in-vehicle network architecture.....	22
2.1. The automotive V-model diagram	32
3.1. Basic functional block diagram of a real-time DSP system	44
3.2. General overview of laboratory setups	50
3.3. The picture of the RT-DAC/USB2 I/O board.....	51
3.4. The block diagram of the RT-DAC/USB2 I/O board.....	52
3.5. The MS Windows jitters comparison.....	54
4.1. Quarter-car passive automotive suspension model	63
4.2. Quarter-car semi-active automotive suspension model	64
4.3. Quarter-car fully active automotive suspension model.....	64
4.4. Half-car passive pitch oriented automotive suspension model.....	66
4.5. Full-car passive automotive suspension model.....	69
4.6. Hysteresis loop of the Bouc-Wen model	70
4.7. System poles diagram	78
4.8. Frequency response of transfer function $F_s(s)$ for varying damping parameter b_s	78
4.9. Frequency response of transfer function $F_t^d(s)$ for varying damping parameter b_s	79
5.1. Photography of the laboratory SAS system.....	85
5.2. Photography of the semi-active suspension system's spring and MR damper unit.....	86
5.3. Scheme of the semi-active suspension system.....	86
5.4. An example SAS system trajectories.....	87
5.5. Kinetic excitation frequency vs. time with no load and after load application due to stairs PWM control of the DC motor	88
5.6. Kinetic excitation frequency vs. time with no load and after load application due to ramp PWM control of the DC motor	88

5.7. Set-point (ramp signal) and real measured frequency vs. time.....	89
5.8. Set-point (stairs sequence signal) and real measured frequency vs. time.....	90
5.9. Structure of the suspension part model.....	91
5.10. Body angular position x_1 vs. time in experiment 1	94
5.11. Body angular position x_1 vs. time in experiment 5	95
5.12. Obtained static profile $b(u_{MR})$ of MR damper	96
5.13. Body angle x_1 and MR damper control u_{MR} vs. time	96
5.14. Body angle x_1 and MR damper control u_{MR} vs. time	97
5.15. Structure of the complete SAS model.....	98
5.16. Wheel angular position x_1 , body angular position x_3 and set-point frequency for the kinetic excitation controller f_{u_1} vs. time	102
5.17. Wheel angular position x_1 , body angular position x_3 and control u_1 vs. time ($f_{u_1}(t) =$ 6.5 Hz)	103
5.18. Body angular position x_3 vs. time ($f_{u_1}(t) = 1.6$ Hz, $u_2 = 30$ %).....	104
5.19. Body angular position x_3 vs. time ($f_{u_1}(t) = 1.6$ Hz, $u_2 = 70$ %).....	104
5.20. Body angular position x_3 vs. time ($f_{u_1}(t) = 1.6$ Hz, $u_2 = 100$ %).....	105
5.21. MR damper characteristics for different coil currents	107
5.22. MR response to the chirp signal	107
5.23. RMS accelerations of the sprung mass for different excitation frequencies	110
5.24. RMS controls of the MR damper for different excitation frequencies	110
5.25. The SAS real-time MATLAB/Simulink model	111
5.26. Estimation of the sprung angular velocity	112
5.27. Continuous skyhook method with and without the state estimator	113
5.28. On-Off skyhook method with and without the state estimator	113
6.1. Wheel tire-road contact forces.....	116
6.2. Burckhardt model longitudinal friction coefficient for different road types.....	118
6.3. Single-wheel model	120
6.4. Double-wheel model.....	121
6.5. Vehicle and wheel speed during a panic braking manoeuver for different road conditions ...	123
6.6. Vehicle slip ratio during panic braking manoeuver for different road conditions	124
6.7. Function $\psi(\lambda_x)$ for different road conditions	125

7.1. Photography of the laboratory ABS.....	131
7.2. Lower wheel angular velocity ω vs. time	133
7.3. Upper wheel angular velocity ω vs. time.....	134
7.4. ABS model diagram	136
7.5. Brake control vs. time, upper and lower wheel angular velocity change over initial wheels velocities vs. time	137
7.6. Slip friction coefficient $\mu(\lambda)$ vs. slip λ	138
7.7. Brake static profile $M_b^s(u_b)$	139
7.8. Upper wheel angular velocity x_1 vs. time	139
7.9. Lower wheel angular velocity x_2 vs. time	140
7.10. An example ABS control experiment.....	141
7.11. An open-loop tests results for laboratory ABS.....	142
7.12. An example of non-reproducible results obtained for laboratory ABS	143
7.13. An example of laboratory ABS sensitivity to applied control values.....	144
7.14. An example of laboratory ABS brake torque repeatability issues.....	145
7.15. The current sensor output filter performance.....	147
7.16. The brake DC motor current controller performance	148
7.17. The new slip controller block diagram	148
7.18. The performance of the new ABS slip controller	150
7.19. The performance of the relay slip controller	151

Notes on the content of the dissertation and the original author's contribution

The paper presents a broad spectrum of issues of the real-time control of automotive systems. To enable and at the same time facilitate the evaluation of the doctoral dissertation the author explicitly points out those parts of the paper which, in his opinion, constitute the original scientific output of his work. However, the author could not limit the presented content only to his own original results. Such results would be incomplete if narrowed down to two control examples stripped of important background. After a brief explanation it becomes clear that the dissertation consists of parts describing original research and knowledge that is generally available. The sections concerning the original results are: *5. SAS laboratory demonstrative system and 7. ABS laboratory demonstrative system.*

Introduction

The main purpose of the dissertation is to present and explore the most important functionalities in automotive systems. In fact, two representative functionalities and the laboratory rigs corresponding to them operating in real time were chosen. The first one relates to automotive driving comfort and the second one to automotive safety. The considered laboratory rigs demonstrating these two functionalities are called SAS (Semi-Active Suspension) and ABS (Anti-lock Braking System). What is also investigated are dynamic models, the parameters of which are determined via identification procedures. Real-time control algorithms are selected. The SAS and ABS rigs are dedicated to conduct real-time experiments and provide measurement signals and control signals. Studies concerning SAS and ABS are real-life, non-simulated experiments and they bring us closer to the research directly conducted in the car.

The real-time control in automotive systems is a very broad field of practical knowledge. The author is fully aware that nowadays this field is developing too fast to track its evolution without omitting some aspects. In spite of this, the author presents by name basic functionalities in vehicles. This can be described as a secondary goal of this dissertation. The history of cars, the state of the present, and even future intentions are also taken into consideration.

The thesis of the dissertation has been formulated: **Automotive automatic control systems operating in real time improve driving safety and driving comfort.** It is justified in the contents of the sections: 4.3, 5.3, 6.3 and 7.3.

Chapter 1 introduces a reader to automotive systems. It starts from the history of automobiles and early automotive electric/electronic systems. The following issues are also considered: the vehicle network, powertrain and drivetrain, safety, comfort, communication and entertainment systems.

Chapter 2 describes how to design and test automotive systems. The emphasis is placed on hardware and software tools, the hardware in the loop and rapid control prototyping methodology.

Chapter 3 is devoted to real-time control systems covering such issues as: digital signals processing and computing, systems and programming languages, control in automotive E/E systems. Finally, the laboratory SAS and ABS rigs manufactured by INTECO are considered as the real-time control research tools. These tools are presented in detail in chapters 5 and 7.

Chapter 4 introduces a reader to the semi-active suspension technology. It presents a large scope of vehicle suspension models. A quarter vehicle suspension model is analyzed. As far as semi-active control algorithms are concerned we deal with classical and advanced control strategies.

Chapter 5 is one of the two main scientific contributions to this dissertation. The SAS system is described, modeled and identified. Finally, magnetorheological control strategies are introduced and tested for the real life system.

In chapter 6, in a similar manner as in chapter 4, the ABS modeling takes place. The wheel slip control is a main goal for drive safety purposes. Different ABS control algorithms are concerned.

Chapter 7 is the second main scientific contribution to this dissertation. The ABS system is described, modeled and identified. A new slip controller based on the brake DC current measurement is shown. The most important issue for the controller construction is that it is fully based on the experimental measurement data.

Conclusions close the dissertation. There are also suggestions for further research.

1. Automotive systems

Every modern mid-class passenger car is nowadays equipped with more electronics and has more computing power than NASA Space Shuttle. In fact the entire vehicle is a huge real-time DES (Distributed Embedded System) consisting of 5 to 80 ECUs (Electronic Control Units) in high-end, luxury cars where ECUs interchange information with each other using up to 5 different communication buses [1]. The number of software controlled functions exceeds 2500 which is about 10 million lines of software code. For instance, the head unit of the 2009 BMW 7 series model is programmed with 4 million lines of code. Currently, the solid-state electronic components control the following: engine management, vehicle braking, steering and driveability, passenger safety and convenience functions, navigation and entertainment. It is worth to mention that the above spectrum of E/E (Electrical/Electronic) and software constitute 40 percent of the vehicle cost, and the majority of features in modern vehicles can only be implemented through the use of pre-programmed electronics.

The number of sophisticated applications integrated into a vehicle also has a great impact on car makers competitive advantages and sales volumes. Rapid growth of the automotive electronics which started around 2000 has changed the automobile definition. Nowadays most people treat cars as appliances. During the last 100 years the automotive industry also created a huge economic and business sector, especially in Germany, France, England or United States. This industry also constitutes a driving force of the economy of many other countries where car manufacturers have their factories or suppliers. It has also created a large number of work places in the vehicle maintenance industry. On the other hand, cars also created a spectrum of problems including accidents, increasing air pollution and, of course, fuel consumption issues.

This chapter introduces the main electronically controlled systems found in contemporary cars. The E/E systems are grouped into domains which include powertrain, driveline, passive and active safety, and comfort systems. The description focuses mainly on electronic aspects of the systems. The overview is preceded by a brief history of automobiles regarding the evolution of automotive industry, its main inventors and aspects which had driven the market to its current status. The historical context is devoted to point the milestones of electronics applications with an emphasis on showing how real-time embedded control has been introduced into vehicles.

1.1. History of automobiles and early automotive E/E systems

The first road vehicles were introduced by the end of the 19th century. Their appearance had been preceded by the invention of a gas-fuelled internal combustion engine in the 1870s by A.N. Otto in Germany. This engine has been modified by Gottlieb Daimler in 1885 and fitted into a primitive bicycle becoming the world's first motorcycle. The modification consisted of the usage of petroleum vapour instead of gas to run the engine. The following year, 1896, is considered to have been the starting point of motor vehicle history. This year Karl Benz patented his Motorwagen, the three-wheeled vehicle with a single-cylinder and four-stroke combustion engine, becoming the automobile inventor. Coincidentally, at the same time Daimler rebuilt a horse carriage by installing a motor engine in it. This vehicle is now known as a forerunner of the modern car. Benz continued working on improvements, and in 1894 he introduced Velo, the world's first production car. In 1901 Paul Daimler and Wilhelm Maybach presented 35HP car model thus creating the look of motor vehicles that was followed by designers for decades. Their new car, called Mercedes after Daimlers's daughter, had a four-cylinder engine placed in front of the passengers (Benz's vehicles placed it under the driver and passenger) covered by a bonnet and mounted behind a characteristic radiator.

In those days, all the vehicles in Europe were produced by technique of hand craftsmanship until the mass production technique was introduced into car assembly process in the United States at the beginning of the 20th century by Henry Ford. The first model of a car manufactured using the principle of the production line was Ford Model T in 1908. It was in production until 1927 receiving several revisions and becoming the second, after Volkswagen Beetle, most selling car in the world history with more than 15 million cars sold. Thanks to inventions introduced to the production line flow, including the introduction of a moving assembly line and the construction simplicity, the Model T production speed reached 1000 per day, and the complete time needed to build a single car has been reduced from 14 hours to about 93 minutes. Thus, the mass production lowered the price of the product enough to be affordable by a large section of the public. Before the Second World War started, the US motor industry developed a lot, and the so-called Big Three American automobile companies emerged (Ford Motor Company, General Motors and Chrysler Motor Corporation). By 1927, General Motors owned such marques as Buick or Chevrolet (co-funded by Louis Chevrolet and General Motor founder William C. Durant) becoming the world's largest car manufacturer selling over 1 million cars per year. It is worth to mention that a popular Chevy remained the best-selling brand in the USA from 1936 until 1976. Another GM marque, luxury Cadillac, went down in history as a manufacturer of the first V8 mass produced engine and the V12 and V16 high performance units. The remaining giant of the US market, Chrysler Motor Corporation, started by Walter P. Chrysler, former GM Buick president owned marques such as Dodge or Plymouth. Their last avant-garde model, Airflow, introduced the future streamlined look - the

first true aerodynamic styling.

Meanwhile in Europe, before the Second World War the automotive industry was rapidly developing in Germany, France, Italy and the United Kingdom. The German pioneers jointly created the Mercedes-Benz brand under Daimler-Benz AG company which entered into history of automobiles several times, for example by inventing the first volume-produced diesel passenger car, the Mercedes-Benz 260 D in 1936, the world's first series-produced four-stroke direct-injected petrol engine, or the first passenger car to feature independent suspension on all four wheels in 1931. Except for the Daimler-Benz company which was identified with luxury and power vehicles, the German market contained other trendsetting companies and marques such as Audi, BMW, Porsche or VW. The Audi Automobilwerke was one of the first German brands to adopt electric lighting and starter motors. The BMW company (Bayerische Motoren Werke) was founded in 1913 as an aero-engine producer and had merged with an aircraft manufacturing factory started by Gustav Otto, the son of Nikolaus Otto, the gas-engine inventor. The BMW entered car manufacturing in 1929 and dominated European sport cars racing before the start of the Second World War. The Porsche and VW stories accelerated after the Second World War although their history is connected with one of the 20th century finest automotive engineers, Ferdinand Porsche who developed the concept of electric car propulsion in 1900 and designed a car for masses, the Volkswagen 'people's car'.

In France there were three great marques: Citroën, Peugeot and Renault. The company founded by André Citroën released the first European mass produced model Type A as early as in 1919 (100 per day) surpassing Opel which introduced this technique in 1924. The brand is also recognized as a marketing leader of its time. For example, they used the Eiffel tower as an advertisement banner between 1925 and 1934 having the marque name emblazoned in lights on the stunt. Additionally, Citroën was the first to target their cars to women by having special, easy to use and small models (electric starter motor instead of crank handle). The Armand Peugeot designed car was the first to adopt pneumatic tires (fitted by Michelin brothers), and sliding gear transmission in 1895. The vehicles under this brand were often awarded during European and world races in 1910s and the company became the French leader in car sales shortly afterwards. Unlike its French competitors who in general designed superior models, the Renault brand focused on mainstream cars for masses and also on commercial vehicles. In general, from the beginning of the motor vehicles boom the division into sport, premium and luxury, and regular vehicles had been made. For instance, in Italy there was Alfa Romeo and Fiat while in the United Kingdom there was Austin and such superior marques as Rolls-Royce, Aston Martin and Jaguar. Apart from cars, the years 1910s, 1920s and 1930s yielded the growth of future automotive suppliers leaders such as Bosch. The Robert Bosch business launched its first automotive lighting system that consisted of a generator, battery, voltage regulator and headlights in 1913 in Audi vehicles, and the

diesel injection pump in 1936. The company was also known as horn, indicators and windshield wipers producer. Another example is Blaupunkt which released its first series-produced car radio in Europe in 1932.

After the Second World War outbreak, the majority of car manufacturers changed their production to airplanes, aircraft engines, tanks or other military vehicles, and they either were forced to do it or they did it of their own accord. After 1945 the car production started again. The vehicles engines, transmission and steering systems, suspension and brakes mechanism were constantly refined and even replaced by modern successors such as disc brakes that were introduced instead of drum brakes into mass-produced Citroën DS-19 in 1955. When it comes to interior refinement, air cooling and air-conditioning were introduced by Packard in 1940 but became very popular, especially in USA, after the war. The visual side of cars experienced the greatest changes either due to passing fads or due to aerodynamic factors. The postwar vehicles mass production started to result in poor quality, especially in USA, and until 1970 most of the cars would start to rust quickly and would become perishable. One of the exceptions was VW Beetle, the appearance of which was old-fashioned (it debuted in 1945) and the car itself was behind in the context of mechanical design. However, the simplicity and durability made this model the best selling car in the world. Until the end of its production in 2003 in Mexico, the total number of manufactured Beetles exceeded 23 million. The decreasing quality of old marques mainstream models also allowed Japanese companies such as Toyota or Suzuki to arise on American and European markets. Currently, the marque founded by Kiichiro Toyoda in 1937 is the world's largest cars and trucks producer and it is known as a pioneer of hybrid technology.

The first electronic subsystems application in vehicles (except for the radio or the turn signal models) is dated back to the late 1950s and early 1960s but due to negative customer feedback they were removed from the automobiles production [2]. Historically, the semiconductors have been installed in cars in 1958 in regulators for generators (variodes) [3]. Starting from 1960s, the first mass produced embedded systems that were microcontroller based were introduced. They were utilized in US military Minuteman I/II intercontinental ballistic missiles and also in the NASA Apollo Guidance Computer [4]. The biggest milestone in automotive industry in the context of electronic and real-time embedded system appliance occurred in 1968. That year VW installed the first series-produced microprocessor based fuel injection system in the 1600 model (Bosch D-Jetronic). This was also the first car with 12V electric system which was the standard that lasted to recent years. In the following years, two major factors had impact on the popularization and a need for electronics in vehicle engine control. Firstly, the solid-state digital electronics components had become available for relatively small cost. Secondly, beginning in the late 1960s, government environmental regulations regarding exhaust emissions and fuel economy had been introduced. The computer based techniques were needed to replace the methods applied at the time in

order to increase engine control performance. These events led to an evolution of electronic systems in automotive design. Apart from powertrain control, another urgent need for improvement in automobiles design has appeared. Again partially due to government-mandated regulations, the vehicle safety concern had been escalated [5, 6, 7]. Even today the data shows that in Europe and also in North America the number of deaths caused by vehicle accidents is 150 per day on average which is similar to a number of aeroplane crash casualties. In 1970s research and observations had proven that almost all car accidents are due to human errors mostly caused by a delayed reaction or taking improper actions in vehicle control during an emergency situation such as braking or obstacles avoidance maneuver [8]. For this reason car manufactures started to develop sophisticated passive and active safety systems which in majority had to be electronically controlled in real-time. The first computerized four-wheels braking assistance system called Sure-Brake was introduced by Chrysler in 1971. Shortly after, other car makers such as Toyota, Ford or GM also presented similar solutions although the modern ABS (Anti-lock Braking System) system ready for mass production was invented in 1978 by Bosch and fitted into a Mercedes-Benz vehicle. In the same time, the first airbag and seat belt pre-tensioner systems started to be installed in series produced cars. In the described advent of electronics introduction in vehicles, a lot of other automobile domains have been equipped with electronically controlled subsystems such as automatic transmission, power-assisted steering or central locking mechanism.

The last 25 years once again changed the automobiles design with an introduction of automobile E/E system employing dedicated communication buses and a huge number of ECUs. The latest electronics features started to appear in luxury class cars at the beginning of the 21st century and have become standard in mid-class models. However, in the last 5 years innovations such as AS (Active Safety) and ADAS (Advanced Driver Assistance Systems) applications together with future technologies such as V2V (Vehicle to Vehicle) and V2I (Vehicle to Infrastructure) have just started to emerge in mass production cars. The next section presents the current vehicles electronic system architecture together with bus systems and actual spectrum of electronically controlled functions of modern cars.

1.2. Automotive E/E systems

Nowadays, in modern motor vehicles, the electrical and electronic system covers almost all of the automobile functionalities. The areas where a large amount of electronics is involved are drivetrain, safety, comfort, chassis/body control, and communication. The drivetrain and powertrain (e.g., the engine and the gearbox) is the first domain where microcontrollers took over the entire operation. The next field where ECUs were introduced was safety (e.g., ABS). The two remaining areas of electronics presence, which are communication, and comfort and convenience, are fairly new and would not be developed without electronics. All the ECUs performing the depicted functions and tasks work either in open or

closed loop using a huge number of sensors and setpoint generators, and acting on highly controllable actuators. There are also sensors signals such as engine speed which are needed in two or more ECUs. Additionally, the control units interchange more and more information and often have mutual influence on each other. In order to reduce cabling between ECUs, the CAN (Controller Area Network) vehicle network had been introduced in 1991 in the luxury Mercedes-Benz 500E. At present, every mid-class vehicle is equipped with at least two communication buses.

The next section describes and characterizes the currently utilized vehicle network systems. Subsequently, the electronically controlled functions are presented including a brief functional overview, main dependencies between subsystems and description of how the components complement each other.

1.2.1. Vehicle network systems

The auto industry adopted bus systems for several reasons. The most obvious is the cost reduction because of the decrease of wiring harness. Apart from financial advantages, the use of networks also simplified vehicles assembly process, connection of the system components and handling of the equipment variants in a vehicle. Due to different requirements for bus systems in functional areas such as drivetrain, chassis, interior or telematics, the networks can be divided into classes (Class A, B, C, C+ and D). The most important technical parameters diverging bus systems are: data transfer rate, interference immunity, presence of detection of transmission errors in the protocol, real-time capabilities and number of network nodes. For example, real-time application of drivetrain and chassis functional areas (e.g., ABS or engine and transmission control units) demand relatively high speed data rates (min. 500 kBit/s), and in telematics domain the emphasis is put primarily on extremely high data rates due to the required capability to stream the audio or video data. Detailed information about vehicle networks classification can be found in [9]. The application of different network types and protocols in the vehicle system domain enforces the need of data exchange between these systems. The coupling of networks is performed via gateways which translate data messages with signals from one bus system to another. The example of such solution is depicted in Figure 1.1. Using this configuration, the information about current vehicle speed available in the Drive CAN can be transferred to Instrument Cluster CAN in order to display the value to the driver, to the MOST (Media Orientated Systems Transport) system in order to adapt the sound volume to the driving speed, and also to Comfort CAN in order to adjust the padding position of the dynamic seats.

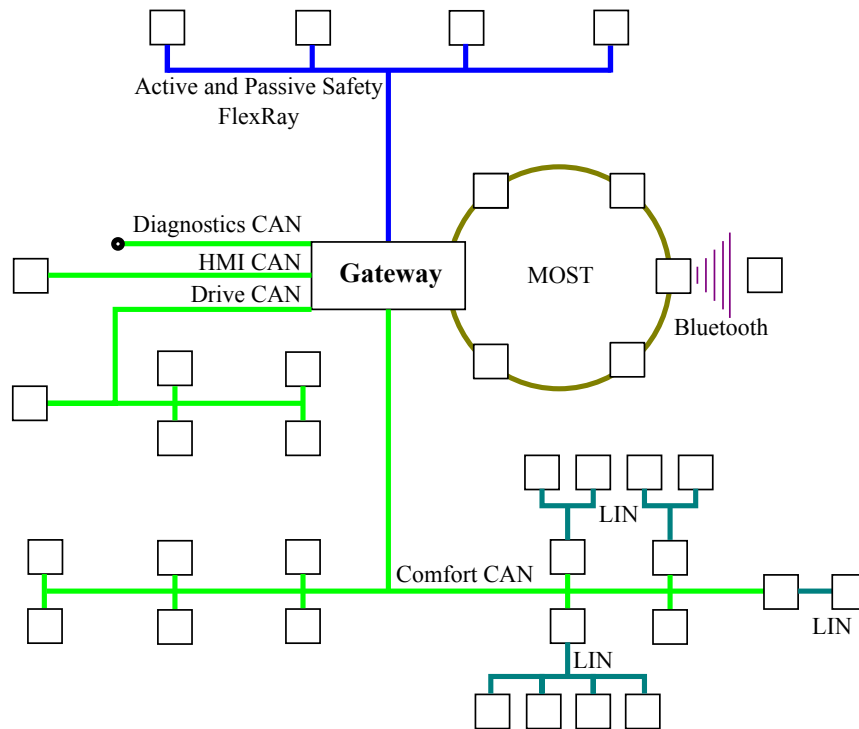


Figure 1.1: An example of in-vehicle network architecture.

1.2.1.1. CAN

The CAN (Controller Area Network) bus is the first bus system introduced in series production automobiles which is the leading serial communication solution used in various domains at the moment. The most common of CAN versions are Low-Speed (ISO 11898-3 2006) and High Speed (ISO 11898-2 2003). The Low-Speed CAN (CAN-B) operates at a bit rate of 5 to 125 kBit/s which is adequate for comfort and convenience functions that do not require response times lower than 100 ms (human being cannot perceive delay periods lower than 100 ms) such as roof control, air-conditioning control, power-window unit, seat adjustment, mirror adjuster or navigation system control. Additionally this CAN bus is also used in vehicle diagnostics protocols like OBD (On-Board Diagnostics). The High-Speed CAN (CAN-C) operates at bit rate of 125 kBit/s to 1 MBit/s and this speed is sufficient for real-time applications in drivetrain and chassis area where fast processes are involved. This version is used in engine-management system, electronic transmission system or vehicle stabilization systems such as ABS or ESP (Electronic Stability Program).

1.2.1.2. LIN

The LIN (Local Interconnect Network) protocol was developed by a consortium of several automotive manufacturers founded in 1998. The goal was to design a cost-effective and simple alternative to Low-Speed CAN to use in body electronics domain. The protocol meant to be simple and dedicated

to non time critical applications. The first production vehicle equipped with LIN was Mercedes-Benz SL introduced in 2001. The LIN bus operates at bit rate up to 20 kBit/s, the bus access is determined by master-slaves principle. It is generally used to connect sensors and actuators in applications such as wipers control, rain and light detection sensors, air-conditioning system, headlights electronics and control of door-lock, power-windows, door-mirrors and power-sunroof.

1.2.1.3. MOST

The MOST (Media Orientated Systems Transport) bus was developed by the MOST Cooperation founded in 1998 by BMW, DaimlerChrysler, Harman/Becker and Oasis SiliconSystems. The aim was to provide cost-effective network for audio, video and data transmission in entertainment and infotainment systems installed mainly in premium class vehicles (DVD, TV, a CD changer, amplifier, radio tuner etc.). It offers a data rate of 24.8 to 150 MBit/s and uses fiber-optic ring for transmission.

1.2.1.4. FlexRay

FlexRay communication network was developed by FlexRay Consortium (BMW, DailmerChrysler and others) starting in 1998. The designed bus system was dedicated to AS areas including X-by-wire (e.g., drive-by-wire, brake-by-wire, steer-by-wire) without mechanical fall-back level and also to drivetrain (as replacement of High-Speed CAN). The new protocol is deterministic, fault-tolerant and high speed with bit rate up to 10 MBit/s. Except AS, the areas of application might be passive-safety systems, chassis/body and comfort systems.

1.2.2. Powertrain and drivetrain systems

1.2.2.1. Engine management system

The modern vehicles gasoline engines (e.g., four-stroke spark-ignition) do not contain such systems as carburettors or contact-breaker (distributor) ignition. The entire engine operation is controlled by microprocessor-based ECU and electromechanical and electronic actuators (ignition coils and sparkplugs, throttle-valve positioner, fuel injectors, fuel-pump, etc.), and sensors (accelerator-pedal position, throttle-valve position, air-mass flow, lambda oxygen sensor, vehicle speed sensor, etc.). The engine ECU of typical US-market vehicle in 2010 had to control about 80 functions with an application containing approximately 25 million instructions. Back in 1990, the values amounted accordingly to 20 and 5 million. This significant growth was the consequence of US and EU regulations for engine emissions of CO, HC and NOX. Among other things, the electronic system (e.g., Bosch Motronic) is responsible for control of the air-fuel ratio and ignition coils and sparkplugs in such a way that the engine operates optimally when it comes to fuel consumption/economy, performance and exhaust gas

emission. The EFI (Electronic Fuel Injection) control systems (speed-density and mass air-flow) differ in specific engine configurations such as gasoline injection systems with intake manifold and gasoline direct injection systems. The electronic ignition control ensures the required spark duration and initiates ignition of air-fuel mixture in the combustion chamber at the proper time. Additionally, the engine management system performs secondary operations such as knock sensing, monitoring of exhaust gas recirculation and diagnostics. In the case of EDC (Electronic Diesel Control, only the fuel injection is regulated. The input for changing the torque of gasoline or diesel engine can be taken either from the driver acceleration pedal or set by other functions like Cruise Control, TCS (Traction Control System), ABS or transmission control. Except for the control of engine operation, the engine management system also provides OBD to monitor and log the engine unit emissions-related equipment.

1.2.2.2. Transmission control system

The vehicle transmission is a gear system enabling optimal operation of engine independently from vehicle speed and load. The device adjusts the ratio of the engine speed to the vehicle wheels speed. The selection of gear ratio can be performed manually by the driver or controlled via an automatic system. Although the automatic transmission system called Hydra-Matic was introduced by GM's model Oldsmobile option as far back as in 1940, nowadays the manual transmissions are still more popular in Europe where 90 percent of vehicles are 'manual'. Essentially, an opposite trend persists in North America and Japan where about 80 percent of vehicles are fitted with automatic transmissions. In general, properly used manual transmission is more efficient in the context of fuel economy especially when engine size is small, thus its popularity in Europe where cost of fuel is considerably high. However, using manual transmission demands more driver fatigue which in turn decreases driver's safety. Also, the variety of road conditions in this region, considerably different than in United States, enforce frequent gear changes. The configuration of the auto gear shift developed by GM engineers, consisting of fluid-coupling mechanism (torque-converter) and a system of planetary gears sets, has been retained until present day. However, the electronically or electrographically controlled clutches replaced the hydraulically or pneumatically actuated ones. Modern self-shifting transmission systems ECU calculates proper gear ratio using driver selected mode (Park, Reverse, Neutral, Drive), accelerator pedal position and engine load. The use of microprocessor based control of the gear shifting strategies improved the performance of the automatic transmission systems respect to fuel economy, and reduced undesirable vehicles dynamics effects such as torque shocks and vibration.

Due to a strong relationship between engine management ECU and transmission control ECU, these two systems often work in strict cooperation which improves the entire vehicle performance. The main advantage of such solution is the reduction of engine torque during gear shifting periods. The integration of these two modules into single ECU called Powertrain Control Module allows for an addition of

such features as EGR (Exhaust Gas Recirculation) and EEC (Evaporative Emission Control). This arrangement also allows the implementation of sophisticated control algorithms such as neural networks incorporated by Mitsubishi in order to 'learn' the driver's habits by monitoring vehicle state variables in order to predict its next action.

Beside the manual and automatic transmission systems, electronic control is also present in semi-automatic gear shifting modules. The electronic clutch control system assists the driver during the gear change operation by steering the clutch lever during the release phase. The electro-hydraulic servo system controlled by ECU automatically handles clutch depressing process based on accelerator pedal position sensor, throttle servo system, engine speed sensor and gearbox state. In addition to the safer and smoother gear changing benefits, the ECU might prevent inappropriate gear change and engine start with gear set.

1.2.3. Safety systems

The safety systems are among the most important domains in auto industry in recent years. The introduction of electronics in active safety, and shortly afterwards, in passive safety systems, significantly improved their performance and also developed a more sophisticated solution the application of which was not possible without microprocessor based sensors and controllers. The passive safety systems, including seat-belts and seat-belts pretensioners, airbags and rollover protection systems, are designed to protect vehicle occupants in the event of crash, while active safety systems operate during pre-crash traffic scenarios and its goal is to prevent the accident occurrence by either assisting the driver during maneuvers or inform and warn the driver about dangerous situations.

1.2.3.1. Passive safety systems

One of the first passive safety systems were seat belts. This mechanical system was patented in the late 19th century although it was first introduced as an option in American cars only after the Second World War. As standard vehicle equipment the seat belt was offered by Saab in 1958 and afterwards the known 3-point safety belt became the required feature of each vehicle. The recent occupant protection systems consist in general of crash detection sensors and passenger occupancy sensing system, a microcontroller and actuators in form of seat belt pretensioners, airbags and rollover protection bars. The impact sensing is realized by either mechanical crash sensors (e.g., mechanical rolamite impact sensor) or electronics based sensors (piezoelectric acceleration sensors or surface micromechanical acceleration sensors). The accident detection elements are mounted in the selected positions on both sides of the vehicle (depending on the vehicle type and system complexity) in the front seat crossmembers or crumple zone (front impact sensing), and B and C-pillars (side impact sensing). The second sensor

group is passenger compartment sensing, performed mainly by OC mats (Occupant Classification mats) installed in the front seats. The OC sensor mat consists of pressure-dependent FSR (Force-Sensitive Resistance) resistance elements which measure the pressure characteristics on the seat surface which provide indirect information about driver and passenger weight and anthropometric profile. Additionally, the seat occupancy sensing system can be equipped with child's safety seat detector. The seat profile of the human body is used to distinguish if a passenger of the vehicle is an adult or a child. This knowledge is useful because in certain cases the deployment of airbags is unwanted even if the seat is occupied. In addition to the presented method of passenger compartment sensing, other techniques are also applied such as ultrasonic sensors or video cameras. The crash detection sensors serve as triggers for ECU to initiate airbag inflation and seat belts tightening and passenger compartment sensors provide additional reference data such as information if a seat is occupied by an object or a person. The main function of seat-belts is to prevent occupants forward displacement caused by inertia force acting on them during the impact. In order to improve protection against injury, the body should be in a position close to backrest of the seat. The seat belt pretensioners system eliminates the seat belt slack by pulling the seat belts tighter achieving 50 to 60 percent absorption of impact energy. The ECU activates a shoulder-belt tightener piston by firing a pyrotechnic propellant charge and it takes approximately 10 ms to tension a seat belt which results in 1 cm passenger frontal travel distance. The next element of the impact protection system are front airbags which can increase the level of energy absorption to 70 percent. It complements seat belts unit by providing an additional head and chest injury protection function in the case of more serious accidents when the first system is not able to prevent hitting of the driver into steering wheel or passenger striking the instrumental panel. To maximize injury protection, the airbag must be fully inflated before the body of the seat occupant reaches its surface (it takes about 10 ms to detect the impact and fire the ignition system and 30 ms to completely fill the airbag using pyrotechnical gas inflators). After the contact, the airbag deflates in order to absorb the impact energy. In the case of side airbags (windows bags, curtains), the time required for crash sensing and activation is even shorter due to a close distance between the occupant and the side of the vehicle body. The last component of the occupant protection system is the rollover protection system which was introduced in cabriolets in order to detect rollover situation (performed by yaw rate sensor and two acceleration sensors on the vehicle's transverse and vertical axes) and protect the passengers by deploying the extendable head restraints. Currently the rollover detection systems are also present in the closed-top vehicles and are used to activate the airbags and seat-belts pretensioners.

1.2.3.2. Active safety systems

Contrary to passive safety systems, the goal of the active safety systems is to prevent the accident occurrence rather than to minimize the crash outcome. Historically, this domain's example, ABS, was

the second system where the electronics were introduced after the engine control units. ABS detects if one or more wheels are about to lock up under braking and if this happens, it makes sure that the brake pressure remains constant or is reduced. By doing so, it prevents the wheels from locking up and the vehicle remains steerable. As a consequence, the vehicle can be braked or stopped quickly and safely. More detailed information about ABS is given in chapter 6. The next system, TCS (Traction Control System) provides a logical extension of ABS during acceleration. The anti-lock braking system prevents the wheels from locking up when the brakes are applied by lowering the wheel brake pressure. The TCS prevents the wheels from spinning by reducing the drive torque at each driven wheel. In addition to this safety-relevant task of ensuring the stability and steerability of the vehicle when accelerating, TCS also improves the traction of the vehicle by regulating the optimum slip. The ESP (Electronic Stability Program) integrates functionalities of ABS and TCS and it is designed to improve driveability through a programmed intervention in the brake system and/or drivetrain. The general role of the system is to prevent the vehicle's tendency to become unstable (oversteered or understeered) in such maneuvers as rapid steering and counter-steering during cornering, lane change with emergency braking or acceleration/deceleration during cornering. The complex algorithm strategies steer the vehicle by applying brake on selected wheels (selective braking) or accelerate the driven wheels. The input to the ESP systems consists of yaw-rate sensor, lateral acceleration sensor, steering-wheel angle sensor, brake-pressure sensors and wheel speed sensors. Additionally the ESP/TCS/ABS ECU can implement automatic brake function such as HHC (Hill Hold Control) which prevents the vehicle rolling backwards when pulling away on a hill, HDC (Hill Descent Control) which assist the driver in braking when driving downhill on a steep terrain.

The next large active safety systems group utilizes the recently adopted sensors in auto industry such as cameras, long range and middle range radars and LiDARs. The complex tracking and recognition algorithms using data from one or more mentioned sensors (sensor data fusion) are able to provide the exact information of the position and velocity of other objects on the road. Moreover, it is possible to determine if a particular object is a car, truck or a pedestrian as well as recognize traffic signs. This highly valuable knowledge enables implementation of more effective solutions in crash preventing areas such as:

- AEB (Autonomous Emergency Braking) - a feature responsible for warning or providing brake support (or fully auto-brake) if the system detects unavoidable collision with an object in the front of the vehicle.
- FCW (Forward Collision Warning) - warns the driver in the event of an imminent collision.
- LDW (Lane Departure Warning) and LKA (Lane Keep Assist/Aid) - these features provide assistance in the case when the vehicle begins to move out of its lane and no turn indicators are

activated. The LDW warns the driver about the detection of such situation and the LKA helps the vehicle stay in the lane by applying counter-steering force to the steering wheel

- CSW (Curve Speed Warning) - this feature identifies potentially dangerous situations when the speed of a vehicle is too high to take a curve and alerts the driver.
- BLIS (Blind Spot Information System) - a feature responsible for monitoring the blind spots and warning the driver if lane change intention is detected.

The number of active safety systems installed in modern premium-class vehicles has been rapidly growing in the recent years and additional systems such as driver drowsiness detection and driver monitoring system, intersection assistant, turning assistant or lane change assistant will become standard in more and more new vehicles due to either legislation or market competition. For example, starting from 2014 the TPMS (Tire Pressure Monitoring System) has to be installed by a manufacturer in all new passenger cars in EU although it was introduced in 1980's and adopted as standard in high volume model Laguna II as early as in 2000.

1.2.4. Comfort and convenience systems

The number of comfort and convenience systems highly depends on vehicle class and manufacturer. Basic functions such as power windows and power sunroof or seat and steering column adjustment are now present in every mid-class vehicle model. Also, the central locking system and remote keyless entry and vehicle immobilization solutions are installed as standard in many modern models. Nowadays a similar trend can be observed in an area of electronically controlled heating, ventilation and air conditioning systems or even Cruise Control and PAS (Power-Assisted Steering). There are, however, more complex solutions in this domain that, among other factors, incorporate additional sensors and are offered only in premium and luxury models or as an option in mid-class vehicles. The example of such systems are active and semi-active suspension systems together with vision-based road conditions detection. Suspension systems are characterized in chapter 4.

The parking aid or parking assistant systems make use of ultrasonic sensors, short range radars or cameras (depending on the option) to effectively support the driver when parking. The ECU of the systems monitors the vehicle surroundings and detects obstacles behind, in front or even all-around the vehicle, and reports this information visually in the cluster display or by acoustic signals. The extended version also measures parallel parking space or even, in the case of automatic parking systems, autonomously parks the vehicle using X-by-wire technology.

Another example of sophisticated comfort systems are the extensions of Cruise Control. The basic function of this common and standard system (especially in US) is to automatically keep the set velocity of the vehicle on the same level. This significantly simplifies the task of driving a car because the driver

does not need to use the acceleration pedal anymore. Although if the ego vehicle catches up with the vehicle in front that is going at a slower speed, or the vehicle in front decreases its speed (for example when exiting the highway), the driver must manually brake and set the speed once again after overtaking. The next generation of this system, ACC (Adaptive Cruise Control), relieves the driver of demanding monitoring of the preceding vehicle incorporating the long range radar or/and camera to track the vehicle travelling in front (target). Using the measured speed of the preceding vehicle, the ACC ECU algorithms adjust the velocity (by braking or accelerating) in order to follow the target even if the set speed is higher. In the case when the target leaves the ego lane, the set speed is obtained again. In most cases the ACC can be turned on while driving more than 40-50 km per hour. Currently, car makers also extend the ACC by adding information about speed limits acquired from either navigation maps or camera TSR (Traffic Sign Recognition) systems which is also considered during the velocity adjustment (ICC - Intelligent Cruise Control). There are also options which work in the lower speed range including full stop (QA - Queue Assist) which is a typical situation for a traffic jam.

The vehicle adaptive and intelligent dynamic lighting control systems comprises another prominent group in this area. The simplest system in this group is an automatic headlamp-leveling control system which adjusts the tilt angle of the low beam to the tilt angle of the vehicle body. This dynamic behavior results in a permanently good visual range with no dazzling of oncoming traffic under all load conditions. The ALS (Adaptive Lightening System) provides such features as cornering lights and adaptive rear lighting system. The first one improves the light pattern of the vehicle while turning by switching supplementary reflectors pivoted laterally based on vehicle speed and steering angle. The rear lighting system is used to determine environmental parameters and conditions (brightness, dirt, visual range) and for example to adjust the stop light luminous intensity up in high sunlight, and down at night. The most sophisticated control system for lighting is Auto High-Low Beam (AHLB) which utilizes a video camera to detect and classify vehicles on the road and intelligently turn on and off the high beam in order not to dazzle other drivers and maximize light pattern of the ego vehicle.

1.2.5. Communication and entertainment systems

The domain of communication and entertainment mostly includes non-critical vehicle electronic systems (GPS navigation, audio/video systems, hands-free calling, connectivity with smart-phones, etc.) except for such features as in-vehicle security or ACN (Automatic Collision Notification) system that automatically dial and inform emergency agencies in case of car crash or incident. The next cutting-edge technologies in these fields developed by researchers and OEMs are V2V and V2I communication. The V2V communication is an automatic communication system which enables the vehicles to exchange information with each other. The V2I communication allows vehicle to report relevant data to the

infrastructure. These two systems might be used in the future to implement more and more intelligent vehicles and provide additional source of information for autonomous vehicles. The increasing number of communication systems fitted in modern cars is raising the risk of cyber-attacks (e.g., hijacking). Thus the role of cyber-security systems is going to be significant in the near future.

2. Automotive systems design, development and testing

In each advanced engineering industry such as military, aerospace or automotive, the introduction of a new product requires considerable effort on the part of engineers involved in the project. Their cooperation and coordination of their work must be very well planned and managed during the entire product development lifecycle so that the goal put ahead of them can be reached. For instance, if a manufacturing company wants to productize a novel ABS controller, then except for the concept of unique control algorithm they must also design hardware (this includes the target microcontroller and vehicle bus communication components), and develop software architecture where this controller is executed. Such complex chain of work and operations needs proper methodology to ensure that the resulting device will behave and perform in a way that its concept assumed. The following chapter mainly focuses on software and hardware tools commonly applied during the development and testing of the controllers embedded software. It also includes the most important software development process methodology used in automotive industry, and basic software quality terms related to it. It must be remembered that the whole development process must not only consider driver comfort, safety, reliability and performance but also a tight hardware cost budget and constraints caused by existing functions, components, platforms, technologies and mechanical design.

2.1. V-Model as automotive systems development process

In automotive industry there are three main company types included during the ECU development process:

- The carmaker, also called car manufacturer or OEM (Original Equipment Manufacturer).
- ECU suppliers for OEMs, also called Tier I.
- Direct suppliers for Tier I companies, called Tier II.

Commonly, during the car development process, the OEM company (e.g., Volvo Car Corporation or General Motors) employs several Tier I suppliers which deliver their ECUs (e.g., ABS controller, ACC controller, ECM (Engine Control Module) controller) to be integrated into a car model. The ECU manufacturers, on the other hand, utilize components such as microcontrollers, sensors or software

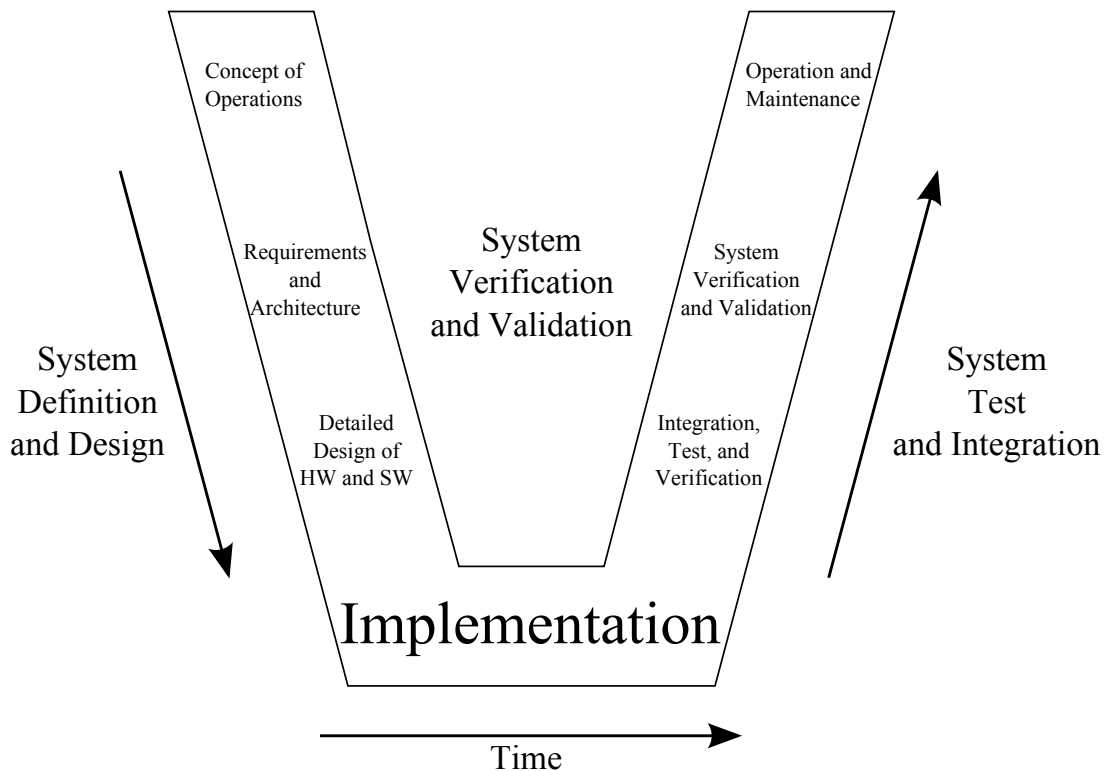


Figure 2.1: The automotive V-model diagram.

packages that come from several different Tier II suppliers. The resulting chain of supply, especially on the OEM and single ECU supplier level, requires effective methodology of cooperation. This guarantees successful integration of ECU delivery inside huge and highly distributed modern vehicle E/E systems. The majority of car makers require the suppliers to meet Automotive SPICE standard (Software Process Improvement and Capability dEtermination) [10]. It is a standard based on ISO/IEC 15504 referring to international automotive industry and it has been developed under the Automotive SPICE initiative by the consensus of several major car manufactures such as Audi, BMW, Ford, Fiat, Volkswagen and Volvo [11].

The common methodology of ECU development used by OEMs is the V-model systems engineering process. The V-model diagram is depicted in Figure 2.1. This process defines and characterizes several development steps that summarize the development of the embedded automotive control system. These steps include software and hardware design, implementation and testing.

First, the system requirements are gathered, analyzed and system specification on the functional system architecture level is prepared. This process strictly relies on tight cooperation between the ECU supplier and carmaker(s). The mentioned activities are performed by system engineers who gather concrete requirements from stakeholders (mainly from car manufacturers), and perform their functional analysis which results in a documentation of functions the system should be able to perform and a specification of how well these functions should be performed [12]. It is very important that such

requirements are achievable, verifiable, consistent and complete due to the fact that the outcome will be utilized as input for subsequent work of software and hardware engineers. To achieve this quality of requirements a system engineer needs to cooperate with persons who possess other competencies (e.g., software architects, hardware engineers) and needs to fully understand the system behavior and its capabilities. The result of the described work is a formal requirements specification document or a list of documents. This documentation is then systematically evaluated and reviewed during the V-cycle development steps. Since process standards used in the automotive industry require traceability, requirements management IT (Information Technology) tools are used to support that. Typically such tools hold information in the database system which allows the system engineer to link specific requirements to other documents (e.g., Software Architecture Design document), and to define the attributes of this requirement, for example by specifying if it is meant to be fulfilled by hardware or software competency. Tools that are commonly used here are IBM Rational DOORS [13] and Dassault Systèmes CATIA REQTIFY [14].

The next phase of the ECU development process is the System Architecture and Design step. Using the created requirements documentation as the basis, the hardware and software architects prepare logical and technical system architecture. The hardware part of the system is designed by choosing the microprocessor(s), actuators, sensors and bus systems. Software engineers plan the software architecture which includes selecting ECU software components and modules, their functionality, connections and interfaces. In this design process, the engineers distribute functions among specific hardware and software components. These activities usually constitute high level system architecture documentation which serves as an initial point for detailed/low level software and hardware design. The design of ECU hardware comprises of selecting the electronic components, PCB layout and the specification of placement of the input and output interfaces. Concurrently, the software architects/engineers design the application software for interfaces of sub-systems or components that resulted from splitting the overall software into modules, interfaces and specific software components alignment (e.g., control algorithms or device drivers). The detailed software/hardware architecture documents will later serve as specification (delivered in the form of text or graphical flowcharts) for appropriate competencies in the step where components and sub-systems development is performed.

The most bottom part of the V-model is the components implementation. During this phase, the hardware engineers prepare PCB layouts and produce the first sample units while control algorithms engineers and software engineers develop the required software components. When hardware design and development is finished, the embedded software can be deployed into a hardware unit, and the component unit testing can be started. Software development and testing is described in details in the next sections.

After component (ECU) unit tests finish, the system integration tests and validation are performed. In

the context of ECU development process, the system integration tests constitute verification of whether the unit works as expected when it is a part of the entire distributed vehicle system. The suppliers are first to conduct this kind of tests. In order to check the ECU behavior in realistic environment it is necessary to simulate other ECUs which interact with the ECU that is being tested. Generally, car suppliers do not have sufficient information about other ECUs in the vehicle communication network. Carmakers deliver a list of signals and messages which are relevant to the ECU under test, and using only these specifications the interactions with other ECUs can be simulated. If the unit passes the required tests, it is delivered to the car manufacturer who performs their own sub-system integration tests of the ECU. Next, the carmaker conducts a complete vehicle integration where all of the vehicle E/E components are connected (including the ECU delivered by other suppliers). This process is generally divided into two phases. First, the stationary lab-car integration is performed, where all non-driving functions and features are evaluated. Afterwards, the dynamic lab-car tests are conducted which basically means real test drives with complete vehicle E/E system present [12]. It is worth to mention that a novel process called Virtual Integration is getting more attention and a number of car suppliers attempt to use it on large scale in the future. The main goal of the new methodology is to perform integration of the system ECUs and sub-systems much earlier in the design cycle using virtual prototyping and simulations [15, 16]. The advantage of such solution is to reduce the cost of development and to identify faults or incompatibilities at the early development stage.

2.2. MBD of embedded real-time control algorithms and software

The embedded software of the ECU, typically containing supplier's proprietary control or advanced perception algorithms make up the essential part and the most significant work product delivered to the customer. The quality, reliability and available functionality, all play a key role in the decision made by a carmaker when choosing the appropriate supplier. On the other hand, the implementation and testing of the automotive software systems is the most time consuming and expensive phase of the development process. Therefore delivering a ready product to the market in a short time becomes the most challenging task. Apart from research on complex control strategies or sensing approaches, the resulting implementation, usually in a form of C-code, must be integrated into basic software components (drivers, operating systems, etc.). Altogether they constitute the ECU software which must fulfil automotive industry domain standards. The most important software standards are:

- IEC 61508 [17],
- ISO 26262 [18],
- MISRA (The Motor Industry Software Reliability Association) C [19].

The first two standards refer to Functional Safety which is nowadays getting more and more attention due to systems such as ADAS and AS. The last standard defines the guidelines for C-code implementation. The main goal for complying to these standards is to produce safe, reliable and faultless software. Additionally many suppliers build their software using AUTOSAR (AUTomotive Open System ARchitecture) [20] framework which, among other benefits, makes the software components reusable in other products. AUTOSAR is an open and standardized automotive software architecture developed by key players in automotive industry in order to establish common standards for the automotive E/E architecture. It is composed of three layers: Basic SW (e.g., drivers), RTE (Runtime Environment) and Application. The RTE layer (abstract middleware) serves as communication exchange channel between SWC (Software Components) implemented in Application layer (e.g., control algorithms) and between Basic SW. The other advantages of using common software reference architecture are reduced development costs and time-to-market [21] thus AUTOSAR has become a state-of-art for automotive electronics.

In order to tackle the concerns described above, the ECU suppliers started to use model based approaches in the context of system engineering, development and testing. Naturally the models are an essential part of the design, analysis and tuning methodology for algorithms and control design. Apart from formal, mathematical or analytical models, the automotive industry also recognizes conceptual and constructive models. In the context of automotive systems, the MBD (Model Based Design/Development) is often interpreted as computerized models family used to support communication, documentation, analysis and synthesis [22]. This method is established as a common framework for the whole design and development process for the entire automotive V-model. The next paragraphs of this section will shortly describe key approaches extensively applied during automotive embedded systems development.

Functional modeling of the system in terms of the entire system architecture and its software components architectures, functionalities and customer requirements is called Model Based System Engineering (MBSE) and Model Based Requirements Engineering (MBRE). Using these techniques, systems engineers utilize models to capture and elicit customer requirements for product functionalities. MBSE and MBRE were originally based on UML [23] and SysML [24] but are now starting to use physical models (also referred to as behavioral or abstract models) to illustrate and describe requirements, to communicate ideas and designs with clients, and to document and manage the designs. In conjunction with written documents, these types of models serve as virtual product description and basis for product realization.

In the domain of control systems development, the MBD is the standard approach in automotive industry when it comes to advanced algorithms concept design and prototyping. In this case the

models of the developed controllers and of the simulated surrounding environment are used during implementation. Algorithm developer begins the development process using the technique called MiL (Model-in-the-Loop) simulation. Various modeling frameworks are used during this phase (see section 2.3.1) in order to obtain the stage of the system model which works according to the requirements. The mathematical and logical model behavior is tested using virtual input vectors generated by the simulation environment. This approach for algorithms verification does not take into account real-time operations or any future embedded target constraints, although it enables the initial calibration and performance assessment in the early stage of the development [25].

As soon as the functional model is finished, it can be implemented. Typically this process is partially auto-generated and partially hand-written, although it is becoming more and more popular to use fully auto-generated code especially during RP (Rapid Prototyping) (see section 2.3.2). Such compiled code is used in SiL (Software-in-the-Loop) simulation concept where the developers still use artificial input data that comes from the simulation environment. At this point the algorithms in binary form can be analyzed in terms of the following: their complexity, the impact of the fixed-point signal representation, or other constraints introduced by the implementation code language (the resulting C-code implementation of the model might prove inefficient or even unreliable). It is worth mentioning that SiL component (software representation of the model) can be verified by previously generated test vectors and reference signals. This technique is called MBT (Model Based Testing) [26, 27].

The next phase of simulation and testing is done using PiL (Processor-in-the-Loop) concept. On the MiL and SiL level, the verification of the control algorithms is typically done on a Windows based PC (x86/x64 based architecture). In the course of PiL step, the embedded target processor execution of code is applied. This permits the assessment of the real-time implementation performance, throughput and execution time (efficiency). We can either emulate the embedded target or apply the evaluation board in which case a partially employed physical signals can be used instead of virtual interface.

When ECU hardware components are finalized, the algorithm code is integrated into the basic software of the component system. This phase of development is called HiL (Hardware-in-the-Loop) simulation testing [28]. The simulation environment is still applied in order to provide input signals into ECU. However the data is now transmitted via communication channels, analog or digital physical interfaces. The functionality of the ECU can now be verified and validated since the hardware and software implementation is in the final production form. This step is used to check the entire software behavior after the integration of algorithms and basic components (device drivers, network controllers, etc.) which are typically implemented either by supplier developers teams (often distributed around the world) and/or by customers themselves. Finally, the ECU is delivered to the customer for integration and further tests described in the previous section. The entire chain of the MiL-SiL-PiL-HiL simulation

and testing requires dedicated and specialized hardware and software tools. These include modeling, simulation frameworks, virtual and rapid prototyping and instrumentation, network monitoring packages, etc. The next section covers the leading tools utilized during the development of automotive embedded systems.

2.3. Software and hardware tools

The presented design and development process of automotive electronics is long-term and complex, hence it requires SW and HW tools to support the entire life-cycle. The tool-sets might be divided into two groups: virtual and experimental. The first section 2.3.1 provides essential information regarding modeling and simulation environments utilized during prototyping and virtual testing. The remaining section 2.3.2 presents typically applied RP process and describes real-world tool-chains that are applied to test SW on the target HW platform.

2.3.1. Modeling and simulation software tools

The modeling and simulation CAE (Computer Aided Engineering) frameworks employed during the ECU software and control algorithms development can be divided into three main categories:

- physical
- mathematical
- system and functional.

However, these domains of software tools frequently overlap since producers of different platforms tend to integrate all applications inside their packages. All these products allow engineers to rapidly build, test, precalibrate and optimize solutions using high-fidelity models the simulation of which provides a broad knowledge on how they operate. The CAE tools also help to identify problems while still working at the computer and before going into the prototype stage, which minimizes cost and time of development. This process is often referred to as Virtual/Conceptual Design, Prototyping, Development and Testing.

The first category, the physical level simulation and model development, is dominated by three companies: Dassault Systèmes, Siemens and Maplesoft. Dassault Systèmes Dymola/CATIA VDL (Vehicle Dynamics Library) software library enables the simulation and modeling of complete wheeled vehicle systems and their related mechanical and control sub-systems in CATIA environment, which is the world leading solution for 3D mechanical design and simulation [29]. The VDL is based on Modelica [30], an open modeling language and includes basic models of engines, transmissions, drivelines, brakes, chassis, suspensions, wheels and tires. The predefined models can be rapidly coupled

and simulated under a variety of different conditions including segment-based road definitions with friction and unevenness, customized tracks and maneuvers. Additionally, 3D visualization of vehicle motion adds many more capabilities of analysis and evaluation. Similar possibilities of physical simulation of mechatronic systems is offered by LMS Imagine.Lab Amesim tool from Siemens. This platform can be utilized to model, simulate and analyze multi-domain, controlled systems and it offers extensive capabilities to control design and validation. The package also comes with a large set of physical libraries for automotive and ground vehicles (engines, electrical systems, transmission, vehicle system dynamics, etc.) [31]. The last supplier, Maplesoft, provides MapleSim, a multi-domain physical modeling and simulation software package equipped with dedicated high performance Vehicle Dynamics library based on powerful Maple math engine. The tool can derive mathematical models (e.g., equations of motion) from a graphically defined system [32]. Except for the above mentioned platforms, automotive industry also employs, among others, ITI SimulationX (physical simulation mainly for mechanics, hydraulics, pneumatics) [33] and MSC Software Adams/Car (suspension, steering, handling, vehicle dynamics, tires) [34].

Contrary to what was just discussed, the second domain implies mathematical modeling (a so-called signal-flow modeling) mainly based on logic or on ODE level instead of on physical relations and mechanic coupling of components. These software tools are mainly utilized during very early stage of development when working on algorithm concepts and their functional design. The most commonly used package is MathWorks MATLAB/Simulink/Stateflow. This well known package is extensively used in the automotive industry and in strictly academic/research areas [35]. The Mathworks MATLAB is an environment framework which allows the user to define, process, transform and plot signals using the simple scripting language and rich, out-of-the-box library of mathematical functions. Simulink and Stateflow which are both MATLAB extensions, constitute a graph filter based framework where signals and data flow are implemented by block diagram. Each block defines inputs signal transfer function which can be: differential equation dynamics, state machine, lookup tables, mathematical expression or PID controller. The diagram is simulated using variable or fixed step solvers in order to analyze the output. Additionally, a huge number of libraries is available all of which add ready to use blocks for Simulink models (examples are: Control System Toolbox, Model Predictive Control Toolbox, Fuzzy Logic Toolbox, Neural Network Toolbox). The second virtual design and development environment is NI (National Instruments) MATRIXx product family [36], a suite for advanced system design and control development. The core of the NI MATRIXx products is SystemBuild, a graphical framework for modeling and simulating complex dynamic systems. Similarly to MathWorks, NI provides integrated text-based script language (MathScript) and extensive library with functions for fuzzy logic design, neural network design and optimization control. The NI platform is equipped with AutoCode C tool

which allows automatic code and documentation generation from the models. The same functionality of generating the production code is also offered by Mathworks MATLAB Coder, Simulink Coder and Embedded Coder products. The first two toolboxes are mainly used to generate experimental code from either MATLAB m-scripts or models for concepts verifications, and the last one is intended for strict production code generation. Although one can find application of MATLAB Coder in production. For example, Delphi successfully utilized this SW package to design and develop a series radar sensor alignment algorithm for automotive active safety system [37]. The dSPACE TargetLink is the second choice for code generation from the Mathworks products family [38]. Nowadays such tools generate code that proves to be as efficient and high-quality as hand-written code in the context of memory consumption and execution time, and its form ensures readability and traceability. Furthermore, the production C-code generators commonly support AUTOSAR framework and are certified for standards such as IEC 61508, ISO 26262 and MISRA C. Typically, they also offer optimization of the ANSI C code for certain fixed or floating point embedded systems Microcontrollers (MCU) or Microprocessors (MPU) including units dedicated for automotive industry like ARM, Freescale, Infineon or Renesas.

It is common for car makers and ECU suppliers to extend simulation environment (especially Simulink) with libraries of mature, complex, realistic vehicles and vehicle surroundings dynamics models. Models implemented in physical modeling software such as MapleSim, SimulationX, Adams/Car, Dymola/CATIA or LMS Imagine.Lab Amesim can be co-simulated or even integrated into Simulink by FMI (Functional Mock-up Interface, a model exchange and co-simulation standard) [39]. Apart from the in-house developed packages, a number of companies offer extensive libraries of well designed, highly customized models fully dedicated to automotive industry simulation. TESIS DYNAware DYNA4 and enDYNA/veDYNA packages provide models for vehicle dynamics and drive train development, engine design and control, energy management and driver assistance systems [40]. In [41], researchers used this software in SiL and HiL testing of the semi-active suspension and Audi engineers use it during multi-ECU HiL tests for virtual characteristic rating of the Vehicle Dynamics Control Systems. Other libraries come from Mechanical Simulation Corporation. The CarSim/TruckSim/SuspensionSim [42] products are used to optimize the design of the General Motors track [43] and they are also utilized in the entire vehicle dynamics simulation in the world's largest driving simulators built by Toyota in order to conduct DiL (Driver-in-the-Loop) tests. Gamma Technologies GT-Suite/GT Power [44] provides precise engine dynamics simulation models especially needed during the ECM development and optimization. This suite helped Porsche engineers improve fuel consumption on highly charged gasoline engines by reducing the intake air temperature. The dSPACE ASM (Automotive Simulation Models) [45] models such as powertrain, electrical systems, vehicle dynamics, are used by Scania for complete truck electronics tests including 33 networked ECUs. The

co-simulation and mixed simulation of models with different levels of details is a high value added to control strategy tests.

Along with simulation models, the automotive industry now heavily uses 3D animations of vehicle motion and of its interactions with the environment. Such visualizations of virtual experiments help to understand and identify problems which may remain undiscovered during the rough data and signal plots analysis. Virtual drives significantly replace real test drives especially during ADAS, AS and IV (Intelligent Vehicles) systems development and testing. The most frequently used software packages are dSPACE MotionDESK [46], TESIS DYNAanimation [47], IPG Automotive CarMaker [48] and TNO PreScan/3DVisu [49]. In general, these products offer landscape generation including traffic signs, buildings, road modeling and programming of the behavior of ego vehicle along with the motion of other vehicles and pedestrians. The software from TESIS is used by Ford for HiL simulation testing of the camera based Lane Keeping System and by BMW for complete vision based driver assistance system which includes parking assistant, lane detection, traffic sign recognition and high-beam assistant. It allows the companies to check and investigate a broader range of road scenario variations than it would be possible during real road testing and it reduces the number of test drives during the development cycle (e.g. in [50] authors presented an approach for dynamic input generation for the development of AS perception algorithms).

The last modeling and simulation category, system and functional, particularly addresses software system prototyping and architecture design. These domain platforms make it possible for software and system engineers to build ECU software architecture (also AUTOSAR based), plan software components and their intercommunication interfaces. Additionally, they allow for integration of control functions models or control strategy C-code (auto-generated or hand-written), for modeling of logic modules using block diagrams, state machines, look-up tables and for simulation of the resulting complete ECU software in order to test and verify the entire software system operation. It is also common that they support automatic code generation which satisfies Functional Safety standards. The most popular platforms are:

- ETAS ASCET-MD (Modeling and Design) [51]
- dSPACE SystemDESK [52]
- ANSYS SCADE Suite [53].

In addition to the described modeling and simulation solutions, suppliers of automotive sensors and sensor-based control ECU also utilize re-simulation tools in the perception and steering algorithms development. This is done more frequently nowadays, since AS systems become more and more common. Such frameworks typically have the ability to use the previously recorded (logged) videos, radars, LiDARs and navigation data in order to reuse the real vehicle environment horizon and e-horizon

input to evaluate algorithms performance, visualize their output, and compare the results. Apart from the in-house developed tools [54], these types of platforms are offered by Elektrobit Assist ADF [55] or Vector vADASdeveloper [56] with BASELABS products family [57] for data fusion and target tracking algorithms development.

2.3.2. RCP and HiL simulation testing software and hardware tools

The RCP (Rapid Control Prototyping) is the process of calibrating control algorithms on prototype hardware to get a tested device up and running before a production-intent electronic control unit (ECU) is available. RCP platforms typically provide a method to import mathematical models and run them on a controller with a real-time OS connected to a real-world I/O. This process is often designed in such a way that manual coding and programming is reduced to an absolute minimum. Usually the models of control algorithms (controllers) are automatically deployed on dedicated multi-purpose real-time hardware platforms using specialized software suites and automatic code generators. The programmed hardware platform that imitates ECU functionality is connected to the required A/D signals and vehicle communication buses (CAN, Ethernet, FlexRay). In a similar way to MiL development, the signals and communication data is often generated by simulation environments. The RBS (Rest Bus Simulation) simulates messages from (partly) non existing control units in the network. This allows to test ECU without building up the complete vehicle bus. In order to transfer artificial data (messages) from a PC based computer to the algorithms running on an RCP platform, the specialized hardware bus interfaces are applied. The most widely used restbus simulation platforms are CANoe from Vector Informatik GmbH [58], EB tresos Busmirror from Elektrobit [59] and INCA software products family from ETAS [60]. All these products offer similar capabilities which are network cluster emulation, ECUs simulation and stimulation, signals and data measurement and analysis, and diagnosis. The solutions come with dedicated hardware interfaces [61, 62, 63] for in-car (on-board) and desktop use.

The most commonly used suppliers of RCP solutions are dSPACE, ETAS and NI. The dSPACE MicroAutoBox II [64] is a compact and robust prototyping system for in-vehicle applications, which enables direct upload of the MATLAB Simulink/Stateflow models. Additionally, execution of the models can be traced and debugged together with data visualization of algorithms input/output on ControlDESK [65] package instruments. The dSPACE software is the most mature product in the context of HiL simulation testing. It has been used in automotive industry since the late 90s, for example by Jaguar for body control system and driver's door module [66], and by Mercedes-Benz for ECS [67].

The ETAS scalable RCP ES900 modules [68] with prototyping software tools INTECRIO and ASCET-RP [69] deliver more capabilities than dSPACE solutions. The user can integrate functions in the form of generic C code, MATLAB/Simulink/Stateflow or ASCET models, or AUTOSAR compliant

software modules and test the control algorithms on the prototype hardware under real-life ambient conditions. The ETAS RP solutions are used by Advanced Engineering department in DENSO during heavy-duty diesel engines soot particulates and nitrogen emissions optimization, and at Daimler AG for testing and validating newly introduced two-stage turbocharger engine management functions directly in the vehicle. The ETAS Group also provides high-end modular HiL solution, LABCAR [70] utilized for example by Robert Bosch GmbH as a real-time model simulation environment.

Based on RT-LAB [71] and other off-the-shelf software and hardware components, RT-LAB Rapid Prototyping Controller [72] is a modular rapid prototyping system for control algorithm development using MATLAB/Simulink and MATRIXx/SystemBuild with powerful data acquisition support, a parameter editor, and a flexible user interface package. This software was successfully used in [73] during real-time validation of the electric power steering (EPS) control and drive control for a switch reluctance motor (SRM) powered by a fuel cell.

Contrary to the previously mentioned platforms, the NI company provides CompactRIO boards [74] as their own RPC solution connected to LabVIEW environment. Ford used this RCP platform to develop embedded control system for fuel cell electric (FCS) vehicle. The NI company is well known as HiL simulation testing systems supplier (PXI Platform [75]) which is utilized by carmakers such as Subaru for the electric motor ECU verification.

Researchers often develop their own specialized, low-cost RCP and HiL environments in order to test novel control strategies. In [76] one might find the dedicated real-time HiL simulator used for the assessment of ACC embedded system.

3. Real-time control systems

In the modern world the vast majority of automatic real-time control systems are digital systems and often distributed systems. The application of analogue techniques for control or steering purpose is minor due to the fact that DCS (Digitally Controlled Systems) are generally less expensive, faster, flexible and easily reconfigurable thus their development and production is more efficient. In the past DCS were present exclusively in the aerospace, defense and military domain. Recently, most of the devices utilized in industrial automation, medical instrumentation, automotive, home-appliance and telecommunication are based on embedded digital controllers. The introduction of discrete and digital signal processing imposes a number of obstructions and challenges especially in dynamic systems control loops. The designers of the algorithms need to consider all the added constraints upon control law development in order to guarantee that the control strategy is realizable in real-time by the dedicated embedded target. Otherwise, the most sophisticated and efficient control algorithm might prove as inoperable and its application, apart from the modeling purpose, could be impossible.

This section provides insight into the current real-time control systems and their application in the auto industry. In section 3.1 an introduction to the real-time digital signals processing and computing is presented. In the next section 3.2 the real-time systems, real-time operating systems and the utilized programming languages are presented. The section 3.3 is devoted to the real-time control and its application to automotive E/E systems. Finally, section 3.4 introduces INTECO's laboratory setups, considered as rapid control prototyping platforms for the research of real-time control algorithms.

3.1. Real-time digital signals processing and computing

In the real-world applications, most of the encountered and utilized signals are analog in nature. Analog signals such as voltage, current or temperature belong to continuous-time signal category and their processing might be conducted with the usage of specialized analog processing system in form of analog electronic, hydraulic or mechanical systems. This approach was applied in the beginning of the engineering and due to its reactive and physical nature is in general considered as real-time. Even today there still exist domains where analog signal processing is the only solution especially in the case of

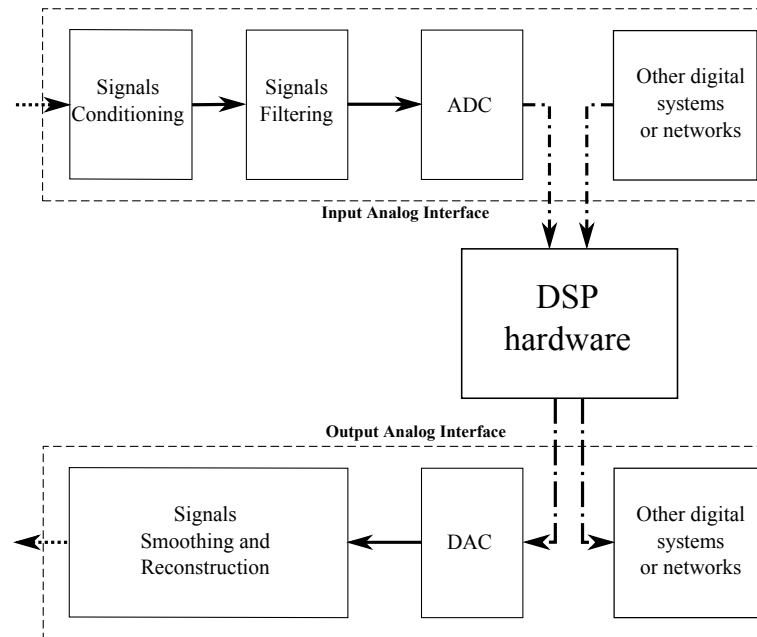


Figure 3.1: Basic functional block diagram of a real-time DSP system.

signal with extremely wide bandwidth [77].

Rapid development of digital computer technology during the so called Digital Revolution brought digital signal processing (DSP) discipline into science and engineering, and replaced analog signal processing in the majority of applications. Initially the application of computers was only off-line (non-real-time), for example, extraction of information or analysis of the recorded data. The following advances in digital integrated circuits, processors and peripheral hardware resulted in cheaper, reliable and smaller devices with the potential to replace classical analog processing systems. Today, the vast majority of real-time systems are digital therefore all computations and data processing, including control, is performed with the use of digital discrete-time signals.

The DSP systems have many advantages over analog processing systems such as [78]:

- flexibility,
- reproducibility,
- reliability,
- complexity.

Flexibility means an ability to reconfigure the digital programmable system (e.g., program upgrade) in the field. Generally, such operation is not feasible for an analog counter-part where analog system hardware must be redesigned. Other attributes are related to the ability of the system to produce the same outputs among units (reproducibility) and during the entire unit life-cycle (reliability). In the recent years the digital electronic components and systems overcame analog-circuits in durability and repeatability. Moreover, digital hardware is cheaper. The last and the most important feature is complexity. Nowadays

only DSP systems are capable of executing a number of sophisticated processing flows, algorithms or computations, the results of which are more precise.

Recently, apart from the mentioned non-real-time application, the typical real-time DSP system consists of several fundamental elements depicted in Figure 3.1. The core block of the system is DSP hardware. This component performs operations on the provided signals which are already digital. The source of the digital signals is either input analog interface or another digital system or communication network. The output of the processing is either transmitted to the connected digital systems or it is converted to an analog form by an output analog interface. However, there are systems where an output of the processing is not forwarded, and the results may be saved on the DSP unit for further analysis or displayed via graphical interface.

The DSP device is capable of handling only the digital signals either in software or in hardware. Software operations on the signals are also referred as programs or algorithms and are realized by a sequence of mathematical or logical commands. The other way to process digital signals is to use specialized logic circuits (configured digital hardware). As a matter of fact, current state-of-market is to combine these two techniques, the result of which is a so-called hybrid DSP system. The main aim of such mixing is that some of the DSP operations and computations are executed faster on a specific DSP platform or its implementation is easier and cheaper. Nowadays the most widely utilized DSP systems are:

- microcontrollers and microprocessors,
- specialized or general-purpose DSP processors,
- FPGAs (Field Programmable Gate Arrays),
- ASICs (Application Specific Integrated Circuits).

The comparison between DSP hardware configurations can be found in [78]. In the subsequent section the software based RTS are briefly introduced.

The surrounding input and output analog interfaces allow interaction with a DSP system. The input analog interface performs operations of converting an analog real-world signal to digital form suitable for further processing by DSP hardware. The source of input to the input analog interface constitutes a specialized sensor which converts physical signal such as temperature, pressure or force into electrical voltage signal. In the most cases the output of the sensor needs conditioning before it is utilized. Signal conditioning includes amplification of the voltage to the required order or shifting its level. Next, the resulting signal is often processed by filters such as anti-aliasing filters or low-pass filters. Once the noise is filtered out, the signal is ready to be converted into digital form by analog-to-digital converter (ADC). Such a conversion, called digitization, is composed of two operations: sampling and quantization. The sampled and quantized digital values are encoded and transmitted by serial or parallel communication

bus to the DSP hardware.

The results of DSP hardware operations are often utilized to control or steer certain plants or processes with the actuators commonly excited by analog voltage or current signals. Since the DSP devices provide digital signals, a conversion to analog signal is required. This is performed by a digital-to-analog converter (DAC). The smoothing filter is often applied afterwards and finally the signal is applied on actuator.

One can note that the analog interface introduces interference in the assumed feedback control loop. Primarily, even without considering the actual DSP hardware execution time, the filtering and signals pre-processing adds delays. Secondly, A/D and D/A conversions generate distortions in the signals values. Therefore, all the mentioned effects in the most cases do not harm the control or processing system performance and are rather omitted during the analysis. The largest influence on the system efficiency and speed has the DSP hardware and its SW components.

3.2. Real-time systems, operating systems and programming languages

The extensive literature provides a multiple number of formal and informal definitions of real-time systems (RTS). Basic definition (IEEE/ANSI) defines the RTS as a device or computer where the calculations are executed concurrently with the external process in order to control, supervise and react to events occurring in the process. Another one, introduced in [79], says that RTS is one of those systems in which the correctness of the system depends not only on the logical result of computation, but also on the time at which the results are produced. Therefore, the real-time control system calculation results must be delivered and applied to external process or controlled plant just on time which means not too late and not too early. The certain time instant when a computation result is expected is called deadline. Typically, a real-time system handles two types of events: periodic and aperiodic. The time-bounds of the cyclic tasks differ depending on the system application and it might be milliseconds (e.g., ABS) or hours (chemical industry) thus a real-time not necessarily needs to be fast although the temporal constraints need to be meet. If the time limit is exceeded then a system might malfunction or its performance might be deteriorated. Depending on how much the deadline is missed, real-time systems are classified as soft, firm and hard. The soft real-time systems are non critical systems where occasionally missed deadline would not cause dramatic impact on the system. The second class also permits rare deadline missing although it needs to follow a certain predefined pattern. In general, the hard real-time systems are critical and no deadline missing is tolerated since it might harm human life or destroy the system and the environment. Therefore, RTS is supposed to be:

- continuous in execution,
- dependent on process,
- concurrent with process,
- predictable,
- precise,
- punctual.

The application of RTS is nowadays wide range and includes such disciplines as real-time artificial intelligence or real-time databases although the real-time control is the most important appliance where such a system (often embedded system) is in the feedback loop of control system. Every embedded digital real-time system needs to be equipped with specialized SW called real-time operating system (RTOS) which would act as a control and measurement environment (measure process signals, execute control algorithms and steer the actuators). Generally, for the control purpose, RTOS needs to punctually execute the control strategy algorithm in the sampling period events equally spaced in time, and simultaneously be able to respond to unpredictable events generated by the controlled process in alarm conditions [80]. Thus RTOS must implement key features and requirements which, among others, are:

- precise and predictable behavior (shall respond in the same time and in the same way to identical events),
- execution dispatching and scheduling (real-time clock, timers, multi-tasking, multi-threading, thread prioritization and preemption),
- memory management and locking mechanisms (semaphores, critical sections handling, shared memory access and synchronization).

There are a number of commercially available embedded RTOS such as VxWorks [81], QNX [82], Nucleus [83] or OSE [84]. Apart from the proprietary solutions one can find Unix or Linux based RTOS distributions and other open-source counterparts (e.g., FreeRTOS [85]). Additionally, the commonly utilized general purpose (non real-time) operating systems such as Windows and Linux may be extended to provide required soft real-time functionalities [86]. Even mobile devices OSs such as Android are successfully applied for real-time control in the research area [87]. The embedded real-time system society defined a number of comprehensive benchmarks for RTOS performance assessment (e.g., RheaStone or MiBench metrics [88]). In the area of feedback control applications, RTOS timing jitter and its impact on control effectiveness and stability still require extensive analysis. The above mentioned delay related to analog interface or the communication in the distributed systems is usually constant (or the worst case scenario delay value is known) although the computation-time delay introduced by DSP system is a random variable. It consists of actual control code execution time and an extra time required by RTOS itself to trigger and execute a control task. It is highly recommended to address the control

algorithm ability to work in real-time during the design phase in order to avoid such a case where control strategy is too time consuming or it does not fulfill performance requirements due to encountered delays.

RTOS serves as environment where the control strategy is executed. The control algorithm needs to be implemented in one of the main real-time programming languages such as C, C++, Ada or RT Java. The most important characteristics of appropriate programming language for real-time application are predictability, portability, flexibility, abstraction and resources handling [89]. At the early algorithm development stage it is more feasible to design the control laws in the high-level languages such as MATLAB/Simulink/Stateflow using desktop workstation running general-purpose OS. Hence, it is common to model the control algorithms and use specialized software to generate real-time programming language code and deploy it the target real-time system (see section 2.3.1). There are also solutions to run the generated code right away on the PC based machine.

The number of areas of RTS application is still growing and nowadays we can find it, among others, in:

- telecommunication (video and audio broadcasting, cellular networking, Internet),
- transportation (on-board control systems for trains and air-crafts, traffic control systems),
- industrial automation (assembly lines, process control),
- medical equipment,
- aerospace (satellites control and tracking, manned and unmanned space mission control),
- defense (missiles / anti-missiles systems, targets tracking).

3.3. Real-time control in automotive E/E systems

The majority of automotive E/E systems described earlier in this chapter require high reliability and have elevated safety requirements. Moreover, a strict and hard real-time property is often required. Illustrative examples of hard real-time systems are found in most of the domains including engine management, powertrain, drivetrain, safety and even comfort and convenience systems. Recent developments towards Connected Cars approach would require a huge adaption effort also in communication and entertainment systems.

A good example of hard real-time automotive system is an air-bag control system. Here, when the monitoring sensor system detects an impact collision the ignition of gas must be triggered within 10 ms to 20 ms. Otherwise, the system might harm the occupant's face and the not properly inflated bag might not absorb a hit.

Another example is an engine management system responsible for spark timing, throttle control and fuel injection. Contrary to the air-bag case, this system requires perfect scheduling of each engine rotation

cycle (e.g., fuel injection processing must be finished before ignition timing is scheduled) and precise timing of the ignition (microseconds).

ABS system is also considered as safety-critical due to its high influence on the vehicle motion. Despite its primary function as skid protection, the system must monitor sensor errors and other meaningful faults. The fail-safe operation must be designed to prevent situations when the driver is not able to apply brakes. Similar approaches must be present for almost all AS and ADAS systems.

All of the above examples show that the entire automotive E/E system is a complex, distributed and embedded real-time system where multiple embedded real-time sub-systems highly depend on each other. A single delay in the calculation in one sub-system or communication delay in the vehicle network might result in severe error in a dependent component.

3.4. INTECO's SAS and ABS laboratory setups

In order to apply and test real-time control algorithms, the modeled system is not sufficient. One can find examples of implemented control strategies using only the model which is not realizable. The verification of the control shall be conducted on the experimental bench. The laboratory setups, manufactured by INTECO company, were selected and utilized during the research. The main reasons for selecting these setups was ease of implementation and of application of the real-time control algorithms, and free access to the measurements and to the control signals. The first one, SAS, mimics quarter car suspension part with controlled semiactive damper. The second one is the commonly known ABS device. From mechanical point of view the setups differ, although the control and measurement part is common for both of the devices - the input and output signals structure is the same. The devices are controlled with PWM (Pulse Width Modulation) signals and incremental encoders output is measured. The shared setup elements are covered in the next section and each device specific and detailed information are covered in the following chapters: SAS in chapter 5 and ABS in chapter 7. The second part of this section presents how MBD methodology and MiL, SiL and HiL approaches are applied to INTECO company hardware and software for real-time control algorithms development.

3.4.1. Laboratory setup's overview

Overview of the laboratory setups is shown in Figure 3.2. In general, the devices are controlled from PC running MATLAB/Simulink environment through specialized control and data acquisition board connected via USB 2.0 interface. The RT-DAC/USB2 I/O board measures incremental encoders signals and generates PWM control signals applied by power unit to the actuators of the devices.

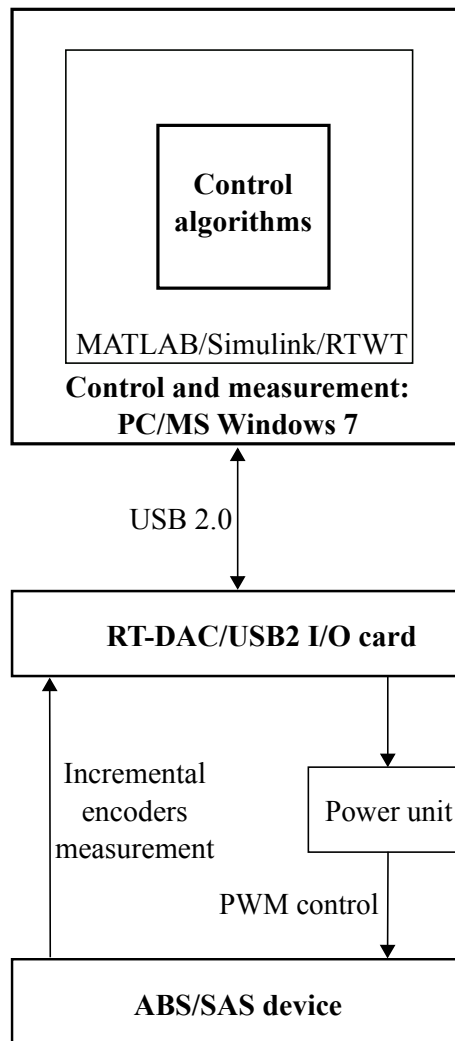


Figure 3.2: General overview of laboratory setups.

3.4.2. RT-DAC/USB2 I/O card

The RT-DAC/USB2 is a multifunction analog and digital I/O board. The device is presented in Figure 3.3. The board enables real-time data acquisition and control in the Microsoft Windows family operating systems environment. The block diagram of the RT-DAC/USB2 card is shown in Figure 3.4. The main element of the board is the Xilinx FPGA chip which processes signals incoming from several sources of information [90]:

- up to 26 digital inputs using LVTTTL standard (output current up 2 mA per channel),
- up to 16 analog inputs with 12 bit resolution (5 mV) and range -10 V to 10 V with programmable gain,
- up 2 channels for high-speed 32 bit timer/counter,
- up 4 channels for incremental encoders.

The card can control the following output signals:



Figure 3.3: The picture of the RT-DAC/USB2 I/O board.

- up to 26 digital outputs using LVTTTL standard,
- up to 4 analog channels with 12 or 14 bit resolution, output range -10 V to 10 V or -5 V to 5 V with $10\text{ }\mu\text{s}$ settling time,
- up to 4 PWM channels with 8 or 12 bit resolution.

The processing unit is communicating with the supervisor environment via USB 2.0 bus. The version of the card utilized to control the mechatronic ABS and SAS devices is the digital only variant RT-DAC/USB2-D version, the detailed specification of which can be found in [90]. The processes in the investigated devices are fast and require very fast controller response. The dedicated FPGA logic performs all time-critical tasks and the connected master PC computer selects the parameters of output signals and acquires real-time data and presents the experimental results. The default configuration of the FPGA chip logic is adapted, although the logic can be reloaded by the user to implement customer specific features like [91]:

- fast, hardware or software triggered, analog or digital data acquisition into the internal buffers,
- hardware-implemented analog signal generation,
- hardware-implemented digital filters of the analog signals,
- hardware-implemented FFT (Fast Fourier Transform).

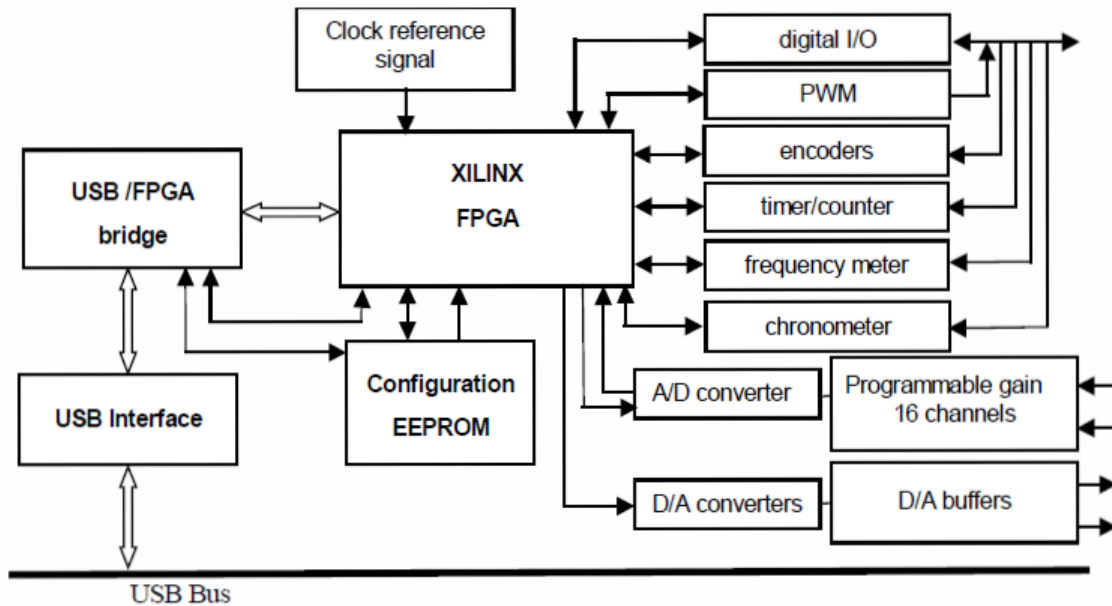


Figure 3.4: The block diagram of the RT-DAC/USB2 I/O board. Source: [90].

3.4.3. PC based real-time control and measurement environment

The discussed RT-DAC/USB2 board can be controlled by real-time applications running on Windows operating systems such as MATLAB/Simulink/Stateflow, LabView or industrial monitoring and control packages (SCADA programs e.g., iFIX or InTouch). In the conducted research activities regarding real-time control, the connection to MATLAB/Simulink is used. In this configuration the PC machine running MS Windows OS and MATLAB/Simulink application and FPGA chip located on the RT-DAC/USB2 board constitute a hybrid HW and SW DSP unit (according to Figure 3.1). The remaining peripherals (see Figure 3.4) are jointly described as Input and Output Analog Interface. Additionally, the system might be considered as distributed DSP system since the communication between FPGA chip and MATLAB/Simulink running on MS Windows OS is realized through USB connection.

The main data processing and calculations (control algorithms) are conducted on MS Windows OS where the MATLAB/Simulink application is executed. The card comes with dedicated software and driver package. Among others, it includes the C language procedures, MATLAB/Simulink blocks and dedicated S-functions. The main software block is the RT-DAC/USB2 Device Driver which enables communication with the board via USB 2.0 by transferring and receiving data frames. This element together with control and measurement logic implemented in the Simulink model are compiled with RTWT (Real-Time Windows Target) toolbox. This solution gives an opportunity to prototype and test the controller for both ABS and SAS systems in real-time. The positions measured by encoders are calculated in FPGA unit. Afterwards they are sent to RT-DAC/USB2 Device Driver via USB and outputted as Simulink model signals. Next, the signals are utilized as feedback to the controller algorithm

code which computes the desired control on their basis. Eventually, the control signals are passed back to RT-DAC/USB2 Device Driver and are sent to the FPGA chip. The board logic accesses control information and handles the adjustment of current or voltage via the power unit actuator. The described pipeline of operations acts as a real-time control and measurement environment.

In order to conduct the above mentioned algorithmic operations in the real-time the MS Windows OS needs to be extended to soft real-time OS since it must respond punctually to equally spaced in time sampling period events. Due to the fact that generally MS Windows is not designed and built for real-time purposes its modification towards real-time regime is not trivial. The commercial and professional RTOS described in section 3.2 are expensive and do not fit into RCP methodology. For example, each time the control algorithm is modified the user needs to compile, integrate and re-flash (program) the specialized SoC (System on the Chip) where the RTOS is executed. Due to the fact that during research and so-called proof of concept development phase the control strategy changes are frequent the mentioned steps are time-consuming and uncomfortable. Another drawback is the debugging and testing capability. When the algorithm code is not executed in the development environment the dedicated tracers and debuggers needs to be utilized and such solution generally does not contain expanded GUIs (Graphical User Interface) which does not support data analysis and problem solving. From the algorithm developer standpoint it is better to work and debug using the well-known MS Windows environment where in general the simulation and results analysis is conducted.

The real-time extension utilized by INTECO RT-CON package relies on modification of MS Windows HAL (Hardware Abstraction Layer). This is accomplished by the preemption of interrupts and the injection of either small footprint RT kernel or RTOS [86]. The RT-CON engine and the software enabling soft RT execution of Simulink models and soft MS Windows RT capabilities is fully transparent for the user. Its engine makes use of MS Windows multimedia event timer. In [92] authors examine the jitter of the periodic tasks excited by several different types of MS Windows timers such as the mentioned multimedia timer or Windows message (WM) timer. The comparison results for 10 ms period are presented in Figure 3.5. One can note that for WM timer the mean value is over 15 ms (which is not accepted for control purposes), and the considered multimedia event timer mean result is correct. Despite the acceptable average mean value of the jitter for the timer utilized by RT-CON, one can note a large jitter that happens occasionally, although this operation satisfies soft RT requirements.

The application of RT-CON and MATLAB/Simulink results in an easy to use soft RT solution. Apart from RT capabilities, the presented environment supports RCP due to the fact that the C-code generated from the MATLAB/Simulink model using the RTWT toolbox is automatically compiled and linked to RT-CON and it is ready to be executed in RT in MS Windows. The entire MATLAB environment may be used to debug and observe the control signals directly during real-time experiments and the recorded

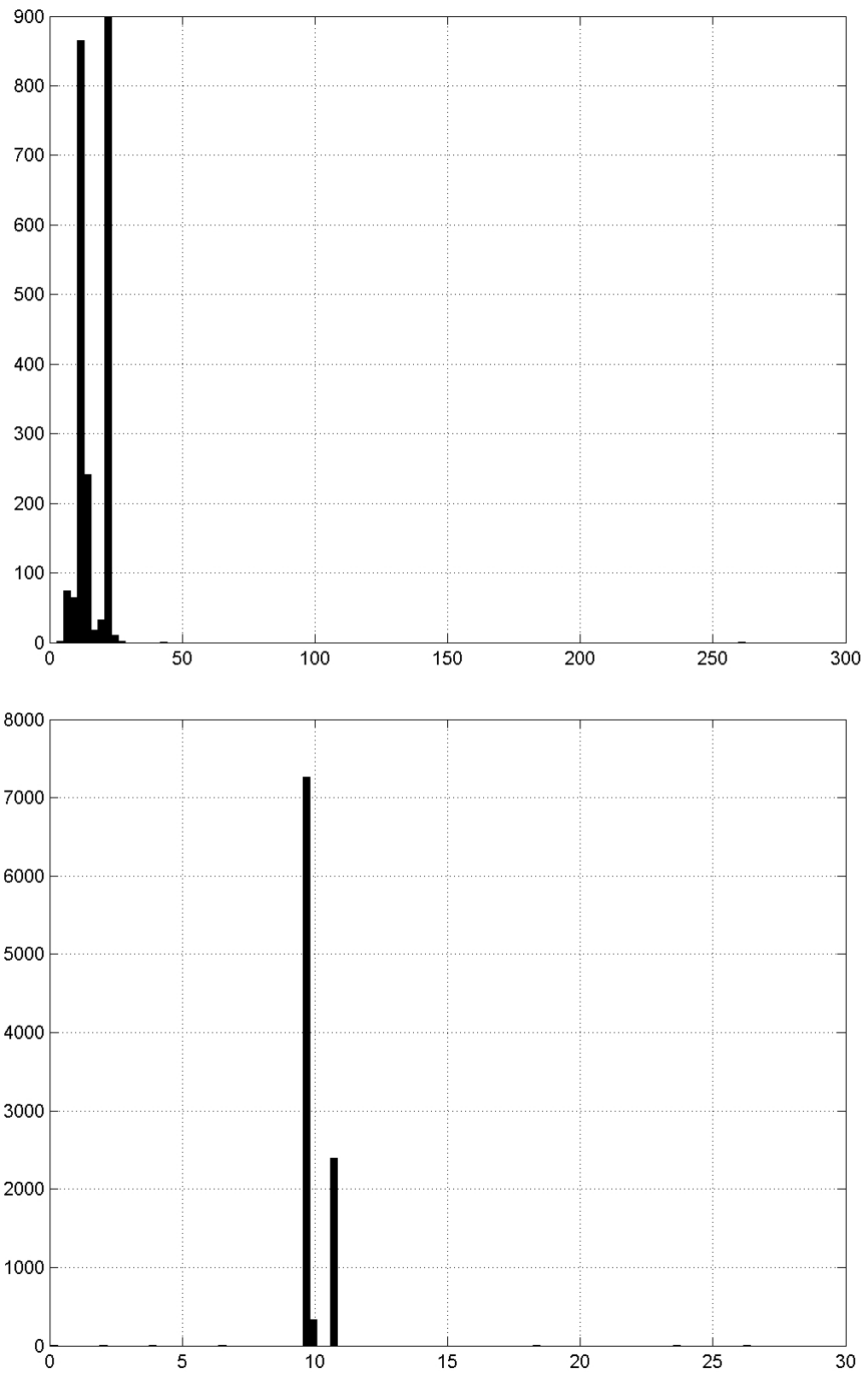


Figure 3.5: The MS Windows jitters comparison. Upper - WM timer, lower - multimedia event timer. Source: [92].

data is easily accessible for further analysis and algorithm refinement. Additionally, there is no need for recompilation of the whole model when, for example, only the parameters have been changed and the entire tool-chain serves as integrated RCP environment - from simulation and modeling, through C-code generation, and up to the execution on the target RT MS Windows platform.

The presented RCP setups supremely fit into MBD methodology. The models of the SAS and ABS devices are presented and their parameters are identified in MATLAB/Simulink environment. Next, they are directly used to develop, tune and test the control algorithms. Consequently, the resulting control strategies are also in the form of MATLAB/Simulink models and might be simply utilized (after C-code generation) in the loop with real hardware (SAS or ABS) without any other effort. This approach provides fast and easy way to verify if the designed algorithm is capable of being executed in RT. For example, the initial version of Neural Network (NN) utilized in section 5.3 was more complex and it was found not to be executable in RT. Due to the integrated RCP environment this problem was quickly discovered and the work towards smaller equivalent NN that is capable to work in RT was started.

To demonstrate the real-time control of the automotive systems, the ABS and SAS laboratory systems are selected and all experiments are conducted with their application. The goal of the research is to present real-time control aspects related to important functions of the vehicles: safety and comfort. The modeling and control approaches applied to laboratory SAS and ABS devices are presented in chapters 5 and 7 respectively.

4. Semi-active suspension systems

This chapter introduces automotive suspension systems. It talks about the conventional passive suspensions designs and the current active and semi-active applications. The chapter is organized as follows: in section 4.1 an introduction to the suspension systems is presented. Typical approaches to modeling of the vehicle suspension are given in section 4.2. Section 4.3 provides an analysis of the main goals of vehicle suspension, and then section 4.4 deals with semi-active suspension control strategies.

4.1. Semi-active suspension application and technology

Automotive suspension is a mechanical construction which supports vehicle chassis on the axels. In general, such a system is composed of a number of spring-type units and dissipative elements. A typical suspension of a modern vehicle can be divided into two groups: dependent and independent. In the dependent suspension the two wheels of an axle are directly linked, thus the vertical motion of one of the wheels influences the remaining one. This type of suspension, which is simpler and inexpensive, is still common as rear suspension and is found in trucks and also in some passenger cars. A typical design is called a solid-axle leaf-spring rear suspension and it is composed of leaf springs and shock absorbers attached to the clamps and vehicle body. In the independent type of suspension, the axle wheels are not directly linked to each other, which is almost always found in the front vehicle suspension. The classic design is the MacPherson strut where the damper is mounted inside the spring (so-called 'coil over oil' arrangement). Regardless of the type of the suspension, its fundamental functions are:

- isolation from vibrations transmitted by road unevenness,
- providing good road holding and handling,
- support the vehicle static weight.

Driver's comfort, driving pleasure and ride quality is often equated with the vertical acceleration of the vehicle body and passenger seats. Road disturbances and irregularities generate vibrations on vehicle's axles which are, in the case when there is no suspension, directly transmitted to the chassis of the vehicle (e.g., the first automobiles and horse carriages were not equipped with suspension). The resulting vertical acceleration of the chassis is uncomfortable to the passengers. The goal is to place

the vibration protection unit (the spring and the shock absorber) between the source of the excitation (vehicle axles) and the passenger compartment in order to reduce the transmission of the force to the vehicle's body. The comfort assessments will be briefly described in section 4.3. The road holding and handling performance depends directly on the forces acting on the tire and the resulting tire deflection. The variations in normal tire loads have negative impact on braking, cornering and traction properties of the vehicle due to the fact that longitudinal and lateral forces generated by the tire directly depend on the normal tire load. In order to effectively support the vehicle static weight the suspension travel (also called rattle space) should be minimized.

Despite of the division of the suspensions into dependent and independent categories, these systems are also divided based on a functional standpoint into uncontrolled and controlled. The conventional passive vehicle suspensions, realized by an elastic spring element (coil spring, air spring or leaf spring) and the passive viscous damper, are designed according to the classical approach which consists of choosing the spring stiffness and the damping rate coefficient. In such a structure there is no real-time control of the suspension. Thus the design process of the suspension characteristics needs the optimization of the system performance in a view of chassis vibrations (comfort) together with the road holding and handling (safety). The suspension compositions having high damping capabilities significantly reduce the vibrations in the vicinity of the resonance frequency, although in the remaining range it is outperformed by low-damped design. The selection criteria of the suspension characteristics depend on vehicle type (e.g., different behavior of the system is expected from an urban vehicle and from a land cruiser), and it is always the result of the compromise and trade-off between hard and soft nature.

The limitations of passive suspension systems had been tackled even before electronic embedded systems were introduced into the auto-industry. An example might be the hydro-pneumatic suspension developed by Citroën in the legendary model DS in 1960s. Controlled suspensions have the ability to obtain better results in the entire working frequency set. In order to achieve improved performance, the system is equipped with sensors, actuators and controllers which are able to change the suspension attributes on-line according to particular needs. This group of smart suspensions has recently been divided into active and semi-active categories. When the micro-controllers started to appear in the automotive industry in 1980s they were incorporated to suspensions. The leader of electronic suspensions in this period was Lotus which presented the fully-fledged electronically controllable fast-reacting hydraulic actuator. This technology was adopted in racing models (Formula I) in circa 1983, and in conventional models afterwards (e.g., Nissan). The active suspension utilizes electronically controlled electro-hydraulic actuators in order to provide external power (force) to the system. This operation enables a significant performance improvement with respect to the passive suspension in each of the above mentioned criteria. However, the system became costly and complex due to the necessity to

apply sensors and actuators. There are also aspects concerning the reliability of such a system and its behavior in a case of mechanical failure. Additionally, the design must consider the energy consumption factor which nowadays, in the era of hybrid and electric cars, is extremely emphasized. In the later years, such solutions were developed and installed in passenger cars by such marques as Mercedes, Volvo and Toyota. Due to unreliable hydraulic systems, high cost and significant power demands, the semi-active technology received much attention. In 1987, Mitsubishi demonstrated the world's first production semi-active electronically controlled suspension system in the passenger model Galant. In the next years manufacturers of another carmakers paid attention to new trends which resulted in the incorporation of semi-active suspensions in some Cadillac models and Chevrolet Corvette. Recently, the semi-active systems have been present in premium models including Audi (e.g., TT or R8), Ferrari, Lamborghini and Mercedes.

The intelligent electronically controlled suspensions (active and semi-active) can be classified in various ways. The most basic one is the division into open-loop and closed-loop systems. The open-loop type incorporates an a-priori setting of constant suspension characteristics (spring and/or damper) according to vehicle weight and the expected road quality [93]. The closed-loop type constitutes the dynamic feedback suspension control which utilizes the vehicle speed and acceleration sensors, and also the suspension deflection sensor in order to control the vehicle motion. Another classification which can be found in literature emphasizes two features: energy input and bandwidth. The energy input aspect applies to the ability of the electronically controlled suspension part to add energy in the suspension system (controllability range). When the system is able to insert energy (in the other words it can lift the vehicle) then it is called active. Otherwise, if it is only capable of removing energy from the system, it is called semi-active. The bandwidth criteria concern the smart suspension reaction time. Using these two aspects such systems are divided into the following categories [94, 93]:

- Active suspensions:
 - Load-leveling (very slow active) suspensions. The load levellers systems have bandwidth within 0.1 Hz to 1 Hz and relatively high power demands around 100 W to 200 W. The main advantage of such systems is an ability to change suspension steady-state condition with the use of controllable springs (e.g., air or gas springs). Since the only controllable variable is the static load, the damping control range is constant.
 - Slow-active suspensions. This group of relatively slow active suspensions where the cut-off frequency is around 1 Hz to 5 Hz (between the body and wheel dynamics) is able to introduce energy into the system. In this case, the actuator generates force the controllability range of which is wide even though the power consumption is large (around 1 kW to 5 kW). An example of such systems is Mercedes-Benz ABC (Active Body Control) and BMW Dynamic

Drive.

- Fully-active (fast active) suspensions. In contrast to the previous group, the fully-active suspension reaction time is relatively fast (around 20 Hz to 30 Hz). Similarly to slow-active suspensions, the controllability range is beyond passivity constraints which raises even higher power request (around 5 kW to 10 kW).
- Semi-active suspensions:
 - Adaptive suspensions. This type of suspensions is often implemented with an open-loop architecture where the damping ratio can be controlled in relatively small bandwidth (around 1 Hz to 5 Hz). Power request is small (max. 20 W). A number of premium class vehicles have the ability to switch suspension operating mode between comfortable and sportive.
 - Fast semi-active suspensions. In the case of the fast semi-active shock absorber, the control actuation bandwidth is large (around 30 Hz to 40 Hz) which enables the effective control in the closed-loop configuration since the wheel-hop natural frequency is around 10 Hz and the typical body natural frequency is around 1 Hz. The power consumption is low (max. 20 W). Such a system is not able to inject energy into the system (passivity constraint).

From the technological point of view the intelligent suspensions classes have their pros and cons with regards to such criteria as structure, weight, cost, ride comfort, handling performance, reliability, dynamic performance, energy recovery and commercial maturity. A very good comparison has been presented in [95] and its results are shown in Table 4.1.

The comparison presented above together with the described features of each technology shed a light on advantages and disadvantages of each solution. One can notice that only the semi-active and fully-active suspensions are capable of full heave vehicle control unlike the load-leveling suspensions (which does not have impact on body and wheel dynamics) and the adaptive suspensions together with a slow-active group (which are able to control body although they do not impact wheel dynamics). The fully-active suspensions get the better of the semi-active ones in terms of an achievable performance. On the other hand, the semi-active suspensions require much less power and preserve the intrinsic stability. In order to improve the performance of the suspensions systems several approaches have been investigated either by carmakers or scientists such as:

- road surface preview (using vision or LiDAR sensors or by utilization of front axle motion as preview for rear axles) [96, 97],
- centralized body control - GCC (Global Chassis Control) [98],
- incorporation of the so called 'full-corner' vehicle architectures (concepts by Michelin Active Wheel and by Siemens VDO e-Corner),

Parameter	Passive suspensions	Semi-active suspensions	Hydraulic or pneumatic active suspensions	Electromagnetic active suspensions
Structure	Simplest	Complex	Most complex	Simple
Weight or volume	Lowest	Low	High	Highest
Cost	Lowest	Low	Highest	High
Ride comfort	Bad	Medium	Good	Best
Handling performance	Bad	Medium	Good	Best
Reliability	Highest	High	Medium	High
Dynamic performance	Passive	Passive	Medium	Good
Energy regeneration	No	No	No	Yes
Commercial maturity	Yes	Yes	Yes	No

Table 4.1: The automotive suspensions comparison. Source: [95].

- application of a new actuation hardware such as frictional dampers or linear electromagnetic motors [99].

Despite the mentioned future technology development, the current trend is to combine semi-active dampers with load-leveling systems.

When it comes to applications and technologies, in the modern vehicles the semi-active suspension is found at three different vibration isolation levels [94]:

1. Wheel-to-chassis (primary suspension used in all road vehicles).
2. Chassis-to-cabin (in the configurations where the driver cabin is separated from the chassis e.g., tractors, trucks or heavy-duty vehicles).

3. Cabin-to-seat (in the configurations where the driver's seat is separated from the cabin e.g., trucks or off-road vehicles).

In all of the above-mentioned levels, the semi-active actuator might come from the three mostly utilized technologies: electrohydraulic (EH), electrorheological (ER) or magnetorheological (MR). All the technologies in contrast to the active suspension make use of controllable damper devices. The controllable damper behavior might be realized with the controllable orifice or controllable fluid.

The EH technology based dampers utilize the classic passive hydraulic (or gas) damper which is modified in order to comprise the electronic electro-magnetic valve instead of passive valve. The introduced variable (controllable) solenoid valve has capabilities of a variable orifice. The damping ratio in such a damper is modified by the change of orifice size. Among other companies, EH dampers are produced by ZF Sachs under the name of CDC (Continuous Damping Control) [100].

The second group of semi-active dampers utilize the properties of so-called smart materials. ER dampers are based on ER fluids (a mixture of oil and micron sized particles which reacts to electrical field change) which change their viscosity due to the applied electric field. The Fludicon GmbH company developed the world's first shock absorber based on the ER technology for light commercial vehicles. The MR technology makes use of MR fluids which are sensitive to the applied magnetic field and respond with transition of rheological properties such as viscosity, plasticity and elasticity. Similar to the ER dampers, the MR dampers response time of the viscosity change is short (about 10 ms). On the other hand, the MR technology has lower power demands than the ER technology and it is more resistant to temperature changes. Additionally, the MR damper usually has a wider operation range (minimum to maximum damping level). The commercial applications of the MR technology are found in the MagneRide damper (installed for example in Chevrolet Corvette) [101] and in a variety of products offered by Mid-Atlantic Rubber / Lord Corporation such as for example RD-8041-1[102].

Apart from the presented technologies, some work and research has recently been conducted examining other technologies which might be exploited in vehicle suspensions. Among them are: air-damping with electronically controlled valves (e.g., Continental Electronic Air Suspension System for motorcycles [103]), the friction dampers, and the most promising one, linear electromagnetic motors. The use of motors as the fast damper like actuators parallel to conventional springs results in the energy recuperation capabilities, and introduce combined active and semi-active features. The Bose Corporation has already tested the prototype version of an active suspension built with linear electromagnetic motors [104]. Another example is Synaptic Damping Control system produced by Magneti Marelli exploiting electronically controlled continuous dampers provided with electro-valves [105].

4.2. Vehicle suspension modeling

In order to design and analyze the automotive suspension, a number of typically employed models have been developed by researchers. Nowadays, when the engineering is mainly computer-aided, mathematical models are popular in performance assessments in the early development stage. The complexity of suspension model depends on its application and purpose. For the control design (comfort, ride and handling) the vehicle suspension is usually modeled using ordinary differential equations, although in advanced studies of aerodynamical or mechanical behavior, distributed models are also utilized. This section covers only the classical ride models for a passenger car, where the vehicle is represented by two components: the sprung masses (vehicle body) and the unsprung masses (wheels and tires). The springs and dampers between those subsystems compose the vehicle suspension and the single-contact point of the tire and road is used. Generally, the control-oriented vehicle models are lumped parameters models derived using Newton's law. Such an approach simplifies the controller synthesis and speeds up the time of simulation and tuning. In the literature one can find a more sophisticated representation of a vehicle which also takes into account the complex tire models (e.g., dynamic tire forces), seats and engine models, and also the driver and passenger models. Due to their complexity such models are usually considered during the final control algorithm verification. The control strategy must first perform correctly in simplified conditions.

In this section, three vehicle suspension models in the increasing complexity level are reviewed: the quarter-car model, the half-car model and finally the full car model.

4.2.1. Quarter vehicle suspension model

The quarter vehicle suspension model represents only the bounce motion of the vehicle body and the single wheel. Such classical spring-mass-damper 2-DOF linear passive suspension model is presented in Figure 4.1. The equations of motion are as follows:

$$\begin{aligned} m_s \ddot{x}_s + b_s (\dot{x}_s - \dot{x}_t) + k_s (x_s - x_t) &= 0 \\ m_t \ddot{x}_t + b_t (\dot{x}_t - \dot{x}_r) + k_t (x_t - x_r) - b_s (\dot{x}_s - \dot{x}_t) - k_s (x_s - x_t) &= 0 \end{aligned} \quad (4.1)$$

where:

- x_s - vertical displacement of the sprung mass from steady-state,
- x_t - vertical displacement of the unsprung mass from steady-state,
- x_r - road displacement,
- m_s - quarter-car mass equivalent,
- m_t - axle and tire mass equivalent,
- b_s - suspension shock absorber damping,

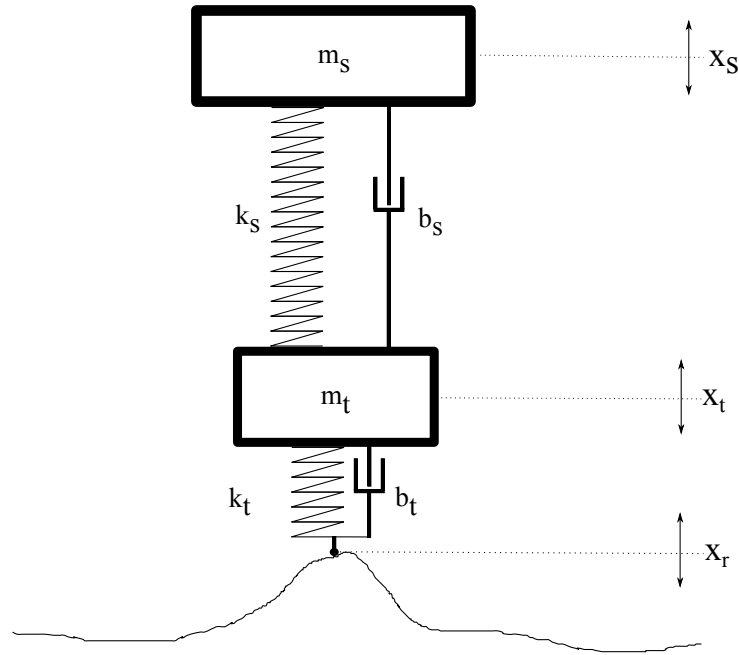


Figure 4.1: Quarter-car passive automotive suspension model.

- k_s - suspension spring stiffness,
- b_t - tire damping,
- k_t - tire stiffness.

The described model is commonly used in the research and automotive industry due to its simplicity and versatility. It is worth to mention that 1-DOF model is also employed and in such a case the tire stiffness and mass are neglected.

The semi-active and active quarter car suspension models are depicted in Figure 4.2 and Figure 4.3 respectively. The governing equations of motion differ from the passive ones only in the addition of either the variable damper in case of the semi-active suspension model (equation (4.2)) or the controllable force in the case of the active model suspension model (equation (4.3)).

$$\begin{aligned}
 m_s \ddot{x}_s + b_s(\dot{x}_s - \dot{x}_t) + k_s(x_s - x_t) &= -b_{sa}(t) \\
 m_t \ddot{x}_t + b_t(\dot{x}_t - \dot{x}_r) + k_t(x_t - x_r) - b_s(\dot{x}_s - \dot{x}_t) - k_s(x_s - x_t) &= b_{sa}(t)
 \end{aligned}
 \tag{4.2}$$

$$\begin{aligned}
 m_s \ddot{x}_s + b_s(\dot{x}_s - \dot{x}_t) + k_s(x_s - x_t) &= F_a \\
 m_t \ddot{x}_t + b_t(\dot{x}_t - \dot{x}_r) + k_t(x_t - x_r) - b_s(\dot{x}_s - \dot{x}_t) - k_s(x_s - x_t) &= -F_a
 \end{aligned}
 \tag{4.3}$$

In the case of the former suspension type, the variable damper $b_{sa}(t)$ modeling function depends on a component type and the required simulation accuracy. The possible approaches are discussed in section 4.2.4. It is common to model the active suspension force actuator as the direct external force input although some of the work in this case will include for example the hydraulic actuator dynamics approximation in the presented model [106].

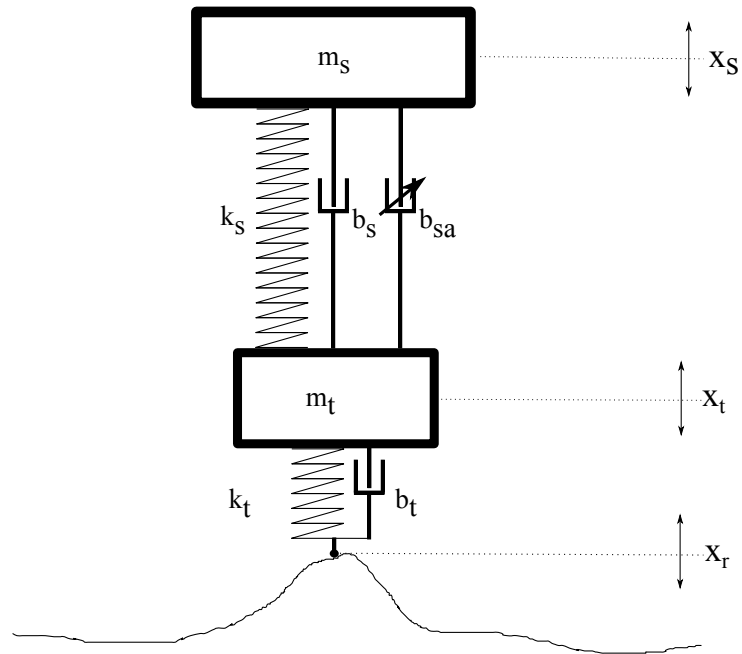


Figure 4.2: Quarter-car semi-active automotive suspension model.

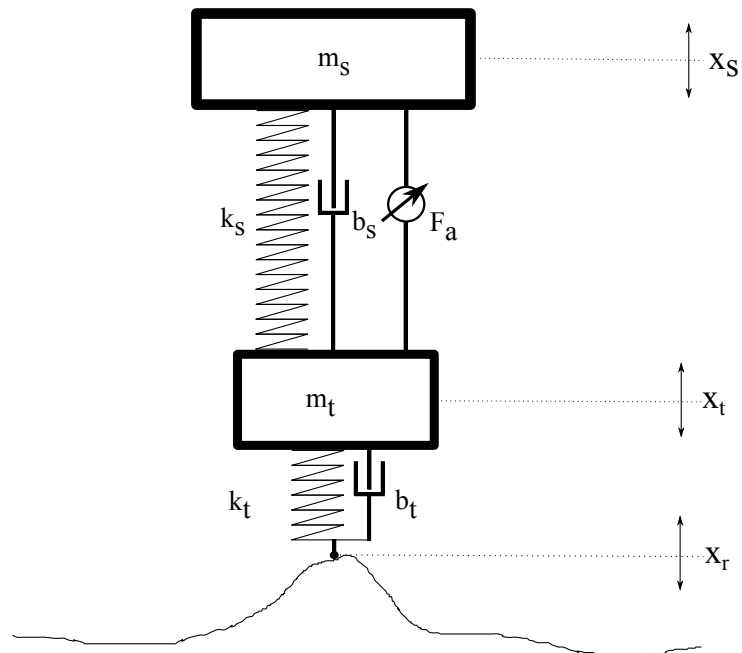


Figure 4.3: Quarter-car fully active automotive suspension model.

4.2.2. Half vehicle suspension model

A more complex half vehicle model extends the trivial quarter suspension model with featuring the pitch motion or roll motion. The half-car vehicle model is the linked system of two quarter-car vehicle models joined using a rigid vehicle body. The so-called bicycle model assumes the vertical motion of front and rear wheels, and the vertical vibration and pitch motion of the vehicle rigid frame center of gravity (c.g.). The passive 4-DOF example of the pitch oriented model is presented in Figure 4.4 and its equations are as follows:

$$\begin{aligned}
& m_s \ddot{x}_s + b_{sr}(\dot{x}_s - l_f \dot{\theta} - \dot{x}_{tr}) + k_{sr}(x_s - l_f \theta - x_{tr}) + \\
& \quad b_{sf}(\dot{x}_s + l_r \dot{\theta} - \dot{x}_{tf}) + k_{sf}(x_s + l_r \theta - x_{tf}) = 0 \\
& I_\theta \ddot{\theta} - k_{sr}(x_s - l_f \theta - x_{tr})l_f - b_{sr}(\dot{x}_s - l_f \dot{\theta} - \dot{x}_{tr})l_f + \\
& \quad k_{sf}(x_s + l_r \theta - x_{tf})l_r + b_{sf}(\dot{x}_s + l_r \dot{\theta} - \dot{x}_{tf})l_r = 0 \\
& m_{tr} \ddot{x}_{tr} - k_{sr}(x_s - l_f \theta - x_{tr}) - b_{sr}(\dot{x}_s - l_f \dot{\theta} - \dot{x}_{tr}) + k_{tr}(x_{tr} - x_{rr}) = 0 \\
& m_{tf} \ddot{x}_{tf} - k_{sf}(x_s + l_r \theta - x_{tf}) - b_{sf}(\dot{x}_s + l_r \dot{\theta} - \dot{x}_{tf}) + k_{tf}(x_{tf} - x_{rf}) = 0
\end{aligned} \tag{4.4}$$

where:

- x_s - vertical displacement of the sprung mass center of gravity (heave or bounce) from steady-state,
- m_s - half-car mass equivalent,
- x_{sr} - vertical displacement of the rear sprung mass from steady-state,
- x_{sf} - vertical displacement of the front sprung mass from steady-state,
- I_θ - pitch inertia of the vehicle body,
- θ - pitch angle of the vehicle body,
- x_{tr} - vertical displacement of the rear unsprung mass from steady-state,
- x_{tf} - vertical displacement of the front unsprung mass from steady-state,
- x_{rr} - rear wheel road displacement,
- x_{rf} - front wheel road displacement,
- m_{tr} - rear axle and tire mass equivalent,
- m_{tf} - front axle and tire mass equivalent,
- b_{sr} - rear wheel suspension shock absorber damping,
- b_{sf} - front wheel suspension shock absorber damping,
- k_{sr} - rear wheel suspension spring stiffness,
- k_{sf} - front wheel suspension spring stiffness,
- k_{tr} - rear wheel tire stiffness,
- k_{tf} - front wheel tire stiffness,
- l_r and l_f - distances of rear and front suspension mounting from its center of gravity (c.g.).

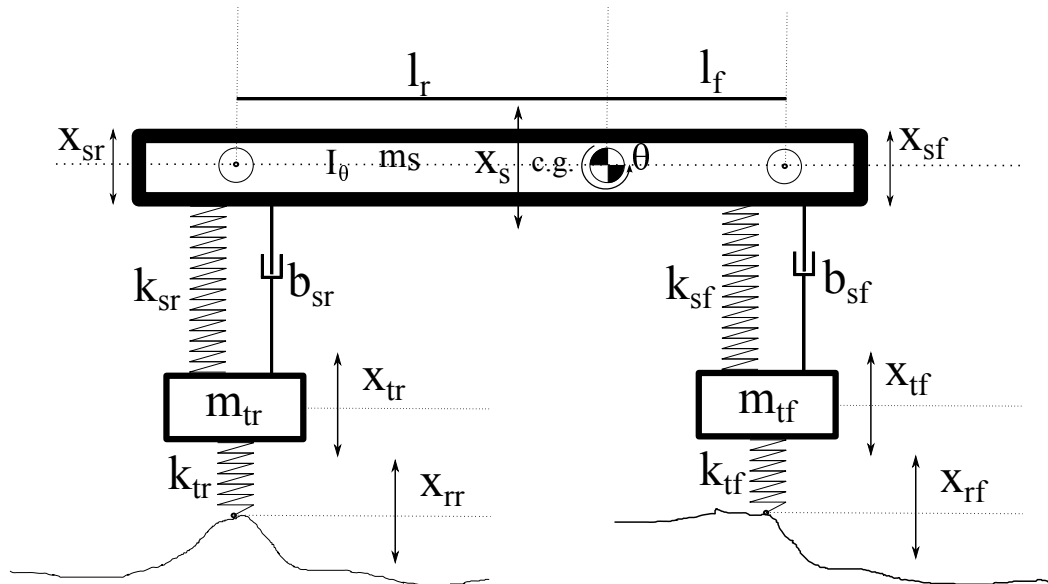


Figure 4.4: Half-car passive pitch oriented automotive suspension model.

This model might be utilized to study, except from wheels vertical motion, the vehicle body behavior in the case of acceleration or braking situations. It is worth to mention that the half vehicle pitch model extension, which includes longitudinal dynamics, is greatly used in the scientific literature for validation. The extended passive vertical nonlinear dynamic half-car model is also considered as a complete (although simplified) description of a motorcycle, and it is particularly interesting for the motorcycle community since pitch dynamics is more critical in two-wheeled vehicles than in four-wheeled ones. The other variant of the half vehicle model is the roll oriented equivalent where side wheels (left and right) are considered instead of front and rear, and the roll motion is investigated. This particular case concentrates on lateral steering scenarios. As one can notice, the tire damping is not present in the model but it might be taken into account. The semi-active and active equivalents of the passive half-car models can be easily introduced by incorporating additional force or controllable dampers to the wheel's suspension parts.

4.2.3. Full vehicle suspension model

The full vehicle linear 7-DOF passive suspension model is depicted in Figure 4.5. The presented model has independent rear and front suspensions, the vehicle body is assumed to be rigid frame and

it allows to investigate vehicle body heave, pitch and roll motion. Each wheelstation is modeled as a quarter-car suspension model although in this case the tire is modeled as a combination of damper and spring. The governing equations are as follows:

$$\begin{aligned}
& m_s \ddot{x}_s + k_{sfr}(x_{sfr} - x_{tfr}) + b_{sfr}(\dot{x}_{sfr} - \dot{x}_{tfr}) + k_{sfl}(x_{sfl} - x_{tfl}) \\
& \quad + b_{sfl}(\dot{x}_{sfl} - \dot{x}_{tfl}) + k_{srr}(x_{srr} - x_{trr}) + b_{srr}(\dot{x}_{srr} - \dot{x}_{trr}) \\
& \quad \quad + k_{srl}(x_{srl} - x_{trl}) + b_{srl}(\dot{x}_{srl} - \dot{x}_{trl}) = 0 \\
& I_\theta \ddot{\theta} - k_{sfr} l_f (x_{sfr} - x_{tfr}) - b_{sfr} l_f (\dot{x}_{sfr} - \dot{x}_{tfr}) - k_{sfl} l_f (x_{sfl} - x_{tfl}) \\
& \quad - b_{sfl} l_f (\dot{x}_{sfl} - \dot{x}_{tfl}) + k_{srr} l_r (x_{srr} - x_{trr}) + b_{srr} l_r (\dot{x}_{srr} - \dot{x}_{trr}) \\
& \quad \quad + k_{srl} l_r (x_{srl} - x_{trl}) + b_{srl} l_r (\dot{x}_{srl} - \dot{x}_{trl}) = 0 \\
& I_\varphi \ddot{\varphi} - k_{sfr} w_r (x_{sfr} - x_{tfr}) - b_{sfr} w_r (\dot{x}_{sfr} - \dot{x}_{tfr}) - k_{srr} w_r (x_{srr} - x_{trr}) \\
& \quad - b_{srr} w_r (\dot{x}_{srr} - \dot{x}_{trr}) + k_{sfl} w_l (x_{sfl} - x_{tfl}) + b_{sfl} w_l (\dot{x}_{sfl} - \dot{x}_{tfl}) \\
& \quad \quad + k_{srl} w_l (x_{srl} - x_{trl}) + b_{srl} w_l (\dot{x}_{srl} - \dot{x}_{trl}) = 0 \tag{4.5} \\
& m_{tfr} \ddot{x}_{tfr} - k_{sfr}(x_{sfr} - x_{tfr}) + k_{tfr}(x_{tfr} - x_{rfr}) \\
& \quad - b_{sfr}(\dot{x}_{sfr} - \dot{x}_{tfr}) + b_{tfr}(\dot{x}_{tfr} - \dot{x}_{rfr}) = 0 \\
& m_{tfl} \ddot{x}_{tfl} - k_{sfl}(x_{sfl} - x_{tfl}) + k_{tfl}(x_{tfl} - x_{rfl}) \\
& \quad - b_{sfl}(\dot{x}_{sfl} - \dot{x}_{tfl}) + b_{tfl}(\dot{x}_{tfl} - \dot{x}_{rfl}) = 0 \\
& m_{trr} \ddot{x}_{trr} - k_{srr}(x_{srr} - x_{trr}) + k_{trr}(x_{trr} - x_{rrr}) \\
& \quad - b_{srr}(\dot{x}_{srr} - \dot{x}_{trr}) + b_{trr}(\dot{x}_{trr} - \dot{x}_{rrr}) = 0 \\
& m_{trl} \ddot{x}_{trl} - k_{srl}(x_{srl} - x_{trl}) + k_{trl}(x_{trl} - x_{rrl}) \\
& \quad - b_{srl}(\dot{x}_{srl} - \dot{x}_{trl}) + b_{trl}(\dot{x}_{trl} - \dot{x}_{rrl}) = 0
\end{aligned}$$

where:

- x_s - vertical displacement of the sprung mass center of gravity (vehicle body) from steady-state,
- m_s - half-car mass equivalent,
- x_{sfr} - vertical displacement of the front right sprung mass from steady-state,
- x_{sfl} - vertical displacement of the front left sprung mass from steady-state,
- x_{srr} - vertical displacement of the rear right sprung mass from steady-state,
- x_{srl} - vertical displacement of the rear left sprung mass from steady-state,
- I_θ - pitch inertia of the vehicle body,
- θ - pitch angle of the vehicle body,
- I_φ - roll inertia of the vehicle body,
- φ - roll angle of the vehicle body,
- x_{tfr} - vertical displacement of the front right unsprung mass from steady-state,

- x_{tfl} - vertical displacement of the front left unsprung mass from steady-state,
- x_{trr} - vertical displacement of the rear right unsprung mass from steady-state,
- x_{trl} - vertical displacement of the rear left unsprung mass from steady-state,
- x_{rfr} - front right wheel road displacement,
- x_{rfl} - front left wheel road displacement,
- x_{rrr} - rear right wheel road displacement,
- x_{rrl} - rear left wheel road displacement,
- m_{tfr} - front right axle, wheel and tire mass equivalent,
- m_{tfl} - front left axle, wheel and tire mass equivalent,
- m_{trr} - rear right axle, wheel and tire mass equivalent,
- m_{trl} - rear left axle, wheel and tire mass equivalent,
- b_{sfr} - front right wheel suspension shock absorber damping,
- b_{sfl} - front left wheel suspension shock absorber damping,
- b_{srr} - rear right wheel suspension shock absorber damping,
- b_{srl} - rear left wheel suspension shock absorber damping,
- k_{sfr} - front right wheel suspension spring stiffness,
- k_{sfl} - front left wheel suspension spring stiffness,
- k_{srr} - rear right wheel suspension spring stiffness,
- k_{srl} - rear left wheel suspension spring stiffness,
- k_{tfr} - front right wheel tire stiffness,
- k_{tfl} - front left wheel tire stiffness,
- k_{trr} - rear right wheel tire stiffness,
- k_{trl} - rear left wheel tire stiffness,
- b_{tfr} - front right wheel tire damping coefficient,
- b_{tfl} - front left wheel tire damping coefficient,
- b_{trr} - rear right wheel tire damping coefficient,
- b_{trl} - rear left wheel tire damping coefficient,
- w_l and w_r - distances of left and right suspension mounting from its center of gravity (c.g.),
- l_r and l_f - distances of rear and front suspension mounting from its center of gravity (c.g.).

The above model is a trivial form of a full car model due to simplified assumptions among which are the elimination of yaw (turning) motion or small angles approximation. The researches often incorporate the advanced version of the described one for example by representing the rear suspension as dependent or adding the anti-roll bars. In the literature one can also find versions of full car models having nonlinearities in form of the Coulomb friction, hysteresis, time delays, uncertainties (e.g., vehicle mass

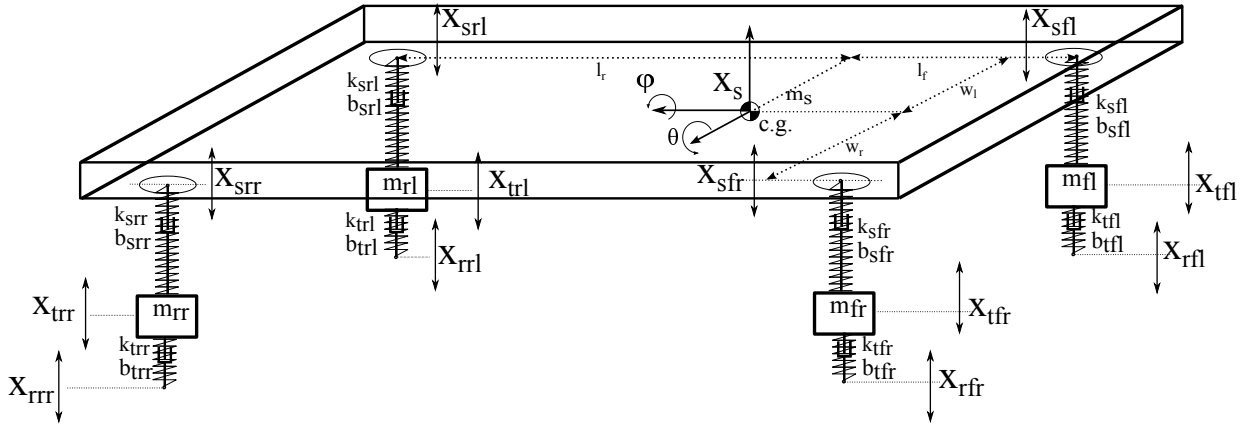


Figure 4.5: Full-car passive automotive suspension model.

uncertainty) or saturations [107]. The presented classical full vehicle ride model can also be extended with additional models of seats, the driver or of the passenger. The one step further is use of a high fidelity complete-car model such as a nonlinear multibody dynamic models having hundreds degrees of freedom [108].

In general, for purposes of control algorithm development, the simple and control-oriented models are more often utilized. Such choice is mainly dictated by the shorter execution time and physical simplicity. During the validation and testing process, the increasing complexity is continuously being introduced which allows to control algorithms optimization based on the obtained results.

4.2.4. Suspension dampers modeling

In the suspension system the damper is the energy dissipative unit and the elastic spring is the storing unit. The described passive suspension models utilize the classic, ideal damping element. It is a representation of a linear passive hydraulic (mono-tube) shock absorber and it is a static model defined as:

$$f_b = f(\dot{x}) = b_s \dot{x} \quad (4.6)$$

In many cases such simplified model is not sufficient to accurately model the damping due to non-linear behavior of dissipative devices. The model is often extended with:

- An addition of the Coulomb friction part which results in a model given by:

$$f_b = f(\dot{x}) = b_s \dot{x} + b_0 \text{sign}(\dot{x}) \quad (4.7)$$

- Consideration of the displacement and acceleration input to damper generated force:

$$f_b = f(x, \dot{x}, \ddot{x}) \quad (4.8)$$

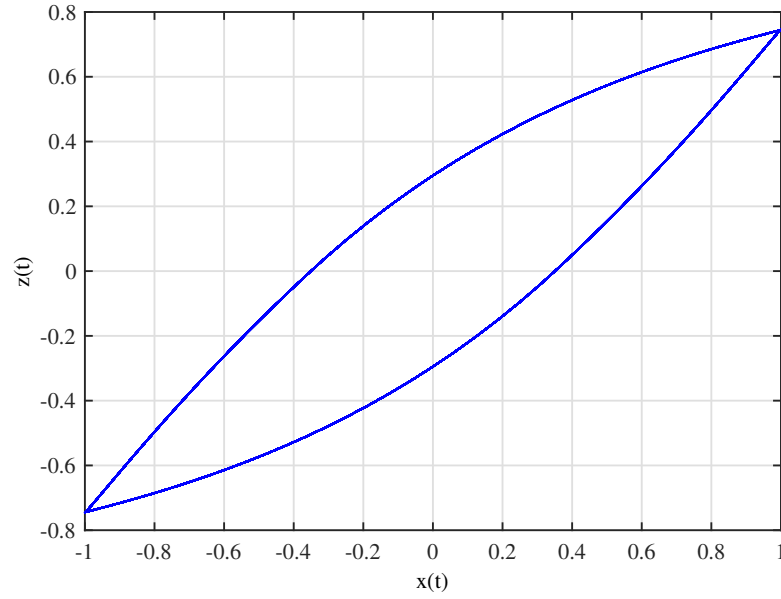


Figure 4.6: Hysteresis loop of the Bouc-Wen model.

On the other hand, the linear characteristics of a damper have some constraints so saturation must be taken into account outside of the working space.

When it comes to controllable dampers, the models become more complex and so the dynamics of the dampers must be included. A number of ideal (static) models of electrohydraulic, electrorheological and magnetorheological dampers have been developed. Nevertheless, characteristics of dampers usually present hysteresis loops, especially when it comes to semi-active devices such as MR dampers or friction dampers. This phenomenon has a huge impact on control design and system analysis and in most cases it must have to be taken into account during modeling. The hysteresis modeling is a known scientific term and over the years several models and approaches to modeling have been proposed, for example: Bingham, Spencer, Dahl, LuGre and other non-linear black-box models (e.g., polynomial) [109]. Among others the most appealing is the Bouc-Wen model [110]. It has recently started to be widely used due its general form and relative simplicity. The model definition is as follows:

$$\dot{z} = -\gamma|\dot{x}|z|z|^{n-1} - \delta\dot{x}|z|^n + \theta\dot{x} \quad (4.9)$$

where x denotes displacement of the suspension from steady-state position, z is the introduced damper's state, and parameters γ , δ , θ and n define the model's hysteresis phenomenon. The model parameters need to be identified and this could be tackled by using LMS (Least Mean Squares) techniques or genetic algorithms. In such a case the damper's force is modeled as:

$$f_b = f(x, \dot{x}, z, u) \quad (4.10)$$

where u is the damper's control signal. An example of the Bouc-Wen model hysteresis loop is presented in Figure 4.6. The hysteresis loop shape is dependent on the model parameters set.

4.2.5. Tire modeling

The main element in the vehicle that interacts with the road is the tire. The tire characteristics vastly affect the entire vehicle performance: handling, traction, ride comfort and fuel consumption. The vehicle maneuvering abilities are point-blank dependent on forces generated under the tires [111]. The tire modeling approach adopted in the above vehicle ride models is the simple representation of tire as spring and damper (often also damping is negligible). The model assumes that there is a single-contact point between the tire and the ground, and this contact is constant (the tire does not jump). For the vertical control oriented purpose (ride comfort) this is often sufficient. In the case of road-holding perspective it turns out that such model is also correct. The lateral and longitudinal forces acting on the tire which have the main influence on the road handling are dependent, among other factors, on the normal force. The vehicle maneuvering performance is the best when lateral and longitudinal forces are maximized. On the other hand the normal force is maximized when the tire deflection is minimized. Due to these facts, the simple model of the tire could be successfully utilized during the computer-aided simulation and control performance assessment.

Except for the described basic model of the tire, during the last fifty years a number of tire dynamics and modeling studies resulted in the creation of a high number of tire models. The developed models vary in accuracy and complexity depending on the purpose and appliance of a specific model. In general, origins of the tire models can be of four possible types: experimental data only, using similarity method, through simple physical model and through complex physical model [112].

The first type of models are empirical models based on measured and preprocessed data obtained during full scale field tests and regression techniques. These models are in the form of mathematical formulas and look-up tables which characterize forces generated by the tire under certain conditions. Among the empirical tire models, the Magic Formula tire model is the one utilized by the majority of researches. The model provides an excellent fit for longitudinal and lateral forces and aligning torque. The generated values depend on normal force, wheel camber angle and eight parameters that have to be identified for a specific tire.

The second category models utilize a so-called similarity approach. The resulting models (often termed 'semi-empirical' models) are also based on measured and interpolated data although they additionally contain structures coming from physical tire models. This type of models is commonly used in vehicle simulations performed in rapid and real-time calculations. Similar to the first group, models from the second group are only concerned with the steady-state situations.

Models that use simple mechanical representation of a tire belong to the third category. This group of models puts more emphasis on theoretical aspects of the tire structure behavior in steady-state conditions. In general, the functions describing lateral and longitudinal slip forces are highly non-linear and also

depend (apart from the mentioned normal force) on the slip ratio, slip angle and tire-road friction coefficient. This analytical model called Tire Brush Model based on the tire thread deformation in the contact patch is used for a small lateral and longitudinal slip. It implies that both the lateral tire force is proportional to the slip angle (lateral slip) and the longitudinal tire force is proportional to the slip ratio (longitudinal slip). The brush model is considered either with a more accurate parabolic normal pressure distribution or a simpler uniform normal force distribution. However, when the tire is exposed to either the combined slip or high pure lateral or longitudinal slip, this relation is no longer accurate. Analytical elastic foundation model has been developed [113] for the larger slip angles and slip ratios cases. While for the combined force generation, the Dugoff tire model is commonly used. The model is not based on either the brush tire model or the elastic foundation. The model assumes a simple uniform vertical pressure distribution on the tire contact patch, and is characterized by independent lateral and longitudinal stiffness parameters, which is beneficial, since the values tend to vary significantly. Apart from the mentioned steady-state tire models, a number of non-steady-state and transient counterparts have been developed, for example the stretched string model or the single-contact point-point transient model. The former approach allows to analyze the oscillatory dynamic behavior of the tire which might be treated as an integral component. This enables study of the so-called wheel shimmy oscillation - the unstable motion (vibration) of a wheel about vertical steering axis. This phenomenon is undesirable especially with front automobile wheels and front motorcycle wheel (wobble). The later approach is simplified to a single-point contact and it is mainly considered for the longitudinal and combined transient slip situation analysis.

The last group of models are advanced dynamic tire models. These complex and commercial models are dedicated to the computer simulation and analysis of the tire detailed performance. The RMOD-K Tire Model and the FTire Tire Model are complex physical models that find application for example in the material stiffness effect research. The MF-Swift Tire Model is more empirically oriented and it is heavily utilized during vehicle-handling studies including anti-lock brakes. The model is based on Magic Formula and enables accurate description of both steady-state, and transient and dynamic tire behavior simulation. The model has become an industry standard and it is sold by TNO company in a package called Delft-Tyre [114]. The Michelin company has developed and patented a tire model called Tame Tire which combines the brush model and thermomechanical component [115].

4.2.6. Road modeling

The road profile is the primary source of vibration generated in the suspension system due to that fact the modeling of the road unevenness is crucial from the control performance standpoint. The accurate and realistic road model is also required for simulations performed during control strategies validation

and benchmarking. The road surface roughness input transmitted to the vehicle suspension model are classified into two categories: a deterministic road and a random road [107]. The first category contains two types of deterministic inputs: periodic and single. Periodic road disturbances in the form of sine waves, square waves, step waves, triangular waves are defined by a mathematical formula. Sine waves are commonly utilized during control design due to the fact that this kind of waveform can be easily adopted to the frequency domain analysis (Body's plots, transmissibility charts). Such a road surface input is non-realistic and it contains only one single frequency each time. Thus, to have more real world excitation input, the second type of experiments in the form of discrete event inputs such as bumps and potholes are also utilized for testing. The advantage of performing experiments with such profiles is to provide a multi-harmonic system excitation (spectrum of a bump is rich in frequencies) which is easily understandable in the time domain and it is realistic [94]. Of course responses obtained during trials with these inputs might serve as complementary and additional test results, aside from the FR (Frequency Response) analysis.

The random or pseudo-random model of the road roughness is much more sophisticated and has more in common with realistic driving situations. The modeling approaches differ among studies and include (but are not limited to):

- broad band white noise [94],
- stationary Gaussian stochastic process, where PSD (Power Spectral Density) is used to describe road surface (British standard BS 7853, 1996, ISO 8608:1995) [108],
- the sum of several sine-waves [108].

All the characterized inputs are common for single contact point tire model. If the complex tire model is introduced then for example for the bump test case the tire might recline on two points. In such cases the more complex road surface spatial model is needed [112].

4.3. Comfort and safety assessment based on quarter vehicle suspension model analysis

This section covers the methods and methodologies applied in order to evaluate the efficiency of a specific suspension system. At first the main aspects of interests regarding criterions of the vehicle suspension performance are described. Afterwards the quarter-car suspension model assessment analysis is performed.

4.3.1. Comfort and safety assessment

Due to the fact that the vehicle is a complex vibrating system, the main objective of the suspension system, which can be treated as a low-pass filter, is to isolate the passengers. On the other hand the safety of a driving vehicle suffering from vibrations inputted from the road surface must also be guaranteed. As stated before, the above mentioned criteria are in contradiction to each other and the trade-off needs to be established.

4.3.1.1. Ride comfort

The ride quality generally concerns a human body comfort. The vibrations originate from a number of external and internal forces. The primary external source is the road unevenness. Other sources might be aerodynamic forces or the work of engine. The assessment of human body comfort specification is very subjective due to the fact that human body sensitivity to vibrations differs among persons. The feeling of comfort depends, for example, on an actual passenger or driver age and his health condition. Generally, the human body is more sensible to horizontal vibrations rather than to vertical vibrations. The vibrations in all directions easily handled by human body are in frequency range of about 1 Hz to 2 Hz which corresponds to the vibration of the walking pace. Lower frequencies cause symptoms such as motion sickness while higher frequencies result in an overall decrease of driver or passengers comfort which might impact the drivers reaction time, accuracy and decision making abilities [94]. In order to objectively study comfort in the vehicle, without modeling of the human body, some simplification need to be considered. Generally, the comfort criteria focus on chassis vertical vibration analysis instead of the real human body vibration analysis. The main goal is to minimize chassis displacement, velocity or acceleration. In order to quantify the ride comfort, a number of criteria have been developed: ISO 2631 standard [116], British Standard BS 6841 [117], VDI 2057 [118], Janeway's criterion [119] and the average absorbed power or RMS (Root Mean Square) of the vertical body acceleration.

4.3.1.2. Road holding and safety

The road handling and holding of the vehicle is mainly concerned by the dynamics of the vehicle tires. Generally the normal load of the each tire should be maximized due to the fact that its value increases the longitudinal and lateral forces of each tire. During the maneuvers such as cornering, accelerating or braking, the maximal longitudinal and lateral forces are expected. The normal load is maximized when the tire deflection is minimized, thus the road holding specification is often considered as tire deflection minimization problem. Such approach is commonly utilized when classical quarter car model is considered where only the vertical motion is addressed.

4.3.2. Quarter vehicle suspension model analysis

The LTI (Linear Time-Invariant) passive simplified quarter-car model is given by the following dynamical equations (please refer to the passive quarter-car model defined in 4.2.1):

$$\begin{aligned} m_s \ddot{x}_s + b_s(\dot{x}_s - \dot{x}_t) + k_s(x_s - x_t) &= 0 \\ m_t \ddot{x}_t + k_t(x_t - x_r) - b_s(\dot{x}_s - \dot{x}_t) - k_s(x_s - x_t) &= 0 \end{aligned} \quad (4.11)$$

The state space representation is as follows:

$$\begin{bmatrix} \ddot{x}_s \\ \dot{x}_s \\ \ddot{x}_t \\ \dot{x}_t \end{bmatrix} = \begin{bmatrix} -\frac{b_s}{m_s} & -\frac{k_s}{m_s} & \frac{b_s}{m_s} & \frac{k_s}{m_s} \\ 1 & 0 & 0 & 0 \\ \frac{b_s}{m_t} & \frac{k_s}{m_t} & -\frac{b_s}{m_t} & -\frac{k_s+k_t}{m_t} \\ 0 & 0 & 1 & 0 \end{bmatrix} \begin{bmatrix} \dot{x}_s \\ x_s \\ \dot{x}_t \\ x_t \end{bmatrix} + \begin{bmatrix} 0 \\ 0 \\ \frac{k_t}{m_t} \\ 0 \end{bmatrix} x_r \quad (4.12)$$

Using the state-space representation, the following transfer functions are defined:

$$F_s(s) = \frac{X_s(s)}{X_r(s)} = \frac{b_s k_t s + k_t k_s}{m_s m_t s^4 + b_s(m_t + m_s)s^3 + (m_s k_s + m_t k_s + m_s k_t)s^2 + b_s k_t s + k_s k_t} \quad (4.13)$$

$$F_t(s) = \frac{X_t(s)}{X_r(s)} = \frac{m_s k_t s^2 + b_s k_t s + k_s k_t}{m_s m_t s^4 + b_s(m_t + m_s)s^3 + (m_s k_s + m_t k_s + m_s k_t)s^2 + b_s k_t s + k_s k_t} \quad (4.14)$$

where $X_s(s)$, $X_t(s)$ and $X_r(s)$ denote the Laplace transform of $x_s(t)$ (vertical displacement of the sprung mass / chassis), x_t (vertical displacement of the unsprung mass / wheel) and x_r (the vertical road disturbance). Additionally the suspension deflection $x_s^d(t) = (x_s(t) - x_t(t))$ and tire deflection $x_t^d(t) = (x_t(t) - x_r(t))$ transforms are described by $X_s^d = X_s(s) - X_t(s)$ and $X_t^d = X_t(s) - X_r(s)$ and the following extra transfers are defined:

$$F_s^d(s) = F_s(s) - F_t(s) = \frac{-m_s k_t s^2}{m_s m_t s^4 + b_s(m_t + m_s)s^3 + (m_s k_s + m_t k_s + m_s k_t)s^2 + b_s k_t s + k_s k_t} \quad (4.15)$$

$$F_t^d(s) = F_t(s) - 1 = \frac{-m_s m_t s^4 - b_s(m_t + m_s)s^3 - (m_s k_s + m_t k_s)s^2}{m_s m_t s^4 + b_s(m_t + m_s)s^3 + (m_s k_s + m_t k_s + m_s k_t)s^2 + b_s k_t s + k_s k_t} \quad (4.16)$$

The defined transfer functions are examined in order to study suspension's performance specifications related to comfort (4.13) and road-holding (4.16). The suspension deflection limits analysis might also be conducted using the transfer function (4.15). The featured model has ability to analyze and consider all the vehicle suspension functions which in this case are:

- ride quality, often represented as sprung mass acceleration \ddot{x}_s ,
- road holding and handling, related to tire deflection $(x_t - x_r)$,
- and vehicle static weight, related to so-called suspension working space or rattle space $(x_s - x_t)$.

In order to perform frequency domain analysis of the defined suspension model, the invariant points of the transfer functions (4.13) and (4.16) are introduced [94]. The transfer function related to comfort $F_s(j\omega)$ has the following invariant points:

- $\omega_s^0 = 0$
- $\omega_s^1 = \frac{1}{m_s m_t \sqrt{2}} \sqrt{m_s m_t (m_s k_t + 2m_s k_s + 2m_t k_s - \sqrt{\lambda})}$
- $\omega_s^2 = \frac{1}{m_s m_t \sqrt{2}} \sqrt{m_s m_t (m_s k_t + 2m_s k_s + 2m_t k_s + \sqrt{\lambda})}$
- $\omega_s^3 = \sqrt{\frac{k_t}{m_t}}$.

where $\lambda = 4m_t^2 k_s^2 - 4m_t k_s m_s k_t + 8m_s k_s^2 m_t + m_s^2 k_t^2 + 4m_s^2 k_s k_t + 4m_s^2 k_s^2$. The road-holding related transfer function $F_t^d(j\omega)$ has three invariant points:

- $\omega_t^0 = 0$
- $\omega_t^1 = \frac{1}{2\sqrt{m_s m_t (m_s + m_t)}} \sqrt{4m_s m_t k_s + 2m_t^2 k_s + 2m_t m_s k_t + 2m_s^2 k_s + k_t m_s^2 - \sqrt{\beta}}$
- $\omega_t^2 = \frac{1}{2\sqrt{m_s m_t (m_s + m_t)}} \sqrt{4m_s m_t k_s + 2m_t^2 k_s + 2m_t m_s k_t + 2m_s^2 k_s + k_t m_s^2 + \sqrt{\beta}}$.

where $\beta = 4m_t^4 k_s^2 + 4m_s^4 k_t^2 + k_t^2 m_s^4 - 12m_s^2 m_t^2 k_s k_t - 8m_t^3 k_s m_s k_t + 24m_s^2 m_t^2 k_s^2 + 16m_s m_t^3 k_s^2 + 16m_s^3 m_t k_s^2 + 4m_t^2 m_s^2 k_t^2 + 4m_t m_s^3 k_t^2 + 4m_s^4 k_s k_t$

To perform the analysis and further discussion, the specified numerical parameters of the quarter-car model are fixed to:

- $m_s = 250$ kg
- $m_t = 45$ kg
- $k_t = 160000$ N m⁻¹
- $k_s = 16000$ N m⁻¹

The remaining b_s would vary during the analysis to show how damping influences the suspension specification. One can notice that invariant points do not depend on the damping coefficient b_s and might be calculated using the fixed parameters. It is also notable that invariant point ω_s^1 is also independent from the spring stiffness parameter k_s . In order to present those values in Body's diagrams, they are calculated and presented as frequency:

- $f_s^0 \approx 0$ Hz
- $f_s^1 \approx 1.64$ Hz
- $f_s^2 \approx 9.49$ Hz
- $f_s^3 \approx 10.42$ Hz
- $f_t^0 \approx 0$ Hz
- $f_t^1 \approx 1.59$ Hz

- $f_t^2 \approx 7.75$ Hz

The model poles diagram is shown in Figure 4.7. One can notice that for the very low damping value $b_s = 1$ N s m⁻¹ the system poles location is close to the right-half plane. Of course if damping is zero then the system becomes unstable and only has an oscillating behavior. With the increase of the b_s the poles move to higher values of real axis. Body's diagrams of transfer functions $F_s(s)$ and $F_t^d(s)$ are presented in Figure 4.8 and Figure 4.9. The invariant points are also marked. The resonance of the comfort transfer function (in the low frequency range between 1 Hz and f_s^1) is filtered by the stiff (higher b_s) damping configuration. On the other hand in the following frequency range f_s^1 to f_s^2 the magnitude is highly reduced by softer dampers (lower b_s). The higher frequencies greater than f_s^3 are also the best filtered by softer dampers. The transfer function related to the road-holding characteristics is best filtered in the low frequencies (lower than f_t^1) by dampers with high damping coefficients. The low frequencies range for both transfer functions is similar and the well performing configuration is common. In the middle frequency range (f_t^1 to f_t^2) similar compatibility (soft damping outperforms stiff damping) is present. The discrepancy occurs in the high frequency range where high damping best filters the road-holding related transfer function, and the ride comfort one is best filtered by stiff damping. It is also worth to mention that tire deflection is reduced when the tire stiffness k_t is high.

The conclusion is that no passive suspension is able to provide the best filtering for both comfort and road-holding objectives. The passive suspension configuration is always a trade-off between criteria. There is a number of publications where the design of optimal or sub-optimal passive suspension is conducted (e.g. [120] or [121]). The application of the controlled suspension where the damping might be changed between soft and stiff in real-time, creates the opportunity to improve the performance of the system in the entire frequency spectrum for both considered objectives.

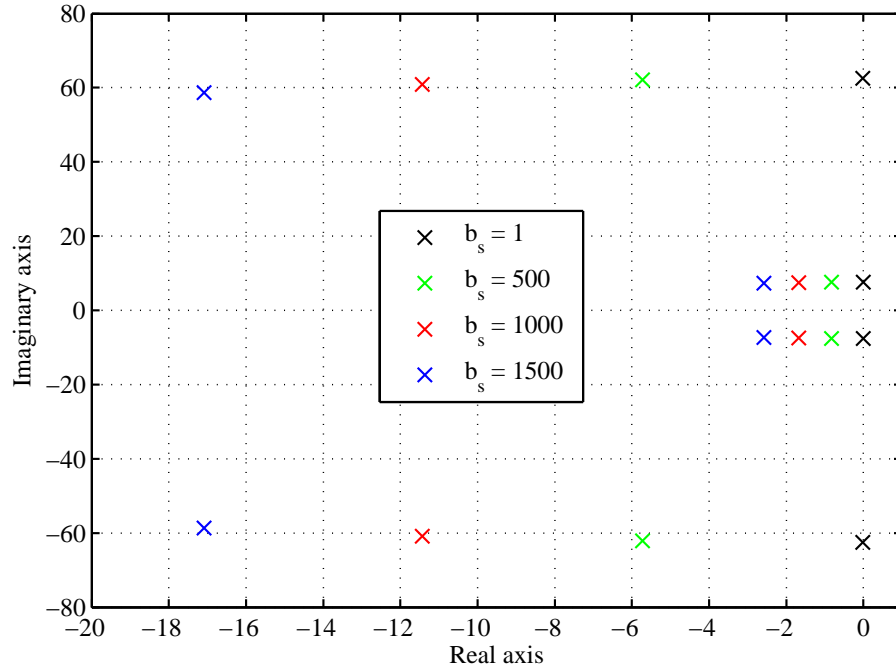


Figure 4.7: System poles diagram.

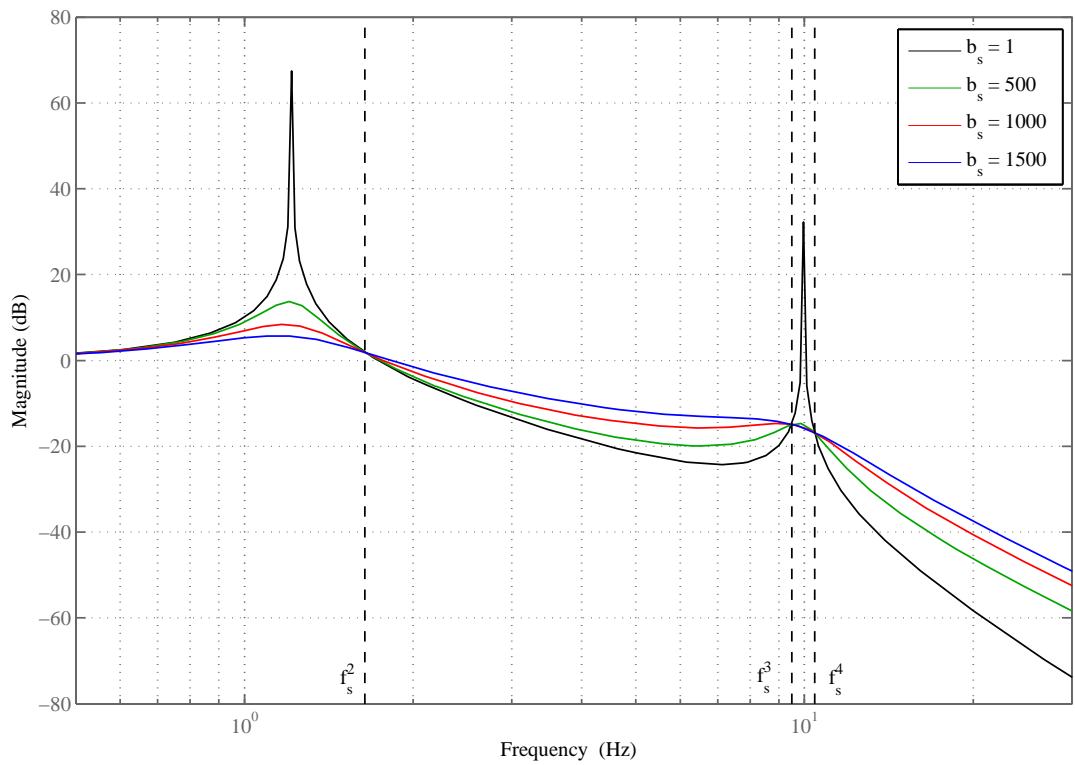


Figure 4.8: Frequency response of transfer function $F_s(s)$ for varying damping parameter b_s .

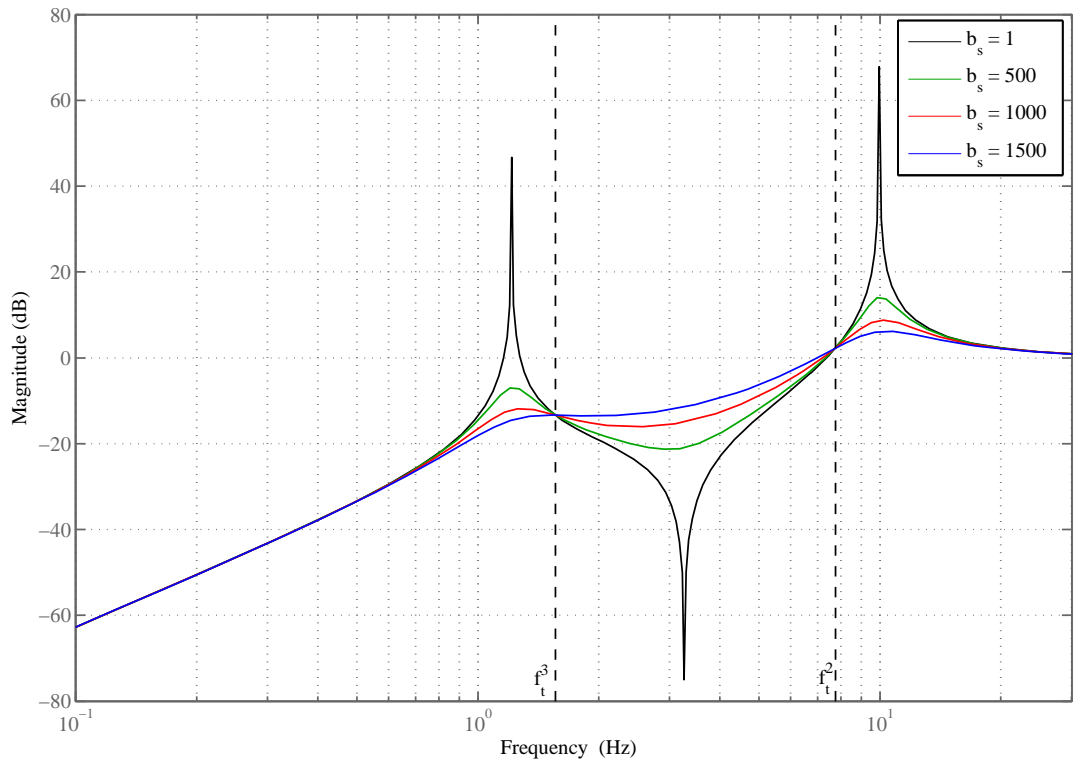


Figure 4.9: Frequency response of transfer function $F_t^d(s)$ for varying damping parameter b_s .

4.4. Control design for semi-active suspension

The control methods for semi-active suspension can be categorized as classical and advanced. The first group consists of relatively simple principles and is oriented towards performance of either comfort or road-handling, or both. The second group refers to more complex and sophisticated approaches which are either an extended or improved version of conventional strategies, or are based on control theory analysis, optimization, etc. This section presents the most important ones. In order to define control laws, the model utilized in section 4.3.2 needs to be re-designed for the controlled, semi-active shock absorber usage. For the sake of clarity the simple first order linear semi-active damper model is considered. The system is defined as follows:

$$\begin{aligned}
 m_s \ddot{x}_s + b_s^{sa} (\dot{x}_s - \dot{x}_t) + k_s (x_s - x_t) &= 0 \\
 m_t \ddot{x}_t + k_t (x_t - x_r) - b_s^{sa} (\dot{x}_s - \dot{x}_t) - k_s (x_s - x_t) &= 0 \\
 \dot{b}_s^{sa} &= b_s^T (b_s - b_s^{sa})
 \end{aligned} \tag{4.17}$$

where b_s is a semi-active damper control value (the steering signal of the examined control laws), b_s^T is a damper dynamics bandwidth and the damper's passivity constraints are b_s^{min} and b_s^{max} .

4.4.1. Classical control laws for semi-active suspension systems

In this section the conventional control strategies applied to semi-active suspension system are presented. The control policies are divided into three groups: comfort oriented, road-handling oriented and hybrid.

4.4.1.1. Comfort oriented control for semi-active suspension

This section briefly covers the well known and common in scientific researches control laws oriented towards comfort.

The two-state Skyhook Damper Control (SH-2). This method, developed in [122], considers a link between chassis (sprung mass) and an abstract point in the sky. The link is an imaginary damper unit the approximation or equivalent of which states the principle of this control strategy operation. The governing equation is as follows:

$$b_s = \begin{cases} b_s^{min} & \text{if } \dot{x}_s \dot{x}_s^d \leq 0 \\ b_s^{max} & \text{if } \dot{x}_s \dot{x}_s^d > 0 \end{cases} \quad (4.18)$$

The linear approximation Skyhook Damper Control (SH-L). This method is a natural extension of SH-2 control strategy with linear approximation. The improved version is as follows:

$$b_s = \begin{cases} b_s^{min} & \text{if } \dot{x}_s \dot{x}_s^d \leq 0 \\ b_s^{sat} \left(\frac{\alpha b_s^{max} \dot{x}_s^d + (1-\alpha) b_s^{max} \dot{x}_s}{\dot{x}_s^d} \right) & \text{if } \dot{x}_s \dot{x}_s^d > 0 \end{cases} \quad (4.19)$$

where $b_s^{sat}(b_s) = \min(\max(b_s, b_s^{min}), b_s^{max})$ is a saturation function and tuning parameter $\alpha \in [0, 1]$.

Acceleration Driven Damper Control (ADD). This control algorithm is in [123] and contrary to the previous strategies it utilizes acceleration of the sprung mass instead of the velocity. The damper control law is as follows:

$$b_s = \begin{cases} b_s^{min} & \text{if } \ddot{x}_s \dot{x}_s^d \leq 0 \\ b_s^{max} & \text{if } \ddot{x}_s \dot{x}_s^d > 0 \end{cases} \quad (4.20)$$

Mixed SH-ADD Damper Control (SH-ADD). This control strategy is a mix of best features of both SH and ADD [124]. The control law is defined as follows:

$$b_s = \begin{cases} b_s^{max} & \text{if } \left((\ddot{x}_s^2 - \alpha \dot{x}_s^2) \leq 0 \wedge \dot{x}_s \dot{x}_s^d > 0 \right) \vee \left((\ddot{x}_s^2 - \alpha \dot{x}_s^2) > 0 \wedge \ddot{x}_s \dot{x}_s^d > 0 \right) \\ b_s^{min} & \text{otherwise} \end{cases} \quad (4.21)$$

where parameter α is the SH-ADD crossover frequency.

Power Driven Damper Control (PDD). Another control law is called PDD and it also makes use of spring stiffness coefficient [125]. In this case the algorithm is as follows:

$$b_s = \begin{cases} b_s^{min} & \text{if } (k_s x_s^d \dot{x}_s^d + b_s^{min} \dot{x}_s^d) \geq 0 \\ b_s^{max} & \text{if } (k_s x_s^d \dot{x}_s^d + b_s^{max} \dot{x}_s^d) < 0 \\ \frac{b_s^{min} + b_s^{max}}{2} & \text{if } x_s^d \neq 0 \wedge \dot{x}_s^d = 0 \\ -\frac{k_s x_s^d}{x_s^d} & \text{otherwise} \end{cases} \quad (4.22)$$

Balance Logic Damper Control. The last control algorithm oriented towards comfort worth mentioning is Balance Logic [126, 127]. The control governing equation is:

$$b_s = \begin{cases} b_s^{min} & \text{if } x_s^d \dot{x}_s^d > 0 \\ k_s |x_s^d| \text{sign}(\dot{x}_s^d) & \text{if } x_s^d \dot{x}_s^d \leq 0 \end{cases} \quad (4.23)$$

4.4.1.2. Road-holding oriented control for semi-active suspension

This section presents road-handling oriented control laws.

The two-state Groundhook Damper Control (GH-2). The two-state Groundhook law is obtained [128] in a similar way to the Skyhook law, although it applies to imaginary fixed point mounted in the ground. The control policy algorithm is as follows:

$$b_s = \begin{cases} b_s^{min} & \text{if } -\dot{x}_t \dot{x}_s^d \leq 0 \\ b_s^{max} & \text{if } -\dot{x}_t \dot{x}_s^d > 0 \end{cases} \quad (4.24)$$

The linear Groundhook Damper Control (GH-L). This is an extended version of the previous control law where damping is controlled in an continuous way, which is:

$$b_s = \begin{cases} b_s^{min} & \text{if } -\dot{x}_t \dot{x}_s^d \leq 0 \\ b_s^{sat} \left(\alpha b_s^{max} \dot{x}_s^d + (1 - \alpha) b_s^{max} \dot{x}_s \right) (\dot{x}_s^d)^{-1} & \text{if } -\dot{x}_t \dot{x}_s^d > 0 \end{cases} \quad (4.25)$$

where α is the tuning parameter.

The displacement-based two-states Groundhook Damper Control. This control law in contrast to conventional groundhook strategy defines control switching condition based on unsprung mass displacement and relative mass velocity [129]. The control algorithm is as follows:

$$b_s = \begin{cases} b_s^{max} & \text{if } x_t \dot{x}_s^d > 0 \\ b_s^{min} & \text{if } x_s \dot{x}_s^d \leq 0 \end{cases} \quad (4.26)$$

4.4.1.3. Dual comfort and road-holding oriented control for semi-active suspension

An example of the dual performance indexes oriented control is **Hybrid Skyhook-Groundhook Damper Control** [130, 131]. The logic combines the mentioned two control polices. The control laws are as follows:

$$b_s = b \left(\alpha b_s^{sh} + (1 - \alpha) b_s^{gh} \right) \quad (4.27)$$

$$b_s^{sh} = \begin{cases} \dot{x}_s & \text{if } \dot{x}_s \dot{x}_s^d > 0 \\ b_s^{min} & \text{if } \dot{x}_s \dot{x}_s^d \leq 0 \end{cases} \quad (4.28)$$

$$b_s^{gh} = \begin{cases} \dot{x}_t & \text{if } -\dot{x}_t \dot{x}_s^d > 0 \\ b_s^{min} & \text{if } -\dot{x}_t \dot{x}_s^d \leq 0 \end{cases} \quad (4.29)$$

where parameter b is a constant gain and the tuning parameter $\alpha \in [0, 1]$.

4.4.2. Advanced control strategies for semi-active suspension systems

The aforementioned conventional semi-active control policies feature (among others):

- Simplicity which results in real-time capabilities. Fast execution time of the control algorithm allows to fully exploit the technology advantage - the minimal reaction time of the MR damper shall be preserved and the control strategy shall produce output within that time.

- Independency from the model. As stated before, the model of the vehicle is highly complex and even if some simplifications are considered then the reduced model has uncertain and variable parameters, such as vehicle mass which depends on the cargo load and the actual number of passengers or wheel mass which depends on the utilized tire and wheel rim.

Nevertheless, most of the benefits of the classical control strategies come with a necessity of measurement of at least two system state signals, such as suspended mass displacement (x_s), velocity (\dot{x}_s), acceleration (\ddot{x}_s) or suspension deflection (x_s^d). The number of sensors increase the cost of the system and the fact that some of the signals are not measured directly and must be reconstructed (e.g., velocity signal from accelerometer) arise issues with accuracy, and leads to control performance decrease. In the literature, the problem of sensors reduction for SH-ADD control law has been tackled in [132], where only a single sensor is considered (accelerometer mounted on the chassis body) leading to results comparable with original SH-ADD algorithm. In [133] authors reduce the number of sensors to one for SH control strategy. Also the other classic control strategies have been improved with the usage of state-of-art control theory tools, the gain-scheduled SH [134], and an adaptive extensions [135, 136] to name a few.

Apart from the model-free control solutions, there is a large number of developed control laws involving techniques usually adopted to control design. The classic PID and Hybrid-Fuzzy PID controllers are developed in [137] and [138] and the sliding-mode control is considered in [139]. Nowadays researches focus on H_∞ control approaches (e.g. [140] or [141]) and LPV (Linear Parameter Varying) technique [142]. There are also case studies utilizing robust VSC (Variable Structure Controllers) [143], LQR control [144] and neural network and backstepping techniques [145]. Some of the authors apply predictive approaches such as MPC (Model Predictive Control) [146] and Hybrid-Model Predictive Control [147]. The sophisticated approaches come with drawbacks such as a need for a-priori ideal model knowledge, requirement for an accurate and full system state measurement or an on-line optimization procedure. Most of the listed features prevent the application of the control laws in the real-time automotive production system. The approach of the auto-industry mostly considers conventional control laws although the optimal and sub-optimal control design is also present and investigated. For example the sub-optimal control approach is proposed and implemented by Mitsubishi company [148] with one sensor measurement only.

5. SAS laboratory demonstrative system

This chapter is devoted to modeling and control of laboratory example of demonstrative semi-active quarter car suspension device. The case study presents an approach on how to mathematically model and identify parameters of the designed model of this particular apparatus. The developed model is used to prototype and virtually test the control algorithms. Next, the designed control laws are executed in real-time in the application to the real world SAS unit, and their performance is compared. The chapter is organized as follows. In the first section 5.1 the system overview is presented. Section 5.2 covers the model development and the following section 5.3 describes the control of SAS in real-time.

5.1. SAS overview

The complete SAS system is presented in Figure 5.1 while Figure 5.2 shows the laboratory setup spring and MR damper elements. The semi-active suspension laboratory system scheme is depicted in Figure 5.3. The device consists of three rotating elements: the eccentricity, the unsprung wheel and the sprung body. The small eccentric aluminium wheel (7) is driven by the DC high-torque flat motor with the gear generating vertical kinematic oscillations. The wheel is composed of the plastic rim (6) and the gum tire (5) and it is attached to the rigid frame through the arm (1). It rolls and oscillates due to the eccentricity movement. The generated wheel vibrations act on the body arm (2) throughout the suspension system which consists of two elements: the magnetorheological rotary damper (3) and the spring (4). Resulting vibrations of the body arm depend on the suspension system and the frequency of rotations of the eccentric disk. The apparatus is equipped with three incremental encoders HEDM-5055 measuring:

- the rotation angle of eccentricity α_0 ,
- the rotational angle α_1 between the wheel arm and the horizontal frame,
- the rotational angle α_2 between the body arm and the wheel arm.

The encoders resolution is 4096 impulses per revolution (accuracy equal to 0.001 534 rad). These three position sensors signals and corresponding reconstructed angular velocities ($\dot{\alpha}_0$, $\dot{\alpha}_1$ and $\dot{\alpha}_2$) constitute system outputs. There are two control input signals:

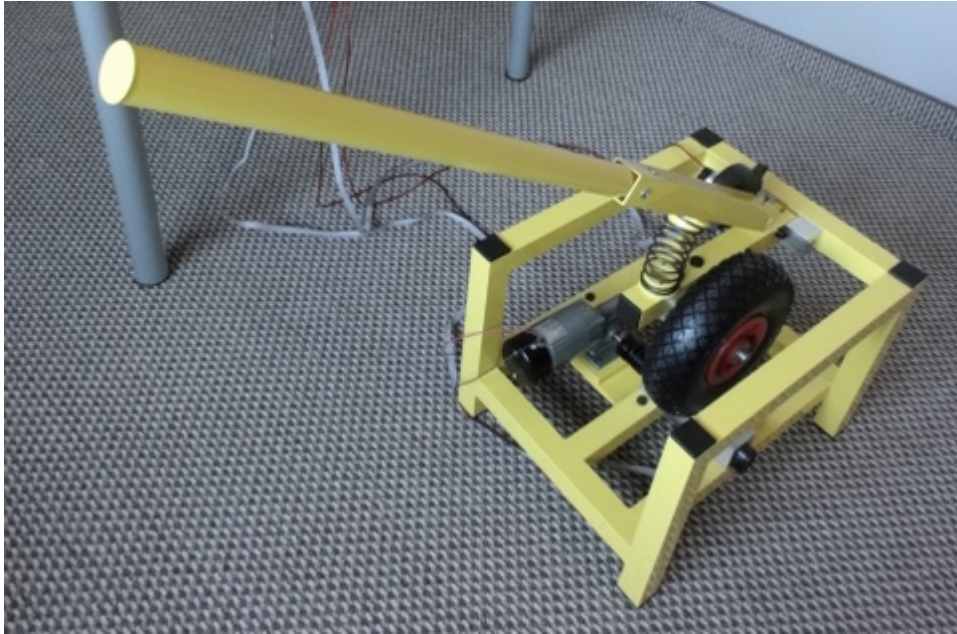


Figure 5.1: Photography of the laboratory SAS system. Source: [149].

- DC current,
- MR damper coil current.

The first PWM signal is designed to stabilize the rotating frequency of the eccentric disk. Since DC flat motor is coupled with the eccentric small wheel, the motor load varies with the angular position α_0 and the suspension system current state. This has a huge impact on the angular velocity and on the resulting small eccentric wheel frequency, and that is why $\dot{\alpha}_0$ controller is introduced (described in detail in section 5.1.1). The second PWM control adjusts the MR rotary brake coil current which in effect changes the damping friction coefficient. The SAS system uses RD-2087-01 MR rotary damper manufactured by Lord Corporation. For detailed brake's description please refer to section 5.1.2. The resolution of both PWM signals is set to 8 bits.

All examined input and output signals are connected to the interface and power supply unit. Control and data acquisition are conducted in MATLAB/Simulink real-time environment using the external RT-DAC/USB2 control and measurement board. System sampling period is set to 0.01 s.

The typical system encoder measured angles are shown in Figure 5.4. The angles α_1 and α_2 represent displacement from the steady-state positions for $\alpha_0 = 0$ (as shown in Figure 5.3). The eccentric wheel frequency is set to 1.35 Hz and the MR damper is inactive in this case (input current PWM is set to zero). One can notice an increasing magnitude of angular oscillations of the body. Reducing these oscillations to minimum via the MR rotary brake control is the goal of the system.

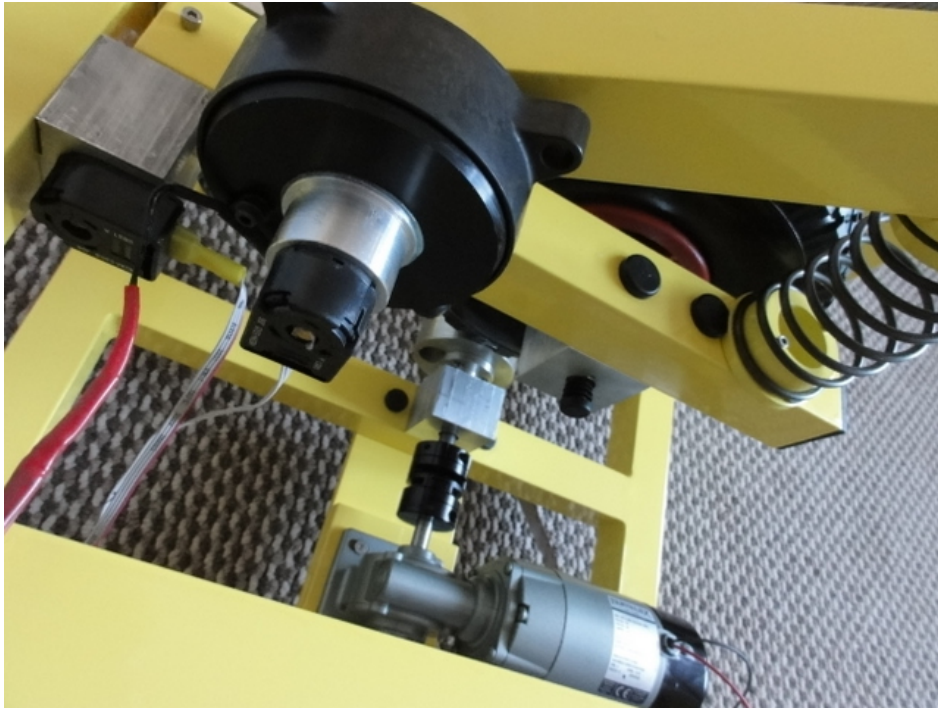


Figure 5.2: Photography of the semi-active suspension system's spring and MR damper unit.

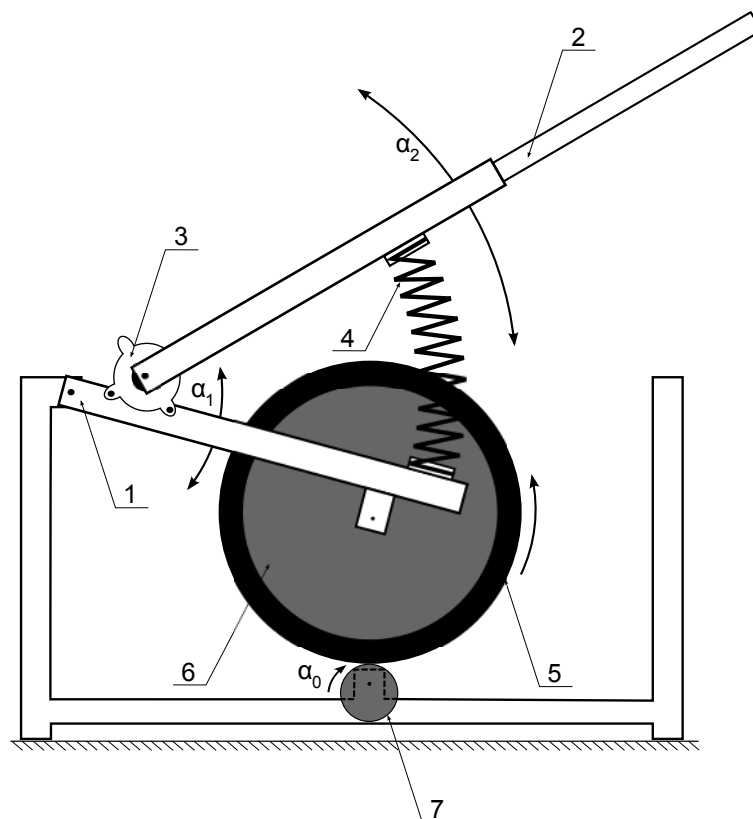


Figure 5.3: Scheme of the semi-active suspension system.

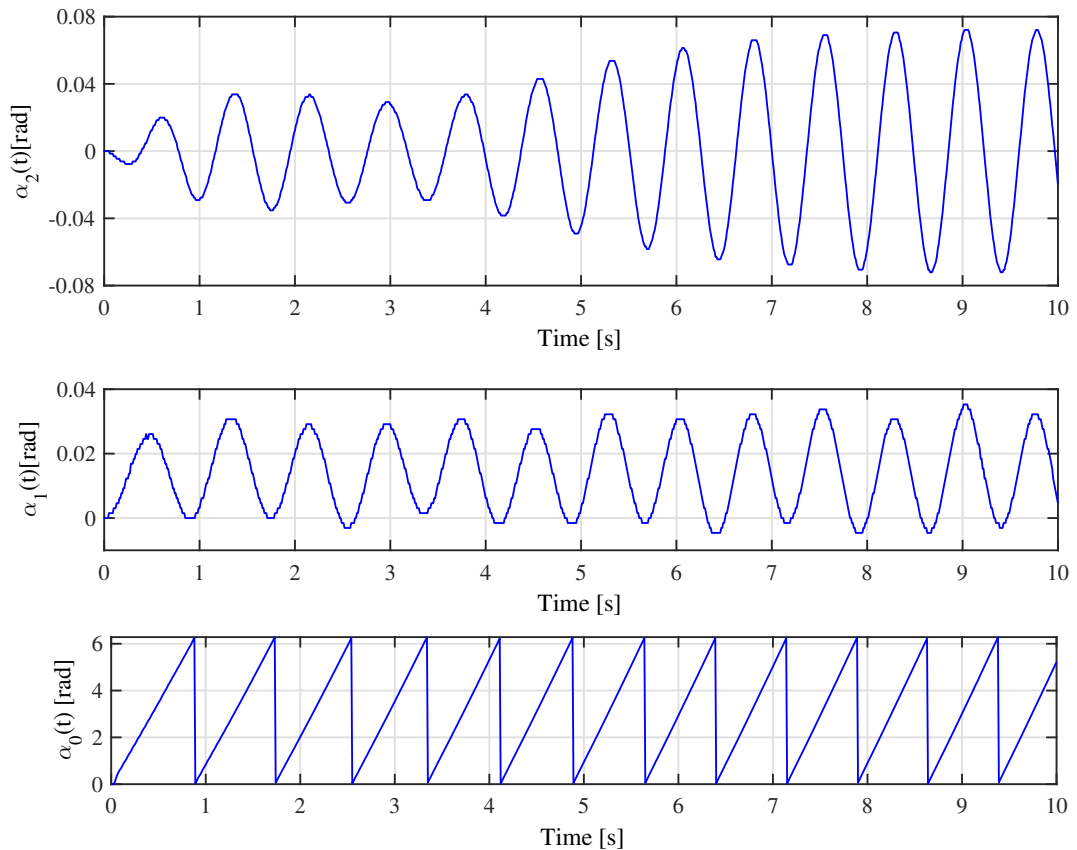


Figure 5.4: An example SAS system trajectories. Angular displacement from stationary point of body arm (α_2) and wheel arm (α_1) vs. time; eccentricity rotational angle α_0 vs. time.

5.1.1. Kinetic excitation controller

The kinetic excitation controller is applied in the SAS device. It is required due to the eccentric wheel angular velocity variations. A stable eccentricity rotation frequency is necessary for the proper model identification and measurement data interpretation. As noticed in section 5.1, the eccentric velocity disturbances are produced by a variable load due to the complex suspension structure and the rotational motion itself. In the first half turn (starting from the lowest position) the eccentricity raises the wheel (high load), while in the second half turn the wheel is lowered (small load). As a result, the kinetic excitation velocity varies around the value designated from the PWM control. Figure 5.5 and Figure 5.6 present the comparison of the kinetic excitation frequency in the case when eccentric wheel is rotating with and without load. One can notice that the application of the load introduces high signal oscillations especially for low frequencies where the differences reach even 2 Hz.

A frequency controller is introduced in [150]. Stabilization and compensation of disturbances is based on two inputs: the angular position (α_0) and angular velocity ($\dot{\alpha}_0$) of the eccentric wheel. In fact, the heuristic controller is a combination of position set-point tracking and velocity stabilization

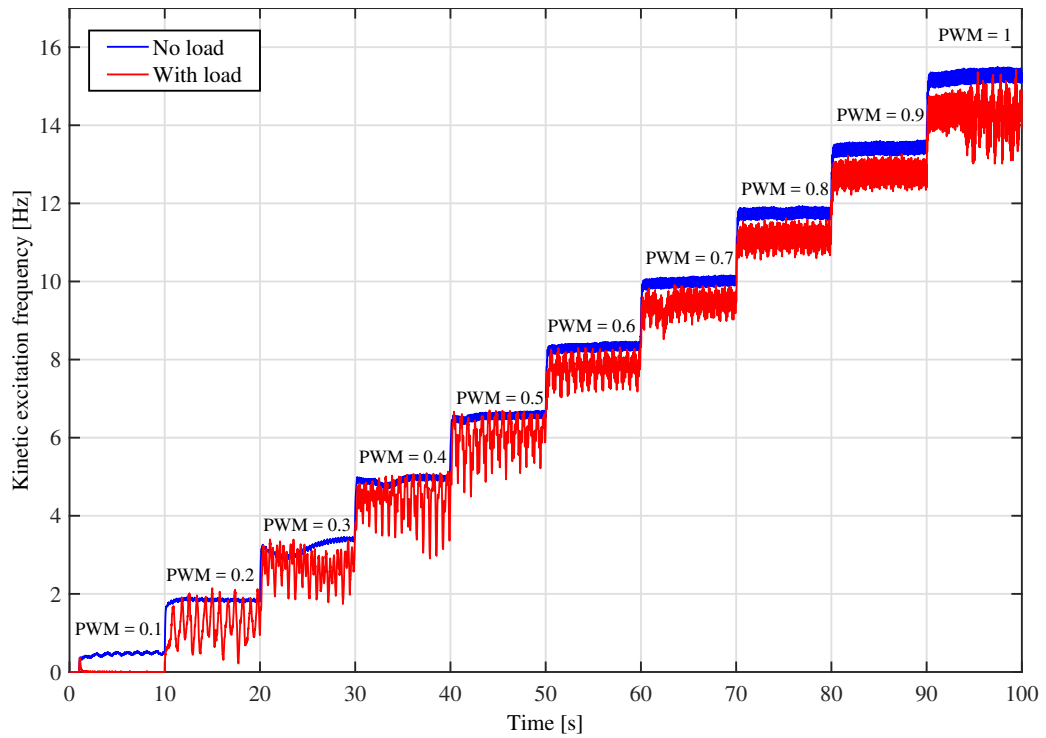


Figure 5.5: Kinetic excitation frequency vs. time with no load and after load application due to stairs PWM control of the DC motor.

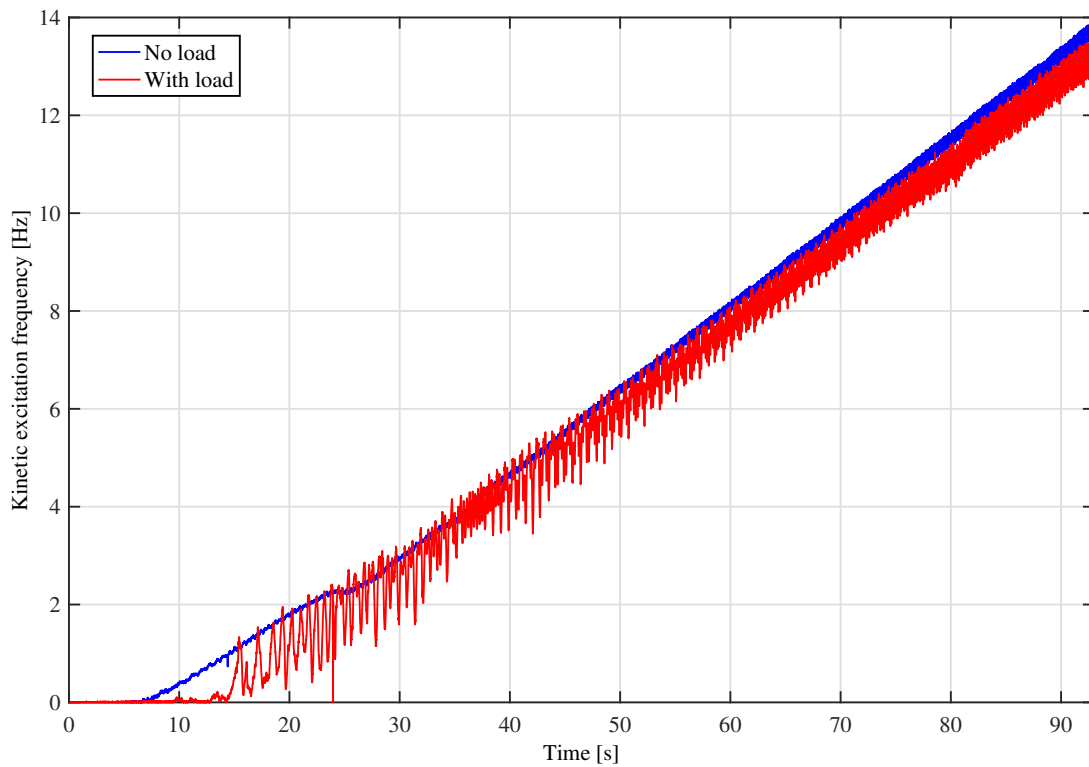


Figure 5.6: Kinetic excitation frequency vs. time with no load and after load application due to ramp PWM control of the DC motor.

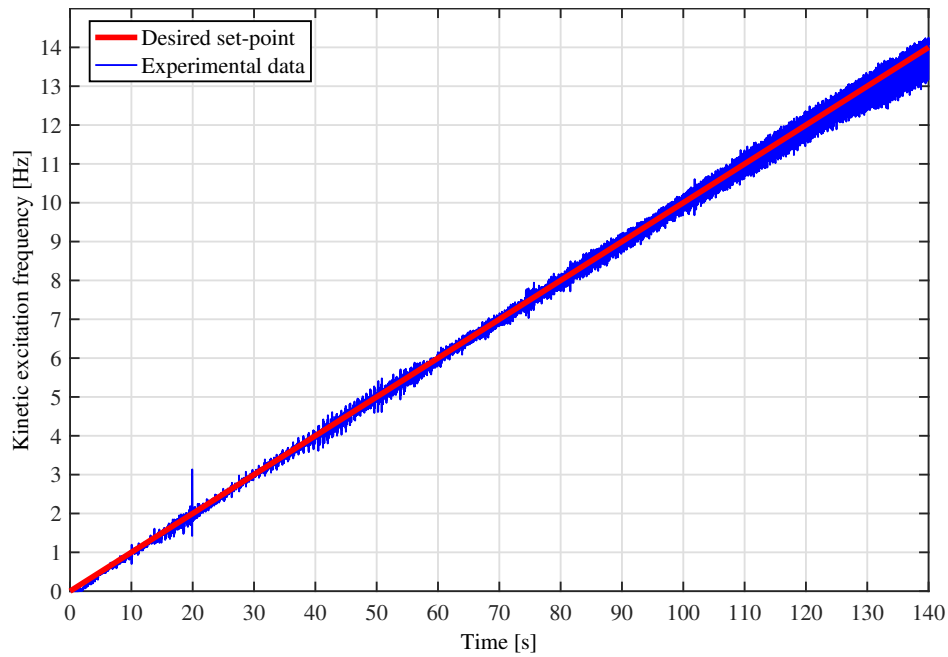


Figure 5.7: Set-point (ramp signal) and real measured frequency vs. time.

controllers (including PID algorithm).

The performance results of the controller operation are shown in Figure 5.7 and Figure 5.8. In both figures a solid line indicates the desired frequency value and the dotted line is an instantaneous frequency calculated from the measured eccentric wheel rotational angle. In comparison to Figure 5.5 and Figure 5.6 the resulting frequency is significantly more stable.

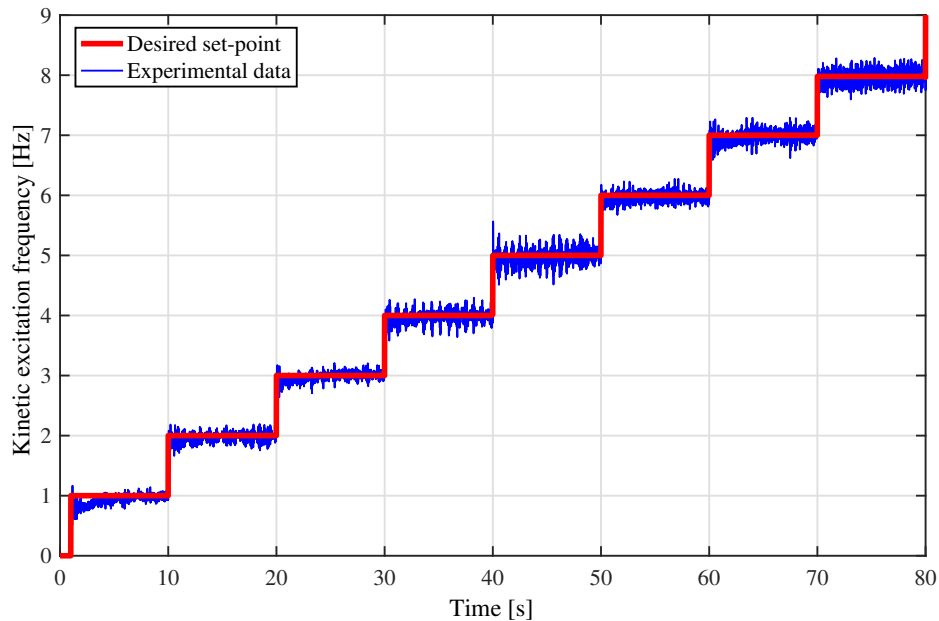


Figure 5.8: Set-point (stairs sequence signal) and real measured frequency vs. time.

5.1.2. MR rotary damper

The Lord RD-2087-01 rotary brake is a compact, magnetorheological fluid proportional brake suitable for a wide variety of applications. The magnetorheological fluid (MRF) is a suspension consisting of micron-sized, magnetizable particles and carrier liquid. In normal conditions (where there is no presence of a magnetic field) the fluid is free-flowing liquid. As the magnetic field is applied, the particles acquire a dipole moment aligned with the external field that causes particles to form linear chains parallel to the field. As a result, the MRF can solidify and restrict its movement ability [151]. The MR dampers use this phenomenon to provide increased torque output. One of the major benefits of the unit is the fast response time. The device reacts to the change of input current (PWM duty cycle) in less than 10 ms. This allows for efficient system control, so that body oscillations can be reduced [152].

5.2. SAS model and model parameters identification

The semi-active system model identification procedure is divided into two parts. Model's identification of the suspension and the wheel-eccentricity are conducted separately. Initially, the wheel arm is lifted to the horizontal position and it is immobilized. This settlement is suitable to obtain the spring and the MR damper parameters separately. Afterwards, the obtained model is rebuilt to take into account the wheel and the eccentricity. The established wheel lock is removed and the missing model parameters are estimated.

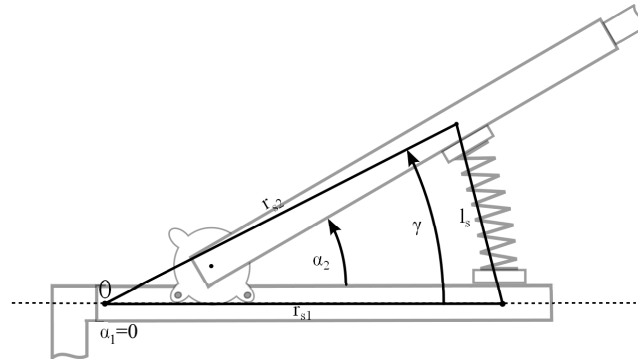


Figure 5.9: Structure of the suspension part model.

5.2.1. Suspension part model identification

The configuration where the wheel arm is locked in the plane position is depicted in Figure 5.9. In this horizontal arrangement the wheel angle (α_1) equals zero and it is considered as ground. A number of variables are introduced:

- r_{s1} - the distance between the spring mount on the wheel arm and the wheel arm axis of rotation,
- r_{s2} - the distance between the spring mount on the body arm and the wheel arm axis of rotation,
- γ - the angle between the wheel arm (the horizontal line) and r_{s2} .

The nonlinear differential equation used to represent dynamics is as follows:

$$I\ddot{\gamma} = k_s r_{s2} l_s(\gamma) - M \cos(\gamma) - k_{MR}(i)\dot{\gamma} \quad (5.1)$$

where

$$l_s(\gamma) = l_{s0} - \sqrt{r_{s1}^2 + r_{s2}^2 - 2r_{s1}r_{s2} \cos(\gamma)} \quad (5.2)$$

As can be noticed, a few simplifications are applied. The MR damper unit is virtually moved to the wheel arm pivot. Both in the discussed model and in the complete one, the mentioned axis acts as the axis of rotation for the two arms. Without this assumption the model becomes much more complex and a lot of problems may occur including the variable moment of inertia of the wheel arm or many geometrical issues. The next reduction concerns the spring. The actual length of the spring is calculated with cosine formula (5.2) using the real r_{s1} , the artificially introduced r_{s1} and the angle γ which slightly differs from the measured body arm angle of rotation α_2 . It is assumed that the spring obeys Hooke's law (k_s - elasticity coefficient, l_{s0} - the length of the no-load spring) and exerted restoring force at the end of the spring is perpendicular to r_{s2} . The simplest MR rotary brake parameter model is implemented in [153] where coefficient $k(i)$ is the function of the magnetic coil current $i(t)$ and the damping is proportional to the angular velocity $\dot{\gamma}$. I_1 is the moment of inertia of the wheel arm with respect to the introduced axis of rotation and M_1 stands for the gravitational moment of the body arm.

There are two primary objectives:

1. Estimate the suspension part model parameters.
2. Obtain the best matching MR damper static profile $k_{MR}(i)$.

In the identification procedure the following parameter reduced state equations are considered:

$$\begin{aligned} \dot{x}_1 &= x_2 \\ \dot{x}_2 &= a_1^1 l_s(x_1) - a_2^1 \cos(x_1) - b x_2 \end{aligned} \quad (5.3)$$

where

$$l_s(x_1) = l_{s0} - \sqrt{r_{s1}^2 + r_{s2}^2 - 2r_{s1}r_{s2} \cos(x_1)} \quad (5.4)$$

$$a_1^1 = \frac{k_s r_{s2}}{I}, a_2^1 = \frac{M}{I}, b = \frac{k_{MR}(i)}{I} \quad (5.5)$$

The distances $r_{s1} = 0.275$ m, $r_{s2} = 0.191$ m, $l_{s0} = 0.189$ m and the initial angular position of the body arm $x_{10} = 0.57$ rad are fixed and their values are measured or calculated directly. The system states denote respectively $x_1 = \gamma$ and $x_2 = \dot{\gamma}$.

In the first step the full set of adjustable parameters a_1^1 , a_2^1 and b are identified by real-time experiments based on the deflection from equilibrium angular position x_{10} with inactive MR rotary brake ($i(t) = 0A$). At this point the parameter b may be treated as the viscous friction coefficient. Five oscillation trajectories are collected (enumerated by i , $i = 1, \dots, 5$) corresponding to the different displacements from the steady-state (starting from the most significant deflection) and only the first $N = 500$ data points are considered. Each one consists of the directly measured γ and a reconstructed velocity $\dot{\gamma}$ and it is denoted as $x^i(n) = \{x_1^i(n), x_2^i(n)\}$ where $n = 0, 1, \dots, N$. The identification of parameters is done in MATLAB System Identification Toolbox and Optimization Toolbox using the grey-box model identification technique [154]. Consider the following quality indexes (cost functions):

$$Q_i(x^i, \bar{x}) = \sum_{j=1}^2 \sum_{n=1}^N (x_j^i(n) - \bar{x}_j(n))^2 \quad (5.6)$$

$$Q(x, \bar{x}) = \sum_{i=1}^5 Q^i(x^i, \bar{x}) \quad (5.7)$$

where $\bar{x} = \{x_1(n), x_2(n)\}$ and it is the trajectory generated by the model at the same time instants for the set of parameters $\{a_1^1, a_2^1, b\}$. x denotes merged experiments data points $\{x^1, x^2, \dots, x^5\}$. The minimization of the cost functions is performed with respect to the unknown set of parameters:

$$Q_i^{min} = \min_{a_1^1, a_2^1, b} Q_i(x^i, \bar{x}) \quad (5.8)$$

$$Q^{min} = \min_{a_1^1, a_2^1, b} Q(x, \bar{x}) \quad (5.9)$$

		a_1^1	a_2^1	b	Q_i^{min}	Q_i
Experiment i	1	526.61	22.07	0.20	2.40	2.44
	2	531.13	22.37	0.19	2.42	2.51
	3	535.59	22.64	0.23	2.06	3.33
	4	538.56	22.76	0.29	2.00	2.76
	5	542.34	22.91	0.43	2.13	2.70
All experiments		528.57	22.07	0.1921	$Q^{min} = 13.74$	

Table 5.1: Identified parameters and quality index values.

The estimation with the quality index in the form of (5.6) finds the best matching parameters for a single trajectory. This is contrary to the procedure that uses formula (5.7) which searches for the unique values common to all experiments.

The obtained results are shown in Table 5.1. Q_i are the quality index values calculated for the corresponding experiments and obtained parameters set for all real-time trajectories. The identified parameters common to all experiments vary at least from these estimated for the trajectories 1 and 2 (the highest displacement from equilibrium point), and deviate at most from the values found for the last experiment (the smallest deflection). One can notice that parameter a_2^1 differs the least among the estimated sets.

The comparison between real-time and commonly modeled trajectories is shown in Figure 5.10 (experiment 1) and in Figure 5.11 (experiment 5). Obviously, the best fit is attained for more significant magnitude oscillations (similar matching appears in the experiment 2). Less satisfactory results have been achieved near the steady-state position, however since our goal is to use the model to simulate the system behavior near the resonant frequency, where magnitude of oscillations rapidly increases, this inaccuracy is acceptable.

Having the model parameters a_1^1 and a_2^1 identified, the MR brake static profile can be obtained. The same mathematical model (5.3) is used although the mentioned parameters a_1^1 and a_2^1 are fixed. In this step the body arm is deflected by approximately the same value from the steady-state angle, however each time a different magnetic coil current $i(t)$ is applied. Twenty-one trajectories have been collected corresponding to the input current PWM duty cycles $u_{MR} = 0.05(i - 1)$ where $i = 1, 2, \dots, 21$. Since the oscillations cycles number decreases due to higher values of u_{MR} , the experiment data samples

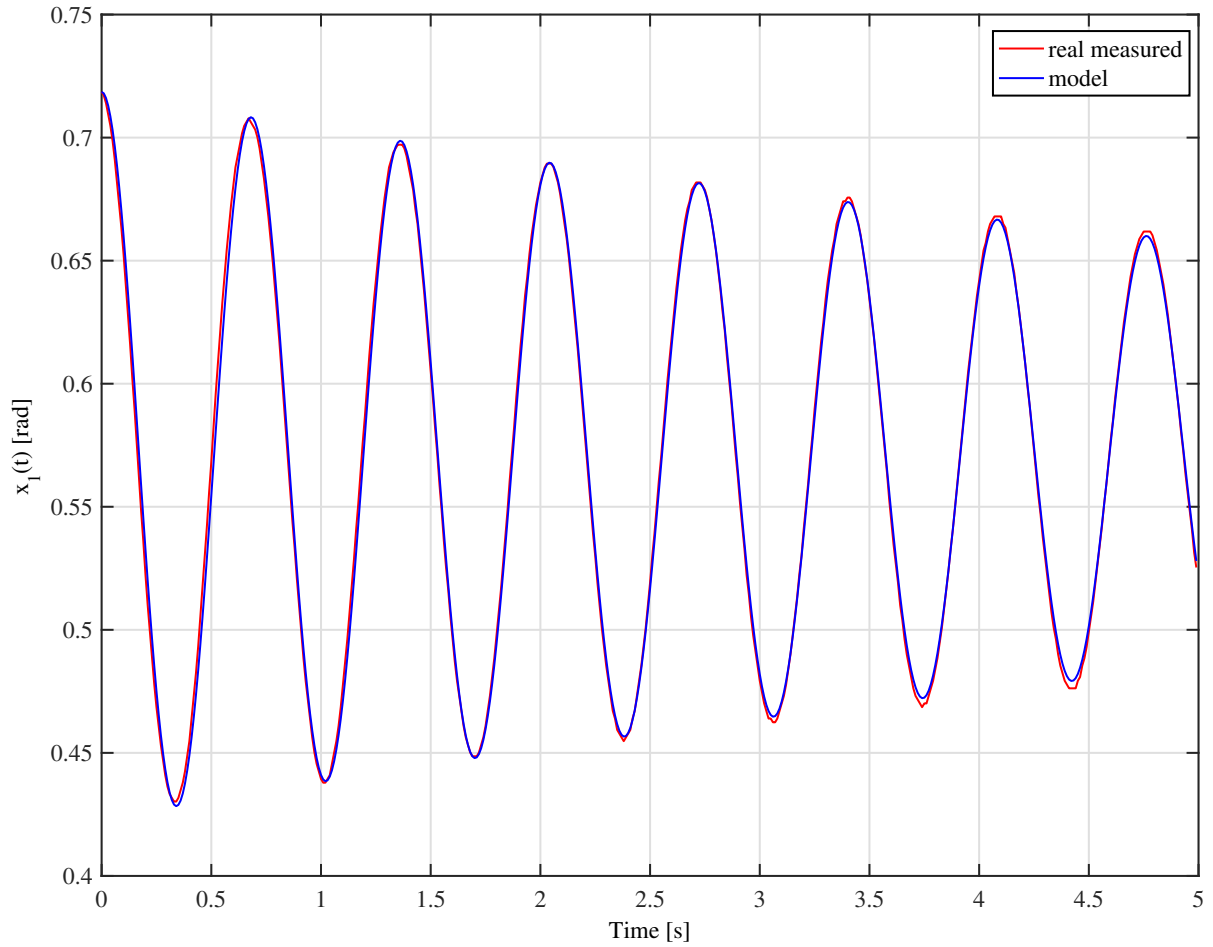


Figure 5.10: Body angular position x_1 vs. time in experiment 1.

number changed from 2700 to 200 and is denoted as N_i . The cost function takes the following form:

$$Q_i(x^i, \bar{x}) = \sum_{j=1}^2 \sum_{n=1}^{N_i} (x_j^i(n) - \bar{x}_j(n))^2 \quad (5.10)$$

and the minimization is performed for each i with respect to an unknown parameter b :

$$Q_i^{min} = \min_b Q_i(x^i, \bar{x}) \quad (5.11)$$

The obtained static profile of the magnetorheological rotary brake as damping coefficient function of u_{MR} is depicted in Figure 5.12. The visible points indicate estimated values b and the solid line is a continuous function (linear interpolation) introduced to test the model in the form:

$$\begin{aligned} \dot{x}_1 &= x_2 \\ \dot{x}_2 &= a_1^1 l_s(x_1) - a_2^1 \cos(x_1) - b(u_{MR})x_2 \end{aligned} \quad (5.12)$$

The verification procedure of the model (5.12) is based on two real-time experiments. The results are shown in Figure 5.13 and Figure 5.14. The figures illustrate the decreasing body angular position

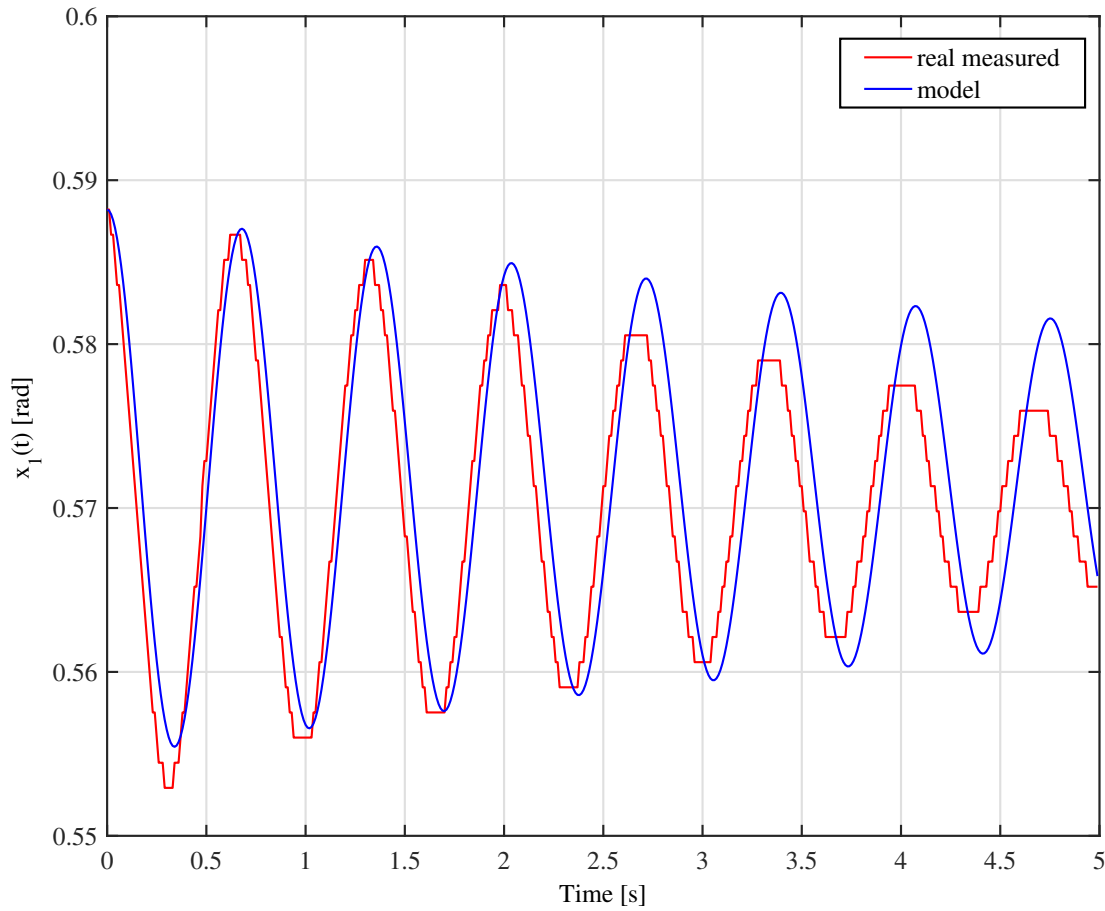
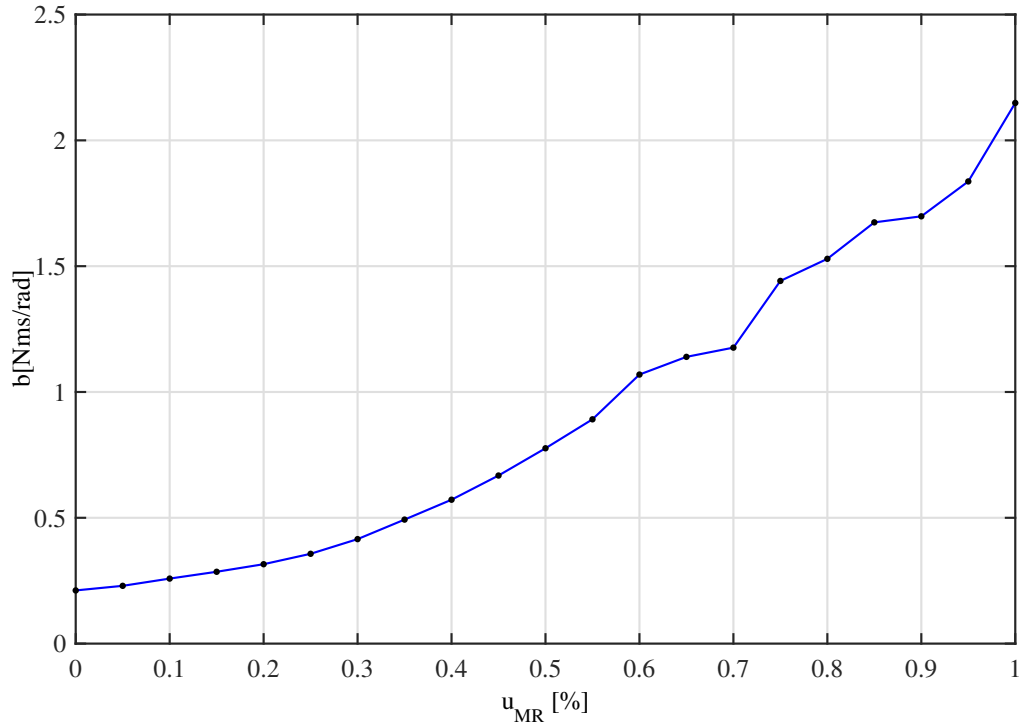
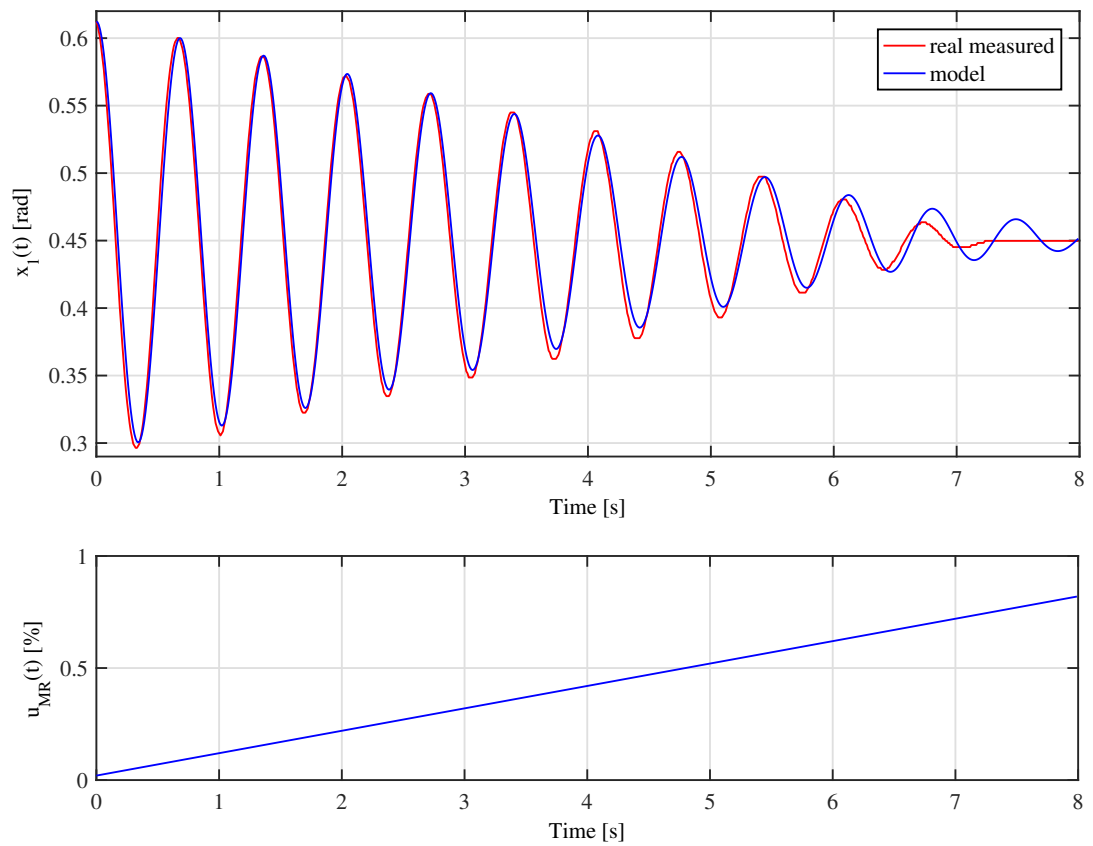
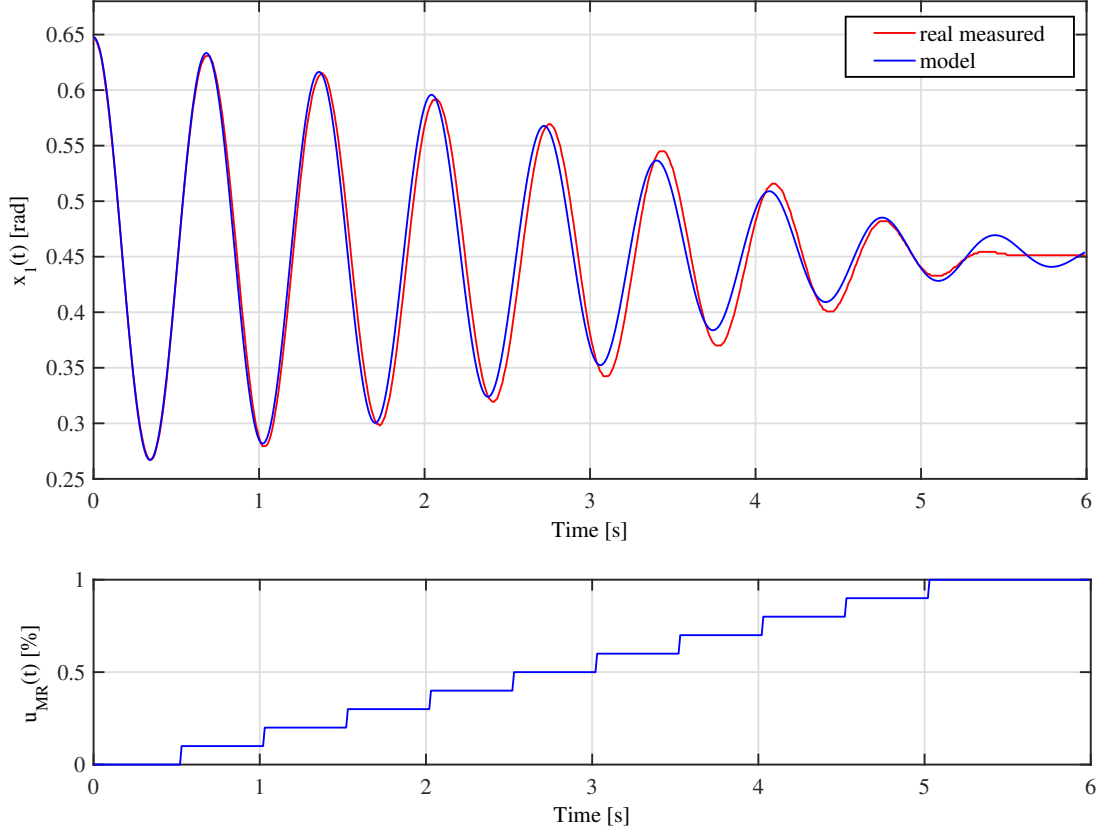


Figure 5.11: Body angular position x_1 vs. time in experiment 5.

oscillations due to the different u_{MR} signal. The real measured vibrations are marked with the red line, and the vibrations obtained from the model with the blue line. As can be noted, in general, modeled trajectories match real data points. The constantly visible error at the end of the motion is acceptable as mentioned above, and can be justified by the implemented model simplifications. The improved MR damper model is presented in section 5.2.3.

At this point with the parameters and the MR static profile obtained one can compute the value of k_s . The rotational inertia I is set to 1.37 kg m^2 and it is calculated using the formula for the moment of inertia of a rod with respect to the axis of rotation at the end of the bar. As a result $k_s = 3.79 \cdot 10^3 \text{ N m}^{-1}$, and the MR static profile is multiplied by the value I and labeled as $k_{MR}(u_{MR})$.

Figure 5.12: Obtained static profile $b(u_{MR})$ of MR damper.Figure 5.13: Body angle x_1 and MR damper control u_{MR} vs. time.

Figure 5.14: Body angle x_1 and MR damper control u_{MR} vs. time.

5.2.2. Identification of the wheel-eccentricity part model

The laboratory device diagram in the natural initial position is shown in Figure 5.15. The system of ordinary differential equations (ODE) representing complete mathematical model is the extended version of (5.1) with a number of changes as follows:

$$\begin{aligned}
 I_1 \ddot{\alpha}_1 &= k_t R \cos(\beta - \alpha_1) l_t(u_1, \alpha_1) + b_t \left(u_1 - \dot{\alpha}_1 R \cos(\beta - \alpha_1) \right) - k_s r_{s1} l_s(\alpha_1, \gamma) - \\
 &\quad - M_1 \cos(\beta - \alpha_1) + k_{MR}(u_2) (\dot{\alpha}_1 - \dot{\gamma}) \\
 I_2 \ddot{\gamma} &= k_s r_{s2} l_s(\alpha_1, \gamma) - M_2 \cos(\gamma) + k_{MR}(u_2) (\dot{\alpha}_1 - \dot{\gamma})
 \end{aligned} \tag{5.13}$$

where

$$\begin{aligned}
 l_s(\alpha_1, \gamma) &= l_{s0} - \sqrt{r_{s1}^2 + r_{s2}^2 - 2r_{s1}r_{s2} \cos(\gamma - \alpha_1)} \\
 l_t(u_1, \alpha_1) &= l_{t0} - \left(H - r - u_1 - R \sin(\beta - \alpha_1) \right)
 \end{aligned} \tag{5.14}$$

The second equation in (5.13) describing the dynamics of the body arm compared to equation (5.1) differs in the spring length calculation manner (the wheel arm rotates, consequently $\alpha_1 \neq 0$), and the static profile of the MR brake is multiplied by the angular velocities difference. The first equation, which is more complex, includes new distances:

- R - the wheel center rotation radius with respect to the pivot 0,

coefficient and b_t is the absorption coefficient of the tire). This approach requires additional model simplifications. It is assumed that the wheel tire does not slip on eccentric wheel during its rotations, and furthermore, that the wheel is always ‘coupled’ with the eccentricity (does not hop). The described behavior is present in the system (sliding is observed for higher eccentric velocities and the wheel jumping occurs near body resonant frequency). However, unless the model is dedicated to the lower eccentric frequency range, it can be successfully applied to reduce body oscillations which is the goal of the controller.

Same way as in section 5.2.1, the identification process is performed using parameter reduced state equations in a form:

$$\begin{aligned}
 \dot{x}_1 &= x_2 \\
 \dot{x}_2 &= a_1^2 \cos(\beta - x_1) l_t(u_1, x_1) + a_2^2 \left(\dot{u}_1 - x_2 R \cos(\beta - x_1) \right) - a_3^2 \cos(\beta - x_1) + \\
 &\quad + k_1^2 k_{MR}(u_2)(x_2 - x_4) - a_4^2 l_s(x_1, x_2) \\
 \dot{x}_3 &= x_4 \\
 \dot{x}_4 &= a_5^2 l_s(x_1, x_3) - a_6^2 \cos(x_3) + k_2^2 k_{MR}(u_2)(x_2 - x_4)
 \end{aligned} \tag{5.16}$$

where

$$l_s(x_1, x_3) = l_{s0} - \sqrt{r_{s1}^2 + r_{s2}^2 - 2r_{s1}r_{s2} \cos(x_3 - x_1)} \tag{5.17}$$

$$l_t(u_1, x_1) = l_{t0} - \left(H - r - u_1 - R \sin(\beta - x_1) \right) \tag{5.18}$$

$$\begin{aligned}
 a_1^2 &= \frac{k_t R}{I_1}, & a_2^2 &= \frac{b_t}{I_1}, & a_3^2 &= \frac{M_1}{I_1} \\
 a_4^2 &= \frac{k_s r_{s1}}{I_1}, & a_5^2 &= \frac{k_s r_{s2}}{I_2}, & a_6^2 &= \frac{M_2}{I_2} \\
 k_1^2 &= \frac{1}{I_1}, & k_2^2 &= \frac{1}{I_2},
 \end{aligned} \tag{5.19}$$

The state variables are adopted as follows: $x_1 = \alpha_1$, $x_2 = \dot{\alpha}_1$, $x_3 = \gamma$ and $x_4 = \dot{\gamma}$. The initial angular position of the wheel arm is obtained through the encoder indications, calculated as the difference between the wheel arm horizontal alignment and the normal position where the wheel lies on the eccentricity. In the result, the measured value x_{10} equals -0.19 rad. To determine the initial angle of the body arm x_{30} in the model (5.13) the following steps are taken:

1. The spring length calculation equation (5.4) in the model (5.3) is modified and takes the following form:

$$l_s(x_1) = l_{s0} - \sqrt{r_{s1}^2 + r_{s2}^2 - 2r_{s1}r_{s2} \cos(x_1 - \theta)} \tag{5.20}$$

2. The introduced θ is set to the wheel arm initial angle x_{10} .

3. The simulation of the revised model with previously identified parameters (5.5) is performed (starting from the formerly steady-state position).
4. The obtained equilibrium of the system is considered as x_{30} and equals approximately 0.36 rad.

The distances R, H, r and l_{t0} as well as the angle β are preliminary measured, although only the last three values are fixed from the beginning. Since the tire stiffness is large, it is difficult to precisely measure loaded tire thickness (expressed as $(H - r - u_1 - R \sin(\beta - x_1))$ in the formula (5.18)) in the system steady-state position. Instead, this value has been set to 0.0185 m (that is 0.0015 m less than no-load tire thickness), and distances R and H are adjusted using simple optimization procedure in such a way that:

- $l_t(u_{1min} = u_1(0), x_{10}) = 0.0015$ and
- $l_t(u_{1max} = 0.045, x_1 = -0.167)$ equals approximately to 0.002.

The angle $x_1 = -0.167$ is the encoder measured position of the wheel arm for the highest eccentric wheel level and the value 0.002 is introduced in order to guarantee that rubber tire is insignificantly more squeezed in the second case. The obtained values of R and H only slightly differ from measured lengths, and finally, the following fixed variables are used in the model (5.16): $R = 0.21$ m, $H = 0.22$ m, $r = 0.075$ m, $l_{t0} = 0.02$ m and $\beta = 0.234$ rad.

In order to obtain the set of final model parameters $p = \{a_1^2, a_2^2, a_3^2, a_4^2, a_5^2, a_6^2, k_1^2, k_2^2\}$ one real-time experiment is conducted. An experiment is performed for a ramp frequency signal applied to a kinetic excitation controller ($f_{u_1}(t) = 0.1 \cdot t$ Hz). The fitting pattern is considered as first $N = 2000$ data points. The PWM control signal u_2 of the MR rotary brake is set to zero. The values $u_1(n)$ where $n = 1, 2, \dots, N$ denote control calculated using formula (5.15) from a rotation angle $\alpha_0(n)$ of the eccentricity. The corresponding trajectory $x(n) = \{x_1(n), x_2(n), x_3(n), x_4(n)\}$ consist of:

- a directly measured $x_1 = \alpha_1$,
- a reconstructed velocity $x_2 = \dot{\alpha}_1$,
- an indirect measured $x_3 = \alpha_2 + \alpha_1$ (see Figure 5.15),
- a velocity $x_4 = \dot{\alpha}_2 + \dot{\alpha}_1$.

Similarly, quality index takes a form:

$$Q(x, \bar{x}) = \sum_{j=1}^4 \sum_{n=1}^N (x_j(n) - \bar{x}_j(n))^2 \quad (5.21)$$

where $\bar{x} = \{x_1(n), x_2(n), x_3(n), x_4(n)\}$ is a trajectory obtained for parameters p .

Again, the cost functions minimization is performed with respect to the unknown parameters \tilde{p} :

$$Q^{min} = \min_{\tilde{p}} Q(x, \bar{x}) \quad (5.22)$$

where \tilde{p} is the subset of the model parameters p . Several selecting approaches as to which parameters to fix and which to estimate are considered. Of course, the values of a_5^2 and a_6^2 are substituted with the

previously identified parameters a_1^1 and a_2^1 as well as k_2^2 is set to inverse value of the adopted $I = I_2$ in section 5.2.1. As it was noted, without further fixings, the optimization procedure tends to find parameters which match a pattern well, however their values do not have a physical meaning. In the course of the research it has been proven that making additional parameters constant during the estimation process does not decrease the quality of the model. In fact, the identified values have a relation to the reality. Initially, the moment of inertia of the wheel arm I_1 is set to the value 0.2116 calculated using a known formula $I_1 = m_1 R^2$ (the wheel mass m_1 is considered as the point mass at the distance R from the axis of rotation) hence $k_1^2 = 4.72$. Having I_1 we can also determine $a_4^2 = 4.92 \cdot 10^3$ using formerly estimated k_s . The last fixed parameter is $a_3^2 = \frac{m_1 g R}{I_1} = 46.71$, where $g = 9.81 \text{ m s}^{-2}$ stands for gravitational acceleration. After determining the fixed values of the model parameters described above, the estimating subset \tilde{p} becomes $\{a_1^2, a_2^2\}$.

As a result of quality index (5.21) minimization, the following parameters are identified: $a_1^2 = 1.08 \cdot 10^5$, $a_2^2 = 1.44 \cdot 10^3$ and the corresponding cost function value equals $Q^{min} = 34.39$. The estimation procedure has been repeated several times to ensure that the minimum is not a local one. The obtained model steady-state is slightly different from the one initially adopted and equals $x_0 = [-0.195 \ 0 \ 0.354 \ 0]^T$. The real-time experiment utilized as a pattern in the identification procedure has been transformed to take into account the new system equilibrium position and it is compared to the obtained modeled trajectory in Figure 5.16. As can be noted, both model states trajectories x_1 and x_3 (blue line) fit the experimental data (red line) well in most of the time instants. In fact, the model behavior is also correct beyond the range of frequencies used in the identification (Figure 5.17).

Having the last two parameters identified, we can calculate the missing parameters $k_t = \frac{a_1^2 I_1}{R} = 1.09 \cdot 10^5$ and $b_t = a_2^2 I_1 = 305.27$. At this point the complete model is identified and the last action is to test and verify the obtained static profile of the MR damper. Initially, the system behavior due to different u_2 values has been tested in a series of experiments similar to the one conducted in section 5.2.1 during the profile determination. As was expected, the modeled and experimental trajectories are similar. The second verification test is based on research of the model reactions to variable u_2 while the eccentricity rotates with constant frequency. Figures 5.18, 5.19 and 5.20 show the model performance for $f_{u_1}(t) = 1.6 \text{ Hz}$ and the MR damper control values u_2 in order 0.3, 0.7 and 1 in the steady-state. In this case the model quality is less satisfactory, however it is acceptable. The differences in the body oscillations amplitude between the modeled (blue line) and the measured values (red line) can be explained by the model simplifications made (mainly by the simple model of the MR brake). In Figure 5.20 we can also observe MR damper's impact on the body vibration frequency.

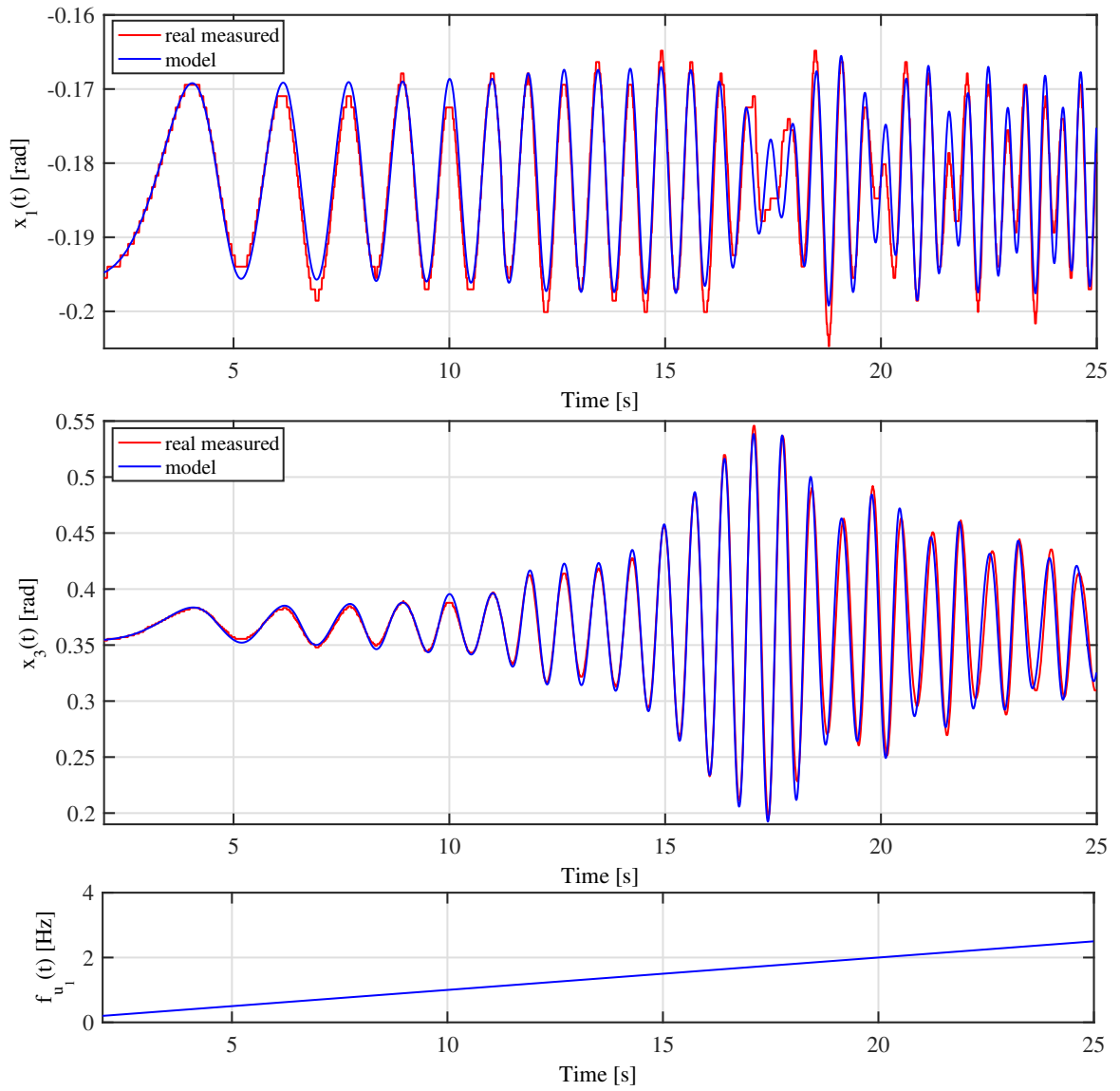


Figure 5.16: Wheel angular position x_1 , body angular position x_3 and set-point frequency for the kinetic excitation controller f_{u_1} vs. time.

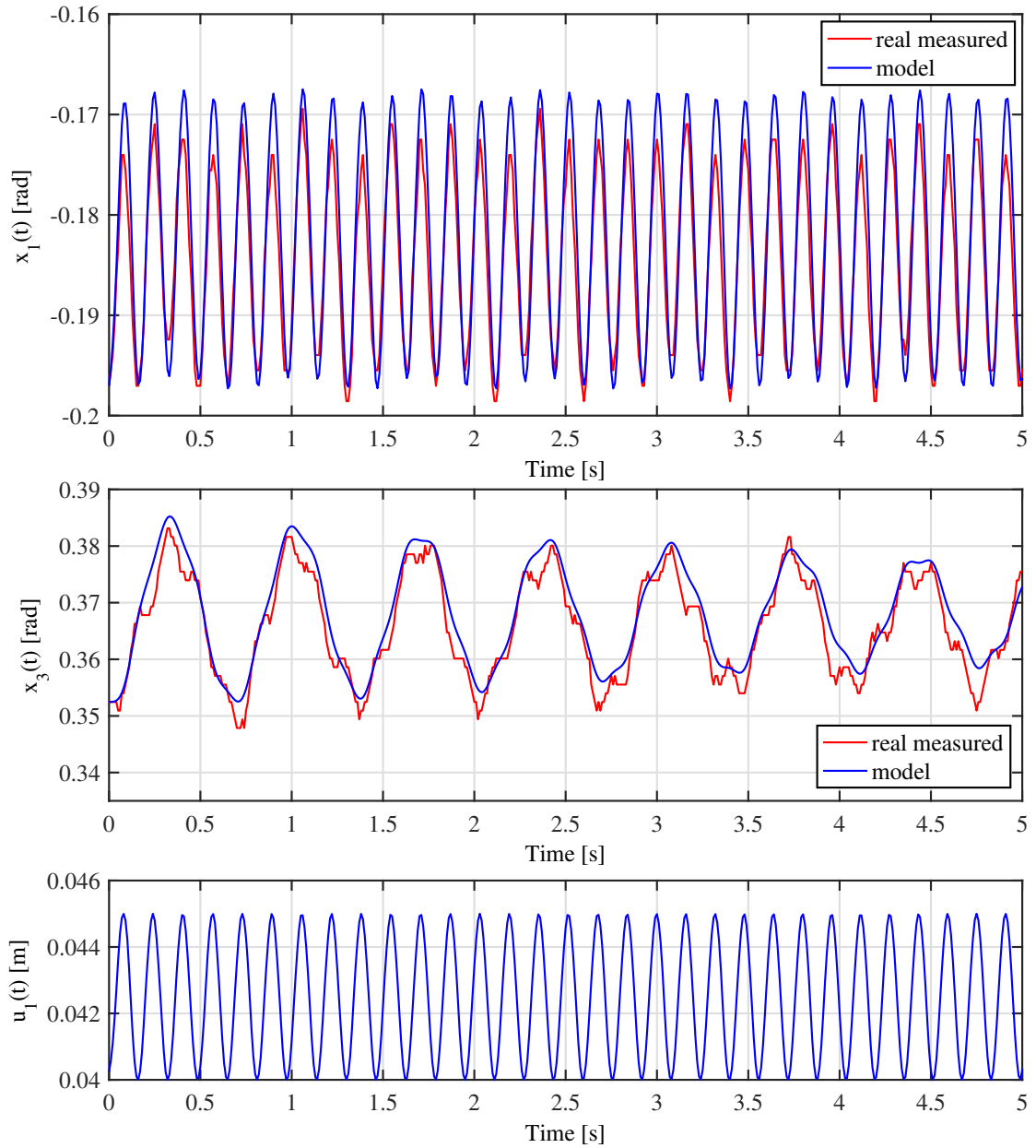


Figure 5.17: Wheel angular position x_1 , body angular position x_3 and control u_1 vs. time ($f_{u_1}(t) = 6.5$ Hz).

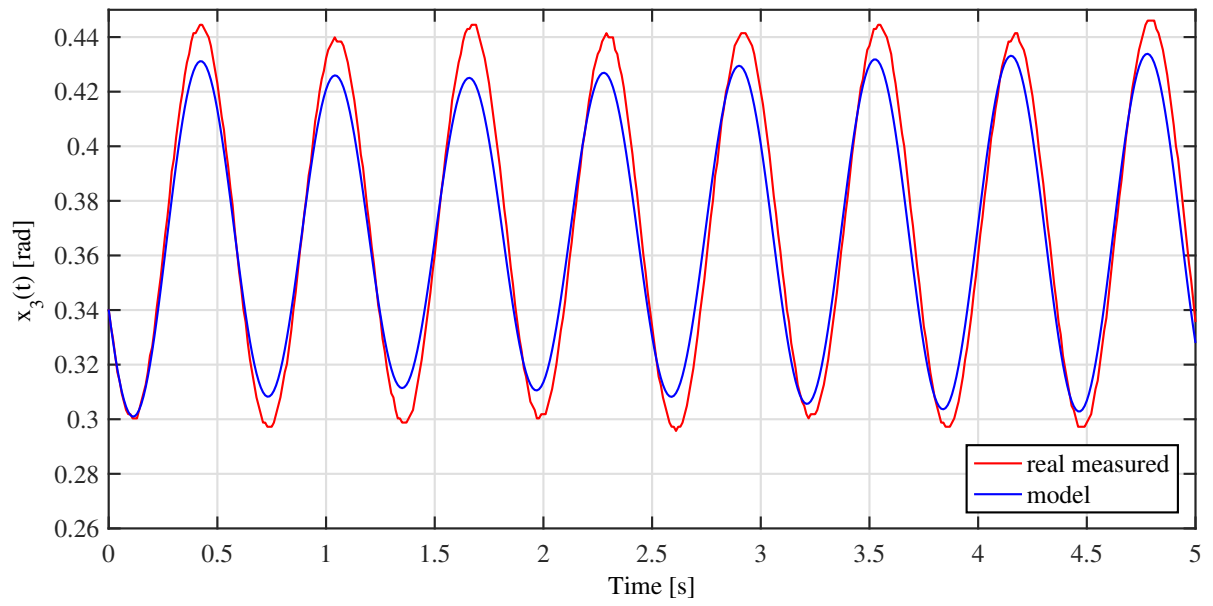


Figure 5.18: Body angular position x_3 vs. time ($f_{u_1}(t) = 1.6$ Hz, $u_2 = 30$ %).

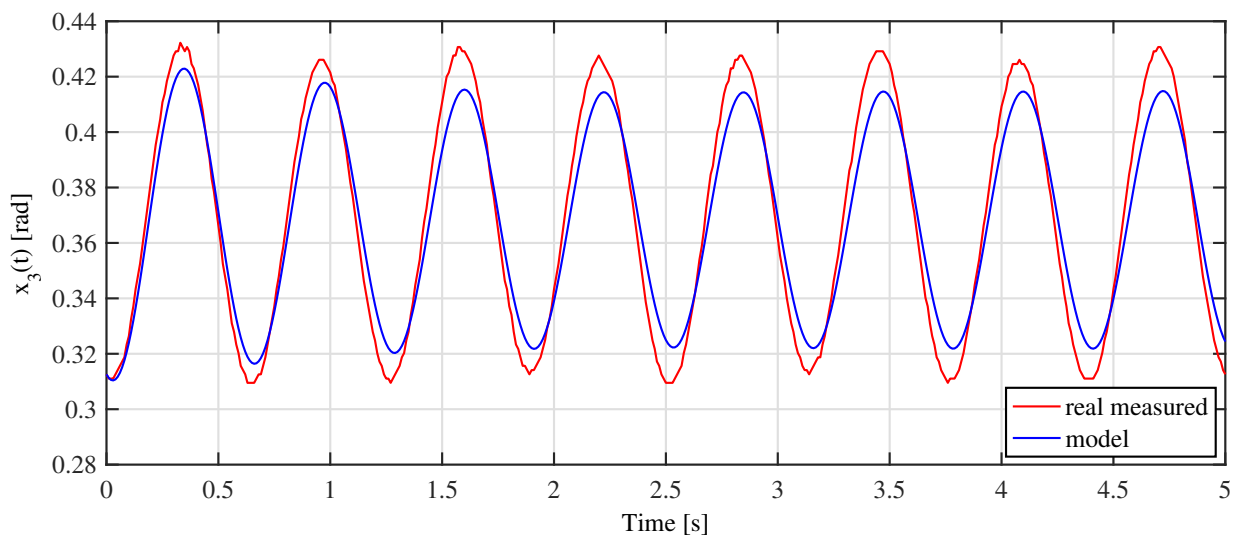


Figure 5.19: Body angular position x_3 vs. time ($f_{u_1}(t) = 1.6$ Hz, $u_2 = 70$ %).

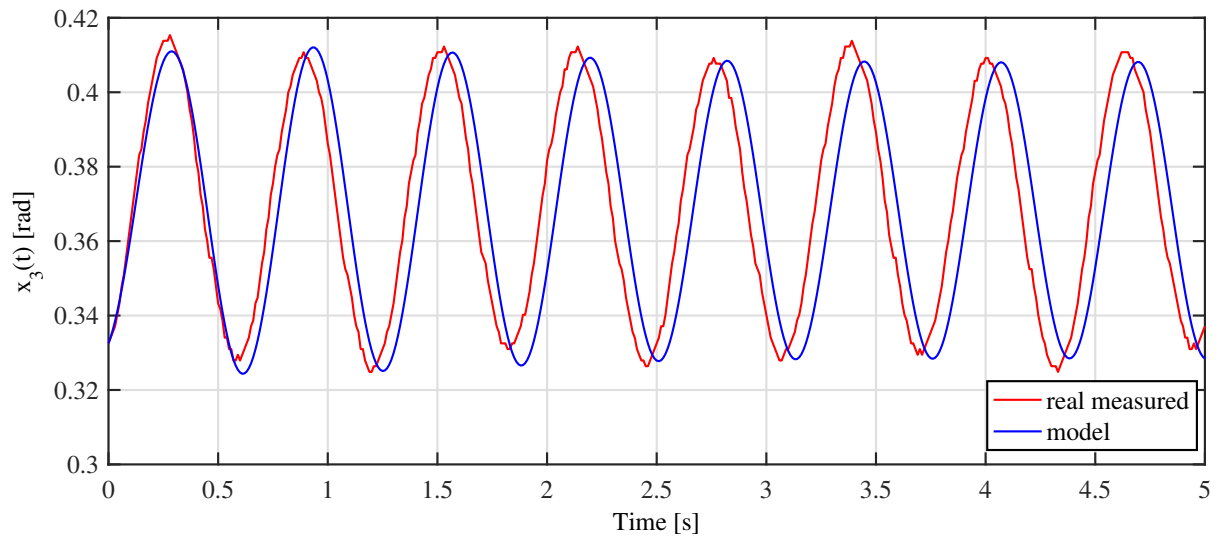


Figure 5.20: Body angular position x_3 vs. time ($f_{u_1}(t) = 1.6$ Hz, $u_2 = 100$ %).

5.2.3. MR-damper model improvement

Consecutive experiments show a poor accuracy of the curve not sufficient to simulate properly the frequency response of the system under varying frequency of the kinematic extortion. The simulated trajectories do not coincide with the real trajectories. Thus a need for a dynamic model of the MR damper occurred. Among many structures encountered in literature, the Bouc-Wen model is selected. The system of equations below shows the MR damper model adopted for the SAS:

$$\begin{aligned}
 T_{MR} &= \alpha(u_2)x_5 + c(u_2)(x_2 - x_4) \\
 \alpha(u_2) &= \alpha_1 + \alpha_2 u_2 \\
 c(u_2) &= c_1 + c_2 u_2 \\
 \dot{x}_5 &= -\gamma|x_2 - x_4|x_5|x_5|^n - \delta(x_2 - x_4)|x_5|^n + \theta(x_2 - x_4)
 \end{aligned} \tag{5.23}$$

The new state variable x_5 describes the hysteresis of the Bouc-Wen model. The model parameters: $\alpha_1, \alpha_2, c_1, c_2, \gamma, \delta, \theta$ and n are identified. The real trajectories of the arm motions are used. The direct measurement of the MR damper torque is unavailable. The experimental data corresponding to the chirp extortion signal is collected. Different values of the current in the MR damper coil (0, 0.1, ...1A) lead to gather the whole family of dynamical trajectories of the MR damper. MR damper characteristics for different coil currents are shown in Figure 5.21. Simulated and real trajectories are shown in Figure 5.22. In this case the chirp signal for the kinematic excitation is applied. The current in the MR damper coil is set to $u_2 = 1A$. The initial values of the c_1 and c_2 parameters are obtained by linearization of the $k_{MR}(u_2)$ function. The other parameters except n , are initialized in a heuristic way. The parameters have been estimated using the Optimization toolbox from MATLAB. The trial and error method has been used for different values of the parameter n .

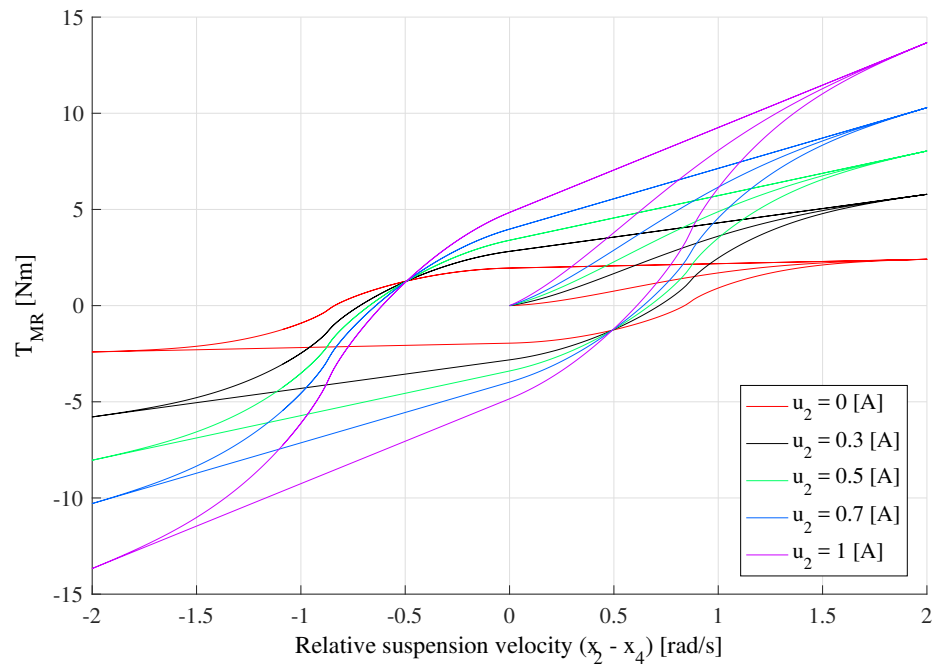


Figure 5.21: MR damper characteristics for different coil currents.

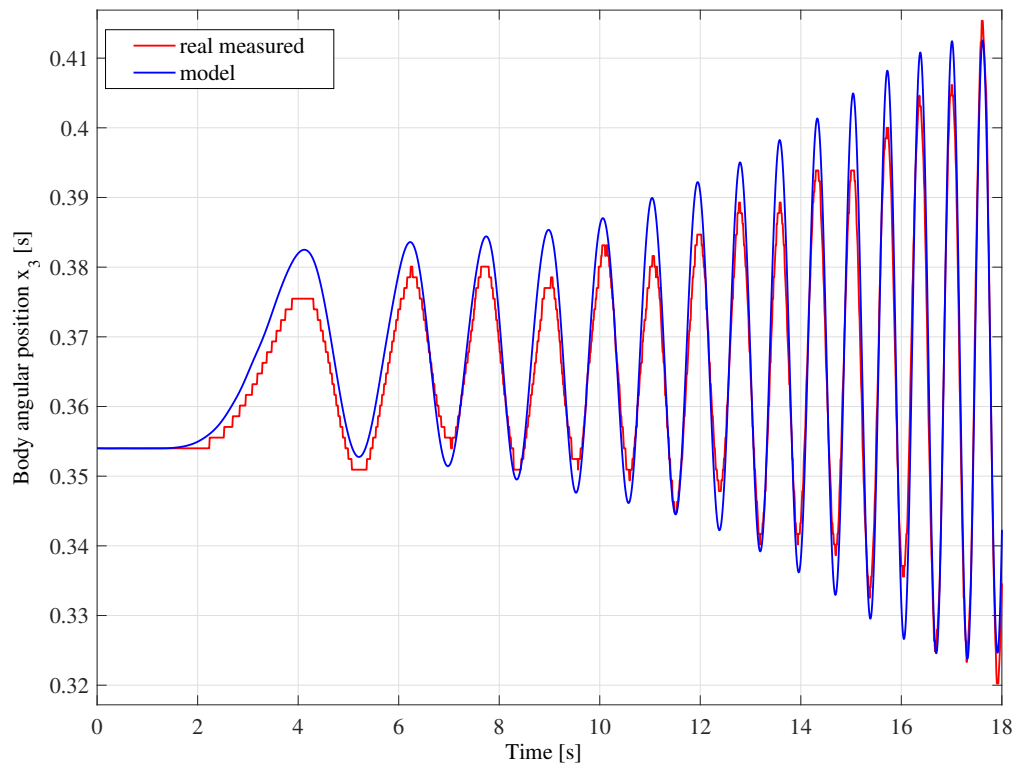


Figure 5.22: MR response to the chirp signal.

5.3. MR damper control strategies for SAS system

Several control strategies of the MR damper for SAS are realized [155]. The correctness and efficiency of the selected algorithms is verified on the basis of the previously identified dynamic model of the system described in sections 5.2.1 and 5.2.2 and the improved MR damper model obtained in section 5.2.3. In order to mimic the real world characteristics of the encoder signals the mathematical model is enriched with quantization blocks of the output encoder signals. This allows to more accurate examination of the controllers due to the fact that dynamics of the real system are rendered in more realistic manner. The following control strategies are considered:

1. On-Off skyhook control.
2. Continuous skyhook control.
3. On-Off balance control.
4. Passive-adaptive control.

The above control algorithms for the SAS system are shown in Table 5.2. One can notice that implemented control methods partially correspond to classical control laws for semi-active suspension systems presented in section 4.4.1. Controller 1 is the adapted version of the two-state Skyhook Damper Control (SH-2), Controller 2 is derived from the linear approximation Skyhook Damper Control (SH-L) and Controller 3 is based on Balance Logic Damper Control.

In order to examine the performance of the controllers the continuous cumulative root-mean-squared (RMS) value of the sprung mass acceleration \dot{x}_4 and control u_2 are chosen as the quality factors. The MATLAB/Simulink model containing both the SAS system model and controllers models is built and it is stimulated by kinematic extortion for the same time range equal to 20 s. Each stimulation is carried out for different kinematic excitation frequency from the range (0, 5) Hz. The inputs to all four controllers are ideal simulated models states. Additionally, controllers 1 and 2 are also tested with quantized equivalents of the model states. Aside from control generated by proposed controllers, the reference constant maximal control signal $u_2(t) = 1$ is also included.

The RMS results for different frequencies of the excitation signal are shown in Figure 5.23 and Figure 5.24. The numbers visible in Figures correspond to the controller numbers. The numbers equipped with stars are used to mark controller versions that are evaluated based on quantized velocities. Controller 4 is not shown in these Figures due to the fact that its performance is unsatisfactory. Controller 2 (among verified control strategies) is the best for reducing the sprung mass acceleration in the entire frequency range. It also demonstrates a lower power consumption in particular beyond the resonance frequency zone. Its version 2* working on quantized velocity achieves slightly worse results. Controllers 1 and 1* also correctly reduce the vibrations, although beyond the resonance zones they are less effective and

No.	Algorithm control laws implemented for the SAS
1.	$u_2 = \begin{cases} 1 & \text{if } x_4(x_4 - x_2) \geq 0 \\ 0 & \text{if } x_4(x_4 - x_2) < 0 \end{cases}$
2.	$u_2 = \begin{cases} \frac{\max\left[c_1, \min\left[c_1 + c_2, \frac{c_{sky}x_4}{x_4 - x_2}\right]\right] - c_1}{c_2} & \text{if } x_4(x_4 - x_2) \geq 0 \\ 0 & \text{if } x_4(x_4 - x_2) < 0 \end{cases}$
3.	$u_2 = \begin{cases} 1 & \text{if } l_s(x_1, x_3)(x_4 - x_2) > 0 \\ 0 & \text{if } l_s(x_1, x_3)(x_4 - x_2) \leq 0 \end{cases}$
4.	$u_2 = \begin{cases} 1 & \text{if } RMS(x_4) \geq RMS(x_2) \\ 0 & \text{if } RMS(x_4) < RMS(x_2) \end{cases}$

$$c_{sky} = 6$$

RMS values are calculated over a time period longer than that of the kinematic excitation

Table 5.2: SAS system control algorithms.

consume more energy than controllers 2 and 2*. Controller 3 in the resonance frequency peak works much worse than all other examined controllers when it comes to vibration reduction. One can also notice that in case of quantized state inputs, controller's 1* performance in terms of power consumption is comparable to the reference constant maximal damping. The results of assessment show that controller's 2 performance is highly dependent on the quality of input signals although this control strategy is the most promising approach for the SAS laboratory system

To improve the controller's 2 (continuous skyhook) operation for the real system where the angular velocities of the rig arms are quantized, a velocity observer is introduced in the form of the nonlinear autoregressive neural network with exogenous inputs (NARX). The following vector $[x_1^q \ x_2^q \ x_3^q \ x_4^q \ u_1]$ composed of the quantized states and control u_1 constitutes the input to the neural network. The output vector from the network forms the estimated velocities $[x_2^e \ x_4^e]$. The neural network consists of 20 neurons, has two layers and uses three antecedent input vectors. The neural network is built on the basis of the Neural Network Toolbox from MATLAB. In order to learn the NARX system the SAS model behavior the simulation data is utilized. The targets are obtained from the simulation model for the kinematic excitation of the chirp type in the resonance frequency range

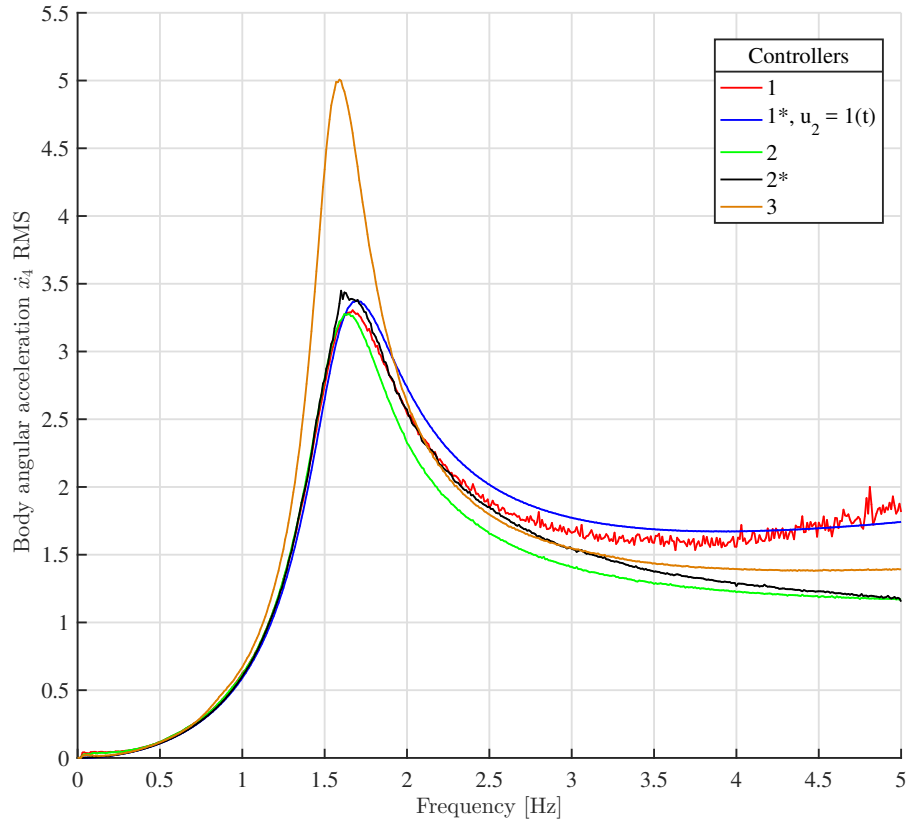


Figure 5.23: RMS accelerations of the sprung mass for different excitation frequencies.

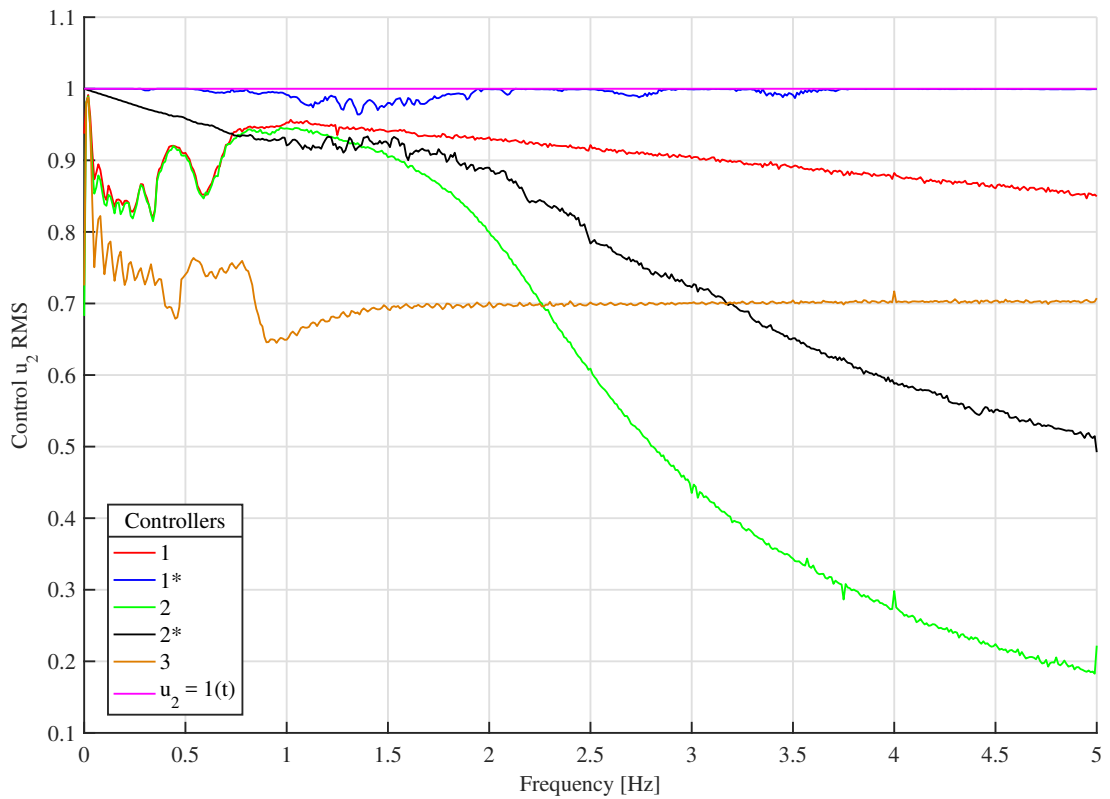


Figure 5.24: RMS controls of the sprung mass for different excitation frequencies.

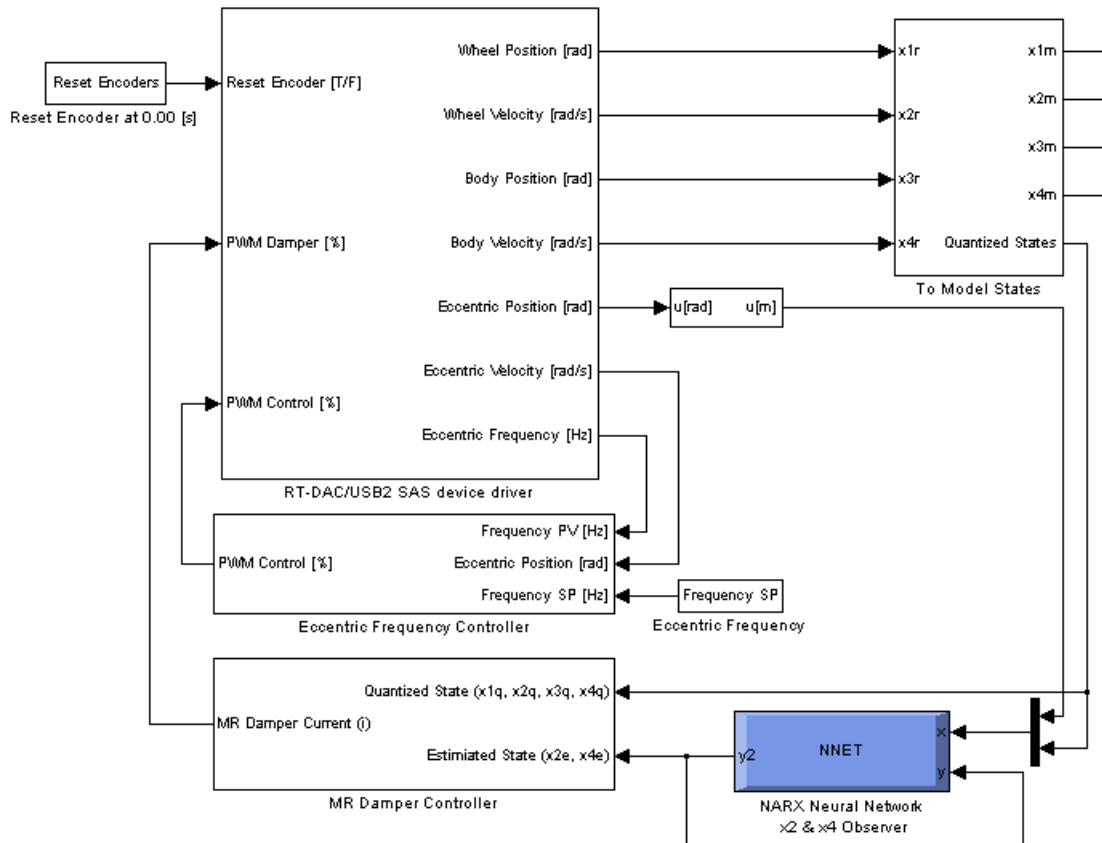


Figure 5.25: The SAS real-time MATLAB/Simulink model.

and the learning is executed by the back propagation of error method. The complexity of NARX system (number of layers and neurons) is chosen arbitrary to retain real-time computation capability of the target MATLAB/Simulink model where the results are finally utilized. After the NARX observer is learned and verified in SAS simulation environment, it is integrated into real-time MATLAB/Simulink model shown in Figure 5.25. The depicted model contains (among others):

- 'RT-DAC/USB2 SAS device driver' block which delivers real measured encoder signals and accepts computed PWM control signals,
- 'To Model States' block responsible for calculation of SAS system model states based on real measured encoder signals,
- 'NARX Neural Network x_2 and x_4 Observer' block,
- 'MR Damper Controller' sub-module accepting both the real measured quantized states and the estimated states from 'NARX Neural Network x_2 and x_4 Observer' block.

This setup is utilized to compare how the selected on-off and continuous skyhook control strategies perform in real world experiments in two configurations:

1. In case when the directly measured system state constitutes the input to controllers,

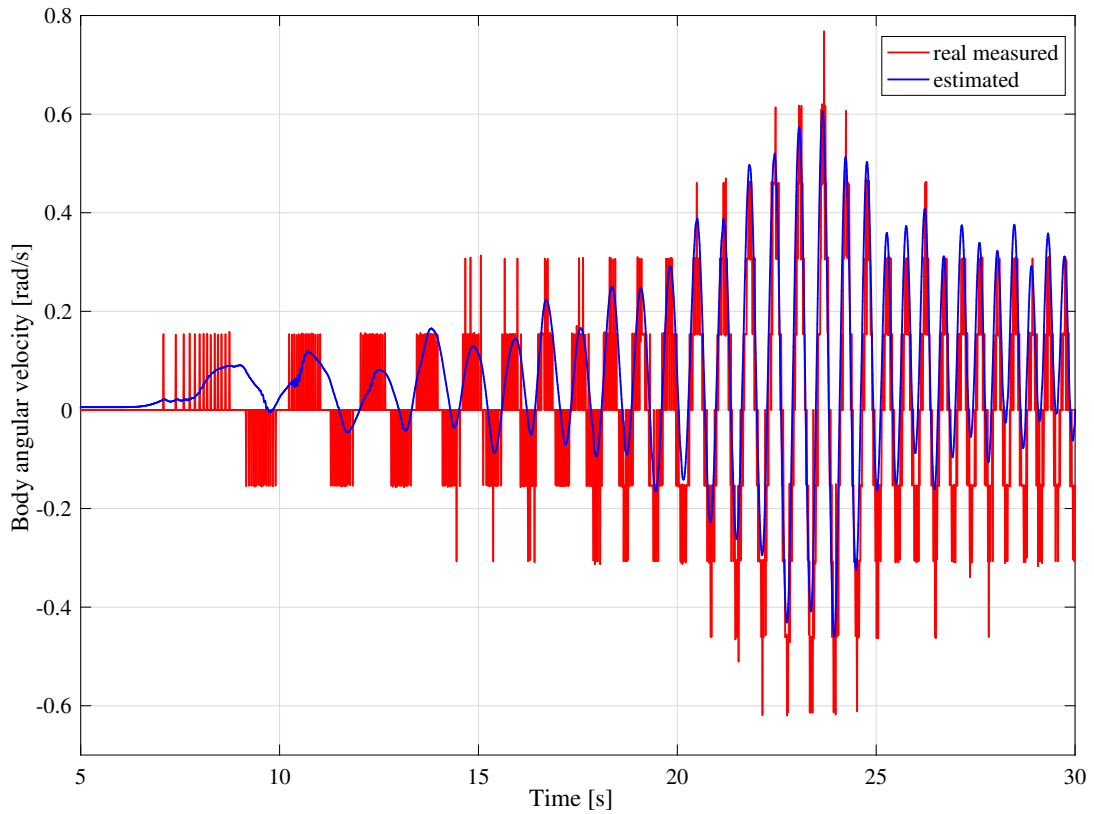


Figure 5.26: Estimation of the sprung angular velocity.

2. In case when the designed NARX system based observer is added into the feedback control loop and controllers utilize estimated system state.

Figure 5.26 illustrates the estimation results of the NARX system based observer for the upper arm and the experimental results of algorithm's performance comparison are shown in Figures 5.27 and 5.28. The presented results are obtained for the chirp excitation. It may be noted that for both control algorithms (on-off and continuous) the introduction of the estimator of the state improved the quality control. The maximum inclination of the sprung mass is in both cases smaller when the estimated state is utilized. The correction effect is more superior in case of continuous skyhook control strategy and this control algorithm achieved the best result. It is worth to mention that both for SAS system model and for real SAS system device the better results are obtained for the continuous skyhook method.

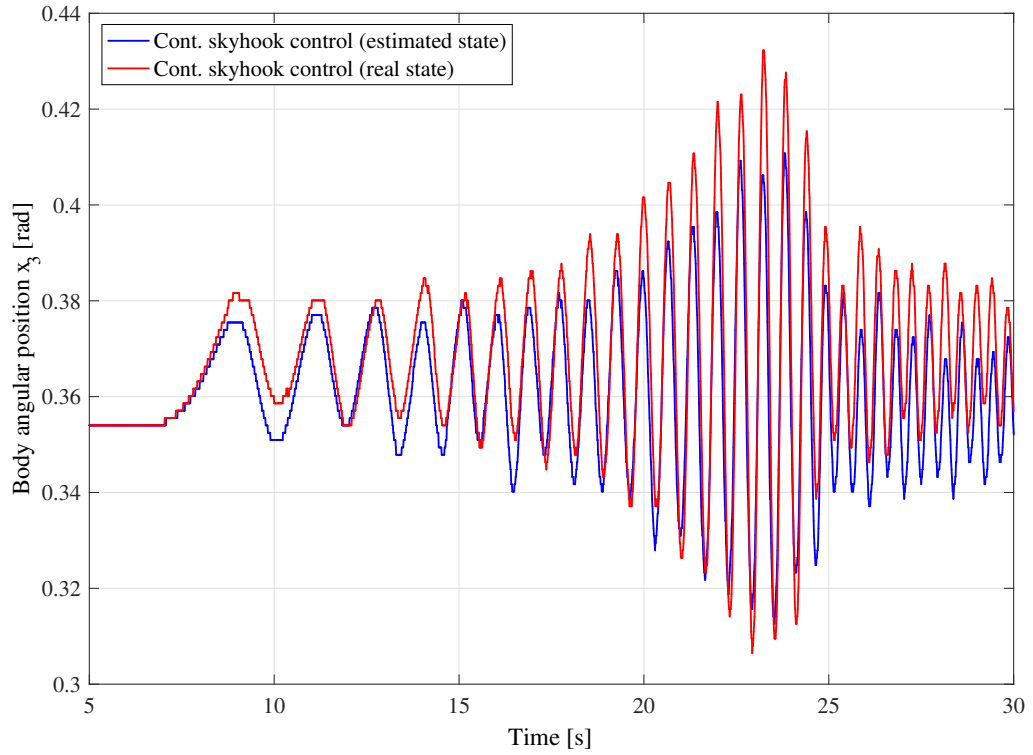


Figure 5.27: Continuous skyhook method with and without the state estimator.

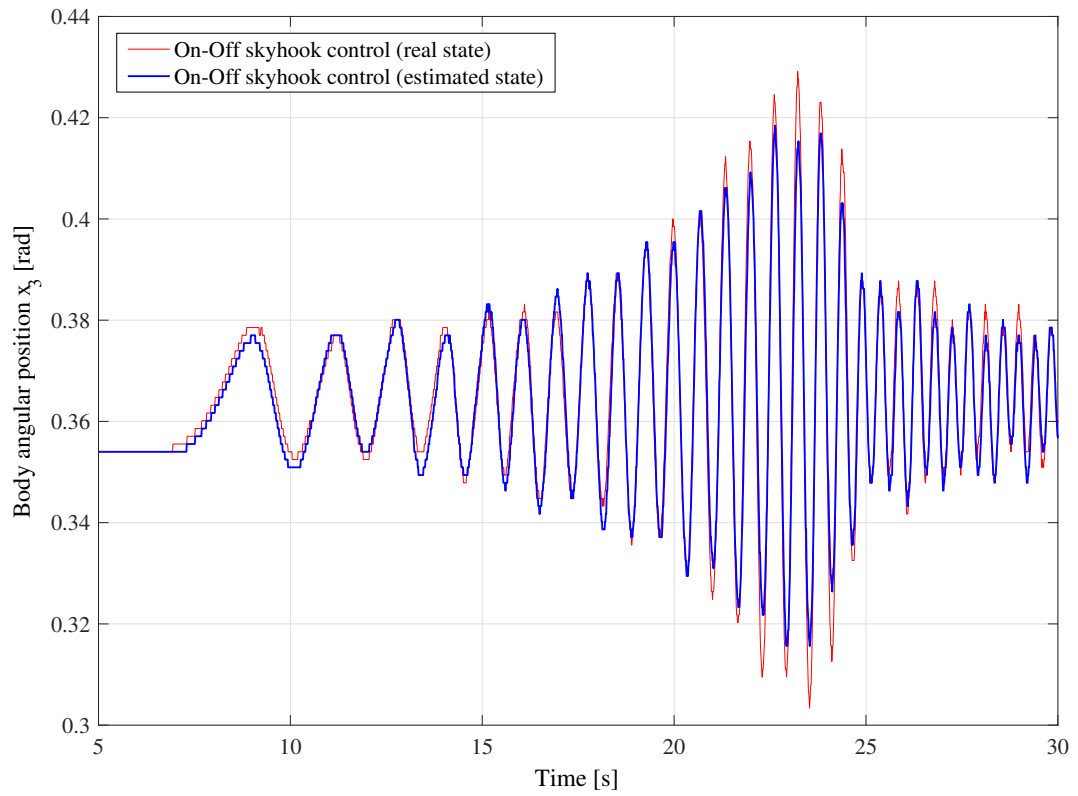


Figure 5.28: On-Off skyhook method with and without the state estimator.

6. Automotive braking systems

The automotive braking systems and anti-lock braking system is described. It is often recognized as the key automotive system that vastly improves road safety. Section 6.1 gives historical overview of automotive braking systems. In section 6.2 the common approaches for modeling of the braking vehicle dynamics are presented. Section 6.3 provides the motivation for ABS and describes its functions and goals. In section 6.4 the ABS system control state-of-art is presented.

6.1. Description of ABS

The first automotive braking solutions appeared together with early motor vehicles at the end of 19th century. Most of the wheels in the first cars were made from steel, and shoe brakes or external shoe brakes were used on the wheels running surfaces. Application of such systems started to decline when rubber tires were introduced in order to ensure more comfortable driving experience. At the beginning of 20th century, band brakes or sprag brakes were introduced although due to increasing speeds of the new vehicle prototypes, more efficient brake systems were needed. Drum brakes (patented by Louis Renault in 1902) started to be fitted in new vehicles in 1920 and remained the standard until 1950s. Simultaneously, the mechanical brake systems consisting of cables, levers and joints were found imprecise and faulty, and the auto-industry adopted hydraulic actuated aircraft solutions. The first European vehicle equipped with hydraulic brake system was Adler Standard in 1926. In 1955 the first mass produced vehicle, Citroen DS-19, was equipped with disc brakes. Improved disc and drum brake systems are still utilized today, and the trend is to fit all the wheels with disc brakes. Nowadays a typical mid-class vehicle is equipped with a hydraulic braking system (consisting of brake pedal, brake servo unit, master cylinder together with brake fluid reservoir, and a pilot pressure valve connected to wheels via pipes and hoses) which has front disc brakes and rear drum brakes. The first anti-lock braking systems were installed in trains in the early 1900s and then applied in B-47 bombers in 1947. Since 1950s the anti-skid systems were commonly installed in commercial and military planes in order to prevent the tires spin-outs and blowing of the tires during landing. At the same time, the problem of locking wheels while braking was addressed in vehicles, and the first automotive ABS device was presented by Ford Motor Company in 1954 called

Lincoln Continental Mark II. The system proved to be too costly and heavy, and was finally put aside. In 1966, Dunlop Maxaret developed the first purpose-built mechanical antiskid automotive system which was fitted into Rolls-Royce, Jaguars and Jensen FF vehicles. In the same year, the Chrysler company introduced a four-wheel ABS device called Sure-Brake. The first rear-wheel ABS with analogue control module and vacuum-controlled actuator of the brake pressure was developed by Ford and Kelsey-Hayes. The system was called Sure-Track and was offered in 1969 Thunderbirds and Lincolns. In general, the analog antiskid systems from 1960s were too slow to shorten the stopping distance although they had increased lateral stability. The age of modern digital electronic automotive anti-lock systems started in 1978 when Bosch company introduced anti-blockier system. Afterwards, other manufacturers such as Bendix, Kelsey-Hayes, Nissan, Teves or Sumitomo developed another electronically controlled anti-lock system which differed in configurations and control approaches. In 1986 Bosch added traction control called ASR (Acceleration Slip Regulation) or TCS (Traction Control System) and in 1995 Bosch ESP (Electronic Stability Program) was introduced which combined the ABS and TCS functionality, and improved vehicle stability through yaw control. In 1980s the ABS systems were only installed in luxury vehicles, and starting from mid 1990s such systems were fitted in more and more models. Finally, since 2004 ABS has been mandatory in all new passenger cars in EU. In the recent years auto-industry has focused on ESC (Electronic Stability Control) systems such as differential braking, Steer-By-Wire or active torque distribution. Also, more attention is paid to GCC (Global Chassis Control) approach which integrates all vehicle active control systems such as braking, steering and suspension (active or semi-active) into a single component.

6.2. Braking vehicle dynamics modeling

The approaches to the braking vehicle dynamics modeling are presented. Section 6.2.1 is devoted to the wheel longitudinal slip phenomenon, and to the modeling of the tire-road dynamics and friction. Section 6.2.2 presents models of the vehicle brake actuators. In section 6.2.3 two versions of vehicle dynamics models are provided.

6.2.1. Longitudinal slip ratio, tire-road dynamics and friction modeling

The most important variable utilized in the tire-road dynamics modeling is longitudinal slip defined as the difference between vehicle velocity (or actual vehicle axle velocity) and the equivalent rotational speed of the tire $r\omega \cos(\alpha_T) - V_x$ (see Figure 6.1). In the case when there is no sideslip (angle α_T) or sideslip is small (straight line braking maneuver) then the expression is reduced to $r\omega - V_x$. The longitudinal slip ratio (normalized velocity difference) is defined only if the vehicle is in motion as

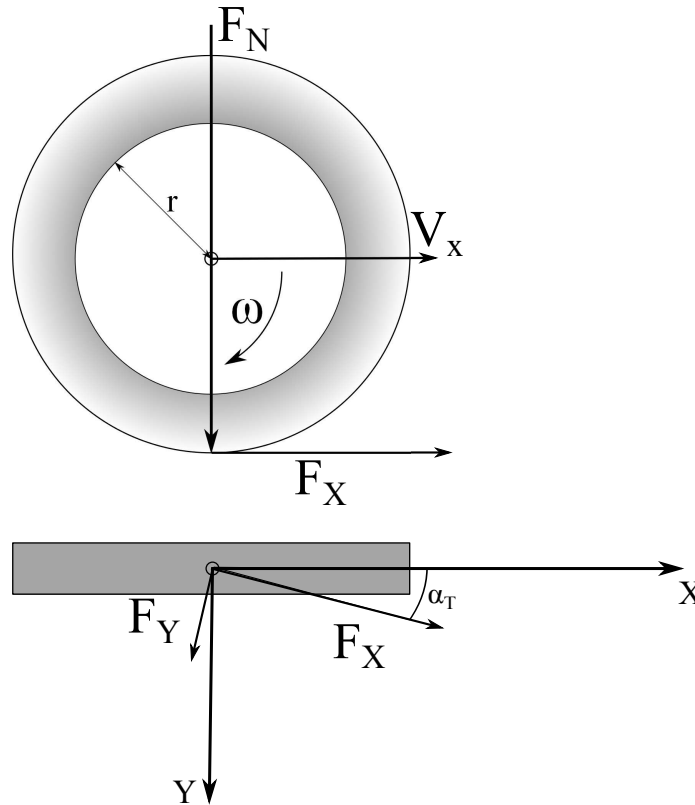


Figure 6.1: Wheel tire-road contact forces.

either:

$$\lambda_x = \frac{r\omega - V_x}{V_x} \quad (6.1)$$

while vehicle is braking or:

$$\lambda_x = \frac{r\omega - V_x}{r\omega} \quad (6.2)$$

while vehicle is accelerating. The value $\lambda_x = 0$ denotes a pure rolling wheel and $\lambda_x = 1$ corresponds to a fully locked wheel ($\omega = 0$).

As shown in Figure 6.1 a vertical force called tire normal load F_N acts on a tire, and it mostly comes from partial vehicle weight. At the contact point between the tire and the road, the force is decomposed to longitudinal and lateral friction forces, F_x and F_y respectively. The modeling of friction is complex (see section 4.2.5) although experimental results show that forces depend on the slip ratio λ_x , normal force F_N and the longitudinal and lateral friction coefficients μ_x and μ_y . Typically, for control oriented models the friction forces are expressed as linear combination of normal load and friction coefficients $F_x = F_N\mu_x$ and $F_y = F_N\mu_y$. The friction coefficients depend on large number of parameters such as λ_x and α_T , and the friction can be modeled by Pacejka's 'Magic Formula', LuGre's model or Dugoff's model. When considering small sideslip angle α_T and concentrating only on longitudinal motion, the Burckhardt model

Road type	C_1	C_2	C_3
Dry asphalt	1.28	23.99	0.52
Dry concrete	1.19	25.16	0.53
Wet asphalt	0.86	33.82	0.35
Cobblestone	1.37	06.46	0.67
Snow	0.19	94.13	0.06

Table 6.1: Burckhardt model parameters.

is widely employed [156]. In this model the longitudinal friction coefficient is expressed as follows:

$$\mu_x(\lambda_x) = C_1(1 - e^{-C_2\lambda_x}) - C_3\lambda_x \quad (6.3)$$

where parameters C_1 , C_2 and C_3 define certain tire-road conditions (see Table 6.1 for example values) and the tire longitudinal friction force is denoted as:

$$F_x = F_N\mu_x(\lambda_x) \quad (6.4)$$

In Figure 6.2 the static maps for all the road types and conditions from Table 6.1 are shown. One can notice that the maximum peak of the longitudinal friction factor for almost all types of road conditions is found for longitudinal slip values around $\lambda_x = 0.1$. In general, the longitudinal friction coefficient which is important from the traction (acceleration and braking) perspective is higher for small longitudinal slip and for small sideslip angle. Since the lateral friction coefficient (which guarantees vehicle steerability) is also higher for small longitudinal slip, keeping longitudinal slip ratio at lower values ensures vehicle controllability.

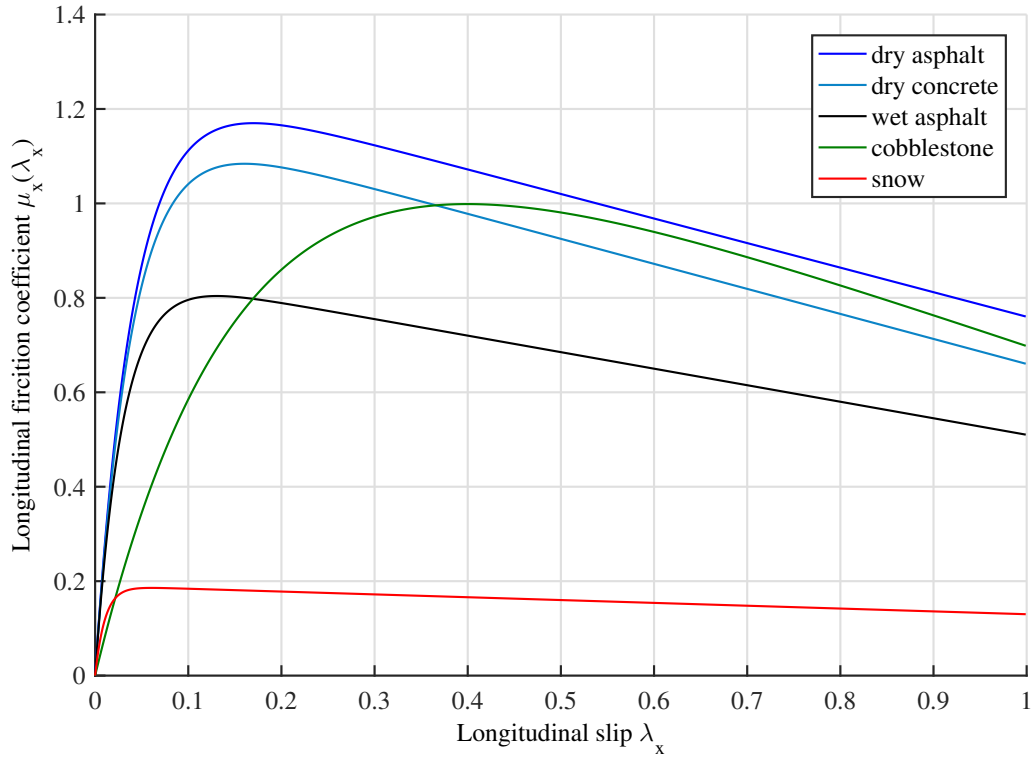


Figure 6.2: Burckhardt model longitudinal friction coefficient for different road types.

6.2.2. Brake actuator modeling

The conventional anti-lock braking systems utilize mainly HAB (Hydraulic Actuated Brakes) and EHB (Electro-Hydraulic Brakes) although a new technology, EMB (Electro-Mechanical Brakes), is gaining popularity. Based on the actuator technology, certain models are employed. In the vast majority of HAB system models, the control of the pressure valve is discrete and it is three-state (e.g. [157]):

$$u_B = \begin{cases} u_B^- = -\tau_B, & \text{decrease pressure action} \\ u_B^0 = 0, & \text{hold pressure action} \\ u_B^+ = \tau_B, & \text{increase pressure action} \end{cases} \quad (6.5)$$

where τ_B is the pressure actuator rate limit. The brake torque depends on the applied braking pressure p_B and it is calculated as:

$$T_B = r_B \mu_B A_B p_B \quad (6.6)$$

where r_B is the effective braking disc radius, μ_B is the friction coefficient of the brake pad and A_B is the brake piston area. The dynamics of the braking torque is modeled as:

$$\dot{T}_B = u_B \quad (6.7)$$

Some of works employ more complex hydraulic system modeling such as [158]:

$$C_F \dot{p}_B = A_1 u_B^1 \sqrt{\frac{2}{\rho}(p_P - p_B)} - A_2 u_B^2 \sqrt{\frac{2}{\rho}(p_B - p_R)} \quad (6.8)$$

where:

- C_F - the brake fluid flow coefficient,
- A_1 and A_2 - orifice areas of the hydraulics valves,
- ρ - the density of the brake fluid,
- p_P - the pressure in the system reservoir,
- p_R - the pressure in the system pump.

The system valves control inputs u_B^1 and u_B^2 are binary (0 or 1) and similarly the braking torque is proportional to brake pressure

$$T_B = k_p p_B \quad (6.9)$$

The other approach is to use only the first order linear system [159] as brake model:

$$\tau_P \dot{p}_B = -p_B + k_B p_B^d \quad (6.10)$$

where τ_P is hydraulics system time constant, k_B is the braking gain and p_B^d is controllable desired brake pressure.

In the EHB systems the direct hydraulic connection between the brake pedal and the wheels brake calipers is separated. The brake pedal is equipped with an electronic position sensor. The measured signal is transmitted by wire to ECU. The ECU is physically integrated into hydraulic unit which is joined with the conventional wheels brake calipers. Such a configuration makes the system more compact (fewer hydraulic circuits are required) and comfortable to the driver because there are no brake pedal vibrations. Contrary to HAB systems, the brake force modulation is continuous and the brake pressure control is more accurate (the brake circuit pressures is measured by the sensors). Modeling of the EHB actuators is similar to the ones used for HAB and when it comes to ABS control design, it is often simplified to the first order systems [160] with or without dead time (control input delays) [158]. More complex modeling of EHB systems can be found in [161, 162, 163].

A brief description of dynamics of the EMB including servo-motor modeling and control can be found in [164, 165, 166]. Generally, the braking torque in such as system is modeled in the following way:

$$T_B = r_B \mu_B F_B \quad (6.11)$$

where r_B is the radius of the disc brake, μ_B is the friction coefficient between disc brake and brake lining and F_B is the clamping force.

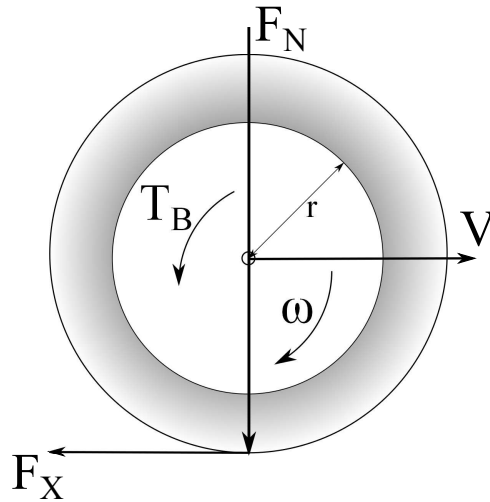


Figure 6.3: Single-wheel model.

6.2.3. Vehicle dynamics modeling

6.2.3.1. Single wheel model

The classic single-corner model is a longitudinal motion oriented version of the quarter-vehicle model presented in section 4.2.1. The system depicted in Figure 6.3 is governed by the following equations:

$$\begin{aligned} J\dot{\omega} - rF_x + T_b &= 0 \\ m\dot{V}_x + F_x &= 0 \end{aligned} \tag{6.12}$$

where

- J - the moment of inertia of the vehicle wheel,
- ω - the radial velocity of the vehicle wheel,
- r - the wheel radius,
- F_x - the longitudinal friction force acting on the vehicle wheel,
- T_b - the braking torque acting on the vehicle wheel,
- m - the quarter vehicle equivalent mass,
- V_x - the longitudinal speed of the vehicle.

It can be noticed that suspension dynamics are neglected. The introduced system analysis with employment of Burckhardt friction model is presented in section 6.3.

6.2.3.2. Double-wheel model

The second model widely employed in braking control algorithms development is the double-wheel model. This model is similar to the pitch motion oriented half-car model introduced in section 4.2.2. In this case the front and the rear wheels from one side of the vehicle are modeled (see Figure 6.4). The

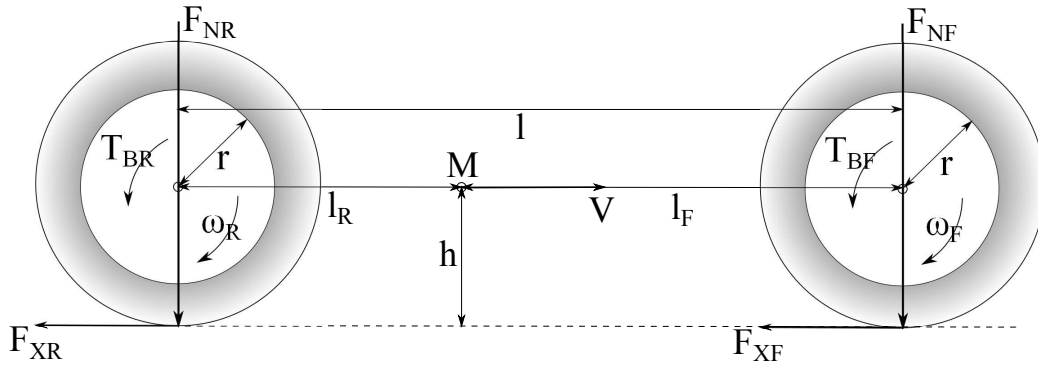


Figure 6.4: Double-wheel model.

system dynamics are governed by the following equations:

$$\begin{aligned}
 J\dot{\omega}_F - rF_{XF} + T_{BF} &= 0 \\
 J\dot{\omega}_R - rF_{XR} + T_{BR} &= 0 \\
 M\dot{V} + F_{XF} + F_{XR} &= 0
 \end{aligned} \tag{6.13}$$

where

- J - moment of inertia of the vehicle front and rear wheel,
- ω_F and ω_R - radial velocity of the front and rear vehicle wheel,
- r - front and rear wheel radius,
- F_{XF} and F_{XR} - longitudinal friction force acting on the front and rear vehicle wheel,
- T_{BF} and T_{BR} - braking torque acting on the front and rear vehicle wheel,
- M - half vehicle equivalent mass,
- V - speed of the vehicle.

In order to consider the load transfer phenomenon between the front and rear vehicle axes, the torque and force balance of the half-car center of mass is calculated:

$$\begin{aligned}
 Mg &= F_{NF} + F_{NR} \\
 Mh\dot{V} &= -F_{NF}l_F + F_{NR}l_R
 \end{aligned} \tag{6.14}$$

which leads to equations to calculate front and rear normal load forces utilized in longitudinal friction modeling:

$$\begin{aligned}
 F_{NF} &= \frac{Mgl_R}{l} - \frac{Mh}{l}\dot{V} \\
 F_{NR} &= \frac{Mgl_F}{l} + \frac{Mh}{l}\dot{V}
 \end{aligned} \tag{6.15}$$

where

- l_F and l_R - the distances from front and rear axles to the center of half-car equivalent mass,
- $l = l_F + l_R$ - the distance between front and rear axles (wheelbase),
- h - the height of the center of half-car equivalent mass,

- g - the gravitational acceleration.

Same as in the single-corner model, the suspension dynamics are not considered.

6.3. ABS functions and wheel slip control goals based on single wheel model analysis

In order to demonstrate ABS system principle application, the simulation of a single wheel model of hard braking situation is presented. The adhesion friction is modeled using the Burckhardt model (6.4) and the remaining parameters are set to typical values of quarter vehicle: $J = 1 \text{ kg m}^2$, $m = 225 \text{ kg}$ and $r = 0.3 \text{ m}$. The maneuvers start at vehicle speed of $V_x(0) = 25 \text{ m s}^{-1}$, normal load is fixed to $F_N = mg$ where $g = 9.81 \text{ m s}^{-2}$ stands for gravitational acceleration. The maneuvers are performed for two different road conditions: dry asphalt and snow. The driver requested braking torque is set to a constant value of $T_b = 500 \text{ N m}$. The resulting system has the form:

$$\begin{aligned} J\dot{\omega} - rmg\mu_x(\lambda_x) + T_b &= 0 \\ m\dot{V}_x + rmg\mu_x(\lambda_x) &= 0 \end{aligned} \quad (6.16)$$

where $\lambda_x = \frac{r\omega - V_x}{V_x}$.

Figures 6.5 and 6.6 illustrate vehicle speed and the resulting slip ratio respectively during the first 2 s of hard braking on dry asphalt and snow. In the case of asphalt road type it can be observed that the vehicle wheel is decreasing the speed rapidly and with the similar rate to the vehicle. The slip ratio rises to approximately 0.04 and stays on this level. The entire braking manoeuvre takes about 3.5 s and the vehicle stops in about 44.5 m. As seen in Figure 6.2, maximal adhesion coefficient for dry asphalt is obtained at slip ratio of about 0.15 thus the braking could be performed better if high slip was reached. Also, the steerability of the vehicle is maintained. In the second case one can notice that the wheel locks after about 0.2 s and the vehicle speed decrease rate is slow. After the slip reaches the value of 1, the vehicle cannot be steered. In this case, the desired slip ratio 0.05 – 0.1 (see Figure 6.2) is not kept which results in about 19.5 s braking time and braking distance greater than 244 m.

To illustrate how the system reacts to the applied constant brake torque in the system equations (6.16), the state variable ω needs to be substituted with λ_x using the slip ratio definition (6.1). The slip ratio derivative is computed as:

$$\dot{\lambda}_x = -\frac{r}{V_x}\dot{\omega} + \frac{r\omega}{V_x^2}\dot{V}_x \quad (6.17)$$

The resulting set of equations is as follows:

$$\begin{aligned} \dot{\lambda}_x + \frac{1}{V_x}\left(\frac{1 - \lambda_x}{m} + \frac{r^2}{J}\right)rmg\mu_x(\lambda_x) + \frac{r}{JV_x}T_b &= 0 \\ m\dot{V}_x + rmg\mu_x(\lambda_x) &= 0 \end{aligned} \quad (6.18)$$

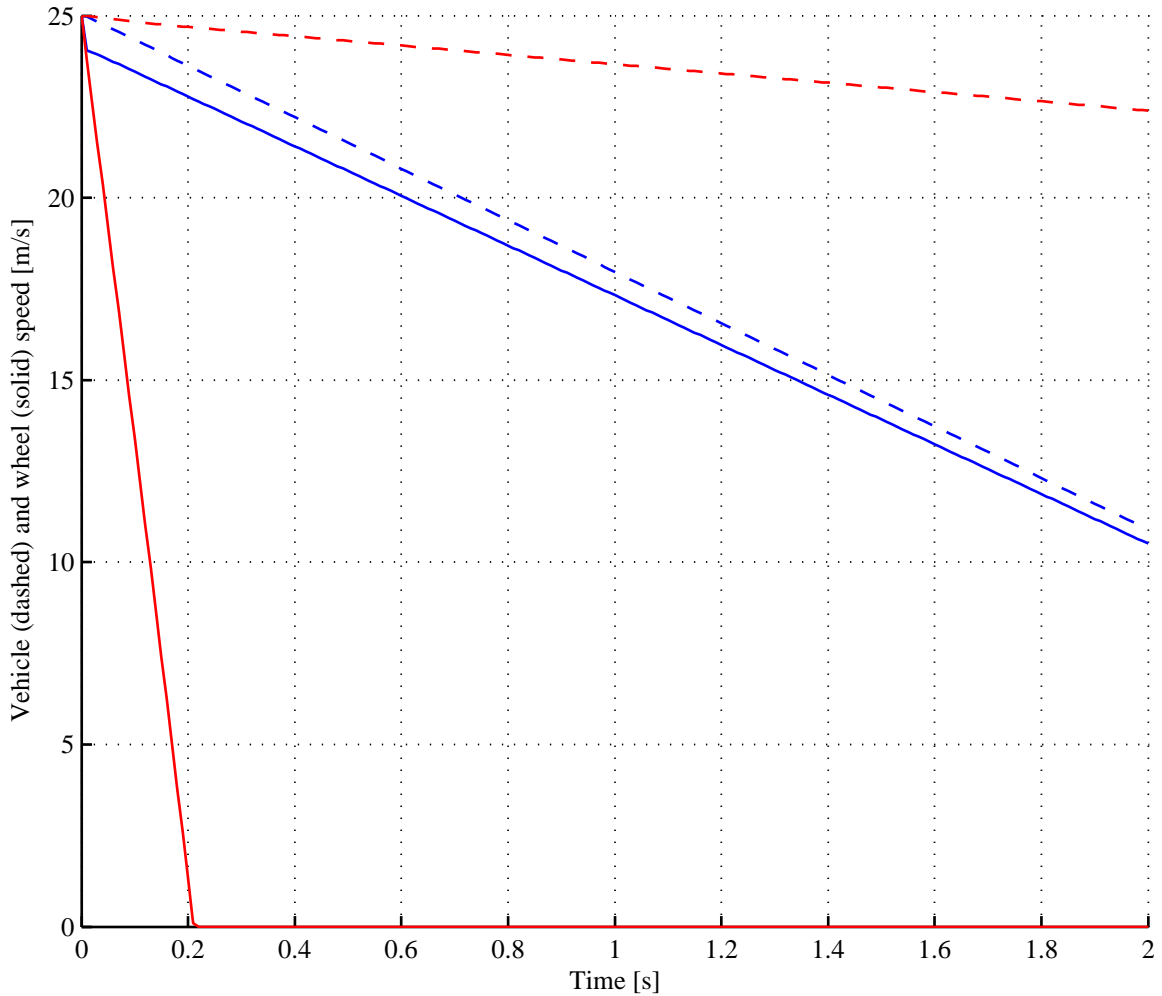


Figure 6.5: Vehicle and wheel speed during a panic braking manoeuvre for different road conditions: blue - dry asphalt and red - snow.

Based on an assumption (see [157]) that the vehicle longitudinal dynamics (second equation) are much slower than the wheel dynamics (first equation) due to large difference in inertia, the V_x is considered as slowly-varying parameter and is neglected in the further analysis. Substituting into the first equation

$V_x = \frac{r\omega}{1-\lambda_x}$ yields:

$$\dot{\lambda}_x = -\frac{1-\lambda_x}{J\omega}(\psi(\lambda_x) - T_b) \quad (6.19)$$

where

$$\psi(\lambda_x) = \left(r + \frac{J}{rm}(1-\lambda_x)\right)mg\mu_x(\lambda_x) \quad (6.20)$$

Examining the equation (6.19) one can notice that the equilibrium points of the system i.e. $\dot{\lambda}_x = 0$ are expressed by $T_b = \psi\lambda_x$. Figure 6.7 shows equilibrium points (intersections between constant T_b lines and $T_b = \psi\lambda_x$ curves) of the system for constant braking torque values $T_b = 100$, $T_b = 500$ and $T_b = 800$ for dry asphalt and snow road conditions. As can be seen, the system might have no equilibrium points, a single equilibrium point or two equilibrium points. In the depicted example for snow road conditions, the

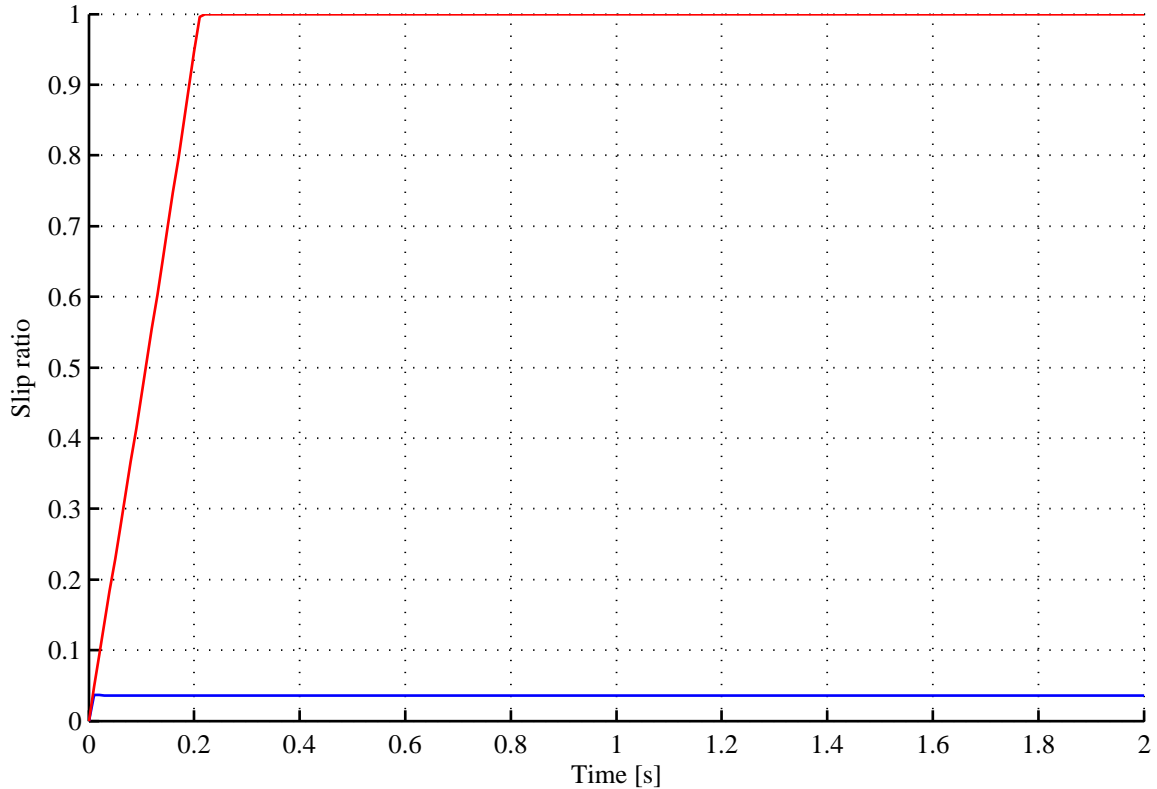


Figure 6.6: Vehicle slip ratio during panic braking manoeuvre for different road conditions: blue - dry asphalt and red - snow.

system would not have any equilibrium points when the braking torque is higher than circa $T_b = 133$ and for dry asphalt road condition higher than circa $T_b = 810$. One can notice that such a case is observed when T_b is higher than maximal value of $\psi\lambda_x$ curve which corresponds to the peak of road adhesion curve. A single equilibrium point or two equilibrium points exist when the braking torque is below the peak. In the example of dry asphalt road conditions, the system has a single equilibrium point when the braking torque is higher than zero and smaller than circa $T_b = 500$, and it has two equilibrium points when the braking torque is higher than circa $T_b = 500$ and below the peak. Further analysis of the stability of such equilibrium points shows that the ones existing on the left hand side of the $\psi\lambda_x$ curve are locally asymptotically stable, and the ones existing on the right hand side are unstable [157].

The presented analysis shows that the goal of the wheel slip control algorithms is to keep the slip value in the vicinity of the peak of friction curve although in the neighbourhood of the stable equilibrium points. If the controlled slip value would exceed the peak and approach the unstable equilibrium point the control of the system would become more difficult and less effective. Thus the ideal controller shall obtain the optimal slip value in the shortest possible time and stabilize the slip value near this point. Due to the fact that in general the optimal point is not known as it depends on the road conditions the ideal control strategy is not realizable in the real world scenarios.

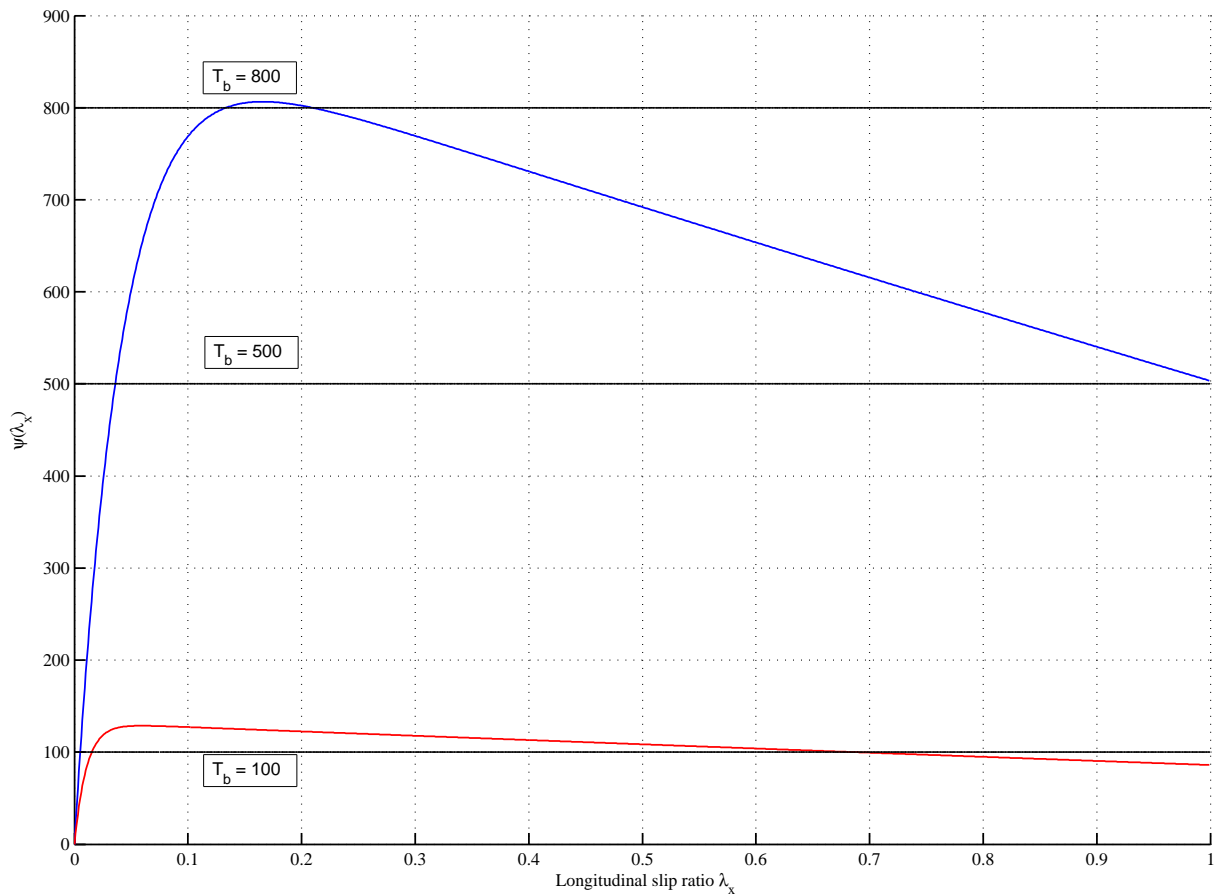


Figure 6.7: Function $\psi(\lambda_x)$ for different road conditions: blue - dry asphalt and red - snow.

6.4. Control design for ABS

The control strategy application selection for ABS systems depends on two main elements: controlled value and brake actuator technology. In ABS systems control of the braking force applied to the wheels is generally based on wheel slip value or wheel acceleration signal or on both quantities. The wheel slip is a non measured value which needs to be calculated from the estimated vehicle velocity signal which tends to be noisy and highly uncertain no matter whether the direct speed sensor is applied or indirect estimation is done. The wheel acceleration signal is measured by wheel encoder and its quality is sufficient. Additionally the wheel slip ratio signal might be corrupted once the tire is bouncing especially on the uneven road. The aforementioned issues regarding wheel slip based control are crucial from a performance point of view and pose a significant factor for control design. The control might be applied either to a continuous brake actuator such as EHB and EMB or a discrete brake actuator which is a traditional HAB regulation scheme: increase, hold or decrease pressure. In case of wheel acceleration only based control there is no set-point value of wheel acceleration to regulate. When slip value is to be controlled then two common approaches are utilized: either the desired slip is set to a fixed value that is sub-optimal for all road conditions or slip set-point value may vary and be adjusted to certain road conditions when

such information is provided to the system or it is estimated on-line in real-time. The classic approach of evaluation of performance of different ABS algorithms and ABS systems configuration is done using the three main objectives: stopping distance, steerability and stability. The braking way criteria depends on initial vehicle velocity and it generally would be minimized when all the vehicle wheels during the braking procedure operate near the peak in friction coefficient characteristics. The steerability objective is critical due to the fact that it enables the vehicle to control its lateral trajectory during braking. It would be preserved if the front wheels lateral friction forces remain in the peaks. The stability criteria is crucial for rear wheels especially when both sides of the vehicle travel on surfaces which differ highly in friction properties such as snow and dry asphalt. In such a case when too large braking force is applied on the wheel rolling on snow (see Figure 6.7) the unwanted and dangerous yaw moment would be generated and it would contribute to vehicle instability by pulling its rear side to the high friction side.

6.4.1. Conventional rule-based ABS control algorithms

Conventional ABS solutions employ HAB system (see 6.2.2) which has three brake pressure control modes: increase, hold and decrease. The ABS controller regulates the pressure using a table or logic rules incorporating a given multiple acceleration and/or slip thresholds. The control strategy defined by such a rules is designed and tuned in order to maximize the friction force between the tire and road surface for different braking scenarios and road conditions. Despite its simplicity and sub-optimal performance the most of standard commercial ABS systems still utilize rule-based wheel acceleration control algorithms due to the fact that are model-free and the required wheel angular velocity measurement is easy and cheap to perform using wheel encoders. The next paragraph presents an example of such an algorithm based on wheel acceleration.

The wheel acceleration is defined as:

$$a_w = \dot{V}_w = r\dot{\omega} \quad (6.21)$$

The ABS control cycles are governed by a set of acceleration thresholds a_1, a_2, \dots, a_i . The number (i) of tunable parameters depends on specific algorithm implementation. One of most common implementations [167, 168] employs a set of four positive thresholds a_1, a_2, a_3 and a_4 where $a_1 < a_2$ and $a_3 < a_4$. At the beginning of the panic braking maneuver the driver presses the brake pedal what results in the increase of the braking pressure. This initial cycle is called Phase 1. When the wheel acceleration is below a given threshold a_1 although still under a_2 ($-a_2 < a_w < -a_1$) the ABS controller holds the braking pressure (Phase 2). As soon as the a_2 threshold is reached the braking pressure is immediately decreased in order to allow the wheel acceleration (Phase 3). When the wheel gains acceleration greater than a_1 then the braking pressure is held again (Phase 4). This cycle lasts until the wheel acceleration obtains value higher than a_4 threshold when the braking pressure is increased in order keep the wheel

slip on efficient value (Phase 5). Next, in the Phase 6, when the acceleration is in range $a_3 < a_w < a_4$ the braking pressure is held and when it goes below a_3 the braking pressure is increased again. As soon as the a_1 threshold is reached again the second ABS cycle starts and in this cycle and in the next ones the braking pressure is decreased immediately (in the first cycle the a_2 threshold triggered the braking pressure decrease). The repetition of consequential cycles keeps the wheel slip in the vicinity of the maximum friction coefficient and prevents the wheel lock. The ABS controller is deactivated when the vehicle velocity is too small.

Apart from the presented algorithm, many other scientific papers considering ABS rule-based controllers have been published. The approaches differ in number of control phases and switching conditions. In [169] a five-phase algorithm is developed where the wheel deceleration is used for switching logic. In [170] a four-phase strategy is applied and control law differs from the presented variant by adding a two extra modes: low-pressure holding mode and high-pressure holding mode. Additionally, the switching mode logic is based not only wheel deceleration but also on elapsed time interval. The good comparison and evaluation of a number of different rule-based controllers is presented in [171].

6.4.2. Other control strategies applications to ABS

In the last thirty years researchers employed various control strategies to ABS. Due to advancement in the hardware development both for sensors, actuators and electronic processing units the more complex approaches were implemented and tested. Simultaneously the progress in the modeling and soft-computing capabilities fostered application of modern control designs placing great emphasis on theoretical basis and intelligent control techniques.

In the eighties a dominant position had conventional rule-based control designs having multiple numbers of discrete states [171, 172]. Apart from this typically commercial solutions the researchers examined various model-based ideas. In [173] a describing-function approach is employed in the design of control and the resulting feedback controller is tested in the field. A discrete-time robust slip controller is developed in [174] based on nonlinear feedback scheme and designed via classical digital control theory. Its effectiveness and robustness is also demonstrated by experiments although the necessity of vehicle speed calculation is a disadvantage of the proposed scheme. In the late 80's automotive companies started to employ more sophisticated ABS control strategies such as Nissan which is evidenced by patenting fuzzy inference application to anti-skid braking systems [175].

During the next decade the most of the researchers focused on either fixed slip value tracking approaches or the emphasis was put on searching for the best desired slip value for actual road condition. In [176] classic sliding-mode controller is proposed and designed for constant slip ratio tracking and its

Lyapunov stability is examined. The industry ABS control strategy based on rules and look-up tables is redesigned in [177] in order to mimic sliding-mode behavior. Another approach regarding SMC is considered in [178] where fixed desired slip is tracked by fuzzy sliding-mode controller (fuzzy control based on sliding-mode control scheme). In order to provide required slip ratio a number of wheel slip observers are tested against direct state feedback input such as Kalman filter or non-linear system model. Other researchers proposed a variable desired slip ratio approach where an extremum search method is used to find an optimal slip set-point (e.g in [179] it is estimated on-line based on friction force observer). The SMC is also combined with fuzzy logic controller in [180] where such a hybrid controller is used as reference model to off-line training of NN controller. A pure fuzzy logic controller is designed in [181] where a logic decision component is utilized to identify current road conditions based on braking torque, slip and slip prediction. Its output constitutes one of the input to complex fuzzy slip ratio controller. Another example of fuzzy logic application is found in [182]. Authors proposed a set of two fuzzy units forming a FMRLC (Fuzzy Model Reference Learning Control) system an extension to MRAC (Model Reference Adaptive Control). Apart from intelligent and hybrid control techniques also another theoretical approaches were explored such as classic feedback linearization control (e.g. in [183] combined with gain scheduling) or an adaptive Lyapunov-based nonlinear control [184]. A review and comparison of several control methods (SMC, conventional threshold, fuzzy logic and PID) is presented in [185]. The outcome from their research is that it is difficult to choose one particular control method due to that fact that each one has its own unique characteristics (advantages and disadvantages) and only a hybrid combination of them could be effective.

Since the 21st century, the part of the research still focused on classic, robust, adaptive and optimal control strategies. The application of PID controller and SMC is presented in [186] and non-linear PID (NPID) is introduced in [187]. The classic PID controller parameters are tuned in advance (gain-scheduled) although the NPID controller structure is fixed (no parameters switching). The simulation and experimental results are presented. The LQR method is used to obtain slip controller gain matrices in [188] and [189]. The designed control recipe is tested in the real vehicle. Another application of adaptive control is presented in [190] where multiple model adaptive control (MMAC) is considered based on backstepping approach. Author designed four slip controllers, each one for different road type and a rule to switch between them. A novel control strategy based on Lyapunov stability theory and Filippov framework is given in [191]. Additionally an optimal target slip ratio estimator is proposed. Apart from unconventional new designs the classic and extended SMC applications were constantly developed for example in [192] and [193] where a new chattering reduction solution is presented - integral switching technique. The other enhancements considered utilization of the fractional order dynamics as sliding mode surface for classic SMC [194] and a grey system modeling [195, 196].

The vast majority of recent publications concern intelligent and hybrid intelligent control strategies. In the domain of fuzzy logic the approach of two FLCs is implemented and tested in the tire test bed in [197]. In the presented system one of the fuzzy controllers is responsible for brake control and the remaining one is used to detect road condition and the resulting optimal slip ratio. Apart from pure fuzzy logic control the researchers combined such a controllers with SMC [198] or extended to model based fuzzy controllers (MBFLC) [199]. The others considered genetic algorithms (GA) to train off-line either fuzzy logic only controller [200, 201] or fuzzy PID and fuzzy NPID controllers [202]. There are also approaches to PID type fuzzy controllers tuned on-line [203] and linear fuzzy PI controllers [204]. The second branch of research emphasis is put on neural networks either trained off-line [205] or on-line for example using steepest descent gradient approach and backpropagation algorithm [206]. There are also attempts to hybrid SMC and control with use of neural network [207]. The most complex solutions tend to combine neural networks and fuzzy logic. Again some of the researchers use GA to train such a systems off-line [208, 209] and the other ones prefer on-line adaptive tuning and learning [210, 211]. Additionally similarly to fuzzy logic only and neural network only application, SMC based fuzzy neural network controllers are designed [212, 213].

7. ABS laboratory demonstrative system

In this chapter the real world laboratory ABS device is investigated. Similarly to the SAS system, at the beginning the model is introduced and the model parameters are obtained. Afterwards, the real-time control approaches are applied. The chapter is organized as follows. Section 7.1 provides an overview of the ABS laboratory bench. The model of the device and its identification is presented in section 7.2. Finally, section 7.3 is devoted to the designed real-time control strategy.

7.1. ABS overview

ABS laboratory system used in experiments consists of two rolling wheels: the car wheel and the car road wheel animating the relative road motion (see Figure 7.1). The upper car wheel remains permanently in a rolling contact with the lower wheel. The car road wheel has a smooth surface which can be covered by a given material to simulate a surface of the road. It is also used to accelerate both wheels to the desired initial angular velocity before the braking action begins. The car road wheel is driven by a powerful flat GPN12LR DC motor. GPN12LR is supplied with a voltage of 24 VDC and a maximum current equal to 11 A. The car wheel is rigidly connected to a disk brake system. This brake system is linked via hydraulic coupling to the brake lever which is driven by the small flat GPN9 DC motor by the tight side and the tightening pulley. This DC motor is supplied with a voltage of 12 VDC and a maximum current equal to 6 A. Both DC motors are controlled with PWM signals with a frequency of 10 kHz to 20 kHz. To prevent unexpected vibrations, the car wheel has a damper attached to the rigid frame. The angular position of two wheels are measured by two identical incremental encoders of HEDM-5055 type. The encoders resolution is 4096 pulses per revolution (quadrature mode), giving the accuracy equal to 0.001 534 rad. The corresponding angular velocities are reconstructed from these two positions using the simple Euler formula. The laboratory rig is directly connected to a power interface. It amplifies the PWM signals and separates them from a PC. Measurements of the DC motors current levels are taken with an integrated LEM CAS 6-NP (brake motor, the nominal current equal to 6 A) and LEM CAS 15-NP (driving motor, the nominal current equal to 16 A) current transducers, utilizing the Hall effect. An analog electronic circuit allows to condition output voltage signal from LEM by changing gain and offset.

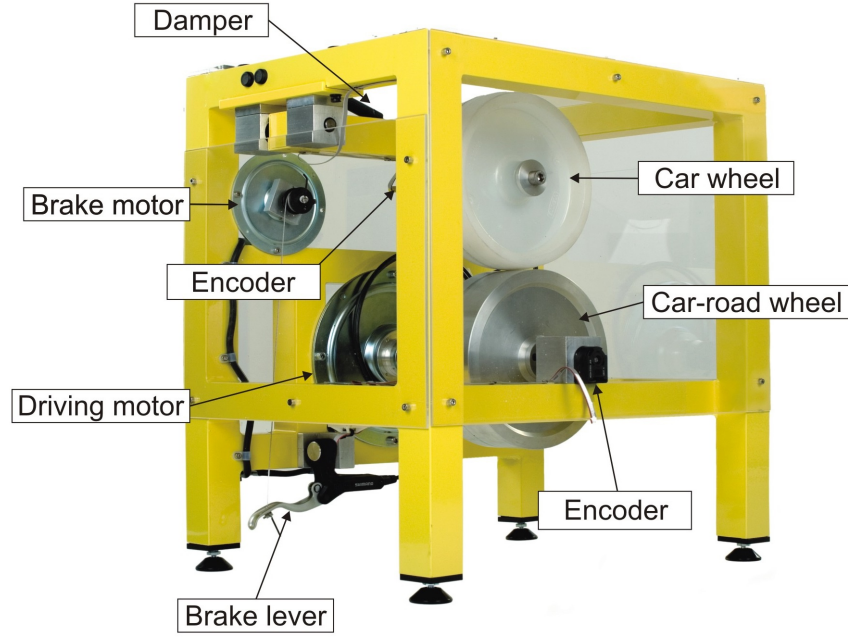


Figure 7.1: Photography of the laboratory ABS. Source: [149].

7.2. ABS modeling and identification

The anti-lock system model identification process is divided into three separate parts [214]. First, only the moments of inertia and wheels bearing friction parameters are identified. In this part the wheels are separated from each other. Next, the complete mathematical model is introduced and the previously estimated parameters are incorporated in order to identify the slip friction curve and the braking torque profile.

7.2.1. Lower wheel with DC motor parameters identification

The goal of this phase of study is to identify the lower wheel moment of inertia and bearing friction coefficients. The lower wheel is coupled with the GPM16LR DC motor which is power supplied to accelerate the wheel, and the upper wheel is removed. The following equations were used during the identification procedure:

$$\dot{i}(t) = \frac{1}{L_i}(U_c u(t) - k_e \omega(t) - R_\omega(t)i(t)) \quad (7.1)$$

$$\dot{\omega}(t) = \frac{1}{J_m + J_l}(k_t(u(t))i(t) - M_l \tanh(\omega(t)) - d_l \omega(t)) \quad (7.2)$$

$$R_\omega(t) = \begin{cases} R + R_m, & \omega(t) \leq \omega_R \\ R_m, & \omega(t) > \omega_R \end{cases} \quad (7.3)$$

$$k_t(u(t)) = \begin{cases} k_t, & \omega(t) \leq \omega_{max} \\ 0, & \omega(t) > \omega_{max} \vee u(t) = 0 \end{cases} \quad (7.4)$$

where

- $U_c = 24 \text{ V}$,
- $k_e = 60.16 \cdot 10^{-3} \text{ V rad}^{-1} \text{ s}$,
- $L_i = 10^{-4} \text{ H}$,
- $k_t = 6 \cdot 10^{-2} \text{ N m A}^{-1}$,
- $R = 1 \text{ } \Omega$,
- $R_m = 0.65 \text{ } \Omega$,
- $J_m = 6.284 \cdot 10^{-4} \text{ kg m}^2$,
- $\omega_{max} = 245 \text{ rad s}^{-1}$,
- $\omega_R = 100 \text{ rad s}^{-1}$.

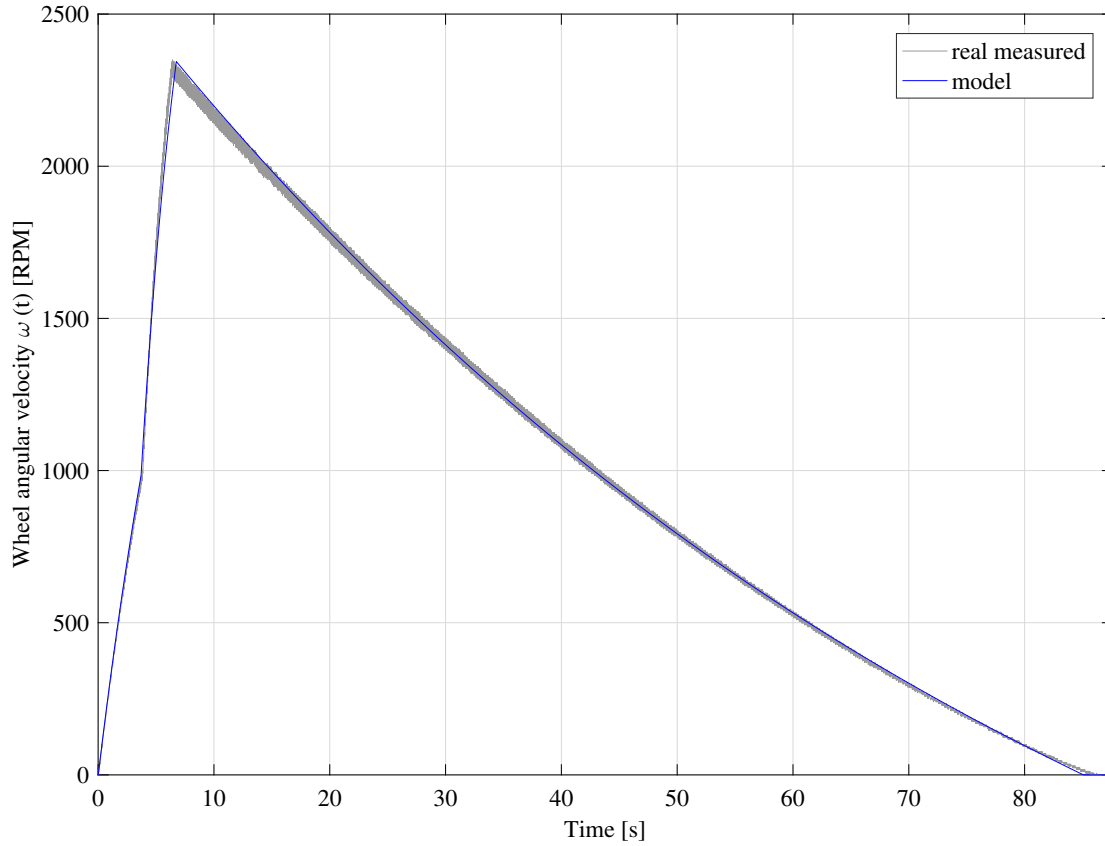
Velocity $\omega(t)$ denotes the lower wheel angular velocity, $i(t)$ stands for motor current and $u(t)$ is the PWM motor control voltage. When control $u(t)$ is set to zero or $\omega(t)$ reaches velocity limit ω_{max} the DC motor power supply is switched off (k_t is set to zero). The variable resistance R_ω is obtained by relays which are used to prevent high current consumption during the early acceleration phase. All motor parameters are taken from the specification sheet [215] except the value R_m . This value (motor resistance) has been increased to include the power supply unit internal resistance [216]. Five real-time trajectories of the wheel velocity $\omega(t)$ have been collected. Each consists of two parts:

- acceleration part for different constant control $u(t) = 0.5, 0.6, \dots, 1$,
- and braking part from the gained ω_{max} velocity.

The current $i(t)$ is not measured. The identification of the parameters J_l (moment of inertia), M_l (static friction torque) and d_l (viscous friction coefficient) is done using the non-linear grey-box model estimation technique [217, 218] from MATLAB System Identification Toolbox and Optimization Toolbox. The following values of the missing parameters are obtained:

- $J_l = 0.0249 \text{ kg m}^2$,
- $M_l = 0.0208 \text{ N m}$,
- $d_l = 4.0 \cdot 10^{-4} \text{ N m s rad}^{-1}$.

The comparison between real-time and modeled trajectories is shown in Figure 7.2. The achieved results of accuracy of fit are satisfactory and the identified parameters will be used in the succeeding identification experiments on the complete model.

Figure 7.2: Lower wheel angular velocity ω vs. time.

7.2.2. Upper wheel parameters identification

The moment of inertia of the upper wheel is identified using constant driving torque. The wheel is lifted to ensure its free motion. The 0.2 kg load weight is applied to the wheel with the inextensible strand and dropped. The wheel angular velocity trajectory is collected during the acceleration and braking phase of the motion. The model used to estimate the required parameters J_u (moment of inertia), M_u (static friction torque) and d_u (viscous friction coefficient) is in the form:

$$\dot{\omega}(t) = \frac{1}{J_u}(M_{mgr}(t) - M_u \tanh(\omega(t)) - d_u \omega(t)) \quad (7.5)$$

$$M_{mgr}(t) = \begin{cases} mgr, & t \leq T \\ 0, & t > T \end{cases} \quad (7.6)$$

where $m = 0.2$ kg, $g = 9.81$ m s⁻², $r = 0.0995$ m.

Velocity $\omega(t)$ denotes upper wheel angular velocity, r is the wheel radius and T is the time when the weight load is reaching the ground and stops to accelerate the wheel. The utilized identification procedure is the same as the one described in the previous section. The estimated parameters are as follows:

- $J_u = 0.0052$ kg m²,

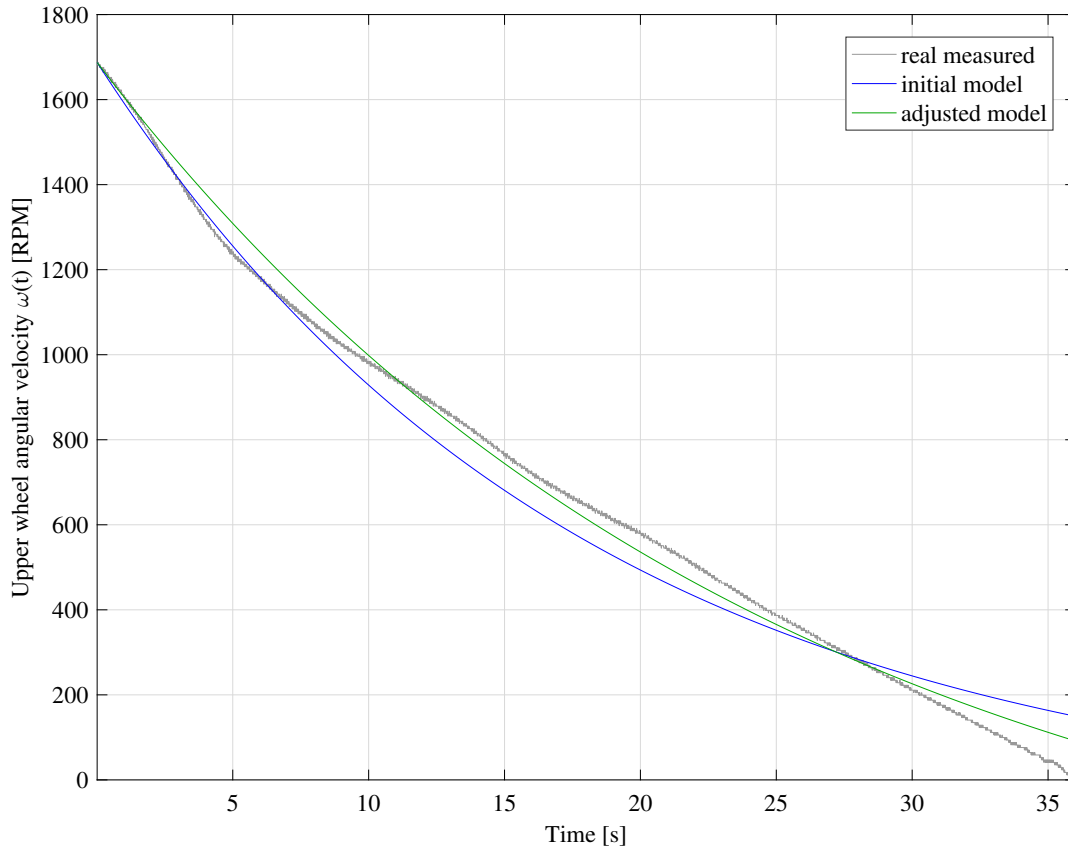


Figure 7.3: Upper wheel angular velocity ω vs. time.

- $M_u = 0.0027 \text{ N m}$,
- $d_u = 2.9 \cdot 10^{-4} \text{ N m s rad}^{-1}$.

Subsequently, the verification experiments are performed when the upper wheel accelerates with the lower wheel and then it is lifted up shortly after the brake starts. Although the proper fit of the model to the data from experiment was used during the identification, it turned out that the friction for large velocities is highly variable and different from that for small velocities experienced during the identification experiment. The bearing friction parameters estimation has been repeated for these verification experiments using the reduced (7.5) model:

$$\dot{\omega}(t) = \frac{1}{J_u} (-M_u \tanh(\omega(t)) - d_u \omega(t)) \quad (7.7)$$

The moment of inertia J_u is fixed with the value obtained previously. The parameters are changed to the following: $M_u = 0.0088 \text{ N m}$, $d_u = 2.08 \text{ N m s rad}^{-1}$. One can notice that all parameters have been changed significantly, especially the static friction coefficient is increased more than 3 times. Figure 7.3 illustrates the comparison of initial and adjusted model trajectories with real time experiment. The less satisfactory results have been achieved between 1700 and 110 RPM, however the new model is performing better for other velocity ranges.

7.2.3. Complete model introduction

Having the parameters of the lower and upper wheel identified, the complete ABS device model is introduced. The laboratory apparatus diagram is depicted in Figure 7.4. The system model state equations of the motion are as follows:

$$J_1 \dot{x}_1(t) = F_n r_1 s \mu(\lambda) - d_1 x_1 - s_1 M_{10} - s_1 M_b \quad (7.8)$$

$$J_2 \dot{x}_2(t) = -F_n r_2 s \mu(\lambda) - d_2 x_2 - s_2 M_{20} \quad (7.9)$$

where $s_1 = \tanh(x_1)$, $s_2 = \tanh(x_2)$, $s = \text{sgn}(r_2 x_2 - r_1 x_1)$, $r_1 = 0.0995$ m, $r_2 = 0.099$ m, $J_1 = J_u$, $d_1 = d_u$, $M_{10} = M_u$, $J_2 = J_l$, $d_2 = d_l$ and $M_{20} = M_l$.

The state x_1 and x_2 denote upper and lower wheel angular velocities respectively, in radians per seconds. The slip between wheels λ (the relative difference of the wheels velocities) is calculated in the following way:

$$\lambda = \begin{cases} \lambda_{21}, & r_2 x_2 \geq r_1 x_1 \wedge x_1 \geq 0 \wedge x_2 > 0 \\ \lambda_{21}, & r_2 x_2 < r_1 x_1 \wedge x_1 < 0 \wedge x_2 < 0 \\ \lambda_{12}, & r_2 x_2 < r_1 x_1 \wedge x_1 \geq 0 \wedge x_2 > 0 \\ \lambda_{12}, & r_2 x_2 \geq r_1 x_1 \wedge x_1 < 0 \wedge x_2 < 0 \\ 1, & \text{otherwise} \end{cases} \quad (7.10)$$

where $\lambda_{21} = \frac{r_2 x_2 - r_1 x_1}{r_2 x_2}$ and $\lambda_{12} = \frac{r_1 x_1 - r_2 x_2}{r_1 x_1}$.

The slip friction curve $\mu(\lambda)$ as well as the braking torque M_b are estimated in the subsequent sections. The normal force F_n is calculated in the following manner (see Figure 7.4):

$$F_n = \frac{M_g + s_1 M_{10} + s_1 M_b + d_1 x_1}{L(\sin(\varphi) - s \mu(\lambda) \cos(\varphi))} \quad (7.11)$$

where $L = 0.37$ m, $\varphi = 1.1451$ rad.

The torque $M_g = 29.6958$ N m has been obtained using the weighing conveyor. The introduced model covers only the braking phase of the device motion from the specified upper and lower wheel initial velocities x_{10} and x_{20} .

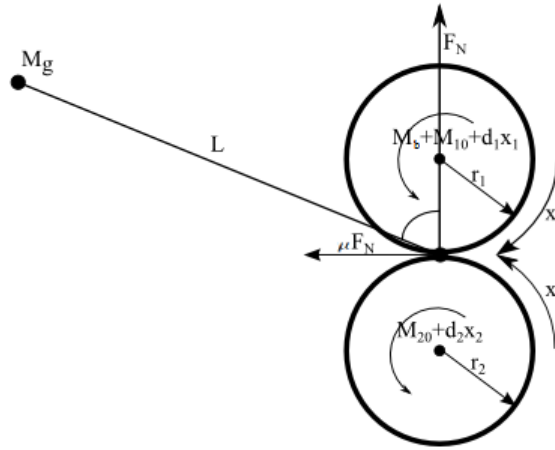


Figure 7.4: The ABS model diagram. Source: [216].

7.2.4. Slip friction curve estimation

The slip friction coefficient function $\mu(\lambda)$ is determined experimentally. From formulas (7.8) and (7.9) one can obtain:

$$s_1 M_b = -\left(\frac{r_1}{r_2}(J_2 \dot{x}_2 + s_2 M_{20} + d_2 x_2) + J_1 \dot{x}_1 + s_1 M_{10} + d_1 x_1\right) \quad (7.12)$$

and then from formulas (7.9), (7.11) and (7.12):

$$\mu(\lambda) = \frac{\frac{L \sin(\varphi)}{r_2} S}{S\left(\frac{L \cos(\varphi) + r_1}{r_2}\right) + J_1 \dot{x}_1 - M_g} \quad (7.13)$$

where

$$S = J_2 \dot{x}_2 + s_2 M_{20} + d_2 x_2 \quad (7.14)$$

The equation (7.13) together with (7.10) are used to calculate slip friction value μ for the corresponding slip λ . The accelerations \dot{x}_1 and \dot{x}_2 have to be observed on the basis of the measured velocities x_1 and x_2 . To obtain the slip friction curve, a number of 21 braking experiments have been performed. In each case the wheels are accelerated to similar initial velocities around 2000 RPMs. Then the brake control is turned on in form of a pulse signal with 50% width, 2 second period and variable amplitude value 0, 0.05, ... 1. In the case when only the upper car-wheel velocity reaches zero angular velocity (lock) during the non-zero control level, the control signal is set to zero unless the wheel accelerated again approximately to 500 RPMs. Figure 7.5 shows one of the performed real-time experiments. For every data point $x^i = [x_1 \ x_2 \ \dot{x}_1 \ \dot{x}_2]$ from all the collected trajectories the pairs (λ^i, μ^i) are calculated. The slip value interval $[0, 1]$ is quantized to set $\lambda_q = 0, 0.01, \dots 1$ and the corresponding λ_q is calculated as mean value. The obtained curve is fitted using 4th degree polynomial (see Figure 7.6) and the slip

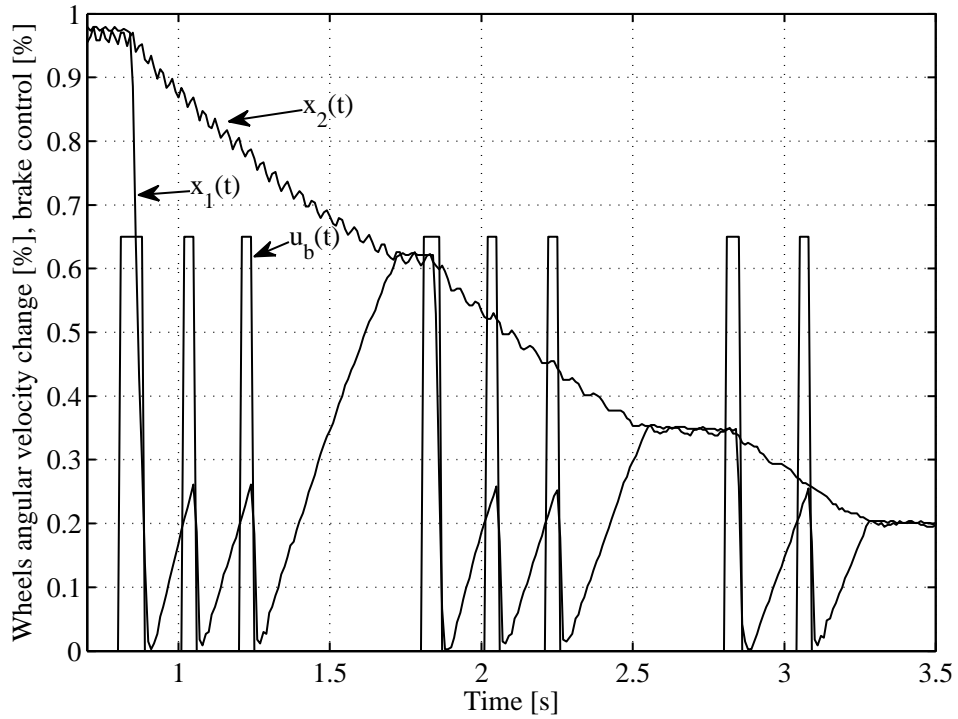


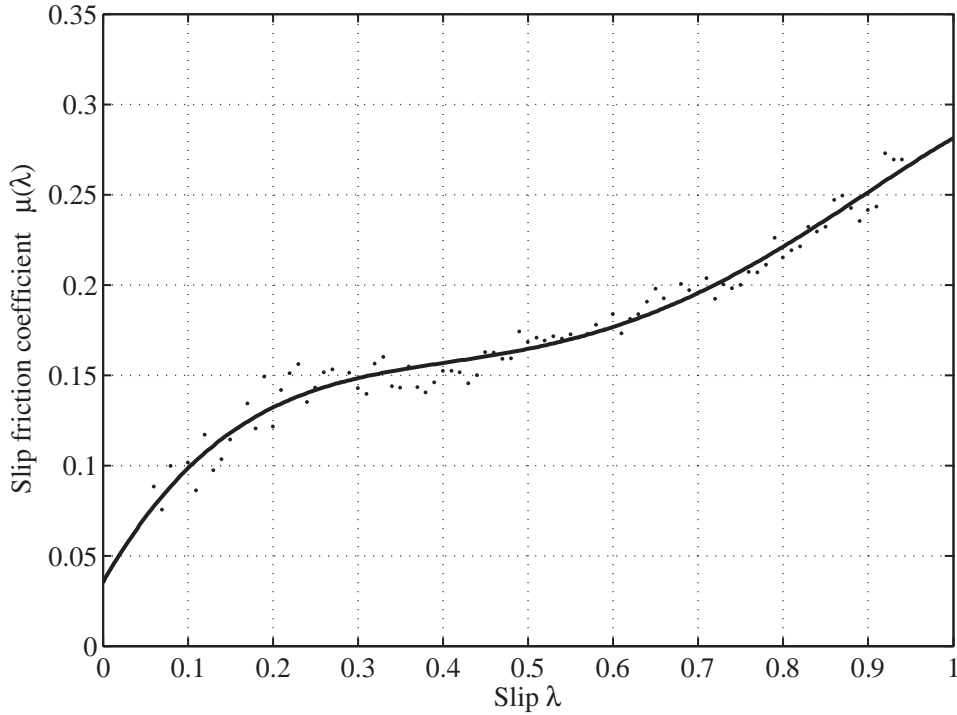
Figure 7.5: Brake control vs. time, upper and lower wheel angular velocity change over initial wheels velocities vs. time.

friction coefficient is approximated by the following formula:

$$\mu(\lambda) = \begin{cases} 0.009, & \lambda < 0.05 \\ \mu_p(\lambda), & \lambda \geq 0.05 \end{cases} \quad (7.15)$$

where

$$\mu_p(\lambda) = p_1\lambda^4 + p_2\lambda^3 + p_3\lambda^2 + p_4\lambda + p_5 \quad (7.16)$$

Figure 7.6: Slip friction coefficient $\mu(\lambda)$ vs. slip λ .

7.2.5. Brake force profile estimation

The ABS device brake torque is modeled with the following first order differential equation with brake control delay:

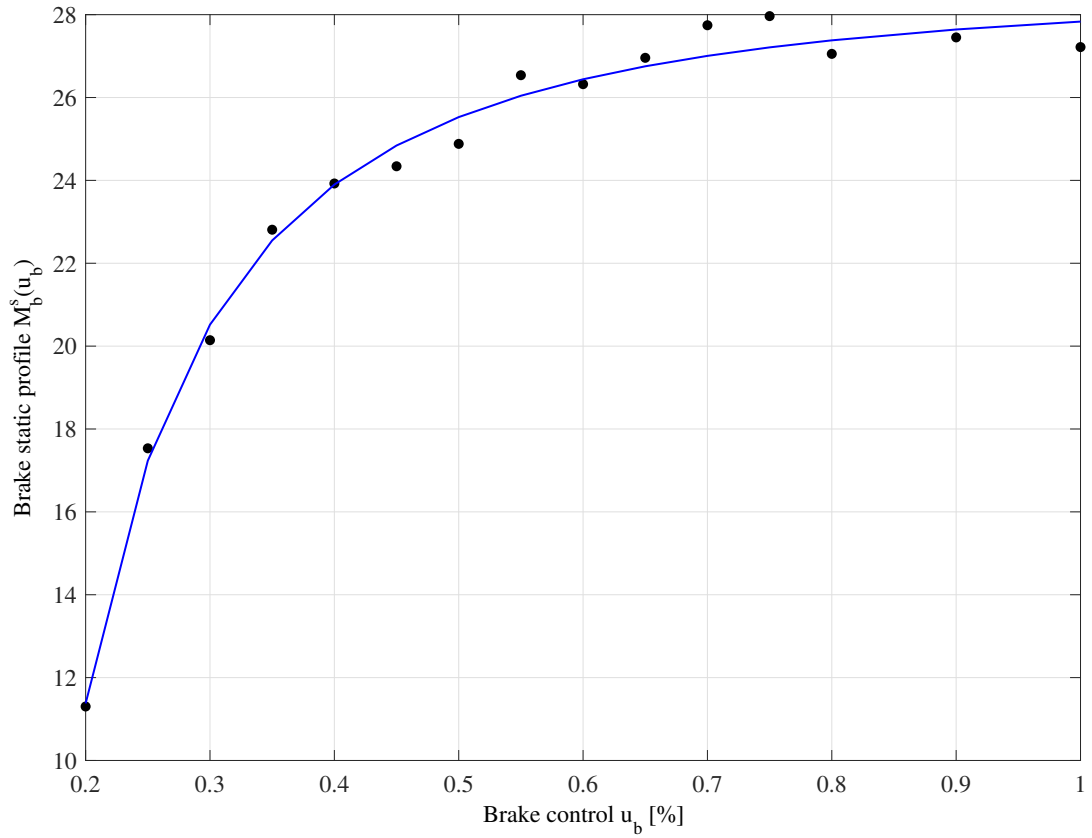
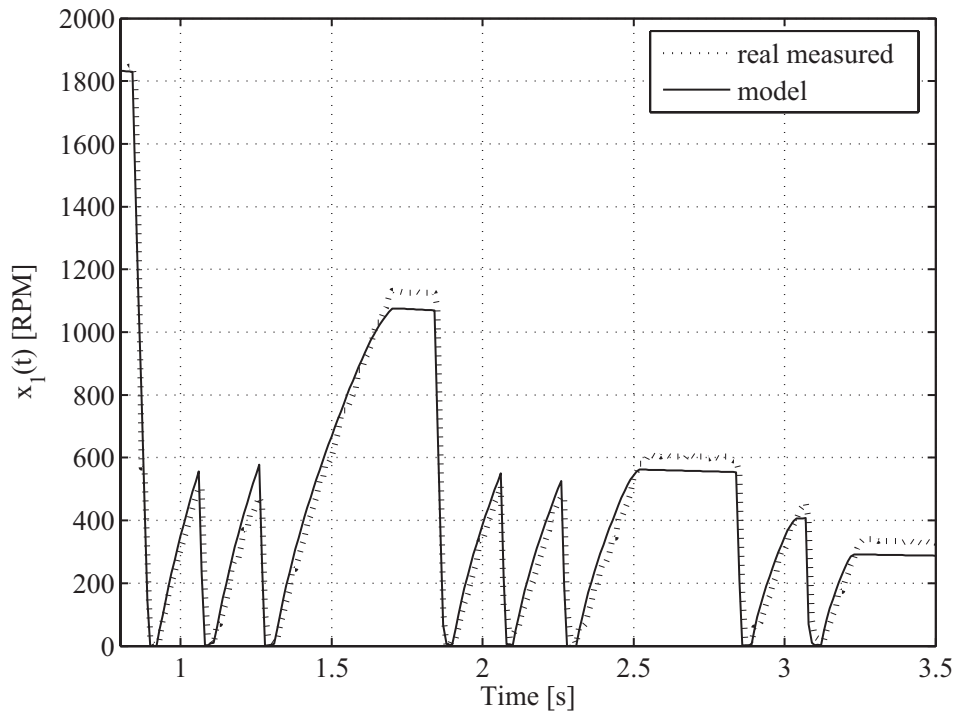
$$\dot{M}_b(t) = c_b(M_b^s(u_b(t - T_d)) - M_b(t)) \quad (7.17)$$

where $T_d = 0.05$.

The M_b denotes the braking torque acting on upper wheel and u_b is the brake motor PWM control. The parameter T_d is a brake torque delay due to small flat DC motor inertia and brake cable influence. The values of parameter T_d and $c_b = 50 \text{ s}^{-1}$ have been arbitrarily set based on experiments. The static profile $M_b^s(u_b)$ is obtained based on experiments utilized in section 7.2.4. Having all other model parameters estimated, only $M_b^s(u_b)$ is identified for different u_b control values. Again the grey-box parameter estimation technique is used. Only the first 500 samples of each experiment are used during identification. The obtained values and resulting static brake profile are shown in Figure 7.7. The function $M_b^s(u_b)$ is described by the following formula:

$$M_b^s(u_b) = \begin{cases} 0.07, & u_b < 0.2 \\ -0.8874u_b^{-1.847} + 28.72, & u_b \geq 0.2 \end{cases} \quad (7.18)$$

The comparison between real-time and complete identified model trajectories is presented in Figure 7.8 and 7.9.

Figure 7.7: Brake static profile $M_b^s(u_b)$.Figure 7.8: Upper wheel angular velocity x_1 vs. time.

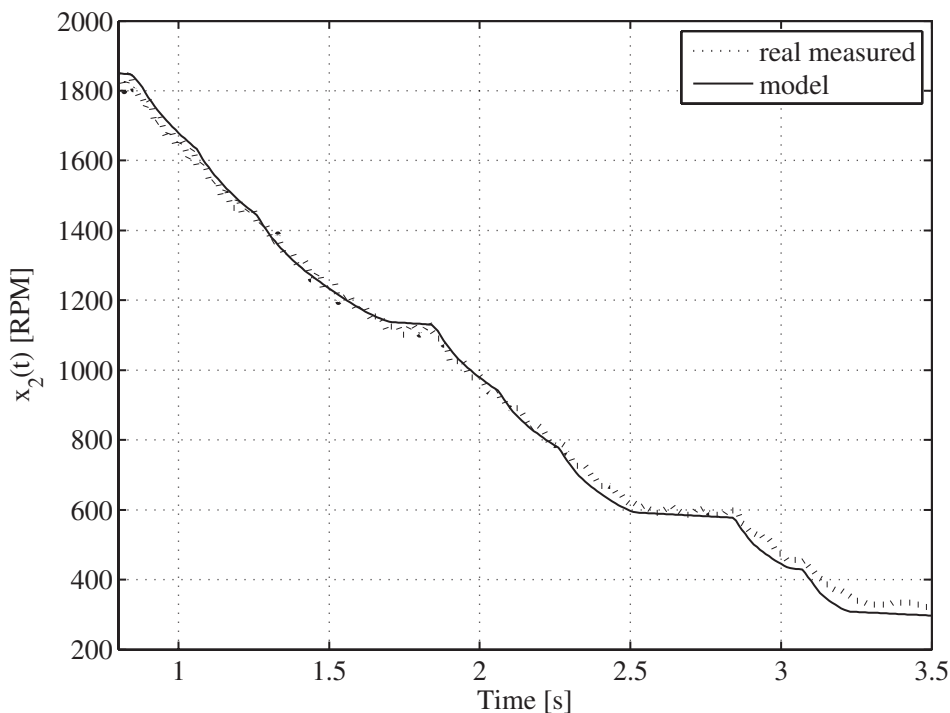


Figure 7.9: Lower wheel angular velocity x_2 vs. time.

7.3. ABS control

In this section real-time control of laboratory system is concerned. First, the need for additional brake DC current measurement is justified based on experience gained during conducted research. Finally, the designed slip controller utilizing added feedback signal is presented.

7.3.1. Motivation to introduce brake DC current measurement

In order to show what challenges, issues and difficulties occur during real-time control of the slip in the laboratory ABS system, an example experiment data is presented in Figure 7.10. The lower plot shows the slip, the filtered signal of the slip and the control, while the upper plot presents rotational velocities of the car and the wheel. The control strategy begins with the jump to control value 0.6 and this value is held for a certain time. In this phase of control one might observe the delays in the reaction of the system to applied control. The first delay is present upon control start (change from 0 to 0.6) - the slip starts approx. 0.05 s after control jump, the second delay occurs when the second phase of control begins (change from 0.6 to 0.39) - the delay is significantly smaller although it also has potential influence to control performance. Next, the control value is kept on constant level 0.39 until the slip closes enough to reference value equal in this case to 0.4. Afterwards, the slip is stabilized on the desired level. During the slip stabilization phase one can note the presence of the slip signal oscillations. They result from the way the slip is obtained, which utilizes the encoder measured signals of both velocities (note that speed

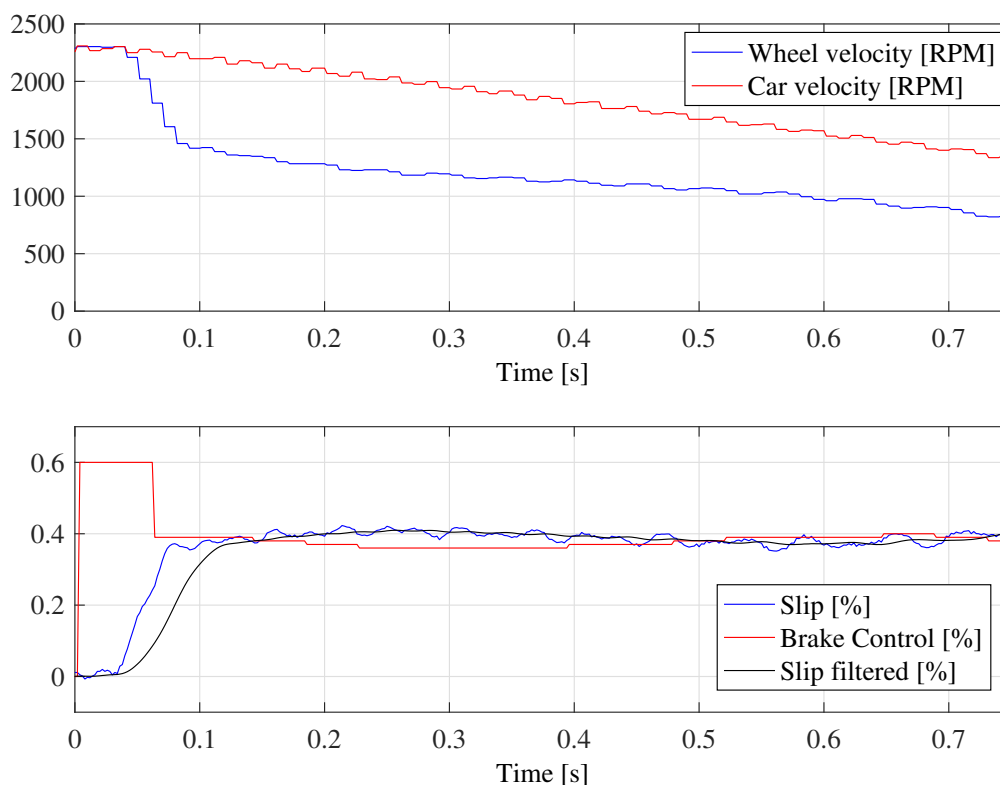


Figure 7.10: An example ABS control experiment.

signals shape). The filtering of the slip (or velocities) is inadequate especially for rapid slip changes (see the lag between filtered and unfiltered slip signal during first control phase). The oscillations in the controlled signal value are undesirable and make it difficult for the controllers.

Considering the presented system properties and the developed model attributes, a number of open-loop experiments have been conducted in order to observe and analyze the system behavior. A set of several tests is presented in Figure 7.11 where each color indicates a separate experiment. It shows runs of the system state (upper plot) and the slip (lower plot) for control consisting of the jump from 0 to 0.6 for fixed time period (common for all experiments) and change to final control value (different for each experiment) which is then kept. In the experiments 1 (black), 2 (red), 3 (blue) and 4 (green) the final control values are as follows: 0.37, 0.38, 0.39 and 0.40. One can note the regularity of the system reaction to increasing final control levels. For higher values the slip is maintained on certain levels and in later stage it is even increasing. On the other hand, for lower values of the control the slip decreases in time.

Based on a large number of experiments conducted in a similar manner as discussed above, the plan was to design a two-part slip controller, that consists of two components:

- I - responsible for rapid reach of the desired slip value,

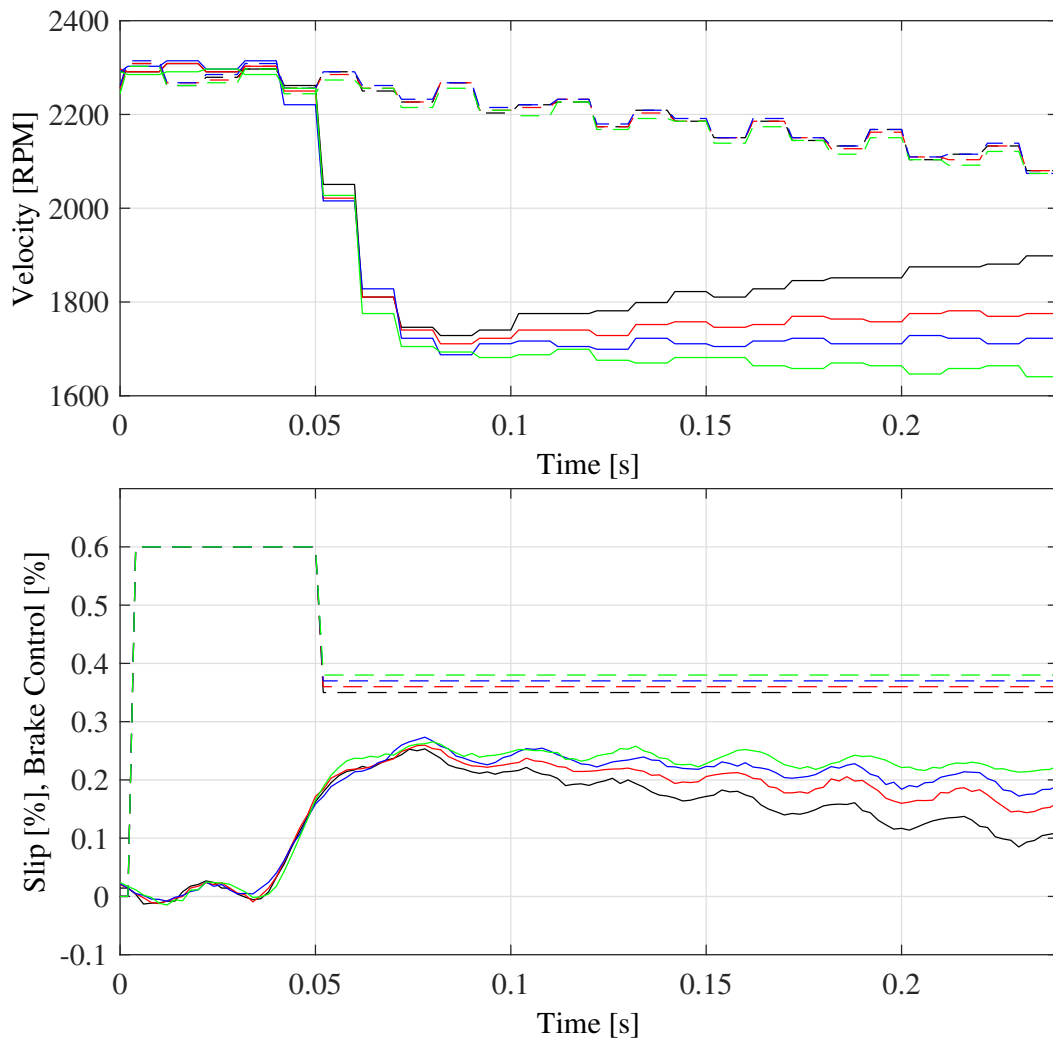


Figure 7.11: An open-loop tests results for laboratory ABS. Each color represents a separate experiment. Upper plot: car velocity - dashed line, wheel velocity - solid line. Lower plot: brake control - dashed line, slip - solid line.

- II - responsible for the slip stabilization around the desired slip value.

The controller I might be in form of NN or heuristic control algorithm and it shall be designed based on experimental data and the system model. The goal of this component is to calculate how long to keep the maximum control value 0.6 and to what value to switch afterwards in order to smoothly reach the desired slip level. The value 0.6 is chosen arbitrarily due to the experimental experience - higher control values introduce too high slip increase rate for the desired values of the slip from the range of $[0.2, 0.4]$. When the slip value is overdriven then it is difficult to reduce it without introducing high oscillations. In the case when the slip level is not accurately obtained, it is much more easy to make a correction. The input to this component is the unfiltered slip value since much attention is paid to rapid slip value changes. The task for the second module, controller II, is to maintain the slip around the desired level.

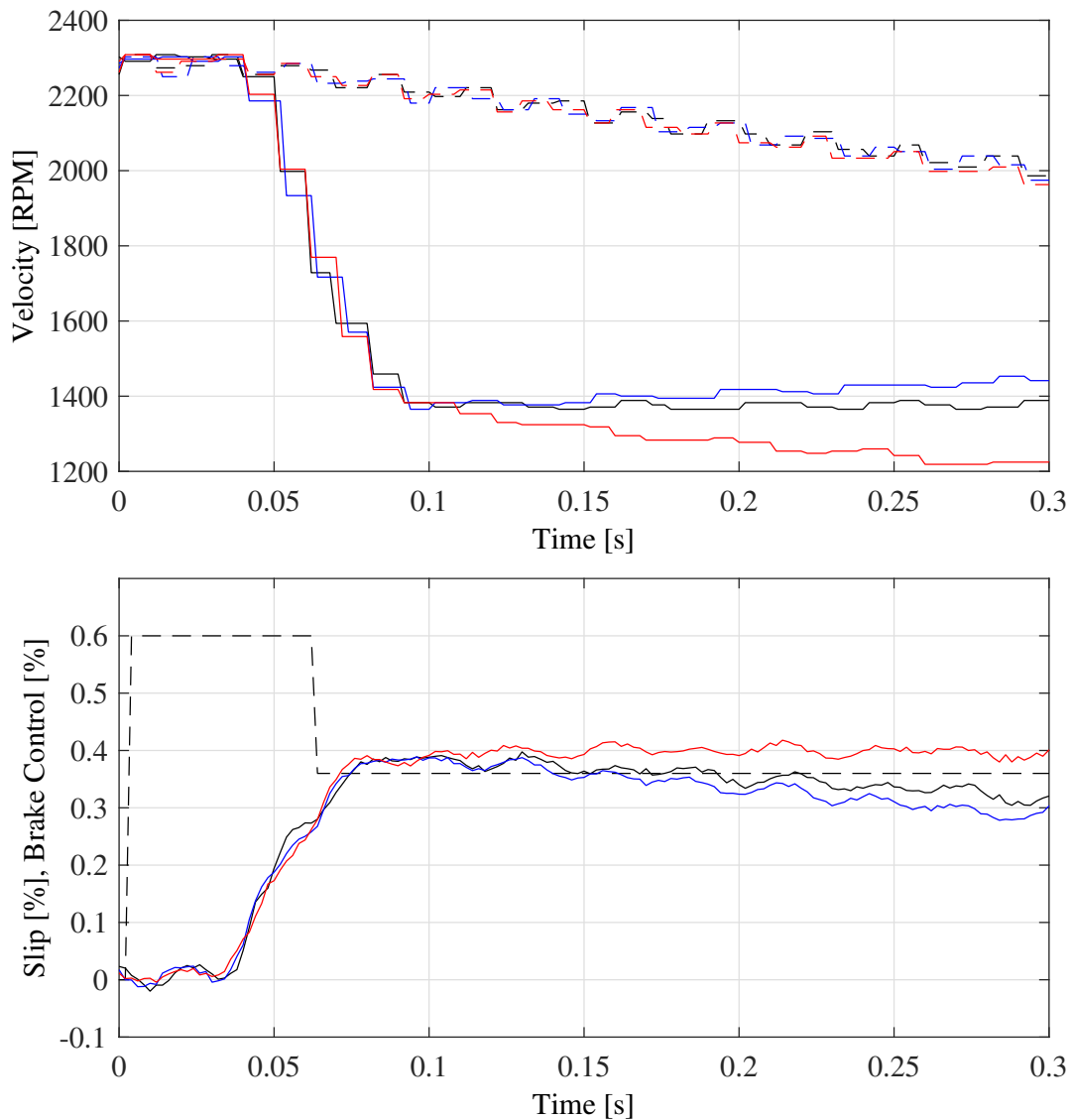


Figure 7.12: An example of non-reproducible results obtained for laboratory ABS. Each color represents a separate experiment. Upper plot: car velocity - dashed line, wheel velocity - solid line. Lower plot: brake control - dashed line, slip - solid line.

The component takes control after I finishes rapid slip increase. The controller shall use filtered slip signal (e.g. the moving average window for 3-5 samples) in order to reduce oscillations.

During ABS system utilization and data collection for presented controller design, a major problem has been observed. The system behavior was known to be not reproducible. Despite similar system state and the same control pattern the obtained results were not consistent. An example of this behavior is shown in Figure 7.12. As previously, the system is working in open-loop and the control signal is identical for all experiments: again the control is set to 0.6 for a certain time and reduced to 0.38 afterwards. One can note that for experiments 1 (black) and 2 (blue) the system response to the applied control is similar, while for the remaining one (red) it is very different. It is notable that system state (see wheel

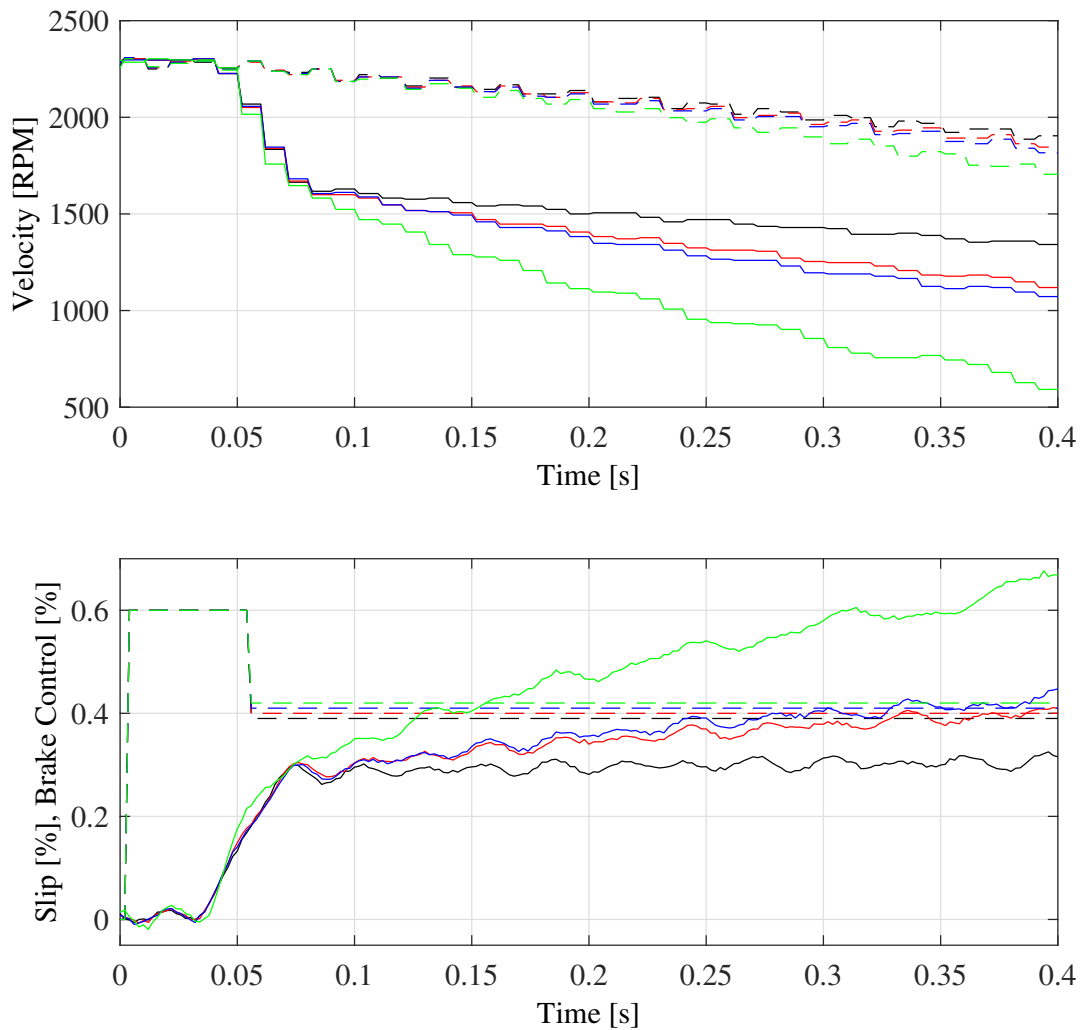


Figure 7.13: An example of laboratory ABS sensitivity to applied control values. Each color represents a separate experiment. Upper plot: car velocity - dashed line, wheel velocity - solid line. Lower plot: brake control - dashed line, slip - solid line.

and car velocities) is similar for all experiments until time instance 0.1 s. After this time the described inconsistency is observed in the state developed by the system.

Another discovered feature of the system is its sensitivity to the applied control values. Figure 7.13 presents results from experiments similar to previous example although in this case the following control values after the jump are different and change from 0.39 to 0.42. The depicted example shows how negligible difference in control level influences the further state of the system. One can notice, that the system state at the time when different control is applied is nearly the same.

Further investigation of the encountered issues revealed mechanical constraints of the utilized brake system. In case of rapid control value changes (adjusting DC motor PWM signal), the torque acting on

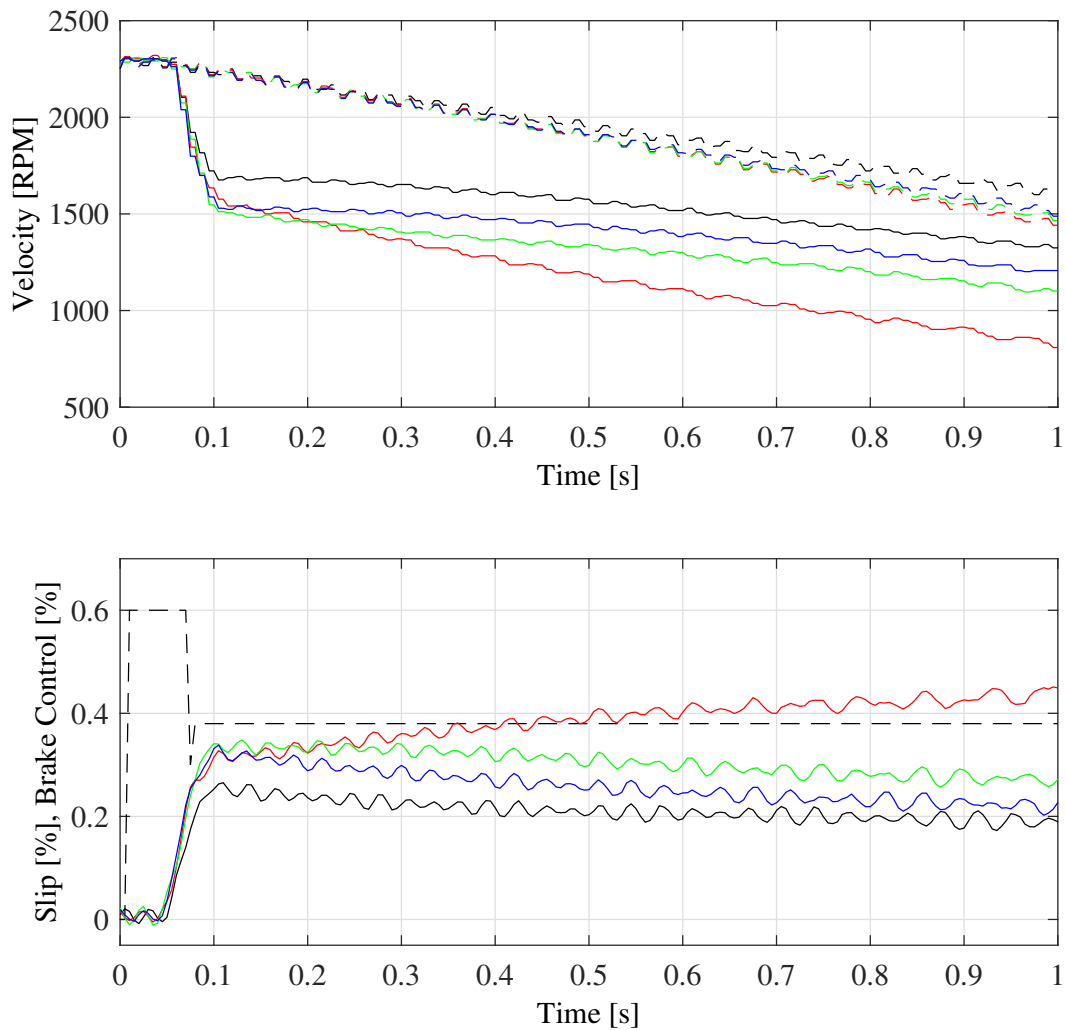


Figure 7.14: An example of laboratory ABS brake torque repeatability issues. Each color represents a separate experiment. Upper plot: car velocity - dashed line, wheel velocity - solid line. Lower plot: brake control - dashed line, slip - solid line.

the brake disc is not always repeatable. Such a condition is shown in Figure 7.14 where the control is first increased, then decreased and once again increased. The braking torque acting on the wheel must be different for all experiments (the system reacts differently), while the applied control is exactly the same in each case.

Due to the described difficulties, the realization of the planned two-part ABS controller based on available measured signals was not possible. In order to obtain confident information about the actual braking torque acting on the wheel, the feedback in the form of brake DC motor current is required.

7.3.2. The new slip controller based on brake DC current measurement

The new ABS slip controller is a combination of hybrid slip controller and brake DC motor current controller [219]. The brake DC motor current controller utilizes the current measurement provided by the Hall effect current sensors which tend to introduce noise to output voltage signal measured on RT-DAC/USB2 I/O board. Additionally, due to the fact that DC motor is controlled by PWM signal, the resulting current is affected by high frequency voltage changes. No filtering is applied to the sensor signal in the measurement board. The signal is filtered only in MATLAB/Simulink control and measurement model.

The measured sensor voltage signal obtained from the A/D converter is in the range $[0.375, 4.625]$ V and the value 2.5 V denotes 0 A current value. Before the voltage signal is converted into corresponding current signal, the filter is applied. In order to smooth the data, the moving-average filter is introduced. The window size is set to 10. The filtered voltage signal is utilized to calculate the current using linear transformation. The bias is set to 2.493 V measured by the A/D converted when the DC motor control is set to 0 V. The gain is set to 104.2 mV A^{-1} . It is based on the sensor technical specification.

Figure 7.15 presents the current sensor output filter response to the DC motor voltage control change. One can notice a noise contained in the raw signal and the filtering effect which enhances the current signal quality.

The DC motor current signal has a direct impact on the braking force moment acting on car wheel. Therefore, it is a key requirement to control the current at the desired level during the braking maneuver. In order to realize such requirement the current controller must be employed. In this work PI controller is designed and tuned for DC motor current control. The input to the controller consists of the current error calculated as the difference between the desired current designated by the root slip controller and the actual current. The output is the DC motor PWM voltage control limited in the range $[30, 50]$ %. The limitation of the controller output is applied in order to prevent high control values which cause rapid wheel velocity decrease which leads to wheel lock-up. The tuning procedure of the proportional gain k_p^b and integral gain k_i^b was conducted using trial and error method. The goal was to find parameters which ensure fast reaching of the desired current and accurate tracking of the set point. The obtained parameters are $k_p^b = 0.1$ and $k_i^b = 0.5$.

The controller performance is depicted in Figure 7.16. The slope of the desired current is driving the controller. The upper plot shows the actual and desired current and the lower plot presents the PI controller output signal. The DC motor current is properly tracking the monotonically increasing reference signal.

In the examined system, the control of a slip is performed by steering the DC motor PWM voltage. Originally, when there is no DC motor current measurement, the control strategy might only be based

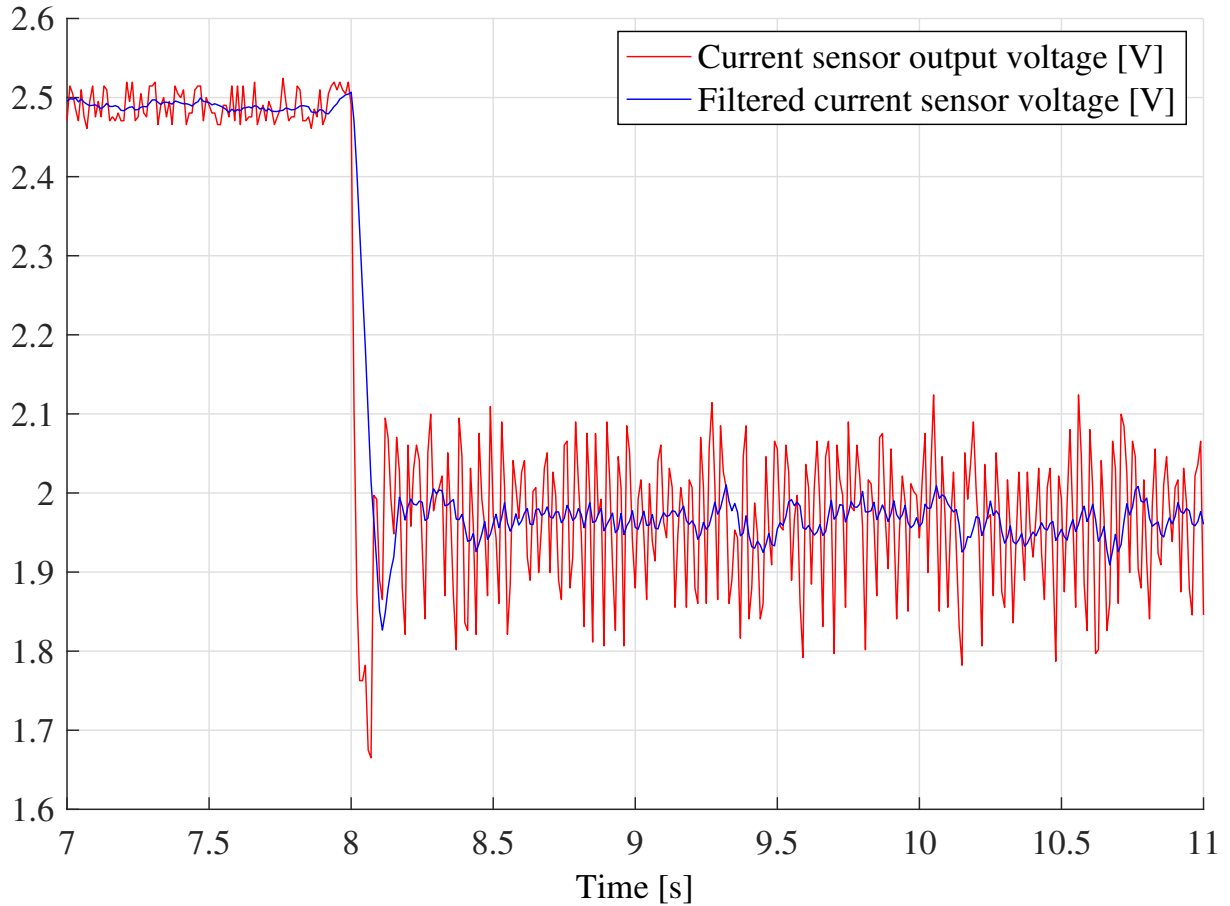


Figure 7.15: The current sensor output filter performance.

on the wheel velocities. With the addition of the mentioned feedback signal from the brake, the control algorithms gain extra input which might be utilized to improve control laws and their performance. For the purpose of this work a daisy chain of system controllers was prepared. The block diagram of the hybrid controller is presented in Figure 7.17. The examined PI current controller is governed by the slip root controller. The role of the master controller (slip root controller) is to provide the desired DC motor current to the slave controller (current controller) in such a way that the desired slip ratio is maintained.

The slip controller is a heuristic controller realized as a combination of PD controller and two-states controller. The control law is as follows:

$$i_d = \begin{cases} i_d^{\max}, & : \lambda_e \geq 0.1 \\ \text{PD}(\lambda_e), & : |\lambda_e| < 0.1 \\ i_d^{\min}, & : \lambda_e \leq -0.1 \end{cases} \quad (7.19)$$

where i_d and λ_e denote the desired current of the brake DC motor and slip error values respectively. The limits of the current (i_d^{\max} and i_d^{\min}) are set to 9 A and 6 A. The lower limit corresponds to the end of brake dead zone (current level, the application of which does not generate braking force). The PD

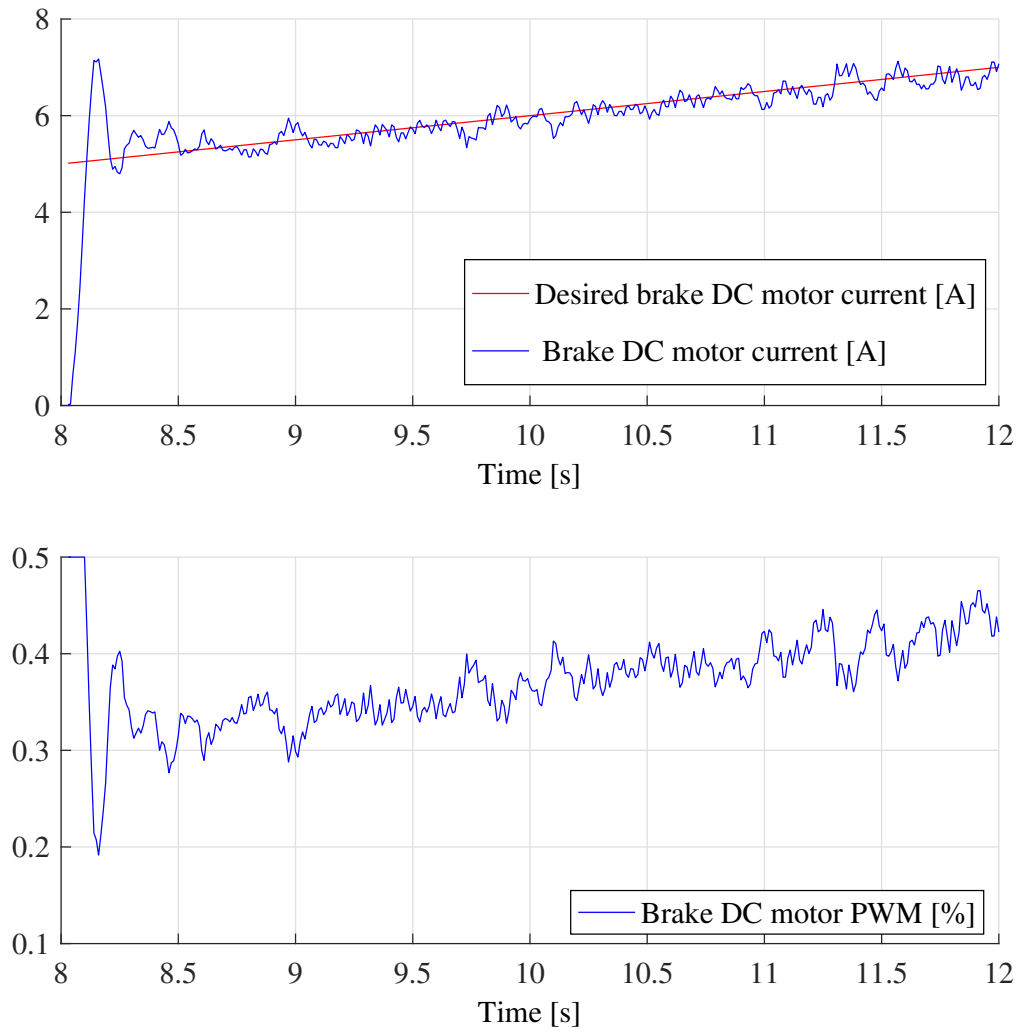


Figure 7.16: The brake DC motor current controller performance.

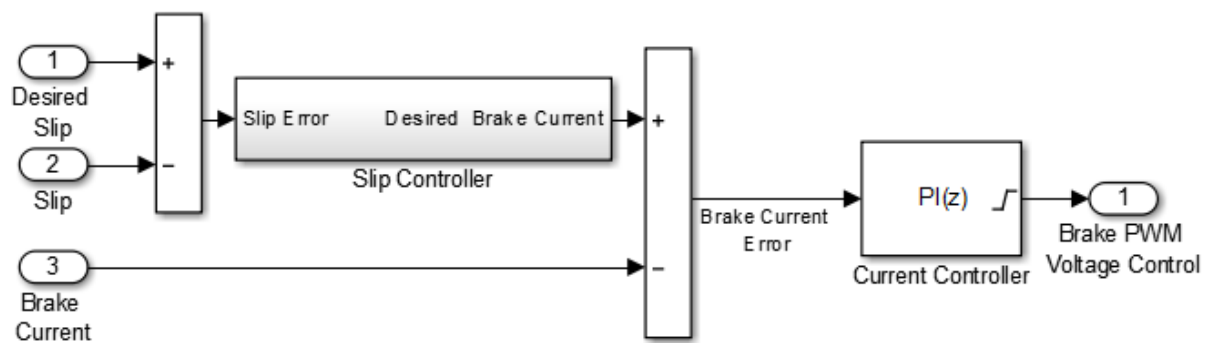


Figure 7.17: The new slip controller block diagram.

controller tunable parameters were obtained based on an experimental observation and the trial and error approach. The proportional gain is set to 20 and derivative gain is set to 1.

The new ABS slip controller performance is compared with classic two-states relay controller. This controller's input is also λ_e although the control variable is the brake DC motor PWM voltage u_b . The control law is as follows:

$$u_b = \begin{cases} u_b^{\max}, & : \lambda_e \geq 0 \\ u_b^{\min}, & : \lambda_e < 0 \end{cases} \quad (7.20)$$

The limits of PWM voltage (u_b^{\max} and u_b^{\min}) are set to 30 and 50 % in order to be compliant with the limits applied to the PI current controller.

The performance assessment of the new ABS slip controller is presented in Figure 7.18 and the behavior of relay controller is depicted in Figure 7.19. The desired slip ratio is set to 0.5 in both cases. The plots time range is limited to a span of approximately 1 s. During the time before the depicted period the wheels are accelerated to the speed of about 2200 RPM. When this happens the controllers are enabled and the braking maneuver begins (the first jumps of control denote the controller's start of operation). After the presented one second period, the wheels speed decreases to the level when slip stabilization is not applicable. One can notice that during the control period the new ABS slip controller outperforms the classic one in the desired slip tracking. The maintained slip is closer to the reference and the oscillations are smaller. Additionally, the observed slip signal is also kept under the reference slip for the most of the control time period.

The presented approach to tackle the issues discussed in section 7.3.1 proved to be correct. The realized solution improved slip control performance and eliminated described difficulties. Thanks to the addition of the current measurement and the implementation of the additional brake DC motor current controller, the problem with non-repetitive results is solved. The experimental results obtained for several identical trails are now similar and comparable.

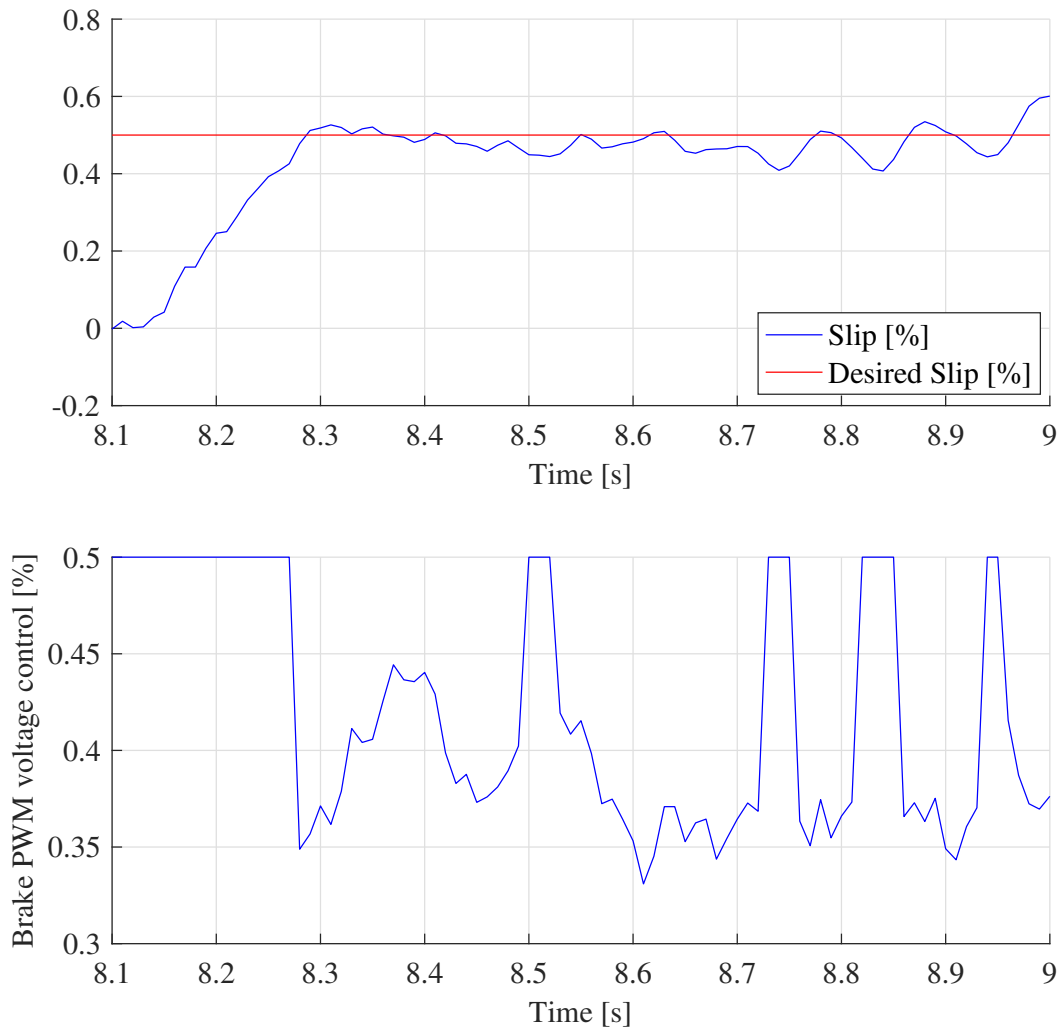


Figure 7.18: The performance of the new ABS slip controller.

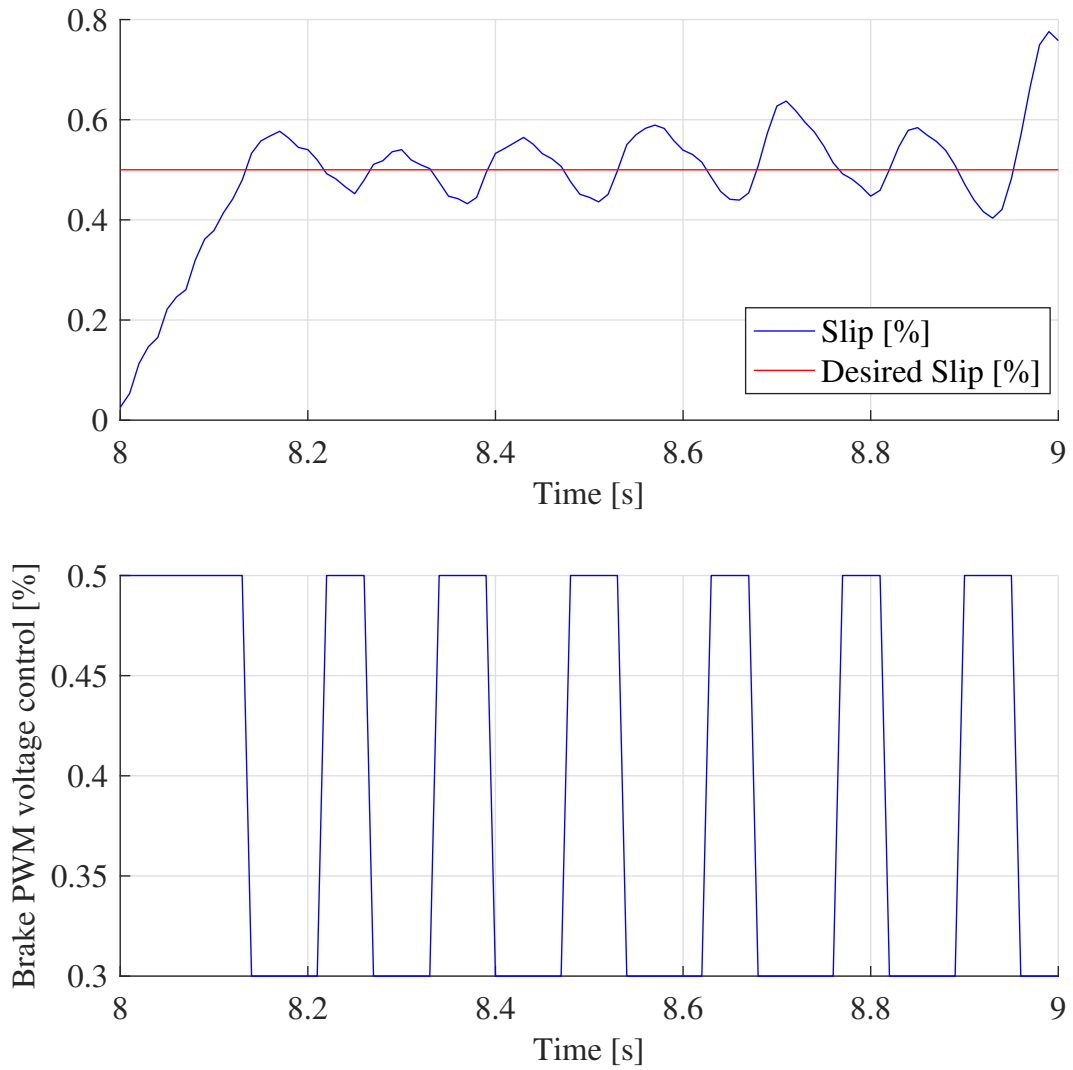


Figure 7.19: The performance of the relay slip controller.

Conclusions

The dissertation consists of 7 chapters. Not all chapters have equal share of references. Chapters 2, 4 and 6 are distinguished by a large number of references, over 50. In principle, this uneven distribution is justified. Chapters 2, 4 and 6 provide a scientific and research background for the implementation of the main thesis of this work: **Automotive automatic control systems operating in real time improve driving safety and driving comfort.**

The dissertation starts with **chapter 1** i.e. “History of automotive systems”. The chapter basically has no references so as not to mix historical and technical topics.

Chapter 2 shows the full range of hardware and software tools required for the design and testing of automotive systems. Successful cooperation of car makers and electronic control systems (ECU) suppliers is indispensable in the car production process. There is a new methodology of the integration of ECU’s and sub-systems much earlier in the design cycle using virtual prototyping and simulations. The quality, reliability and available functionality is taken into account by a car maker to choose ECU suppliers.

The implementation and testing of the automotive software systems is the most time consuming and expensive phase of the development process. The resulting implementation, usually in a form of C-code, must be integrated into basic software components (drivers, operating systems, etc.). They constitute the ECU software standards. The standards listed below are the most commonly used: IEC 61508, ISO 26262 and MISRA (Motor Industry Software Reliability Association) and AUTOSAR (AUTomotive Open System ARchitecture). The first two relate to Functional Safety. The last defines the guidelines for C-code implementation.

MBD (Model Based Design/Development) or MBRE (Model Based Requirements Engineering) are used as computerized models family to support communication, documentation, analysis and synthesis. Actually, the whole chain of simulations: MiL, SiL, HiL and PiL is tested. In MiL (Model-in-the-Loop) simulation, an algorithm begins to be developed. The compiled code is used in SiL (Software-in-the-Loop) simulation where one deals with artificial input data. When ECU hardware components are finalized, the algorithm code is integrated into the basic software of the system. It is

called HiL (Hardware-in-the-Loop) simulation testing. In the course of PiL (Processor-in-the-Loop) step, the embedded target processor execution of code is applied. The section also includes CAE (Computer Aided Engineering) and RCP (Rapid Control Prototyping). It is the process of calibrating control algorithms on prototype hardware to get a tested device up and running before a production-intent ECU is available.

In **chapter 3** several aspects of real-time control are considered. The MS Windows jitters comparison: WM timer and multimedia event timer are illustrated. The USB 2.0 I/O board manufactured by INTECO is presented. Beside the extended MS Windows operating system, tis board is responsible for real-time transitions.

Chapter 4 broadly represents semi active and active suspension systems. The semi-active suspension is found at three different vibration isolation levels: wheel-to-chassis, chassis-to-cabin and cabin-to-seat. A number of vehicle suspension models are investigated. These are: quarter-car passive automotive suspension model, quarter-car semi-active automotive suspension model, quarter-car fully active automotive suspension model, half-car passive pitch oriented automotive suspension model and full-car passive automotive suspension model.

There are also models of a damper, tire and road. There is a general assessment of a driving comfort and safety. As far as the control of SAS is concerned, different technical groups are introduced. There is the *Comfort oriented control for semi-active suspension* group. In this group the following control algorithms are described: Two-state Skyhook Damper Control (SH-2), the linear approximation Skyhook Damper Control (SH-L), Acceleration Driven Damper Control (ADD), Mixed SH-ADD Damper Control (SH-ADD), Power Driven Damper Control (PDD) and Balance Logic Damper Control.

The other group is *Road-holding oriented control for semi-active suspension*. In this group the following control algorithms are described: the two-state Groundhook Damper Control (GH-2), the linear Groundhook Damper Control (GH-L) and the displacement-based two-states Groundhook Damper Control.

The other group name is *Dual comfort and road-holding oriented control for semi-active suspension* with the control algorithm name Hybrid Skyhook-Groundhook Damper Control. Finally the *Advanced control strategies for semi-active suspension systems* are considered.

Chapter 6 gives an exhaustive illustration of automotive braking systems. The following models are considered: the brake actuator, vehicle dynamics – single-wheel, vehicle dynamics – double-wheel. The general reference to the sliding control goes to various control algorithms met by ABS from conventional ABS algorithm to various control strategies.

The dissertation ends in **chapter 5** and **chapter 7**. These sections contain the original achievements of the author. Experiments on modeling, identification and control of driving comfort (SAS) and driving

safety (ABS) are undeniable author's contributions to this area of knowledge. The main result of **chapter 5** is the identification of SAS model parameters. Identification corresponds to different parts of the dynamical SAS model, for example to the wheel-eccentricity part model, etc. A high quality and accuracy of the identification is illustrated in Figures 5.16 and 5.17 where the real and modeled response of car body position to the chirp signal are shown. Due to poor accuracy of the frequency response of the system under varying frequency of the kinematic extortion (the simulated trajectories do not coincide with the real trajectories) a new model of the MR damper has been introduced.

Beside the identification procedures, several control strategies of the MR damper for SAS have been realized. The correctness and efficiency of the proposed algorithms has been verified on the basis of the previously identified dynamic model. It must be stressed that the results of damping and driving comfort are obtained on an experimental basis. This means that the proposed control algorithms are directly verified based on the real SAS system see Figures from 5.23 to 5.28 and Table 5.2.

Another part of the work, which reveals the author's most original results, is **chapter 7**. It starts with the identification of the model parameters: the lower wheel with the DC motor and the upper wheel. The slip friction coefficient function is determined experimentally, see Figure 7.6. High accuracy and quality of the identification experiment are observed, see Figure 7.8 (the upper wheel angular velocity) and Figure 7.9 (the lower wheel angular velocity). One can compare the real and simulated responses.

Finally, the author has an observation that the ABS system does not operate repeatedly. **Subsection 7.3.1** describes challenges, issues and difficulties that occur during real-time control of the slip in the ABS system. The observation becomes a motivation to introduce a brake DC current measurement. The new measurement made it possible to construct a completely new slip regulator. The new ABS slip controller is a combination of the hybrid slip controller and brake DC motor current controller. In the author's opinion, the identification and control of slip due to additional DC current measurement is undoubtedly an important experimental result. Same way as in the case of SAS, the author has limited confidence in results which are purely modeled.

Some words about future research intentions should be added. It is proposed to use neural networks in SAS and ABS control algorithms. This area of research requires some more work, especially because the author is familiar with this subject and has already taken the first steps in integrating and learning neural networks in the control. In his professional life the author is connected with the automotive industry so there is a natural opportunity for further research in this field.

Bibliography

- [1] Robert Bosch GmbH. *Safety Comfort and Convenience Systems*. Robert Bosch GmbH, 2006. ISBN: 0-8376-1391-4.
- [2] William B. Ribbens. *Understanding Automotive Electronics*. 6th. Elsevier Science (USA), 2003.
- [3] Robert Bosch GmbH. *Automotive Electrics and Automotive Electronics: Systems and Components, Networking and Hybrid Drive*. 5th. Robert Bosch GmbH, 2007. ISBN: 978-3-658-01783-5.
- [4] Shibu K. V. *Introduction to Embedded Systems*. Tata McGraw Hill Education Private Limited, 2009. ISBN: 978-0-07-014589-4.
- [5] R.H. Barnard. “An Introduction to Modern Vehicle Design”. In: ed. by Julian Happian-Smith. Butterworth-Heinemann, 2002. Chap. Automotive engineering development, pp. 1–28.
- [6] H. Morris. “An Introduction to Modern Vehicle Design”. In: ed. by Julian Happian-Smith. Butterworth-Heinemann, 2002. Chap. Control systems in automobiles, pp. 333–370.
- [7] J. Happian-Smith and Eric Chowanietz. “An Introduction to Modern Vehicle Design”. In: ed. by Julian Happian-Smith. Butterworth-Heinemann, 2002. Chap. Future trends in automobile design, pp. 553–572.
- [8] Michel Parent. “Intelligent Vehicle Technologies: Theory and Applications”. In: ed. by Ljubo Vlacic, Michel Parent, and Fumio Harashima. Butterworth-Heinemann, 2001. Chap. The car of the future, pp. 3–19.
- [9] Nicolas Navet and Françoise Simonot-Lion. *Automotive Embedded Systems Handbook*. 1st. Boca Raton, FL, USA: CRC Press, Inc., 2008. ISBN: 084938026X, 9780849380266.
- [10] Automotive SIG. *Automotive SPICE Process Assessment Model*. http://www.automotivespice.com/fileadmin/software-download/automotiveSIG_PAM_v25.pdf. [Online]. 2015.
- [11] M. Mueller, K. Hoermann, L. Dittmann, and J. Zimmer, eds. *Automotive SPICE in Practice: Surviving Implementation and Assessment*. Rocky Nook, 2008. ISBN: 978-1-933952-29-1.

-
- [12] J. Weber. *Automotive Development Processes: Processes for Successful Customer Oriented Vehicle Development*. Springer-Verlag Berlin Heidelberg, 2009. ISBN: 978-3-642-01252-5.
- [13] International Business Machines Corp. *IBM Rational DOORS*, Web Page. <http://www-03.ibm.com/software/products/en/ratidoor>. [Online]. 2015.
- [14] Dassault Systèmes. *Dassault Systèmes CATIA REQTIFY*, Web Page. <http://www.3ds.com/products-services/catia/capabilities/requirements-engineering/reqtify/>. [Online]. 2015.
- [15] P. Giusto, J-Y. Brunel, A. Ferrari, E. Fourgeau, L. Lavagno, and A. Sangiovanni-Vincentelli. “Automotive Virtual Integration Platforms: Why’s, What’s, and How’s”. In: International Conference on Computer Design: VLSI in Computers and Processors. IEEE, 2002.
- [16] P. Giusto and T. Demmeler. “Rapid design exploration of safety-critical distributed automotive applications via virtual integration platforms”. In: *The Journal of Systems and Software* 70 (2004), pp. 245–262.
- [17] IEC. *IEC 61508 Functional Safety*. <http://www.iec.ch/functionalsafety/>. [Online]. 2015.
- [18] ISO. *ISO 26262 Road vehicles – Functional safety – Part 1-10*. <http://www.iso.org/>. [Online]. 2015.
- [19] MISRA Consortium. *MISRA C:2012 (MISRA C3)*. <http://www.misra.org.uk/>. [Online]. 2015.
- [20] AUTOSAR (AUTomotive Open System ARchitecture). *Specifications, Release 4.2*. <http://www.autosar.org/>. [Online]. 2015.
- [21] Silverio Martínez-Fernández, Claudia P. Ayala, Xavier Franch, and Elisa Y. Nakagawa. “A Survey on the Benefits and Drawbacks of AUTOSAR”. In: *Proceedings of the First International Workshop on Automotive Software Architecture*. WASA ’15. Montréal, QC, Canada: ACM, 2015, pp. 19–26. ISBN: 978-1-4503-3444-0. DOI: 10.1145/2752489.2752493. URL: <http://doi.acm.org/10.1145/2752489.2752493>.
- [22] M. Torngren, D.J. Chen, D. Malvious, and J. Axelsson. “Model-Based Development of Automotive Embedded Systems”. In: *Automotive Embedded Systems Handbook*. Ed. by N. Navet and F. Simonot-Lion. Taylor & Francis Group, LLC, 2009. Chap. 10. ISBN: 978-0-8493-8026-6.
- [23] Object Management Group, Inc. *OMG Unified Modeling Language (OMG UML), version 2.4.1*. <http://www.omg.org/spec/UML/2.4.1/>. [Online]. 2015.
- [24] Object Management Group, Inc. *OMG Systems Modeling Language (OMG SysML), version 1.3*. <http://www.omg.org/spec/SysML/1.3/>. [Online]. 2015.

-
- [25] Winfred K.N. Anakwa, H.P. Roca, J. Lopez, and A. Malinowski. "Environments for rapid implementation of control algorithms and hardware-in-the-loop simulation". In: vol. 3. 28th Annual Conference of the Industrial Electronics Society (IECON 02). IEEE, 2002.
- [26] P. Skruch, M. Panek, and Bogdan Kowalczyk. "Model-Based Testing in Embedded Automotive Systems". In: *Model-Based Testing for Embedded Systems*. Ed. by J. Zander, I. Schieferdecker, and P.J. Mosterman. CRC Press, 2011. Chap. 19. ISBN: 978-1-4398-1845-9.
- [27] P. Skruch and G. Buchala. "Model-Based Real-Time Testing of Embedded Automotive Systems". In: *SAE Int. J. Passeng. Cars – Electron. Electr. Syst.* 7.2 (2014).
- [28] H.K. Fathy, Z.S. Filipi, J. Hagena, and J.L. Stein. "Review of Hardware-in-the-Loop Simulation and Its Prospects in the Automotive Area". In: SPIE, Modeling and Simulation for Military Applications (6228:62880E). 2006.
- [29] Dassault Systèmes. *Dassault Systèmes Dymola / CATIA*, Web Page. <http://www.3ds.com/products-services/catia/products/dymola>. [Online]. 2015.
- [30] Modelica Association. *Modelica- A Unified Object-Oriented Language for Systems Modeling, Language Specification, Version 3.3*. <https://www.modelica.org/documents/ModelicaSpec33.pdf>. [Online]. 2015.
- [31] Siemens. *Siemens LMS Imagine.Lab Amesim*, Web Page. http://www.plm.automation.siemens.com/en_us/products/lms/imagine-lab/amesim/index.shtml. [Online]. 2015.
- [32] Maplesoft. *MapleSim*, Web Page. <http://www.maplesoft.com/products/Maplesim/>. [Online]. 2015.
- [33] ITI. *ITI SimulationX*, Web Page. <http://www.itisim.com/simulationx/>. [Online]. 2015.
- [34] MSC Software. *Adams/Car*, Web Page. <http://www.mscsoftware.com/product/adamscar/>. [Online]. 2015.
- [35] The MathWorks, Inc. *MATLAB / Simulink / Stateflow*, Web Page. <http://www.mathworks.com/products/>. [Online]. 2015.
- [36] National Instruments. *MATRIXx*, Web Page. <http://sine.ni.com/nips/cds/view/p/lang/en/nid/12153>. [Online]. 2015.
- [37] The MathWorks, Inc. *Delphi Develops Radar Sensor Alignment Algorithm for Automotive Active Safety System*. [Online]. 2015.
- [38] dSPACE GmbH. *TargetLink, Automatic production code generator*, Web Page. <http://www.dspace.com/en/pub/home/products/sw/pcgs/targetli.cfm>. [Online]. 2015.

- [39] Modelica Association. *Functional Mock-up Interface (FMI)*, Web Page. <https://www.fmi-standard.org/>. [Online]. 2015.
- [40] TESIS DYNAware GmbH. *DYNA4 package and enDYNA/veDYNA*, Web Page. <http://www.thesis-dynaware.com/>. [Online]. 2015.
- [41] Medha Santosh Jambhale, J Kale, Mangesh Ramesh Saraf, Arunraj Kumar Govindhasamy, and Karl-Eric Kostlin. "Use of Software / Hardware-in-Loop Technique for Development of Semi-Active Suspension". In: *SAE Technical Paper*. SAE International, Jan. 2015. DOI: 10.4271/2015-26-0007. URL: <http://dx.doi.org/10.4271/2015-26-0007>.
- [42] Mechanical Simulation CorporationTM. *CarSim, TruckSim, SuspensionSim*, Web Page. <https://www.carsim.com/products/>. [Online]. 2015.
- [43] Joseph P. Ryan, Michael W. Neal, James W. Mero, and Frank J. Taverna. "Design of the Milford Road Course". In: *SAE Technical Paper*. SAE International, Apr. 2005. DOI: 10.4271/2005-01-0385. URL: <http://dx.doi.org/10.4271/2005-01-0385>.
- [44] Gamma Technologies. *GT-Suite/GT Power*, Web Page. <https://www.gtisoft.com/>. [Online]. 2015.
- [45] dSPACE GmbH. *Automotive Simulation Models (ASM)*, Web Page. https://www.dspace.com/en/inc/home/products/sw/automotive_simulation_models.cfm. [Online]. 2015.
- [46] dSPACE GmbH. *MotionDesk*, Web Page. <https://www.dspace.com/en/inc/home/products/sw/experimentandvisualization/modesk.cfm>. [Online]. 2015.
- [47] TESIS DYNAware GmbH. *DYNAanimation*, Web Page. <http://www.thesis-dynaware.com/>. [Online]. 2015.
- [48] IPG Automotive. *CarMaker*, Web Page. <http://ipg.de/simulationsolutions/carmaker/>. [Online]. 2015.
- [49] TASS International B.V. *PreScan*, Web Page. <https://www.tassinternational.com/prescan>. [Online]. 2015.
- [50] Dariusz Cieślak, Krzysztof Kogut, Maciej Różewicz, and Mateusz Orłowski. "Dynamic Input Generation for the Development of Active Safety Perception Algorithms". In: *SAE Technical Paper*. SAE International, Apr. 2016.
- [51] ETAS. *ASCET-MD (Modeling & Design)*, Web Page. http://www.etas.com/en/products/ascet_md_modeling_design.php. [Online]. 2015.
- [52] dSPACE GmbH. *SystemDesk*, Web Page. http://www.dspace.com/en/pub/home/products/sw/system_architecture_software/systemdesk.cfm. [Online]. 2015.

- [53] ANSYS. *SCADE Suite, Web Page*. <http://www.ansys.com/Products/Simulation+Technology/Systems+&+Embedded+Software/ANSYS+SCADE+Suite>. [Online]. 2015.
- [54] Pawel Skruch, Rafal Dlugosz, Krzysztof Kogut, Pawel Markiewicz, Dominik Sasin, and Maciej Rozewicz. “The Simulation Strategy and Its Realization in the Development Process of Active Safety and Advanced Driver Assistance Systems”. In: *SAE Technical Paper*. SAE International, Apr. 2015. DOI: 10.4271/2015-01-1401. URL: <http://dx.doi.org/10.4271/2015-01-1401>.
- [55] Elektrobit. *EB Assist ADTF, Web Page*. <https://automotive.elektrobit.com/products/eb-assist/adtf/>. [Online]. 2015.
- [56] Vector Informatik GmbH. *vADASdeveloper, Web Page*. http://vector.com/vi_vadasdeveloper_en.html. [Online]. 2015.
- [57] BASELABS. *BASELABS products and services, Web Page*. <https://www.baselabs.de/>. [Online]. 2015.
- [58] Vector Informatik GmbH. *CANoe, Web Page*. http://vector.com/vi_canoe_en.html. [Online]. 2015.
- [59] Elektrobit. *EB tresos Busmirror, Web Page*. <https://automotive.elektrobit.com/products/ecu/eb-tresos/busmirror/>. [Online]. 2015.
- [60] ETAS. *INCA Software Products, Web Page*. http://www.etas.com/en/products/inca_software_products.php. [Online]. 2015.
- [61] Vector Informatik GmbH. *Hardware Bus Interfaces, Web Page*. http://vector.com/vi_interfaces_en.html. [Online]. 2015.
- [62] Elektrobit. *EB tresos Hardware, Web Page*. <https://automotive.elektrobit.com/products/ecu/eb-tresos/hardware/>. [Online]. 2015.
- [63] ETAS. *Hardware Products, Web Page*. http://www.etas.com/en/products/hardware_products.php. [Online]. 2015.
- [64] dSPACE GmbH. *MicroAutoBox II, Web Page*. <http://www.dspace.com/en/pub/home/products/hw/micautob.cfm>. [Online]. 2015.
- [65] dSPACE GmbH. *ControlDesk Next Generation, Web Page*. <http://www.dspace.com/en/pub/home/products/sw/experimentandvisualization/controldesk.cfm>. [Online]. 2015.
- [66] I.R. Kendall and R.P. Jones. “An investigation into the use of hardware-in-the-loop simulation testing for automotive electronic control systems”. In: *Control Engineering Practice 7* (1999), pp. 1343–1356.

- [67] R. Isermann, J. Schaffnit, and S. Sinsel. “Hardware-in-the-loop simulation for the design and testing of engine-control systems”. In: *Control Engineering Practice* 7 (1999), pp. 643–653.
- [68] ETAS. *ES900 Prototyping and Interface Modules*, Web Page. http://www.etas.com/en/products/compact_es900_rapid_prototyping_modules.php. [Online]. 2015.
- [69] ETAS. *ASCET-RP (Rapid Prototyping)*, Web Page. http://www.etas.com/en/products/ascet_rp_rapid_prototyping.php. [Online]. 2015.
- [70] ETAS. *LABCAR*, Web Page. http://www.etas.com/en/products/solutions_labcar_component_overview.php. [Online]. 2015.
- [71] OPAL-RT TECHNOLOGIES, Inc. *RT-LAB*, Web Page. <http://www.opal-rt.com/product/rt-lab-professional-real-time-digital-simulation-software>. [Online]. 2015.
- [72] OPAL-RT TECHNOLOGIES, Inc. *PC/104 Rapid Control Prototyping (RCP)*, Web Page. <http://www.opal-rt.com/product/pc104-rapid-control-prototyping-rcp>. [Online]. 2015.
- [73] X. Chen, M. Salem, T. Das, and X. Chen. “Real Time Software-in-the-loop Simulation for Control Performance Validation”. In: *SIMULATION* 84.8/9 (2008), pp. 457–471.
- [74] National Instruments. *NI CompactRIO*, Web Page. <http://www.ni.com/compactrio/>. [Online]. 2015.
- [75] National Instruments. *NI PXI Platform*, Web Page. <http://www.ni.com/pxi/>. [Online]. 2015.
- [76] M. Short and M.J. Pont. “Assessment of high-integrity embedded automotive control systems using hardware in the loop simulation”. In: *The Journal of Systems and Software* 81 (2008), pp. 1163–1183.
- [77] John G. Proakis and Dimitris G. Manolakis. *Digital Signal Processing (3rd Ed.): Principles, Algorithms, and Applications*. Upper Saddle River, NJ, USA: Prentice-Hall, Inc., 1996. ISBN: 0-13-373762-4.
- [78] S.M. Kuo, B.H. Lee, and W. Tian. *Real-Time Digital Signal Processing: Implementations and Applications*. Wiley, 2006. ISBN: 9780470035511.
- [79] John A. Stankovic. “Misconceptions About Real-Time Computing: A Serious Problem for Next-Generation Systems”. In: *Computer* 21.10 (Oct. 1988), pp. 10–19. ISSN: 0018-9162. DOI: 10.1109/2.7053. URL: <http://dx.doi.org/10.1109/2.7053>.
- [80] Joseph Mattai. *Real-Time Systems: Specification, Verification, and Analysis*. Ed. by Mathai Joseph. Upper Saddle River, NJ, USA: Prentice Hall PTR, 1995. ISBN: 0134552970.
- [81] Wind River. *VxWorks - Wind River*, Web Page. <https://www.windriver.com/products/vxworks/>. [Online]. 2017.

- [82] QNX Software Systems Limited. *QNX*, *Web Page*. <http://www.qnx.com/content/qnx/en.html>. [Online]. 2017.
- [83] Mentor Graphics. *Nucleus*, *Web Page*. <https://www.mentor.com/embedded-software/nucleus/>. [Online]. 2017.
- [84] ENEA. *ENEA OSE*, *Web Page*. <http://www.enea.com/products/operating-systems/enea-ose/>. [Online]. 2017.
- [85] Real Time Engineers Ltd. *FreeRTOS*, *Web Page*. <http://www.freertos.org/>. [Online]. 2017.
- [86] Andrzej Turnau. “Target Control of Nonlinear Systems in Real Time - Intelligent and Time-optimal Algorithms”. In: *Dissertations, Monographies*. Vol. 102. Uczelniane Wydawnictwa Naukowo-Dydaktyczne AGH im. S. Staszica w Krakowie, 2002.
- [87] Krzysztof Kołek. “Development of C-language real-time controller for Android OS”. In: *Design, development and implementation of real-time systems*. Ed. by Leszek Trybus and Marcin W. Mastalerz. Scientific Papers of the Polish Information Processing Society Scientific Council. Polish Information Processing Society — Warszawa, 2013.
- [88] Roman Gumzej. *Real-time Systems' Quality of Service*. 1st ed. Springer-Verlag London, 2010. ISBN: 978-1-84882-848-3.
- [89] Alan Burns and Andy Wellings. *Real-Time Systems and Programming Languages: Ada, Real-Time Java and C/Real-Time POSIX*. 4th. USA: Addison-Wesley Educational Publishers Inc, 2009. ISBN: 0321417453, 9780321417459.
- [90] INTECO Sp. z o. o. *User's Manual: RT-DAC/USB2 I/O Board*. [Online]. INTECO Sp. z o. o. 2010.
- [91] INTECO Sp. z o. o. *RT-DAC/PCI: Applications*. <http://www.inteco.com.pl/>. [Online]. 2015.
- [92] Krzysztof Kołek and Andrzej Turnau. “FPGA as a part of MS Windows control environment”. In: *Computer Science* 8.3 (2013), p. 61. ISSN: 2300-7036. URL: <https://journals.agh.edu.pl/csci/article/view/201>.
- [93] W. Kruger, O. Vaculin, and M. Spieck. “Semi-Active Suspension Systems for Road and Off-Road Vehicles - an Overview”. In: *Journal of Middle European Construction and Design of Cars - MECCA 01/2004 2* (2004), pp. 1–14.
- [94] S.M. Savaresi, C. Poussot-Vassal, C. Spelta, O. Sename, and L. Dugard. *Semi-Active Suspension Control Design for Vehicles*. Elsevier Ltd, 2010. ISBN: 978-0-08-096678-6.

- [95] X.D. Xue, K.W.E. Cheng, Z. Zhang, J.K. Lin, D.H. Wang, Y.J. Bao, M.K. Wong, and N. Cheung. “Study of Art of Automotive Active Suspensions”. In: 4th International Conference on Power Electronics Systems and Applications. 2011.
- [96] K. Arunachalam and P. Mannar Jawahar and P. Tamilporai. “Active Suspension System with Preview Control - A Review”. In: *SAE Technical Paper*. The Automotive Research Association of India, Aug. 2003.
- [97] M. H. Kim and S. B. Choi. “Estimation of road surface height for preview system using ultrasonic sensor”. In: *2016 IEEE 13th International Conference on Networking, Sensing, and Control (ICNSC)*. Apr. 2016, pp. 1–4.
- [98] Carlos A. Vivas-López, Diana Hernández-Alcantara, Juan C. Tudón-Martínez, and Ruben Morales-Menendez. “Review on Global Chassis Control”. In: *IFAC Proceedings Volumes 46.2* (2013), pp. 875–880. ISSN: 1474-6670. DOI: <http://dx.doi.org/10.3182/20130204-3-FR-2033.00040>.
- [99] D. Hrovat. “Survey of Advanced Suspension Developments and Related Optimal Control Applications”. In: *Automatica* 33.10 (Oct. 1997), pp. 1781–1817. ISSN: 0005-1098.
- [100] ZF Friedrichshafen AG. *CDC - variable damping system, Web Page*. https://www.zf.com/brands/en_de/sachs/products_sachs/products_pc_sachs/cdc/cdc.html. [Online]. 2017.
- [101] BWI GROUP. *MagneRide Suspension System*. <http://www.magneride.com/>. [Online]. 2017.
- [102] Mid-Atlantic Rubber, Inc. *LORD MAGNETO-RHEOLOGICAL (MR)*. <http://www.lordmrstore.com/lord-mr-products/>. [Online]. 2017.
- [103] Continental AG. *Electronic Air Suspension System*. http://www.continental-automotive.com/www/automotive_de_en/themes/two_wheelers/elektronische_luftfedersysteme_en.html. [Online]. 2017.
- [104] W. D. Jones. “Easy Ride: Bose Corp. Uses Speaker Technology to Give Cars Adaptive Suspension”. In: *IEEE Spectr.* 42.5 (May 2005), pp. 12–14. ISSN: 0018-9235. DOI: 10.1109/MSPEC.2005.1402708. URL: <http://dx.doi.org/10.1109/MSPEC.2005.1402708>.
- [105] Magneti Marelli S.p.A. *Synaptic Damping Control*. http://www.magnetimarelli.com/business_areas/suspension-systems/shock-absorbers/synaptic-damping-control. [Online]. 2017.
- [106] A. Alleyne and J. K. Hedrick. “Nonlinear adaptive control of active suspensions”. In: *IEEE Transactions on Control Systems Technology* 3.1 (Mar. 1995), pp. 94–101. ISSN: 1063-6536. DOI: 10.1109/87.370714.

- [107] X. Dong. “State-of-the-art of vehicle intelligent suspension control system”. In: *Handbook of Vehicle Suspension Control Systems*. Ed. by H. Liu, H. Gao, and P. Li. The Institution of Engineering and Technology, London, United Kingdom, 2014. Chap. 1. ISBN: 978-1-84919-634-5.
- [108] E. Guglielmino, T. Sireteanu, C.W. Stammers, G. Ghita, and M. Giuclea. *Semi-active Suspension Control: Improved Vehicle Ride and Road Friendliness*. Springer-Verlag London Limited, 2008. ISBN: 978-1-84800-230-2.
- [109] MT Braz-César and Rui Barros. “Properties and numerical modeling of MR dampers”. In: *ICEM15-15 th International Conference on Experimental Mechanics*. 2012.
- [110] Mohammed Ismail, Fayçal Ikhouane, and José Rodellar. “The Hysteresis Bouc-Wen Model, a Survey”. In: *Archives of Computational Methods in Engineering* 16.2 (2009), pp. 161–188. ISSN: 1886-1784. DOI: 10.1007/s11831-009-9031-8.
- [111] R. N. Jazar. *Vehicle Dynamics: Theory and Applications*. Springer Science+Business Media, LLC, 2008. ISBN: 978-0-387-74243-4.
- [112] H. Pacejka. *Tire and Vehicle Dynamics*. 3rd. Elsevier Ltd., 2012. ISBN: 978-0-08-097016-5.
- [113] R. Rajamani. *Vehicle Dynamics and Control*. 2nd. Springer Science+Business Media, LLC, 2012. ISBN: 978-1-4614-1432-2.
- [114] TASS International. *Delft-Tyre, Web Page*. <https://www.tassinternational.com/delft-tyre>. [Online]. 2017.
- [115] P. Fevrier, H. Martin, and G. Fandard. *Method for simulating the thermomechanical behavior of a tire rolling on the ground*. Patent. US, Oct. 2012.
- [116] ISO 2631-1. *Mechanical vibration and shock – Evaluation of human exposure to whole-body vibration*. Tech. rep. Geneva, CH: International Organization for Standardization, May 1997.
- [117] British Standard 6841. *Guide to measurement and evaluation of human exposure to whole-body mechanical vibration and repeated shock*. Tech. rep. BSI, Sept. 1987.
- [118] Richtlinie VDI 2057. *Einwirkung mechanischer Schwingungen auf den Menschen - Ganzkörper-Schwingungen*. Richtlinie. VDI, Sept. 2002.
- [119] R. N. Janeway. “Human Vibration Tolerance Criteria and Applications to Ride Evaluation”. In: *SAE Technical Paper*. SAE International, Feb. 1975. DOI: 10.4271/750166. URL: <http://dx.doi.org/10.4271/750166>.

- [120] A.F. Naudé and J.A. Snyman. “Optimisation of road vehicle passive suspension systems. Part 1. Optimisation algorithm and vehicle model”. In: *Applied Mathematical Modelling* 27.4 (2003), pp. 249–261. ISSN: 0307-904X.
- [121] G Verros, S Natsiavas, and C Papadimitriou. “Design optimization of quarter-car models with passive and semi-active suspensions under random road excitation”. In: *Journal of Vibration and Control* 11.5 (2005), pp. 581–606.
- [122] D. Karnopp, M. Crosby, and R. Harwood. “Vibration control using semi-active force generators”. In: *Journal of Engineering for Industry* 96.2 (1974), pp. 619–626.
- [123] S. Savaresi, E. Silani, and S. Bittanti. “Semi-active suspensions: an optimal control strategy for a quarter-car model”. In: 1st IFAC Symposium on Advances in Automotive Control (AAC). Salerno, Italy, 2004, pp. 572–577.
- [124] S. Savaresi and C. Spelta. “Mixed Sky-Hook and ADD: Approaching the Filtering Limits of a SemiActive Suspension”. In: *Journal of Dynamic Systems Measurement and Control* 129.4 (2007).
- [125] R. Morselli and R. Zanasi. “Control of a port hamiltonian systems by dissipative devices and its application to improve the semi-active suspension behavior”. In: *Mechatronics* 18.7 (2008), pp. 364–369.
- [126] C.W. Stammers and T. Sireteanu. “Vibration control of machines by use of semi-active dry friction damping”. In: *Journal of Sound and Vibration* 209.4 (1998), pp. 671–684. ISSN: 0022-460X. DOI: 10.1006/1997.1289.
- [127] S. Rakheja and S. Sankar. “Vibration and Shock Isolation Performance of a Semi-Active “On-Off” Damper”. In: *ASME. J. Vib., Acoust., Stress, and Reliab* 107.4 (1985), pp. 398–403. DOI: 10.1115/1.3269279.
- [128] M. Valasek, M. Novak, Z. Sika, and O. Vaculin. “Extended Ground-Hook - New Concept of Semi-Active Control of Truck’s Suspension”. In: *Vehicle System Dynamics* 27.5-6 (1997), pp. 289–303. DOI: 10.1080/00423119708969333.
- [129] J-H. Koo, M. Ahmadian, M. Setareh, and T. Murray. “In Search of Suitable Control Methods for Semi-Active Tuned Vibration Absorbers”. In: *Journal of Vibration and Control* 10 (2004), pp. 163–174. DOI: 10.1177/1077546304032020.
- [130] V. Sankaranarayanan, S. Oncu, D. Ozcan, and L. Guvenc. “Vehicle Chassis Control Using Adaptive Semi-Active Suspension”. In: 17th World Congress, The International Federation of Automatic Control. 2008.

- [131] I. Patil and K. Wani. “Design and Analysis of Semi-active Suspension Using Skyhook, Ground Hook and Hybrid Control Models for a Four Wheeler”. In: SAE Technical Paper 2015-26-0084. 2015.
- [132] S. Savaresi and C. Spelta. “A single-sensor control strategy for semi-active suspensions”. In: *IEEE Transaction on Control System Technology* 17.1 (2009), pp. 143–152.
- [133] X. Song. “Cost-Effective Skyhook Control for Semiactive Vehicle Suspension Applications”. In: *The Open Mechanical Engineering* 3 (2009), pp. 17–25.
- [134] K.-S. Hong, H.-C. Sohn, and J.-K. Hedrick. “Modified skyhook control of semi-active suspensions: A new model, gain scheduling, and hardware-in-the-loop tuning”. In: *ASME Journal of Dynamic Systems, Measurement, and Control* 124.1 (2002), pp. 158–167.
- [135] K. Yi and B.S. Song. “A new adaptive sky-hook control of vehicle semi-active suspensions”. In: *Proceedings of the Institution of Mechanical Engineers, Part D: Journal of Automobile Engineering* 213.3 (1999), pp. 293–303. DOI: 10.1243/0954407991526874.
- [136] X. Song, M. Ahmadian, and S. Southward. “Analysis and strategy for superharmonics with semiactive suspension control systems”. In: *ASME Journal of Dynamic Systems, Measurement, and Control* 129.6 (2007), pp. 795–803.
- [137] B. Kasemi, A.G.A. Muthalif, M.M. Rashid, and S. Fathima. “Fuzzy-PID Controller for Semi-Active Vibration Control Using Magnetorheological Fluid Damper”. In: *Procedia Engineering* 4 (2012), pp. 1221–1227.
- [138] D. Singh and M.L. Aggarwal. “Passenger seat vibration control of a semi-active quarter car system with hybrid Fuzzy–PID approach”. In: *International Journal of Dynamics and Control* (2015), pp. 1–10. DOI: 10.1007/s40435-015-0175-0.
- [139] M. El-Kafafy, S. El-Demerdash, and A. Rabeih. “Automotive Ride Comfort Control Using MR Fluid Damper”. In: *Engineering* 4.4 (2012), pp. 179–187. DOI: 10.4236/eng.2012.44024.
- [140] O. Sename and L. Dugard. “Robust H control of quarter-car semi-active suspensions”. In: *In Proceedings of the European Control Conference (ECC) Cambridge, England* (2003).
- [141] H. Dua, K.Y. Szeb, and J. Lam. “Semi-active H1 control of vehicle suspension with magneto-rheological dampers”. In: *Journal of Sound and Vibration* 283 (2005), pp. 981–996.
- [142] C. Poussot-Vassal, O. Sename, L. Dugard, P. Gaspar, Z. Szabo, and J. Bokor. “A new semi-active suspension control strategy through LPV technique”. In: *Control Engineering Practice* 16 (2008), pp. 1519–1534.

- [143] F. Pozo, M. Zapateiro, L.Achoa, Y. Vidal, and NingsuLu N. Luo Yolanda Vidala. “Experimental study of semiactive VSC techniques for vehicle vibration reduction”. In: *Journal of the Franklin Institute* 350 (2013), pp. 1–18.
- [144] D. Asha, Silje Helene Olsen Storhaug, and Hamid Reza Karimi. “LQG Control of a Semi-active Suspension System Equipped with MR Rotary Brake”. In: *Proceedings of the 11th WSEAS International Conference on Instrumentation, Measurement, Circuits and Systems, and Proceedings of the 12th WSEAS International Conference on Robotics, Control and Manufacturing Technology, and Proceedings of the 12th WSEAS International Conference on Multimedia Systems; Signal Processing*. IMMURO’12. Rovaniemi, Finland: World Scientific, Engineering Academy, and Society (WSEAS), 2012, pp. 176–181. ISBN: 978-1-61804-085-5.
- [145] M.Zapateiro, N. Luo, H.R. Karimi, and J. Vehi. “Vibration control of a class of semiactive suspension system using neural network and backstepping techniques”. In: *Mechanical Systems and Signal Processing* 23 (2009), pp. 1946–1953.
- [146] M. Canale, M. Milanese, and C. Novara. “Semi-active suspension control using fast model-predictive techniques”. In: *IEEE Transaction on Control System Technology* 14.6 (2006), pp. 1034–1046.
- [147] N. Giorgetti, A. Bemporad, H. Tseng, and D. Hrovat. “Hybrid model predictive control application toward optimal semi-active suspension”. In: *International Journal of Control* 79.5 (2006), pp. 521–533.
- [148] Y. Wang and K. Utsunomiya. *Sub-optimal Control Design of a Semi-active Vibration Reduction System*. Tech. rep. Cambridge, MA, 02139 USA: Mitsubishi Electric Research Laboratories, 2013.
- [149] INTECO Sp. z o. o. *INTECO Sp. z o. o., Web Page*. [Online]. INTECO Sp. z o. o.
- [150] Przemysław Gorczyca, Krzysztof Kogut, Krzysztof Kołek, Maciej Rosół, and Andrzej Turnau. “Wymuszenie kinematyczne zawieszenia pojazdu - Kinematic excitation of the vehicle suspension”. In: *Projektowanie, analiza i implementacja systemów czasu rzeczywistego*. Ed. by Leszek Trybus and Sławomir Samolej. Warszawa: Wydawnictwa Komunikacji i Łączności, 2011. ISBN: 878-83-206-1822-8.
- [151] D. H. Wang and W. H. Liao. “Magnetorheological fluid dampers: a review of parametric modelling”. In: *Smart materials and structures* 20 (2011).
- [152] Bogdan Sapiński. *Magnetorheological Dumpers in Vibration Control*. Cracow: AGH University of Science and Technology Press, 2006.

- [153] Krzysztof Kogut. "Semi-active Suspension System Modelling and Parameters Identification". In: *Automatyka/Automatics* 16 No. 1 (2012), pp. 15–24.
- [154] Andrzej Turnau. "Model identification Dedicated to the Time-Optimal Control". In: *17th IFAC World Congress, 7-11 July, Seoul* (2008), pp. 2655–2660.
- [155] Krzysztof Kogut. "Real-time MR damper control strategies for quarter car suspension". In: *Design, development and implementation of real-time systems*. Ed. by Marcin W. Mastalerz Leszek Trybus. Warszawa, Heidelberg: Polish Information Processing Society, 2013, pp. 55–65.
- [156] Manfred Burekhardt. *Fahrwerktechnik: Radschlupf-Regelsysteme*. Germany, Wurtzburg: Vogel-Verlag, 1993.
- [157] S. M. Savaresi and M. Tanelli. *Active Braking Control Systems Design for Vehicles*. Springer-Verlag London Limited, 2010. ISBN: 978-1-84996-349-7.
- [158] A. Mirzaei, M. Moallem, B. Mirzaeian, and B. Fahimi. "Design of an optimal fuzzy controller for Antilock Braking Systems". In: *2005 IEEE Vehicle Power and Propulsion Conference*. 2005, pp. 823–828. DOI: 10.1109/VPPC.2005.1554541.
- [159] J. S. Lin and W. E. Ting. "Nonlinear control design of anti-lock braking systems with assistance of active suspension". In: *IET Control Theory Applications* 1.1 (Jan. 2007), pp. 343–348. ISSN: 1751-8644. DOI: 10.1049/iet-cta:20050218.
- [160] F. Z. Li, R. F. Hu, and H. X. Yao. "The Performance of Automobile Antilock Brake System Based on Fuzzy Robust Control". In: *Intelligent Computation Technology and Automation (ICICTA), 2010 International Conference on*. Vol. 3. 2010, pp. 870–873. DOI: 10.1109/ICICTA.2010.37.
- [161] Guirong Zhuo, Hui Shen, Shenchen Wu, and Yilin Ren. "Antilock Brake Control System for Four-Wheel-Drive Electric Vehicle with Electro-hydraulic Braking based on Precise Control of Hydraulic Braking Force". In: *SAE Technical Paper*. SAE International, Apr. 2015. DOI: 10.4271/2015-01-1573.
- [162] Luigi Petruccelli, Mauro Velardocchia, and Aldo Sorniotti. "Electro-Hydraulic Braking System Modelling and Simulation". In: *SAE Technical Paper*. SAE International, Oct. 2003. DOI: 10.4271/2003-01-3336.
- [163] Zhe Xiong, Xiaofei Pei, Xuexun Guo, and Chengcai Zhang. "Model-Based Pressure Control for an Electro Hydraulic Brake System on RCP Test Environment". In: *SAE Technical Paper*. SAE International, Sept. 2016.
- [164] N. Cesario, F. Tagliatalata, and M. Lavorgna. "Adaptive Control Strategies for Electro-Mechanical Brakes". In: *SAE Technical Paper*. SAE International, Oct. 2007. DOI: 10.4271/2007-01-3944.

- [165] S. Semmler, D. Fischer, R. Isermann, R. Schwarz, and P. Rieth. “ESTIMATION OF VEHICLE VELOCITY USING BRAKE-BY-WIRE ACTUATORS”. In: *IFAC Proceedings Volumes 35.1* (2002), pp. 169–174. ISSN: 1474-6670.
- [166] K. Yang, J. Li, Y. Li, H. Wan, Z. Wang, C. Li, and S. Tan. “Simulation of Fuzzy PI Controller for ABS based on Electromechanical brake system”. In: *Vehicular Electronics and Safety, 2006. ICVES 2006. IEEE International Conference on*. Dec. 2006, pp. 407–412. DOI: 10.1109/ICVES.2006.371625.
- [167] U. Kiencke and L. Nielsen. *Automotive Control Systems For Engine, Driveline, And Vehicle*. Springer-Verlag Berlin Heidelberg, 2005. ISBN: 3-540-23139-0.
- [168] Konrad Reif, ed. *Brakes, Brake Control and Driver Assistance Systems*. Springer Vieweg, 2014. ISBN: 978-3-658-03978-3.
- [169] William Pasillas-Lépine. *Hybrid Modelling and Limit Cycle Analysis for a Class of Five-phase Anti-lock Brake Algorithms*. 2006.
- [170] C-Y Kuo and E C Yeh. “A Four-Phase Control Scheme of an Anti-Skid Brake System for all Road Conditions”. In: *Proceedings of the Institution of Mechanical Engineers, Part D: Journal of Automobile Engineering* 206.4 (1992), pp. 275–283. DOI: 10.1243/PIME\PROC\1992_206_188_02.
- [171] H. Ouwerkerk and R. R. Guntur. “Skid Prediction”. In: *Vehicle System Dynamics* 1.2 (1972), pp. 67–88. DOI: 10.1080/00423117208968422.
- [172] Satohiko Yoneda, Yasuo Naitoh, and Hideo Kigoshi. “Rear Brake Lock-Up Control System of Mitsubishi Starion”. In: *SAE Technical Paper*. SAE International, Feb. 1983. DOI: 10.4271/830482.
- [173] R. T. Fling and R. E. Fenton. “A describing-function approach to antiskid design”. In: *IEEE Transactions on Vehicular Technology* 30.3 (1981), pp. 134–144. ISSN: 0018-9545. DOI: 10.1109/T-VT.1981.23895.
- [174] H. S. Tan and M. Tomizuka. “A Discrete-Time Robust Vehicle Traction Controller Design”. In: *1989 American Control Conference*. June 1989, pp. 1053–1060.
- [175] H. Takahashi and Y. Ishikawa. *Antiskid brake control system based on fuzzy inference*. US Patent 4,842,342. June 1989. URL: <https://www.google.ch/patents/US4842342>.
- [176] Y. K. Chin, W. C. Lin, D. M. Sidlosky, D. S. Rule, and M. S. Sparschu. “Sliding-Mode ABS Wheel-Slip Control”. In: *1992 American Control Conference*. 1992, pp. 1–8.

- [177] P. E. Wellstead and N. B. O. L. Pettit. "Analysis and redesign of an antilock brake system controller". In: *IEE Proceedings - Control Theory and Applications* 144.5 (1997), pp. 413–426. ISSN: 1350-2379. DOI: 10.1049/ip-cta:19971441.
- [178] C. Unsal and P. Kachroo. "Sliding mode measurement feedback control for antilock braking systems". In: *IEEE Transactions on Control Systems Technology* 7.2 (1999), pp. 271–281. ISSN: 1063-6536. DOI: 10.1109/87.748153.
- [179] S. Drakunov, U. Ozguner, P. Dix, and B. Ashrafi. "ABS control using optimum search via sliding modes". In: *IEEE Transactions on Control Systems Technology* 3.1 (1995), pp. 79–85. ISSN: 1063-6536. DOI: 10.1109/87.370698.
- [180] Y. S. Kueon and J. S. Bedi. "Fuzzy-neural-sliding mode controller and its applications to the vehicle anti-lock braking systems". In: *Proceedings IEEE Conference on Industrial Automation and Control Emerging Technology Applications*. 1995, pp. 391–398. DOI: 10.1109/IACET.1995.527594.
- [181] G. F. Mauer. "A fuzzy logic controller for an ABS braking system". In: *IEEE Transactions on Fuzzy Systems* 3.4 (1995), pp. 381–388. ISSN: 1063-6706. DOI: 10.1109/91.481947.
- [182] J. R. Layne, K. M. Passino, and S. Yurkovich. "Fuzzy learning control for antiskid braking systems". In: *IEEE Transactions on Control Systems Technology* 1.2 (1993), pp. 122–129. ISSN: 1063-6536. DOI: 10.1109/87.238405.
- [183] Yong Liu and Jing Sun. "Target slip tracking using gain-scheduling for antilock braking systems". In: *American Control Conference, Proceedings of the 1995*. Vol. 2. 1995, 1178–1182 vol.2. DOI: 10.1109/ACC.1995.520935.
- [184] J. S. Yu. "A robust adaptive wheel-slip controller for antilock brake system". In: *Proceedings of the 36th IEEE Conference on Decision and Control*. Vol. 3. 1997, 2545–2546 vol.3. DOI: 10.1109/CDC.1997.657714.
- [185] C. Jun. "The Study of ABS control system with different control methods". In: *Proceedings of the 4th International Symposium on Advanced Vehicle Control*. 1998, pp. 623–628.
- [186] Byung-Ryong Lee and Kyu-Hyun Sin. "Slip-ratio control of ABS using sliding mode control". In: *Proceedings KORUS 2000. The 4th Korea-Russia International Symposium On Science and Technology*. Vol. 3. 2000, 72–77 vol. 3. DOI: 10.1109/KORUS.2000.866062.
- [187] F. Jiang and Z. Gao. "An application of nonlinear PID control to a class of truck ABS problems". In: *Proceedings of the 40th IEEE Conference on Decision and Control (Cat. No.01CH37228)*. Vol. 1. 2001, 516–521 vol.1. DOI: 10.1109/2001.980154.

- [188] I. Petersen, T. A. Johansen, J. Kalkkuhl, and J. Lüdemann. “Wheel slip control in ABS brakes using gain scheduled constrained LQR”. In: *2001 European Control Conference (ECC)*. 2001, pp. 606–611.
- [189] T. A. Johansen, I. Petersen, J. Kalkkuhl, and J. Ludemann. “Gain-scheduled wheel slip control in automotive brake systems”. In: *IEEE Transactions on Control Systems Technology* 11.6 (2003), pp. 799–811. ISSN: 1063-6536. DOI: 10.1109/TCST.2003.815607.
- [190] Ren-Guang Wang, Zhao-Du Liu, Zhi-Quan Qi, Yue-Feng Ma, and Hai-Feng Cui. “Multiple Model Adaptive Control of Antilock Brake System via Backstepping Approach”. In: *2005 International Conference on Machine Learning and Cybernetics*. Vol. 1. 2005, pp. 591–595. DOI: 10.1109/ICMLC.2005.1527013.
- [191] Z. Wei and G. Xuexun. “An ABS Control Strategy for Commercial Vehicle”. In: *IEEE/ASME Transactions on Mechatronics* 20.1 (2015), pp. 384–392. ISSN: 1083-4435. DOI: 10.1109/TMECH.2014.2322629.
- [192] M. Schinkel and K. Hunt. “Anti-lock braking control using a sliding mode like approach”. In: *Proceedings of the 2002 American Control Conference (IEEE Cat. No.CH37301)*. Vol. 3. 2002, 2386–2391 vol.3. DOI: 10.1109/ACC.2002.1023999.
- [193] A. Harifi, A. Aghagolzadeh, G. Alizadeh, and M. Sadeghi. “Designing a Sliding Mode Controller for Antilock Brake System”. In: *EUROCON 2005 - The International Conference on "Computer as a Tool"*. Vol. 1. 2005, pp. 258–261. DOI: 10.1109/EURCON.2005.1629910.
- [194] Yinggan Tang, Xiangyang Zhang, Dongli Zhang, Gang Zhao, and Xinping Guan. “Fractional order sliding mode controller design for antilock braking systems”. In: *Neurocomputing* 111 (2013), pp. 122–130. ISSN: 0925-2312.
- [195] Y. Oniz, E. Kayacan, and O. Kaynak. “Simulated and experimental study of antilock braking system using grey sliding mode control”. In: *2007 IEEE International Conference on Systems, Man and Cybernetics*. 2007, pp. 90–95. DOI: 10.1109/ICSMC.2007.4413975.
- [196] E. Kayacan, Y. Oniz, and O. Kaynak. “A Grey System Modeling Approach for Sliding-Mode Control of Antilock Braking System”. In: *IEEE Transactions on Industrial Electronics* 56.8 (2009), pp. 3244–3252. ISSN: 0278-0046. DOI: 10.1109/TIE.2009.2023098.
- [197] J. A. Cabrera, A. Ortiz, J. J. Castillo, and A. Simon. “A fuzzy logic control for antilock braking system integrated in the IMM tire test bench”. In: *IEEE Transactions on Vehicular Technology* 54.6 (2005), pp. 1937–1949. ISSN: 0018-9545. DOI: 10.1109/TVT.2005.853479.

- [198] Chih-Min Lin and C. F. Hsu. “Self-learning fuzzy sliding-mode control for antilock braking systems”. In: *IEEE Transactions on Control Systems Technology* 11.2 (2003), pp. 273–278. ISSN: 1063-6536. DOI: 10.1109/TCST.2003.809246.
- [199] R. E. Precup, S. V. Spătaru, M. B. Rădac, E. M. Petriu, S. Preitl, C. A. Dragoș, and R. C. David. “Experimental Results of Model-Based Fuzzy Control Solutions for a Laboratory Antilock Braking System”. In: *Human – Computer Systems Interaction: Backgrounds and Applications 2: Part 2*. Ed. by Zdzisław S. Hippe, Juliusz L. Kulikowski, and Teresa Mroczek. Berlin, Heidelberg: Springer Berlin Heidelberg, 2012, pp. 223–234. ISBN: 978-3-642-23172-8. DOI: 10.1007/978-3-642-23172-8_16.
- [200] A. Mirzaei, M. Moallem, and B. Mirzaeian. “Designing a Genetic-Fuzzy Anti-Lock Brake System Controller”. In: *Proceedings of the 2005 IEEE International Symposium on, Mediterrean Conference on Control and Automation Intelligent Control, 2005*. 2005, pp. 1246–1250. DOI: 10.1109/2005.1467194.
- [201] A. Mirzaei, M. Moallem, B. M. Dehkordi, and B. Fahimi. “Design of an Optimal Fuzzy Controller for Antilock Braking Systems”. In: *IEEE Transactions on Vehicular Technology* 55.6 (2006), pp. 1725–1730. ISSN: 0018-9545. DOI: 10.1109/TVT.2006.878714.
- [202] Abdel Badie Sharkawy. “Genetic fuzzy self-tuning PID controllers for antilock braking systems”. In: *Engineering Applications of Artificial Intelligence* 23.7 (2010), pp. 1041–1052. ISSN: 0952-1976. DOI: <http://dx.doi.org/10.1016/j.engappai.2010.06.011>.
- [203] Chih-Keng Chen and Ming-Chang Shih. “PID-Type Fuzzy Control for Anti-Lock Brake Systems with Parameter Adaptation”. In: *JSME international journal. Series C, Mechanical systems, machine elements and manufacturing* 47.2 (June 2004), pp. 675–685. ISSN: 13447653. DOI: 10.1299/jsmec.47.675.
- [204] M. B. Radac, R. E. Precup, S. Preitl, J. K. Tar, and E. M. Petriu. “Linear and fuzzy control solutions for a laboratory Anti-lock Braking System”. In: *2008 6th International Symposium on Intelligent Systems and Informatics*. 2008, pp. 1–6. DOI: 10.1109/SISY.2008.4664947.
- [205] Velimir Ćirović, Dragan Aleksendrić, and Dušan Smiljanić. “Longitudinal wheel slip control using dynamic neural networks”. In: *Mechatronics* 23.1 (2013), pp. 135–146. ISSN: 0957-4158. DOI: <http://dx.doi.org/10.1016/j.mechatronics.2012.11.007>.
- [206] Amir Poursamad. “Adaptive feedback linearization control of antilock braking systems using neural networks”. In: *Mechatronics* 19.5 (2009), pp. 767–773. ISSN: 0957-4158.

- [207] Chih-Min Lin and C. F. Hsu. “Neural-network hybrid control for antilock braking systems”. In: *IEEE Transactions on Neural Networks* 14.2 (2003), pp. 351–359. ISSN: 1045-9227. DOI: 10.1109/TNN.2002.806950.
- [208] Yonggon Lee and S. H. Zak. “Designing a genetic neural fuzzy antilock-brake-system controller”. In: *IEEE Transactions on Evolutionary Computation* 6.2 (2002), pp. 198–211. ISSN: 1089-778X. DOI: 10.1109/4235.996019.
- [209] Velimir Ćirović and Dragan Aleksendrić. “Adaptive neuro-fuzzy wheel slip control”. In: *Expert Systems with Applications* 40.13 (2013), pp. 5197–5209. ISSN: 0957-4174. DOI: <http://dx.doi.org/10.1016/j.eswa.2013.03.012>.
- [210] Guan-Ming Chen, Wei-Yen Wang, Tsu-Tian Lee, CW Tao, et al. “Observer-based direct adaptive fuzzy-neural control for anti-lock braking systems”. In: *International Journal of Fuzzy Systems* 8.4 (2006), pp. 208–218.
- [211] W. Y. Wang, I. H. Li, M. C. Chen, S. F. Su, and S. B. Hsu. “Dynamic Slip-Ratio Estimation and Control of Antilock Braking Systems Using an Observer-Based Direct Adaptive Fuzzy Neural Controller”. In: *IEEE Transactions on Industrial Electronics* 56.5 (2009), pp. 1746–1756. ISSN: 0278-0046. DOI: 10.1109/TIE.2008.2009439.
- [212] Andon V. Topalov, Yesim Oniz, Erdal Kayacan, and Okay Kaynak. “Neuro-fuzzy control of antilock braking system using sliding mode incremental learning algorithm”. In: *Neurocomputing* 74.11 (2011), pp. 1883–1893. ISSN: 0925-2312. DOI: <http://dx.doi.org/10.1016/j.neucom.2010.07.035>.
- [213] Y. E. Mao, Y. Zhang, and T. Liu. “The sliding mode controller for automotive ABS based on the fuzzy neural network”. In: *2010 Sixth International Conference on Natural Computation*. Vol. 3. 2010, pp. 1410–1413. DOI: 10.1109/ICNC.2010.5582534.
- [214] Krzysztof Kogut. “Anti-lock braking system modelling and parameters identification”. In: *2014 19th International Conference on Methods and Models in Automation and Robotics (MMAR)*. Sept. 2014, pp. 342–346.
- [215] PML Motors Co., LTD. *Motor Specification Sheet*. <http://www.pml.com.cn/>. [Online]. 2014.
- [216] INTECO Sp. z o. o. *ABS User’s Manual*. <http://www.inteco.com.pl/>. [Online]. 2014.
- [217] Pieter Eykhoff. *System identification: parameter and state estimation*. London: Wiley, 1974.
- [218] Neil Gershenfeld. *Mathematical Modeling*. United Kingdom, Cambridge: Cambridge University Press, 1999.

- [219] Krzysztof Kogut, Krzysztof Kołek, Maciej Rosół, and Andrzej Turnau. “A new current based slip controller for ABS”. In: *XIX Polish Control Conference*. To be presented and published at XIX Polish Control Conference 18-21 June 2017 in Krakow University of Science and Technology. 2017.